The Design and Synthesis of Peptides and Small Molecules to Control Immune Checkpoints

Deanne Hayward

School of Pharmacy

University of East Anglia

October 2023

Thesis submitted in partial fulfilment of the requirements for the degree of Doctor of Philosophy of the University of East Anglia.

© This copy of the thesis has been supplied on condition that anyone who consults it is understood to recognise that its copyright rests with the author and that use of any information derived therefrom must be in accordance with current UK Copyright Law. In addition, any quotation or extract must include full attribution.

Declaration

This thesis has been submitted to the University of East Anglia for the degree of Doctor of Philosophy and is, to the best of my knowledge, original except where stated, referenced and acknowledged.

Deanne Hayward

Abstract

Presented within this thesis is research on the identification of novel small molecule and peptide inhibitors for the immune checkpoint protein-protein interaction, programmed cell death 1 and programmed cell death ligand 1 (PD-1/PD-L1). The discovery of PD-1/PD-L1 has been invaluable to the effectiveness of immunotherapy treatment for cancer.

In chapter one the need for new inhibitors for PD-1/PD-L1 is outlined, along with the structure of this interaction and approach for inhibition with mAbs. A literature review of small molecule inhibitors designed from the interactions of peptide inhibitors of proteins is presented, outlining inspiration for the synthetic work.

Chapter two describes the design and synthesis of a light-activated peptide inhibitor of PD-1/PD-L1. A linear peptide PD-1/PD-L1 inhibitor, was analysed *via* an alanine scan to determine which amino acids were essential for inhibiting PD-1/PD-L1. Following this, an azobenzene photo-switch was successfully inserted into the backbone of the peptide. The light-switching capabilities of peptide were confirmed using UV-Vis spectroscopy and analytical HPLC. Following this, the inhibitory activity of the peptide was demonstrated, exhibiting the ability to selectively bind to PD-1/PD-L1 following irradiation. Biological evaluation of the photo-switchable peptide was performed in a cell-based PD-1/PD-L1 assay.

In chapter three, the application of the linear peptide to peptide-directed binding was investigated. The peptide was split in two distributing vital residues based on the information described in chapter two. The synthesis of semi-peptides is discussed, followed by the modification of the peptides with turn-mimicking motif and a library of small molecule fragments to form peptide-small molecule hybrids. The inhibitory activity of these hybrids was tested using a homologous time-resolved fluorescence assay, identifying several peptide-small molecule hybrids capable of inhibiting PD-1/PD-L1 at nanomolar concentrations.

Chapter four presents the investigation into inverse electron demand Diels-Alder reactions using 1,2,4,5-tetrazine derivatives for use as a turn mimicking motif. The successful synthesis of 1,2,4,5-tetrazine derivatives for solid phase peptide synthesis

will be discussed, alongside the use of these compounds in iEDDA reactions. The synthesis of iEDDA precursors was successful, and the investigation of their utility in the generation of peptide-small molecule hybrids is discussed.

The work described in chapter five follows the synthesis of cyclic peptide inhibitors for PD-1/PD-L1, and the investigation of these conformationally restrained molecules for application in peptide directed binding.

Access Condition and Agreement

Each deposit in UEA Digital Repository is protected by copyright and other intellectual property rights, and duplication or sale of all or part of any of the Data Collections is not permitted, except that material may be duplicated by you for your research use or for educational purposes in electronic or print form. You must obtain permission from the copyright holder, usually the author, for any other use. Exceptions only apply where a deposit may be explicitly provided under a stated licence, such as a Creative Commons licence or Open Government licence.

Electronic or print copies may not be offered, whether for sale or otherwise to anyone, unless explicitly stated under a Creative Commons or Open Government license. Unauthorised reproduction, editing or reformatting for resale purposes is explicitly prohibited (except where approved by the copyright holder themselves) and UEA reserves the right to take immediate ‘take down’ action on behalf of the copyright and/or rights holder if this Access condition of the UEA Digital Repository is breached. Any material in this database has been supplied on the understanding that it is copyright material and that no quotation from the material may be published without proper acknowledgement.

Contents

Title ..... **i**
Declaration ..... **ii**
Abstract ..... **iii**
Contents ..... **v**
Abbreviations ..... **ix**
Acknowledgements ..... **xi**
Chapter 1 Literature Review **1**
1.1 Programmed cell death 1 and programmed cell death ligand 1 2
1.1.1 Drawbacks of antibody treatment 3
1.1.2 PD-1/PD-L1 structure 4
1.2 Using cyclic peptides to target PPIs 6
1.2.2 Methods for discovering novel cyclic peptides 9
1.2.3 Transferring peptide side chain functionality to small molecule scaffolds 11
1.2.4 Mimicking peptide side chain interactions to enhance small molecule binders 20
1.2.5 Using peptide side-chain functionality to inspire small molecule design 23
1.3 Conclusion 26
1.4 Thesis outline 27
1.5 References 28
Chapter 2 The Design, Synthesis and Biological Evaluation of Photo-switchable Peptide Inhibitors of PD-1/PD-L1 ..... **34**
2.1 Introduction 35
2.1.1 Restricting peptide secondary structure 35
2.1.2 Peptide inhibitors of PD-1/PD-L1 36
2.2 Photo-switchable molecules 40
2.2.1 Azobenzenes 43
2.2.2 Azobenzene modified peptides 43
2.3 Chapter Aims 44
2.4 Results and Discussion 45
2.4.1 Structural investigation of CLP003 45
2.4.2 Protein interaction of alanine scan peptides 48
2.4.3 Synthesis of AMPP 51
2.4.4 The design of azobenzene peptides 53

2.4.5 Photo-switching peptides 54
2.4.6 Photo stability of azobenzene peptides 56
2.4.7 Peptides 2.51-2.56's ability to inhibit PD-1/PD-L1 57
2.4.8 Thermal stability of 2.51 57
2.4.9 The cellular inhibition of PD-1/PD-L1 by 2.51 58
2.5 Work towards red-light photo-switches 59
2.6 Conclusion 62
2.7 Experimental 63
2.7.1 Materials and solvents 63
2.7.2 Instrumental techniques 63
2.7.3 Solid phase peptide synthesis 64
2.7.4 Synthesis of AMPP 67
2.7.5 Synthesis of fluorinated AMPP 69
2.7.6 Photo-switching of peptides 2.51-2.56 71
2.7.7 Thermal stability of 2.51 71
2.7.8 PD-1/PD-L1 HTRF binding assay 71
2.7.9 PD-1/PD-L1 cell-based assay 72
2.8 References 73
Chapter 3 Peptide-Directed Binding to Identify Peptide-Small Molecule Hybrids that Inhibit PD-1/PD-L1 77
3.1 Introduction 78
3.1.1 Small molecules can control protein-protein interactions 78
3.1.2 Small molecules that target PD-1/PD-L1 78
3.1.3 Methods to identify novel small molecules for PPIs 83
3.1.4 Peptide-directed binding 85
3.2 Chapter Aims 87
3.3 Results and Discussion 87
3.3.1 Semi peptides 87
3.3.2 The synthesis of semi-peptide 1 (-NWRWLPP, 3.14) 89
3.3.3 The synthesis of semi-peptide 1 (-NWRWLPP, 3.14) with the turn mimic Fmoc-2-aminobenzoic acid (3.16) 90
3.3.4 The synthesis of semi-peptide 1(-NWRWLP, 3.14) with turn mimic Fmoc-2-aminophenylacetic acid (3.27) 92
3.3.5 The synthesis of semi-peptide 1(-NWRWLPP, 3.14) with the turn mimic cis-2-Fmoc-aminocyclohexanecarboxylic acid (3.30) 94
3.3.6 Testing peptide-small molecule hybrids 98

3.3.7 Small molecule fragments functionalised with a carboxylic acid 98
3.3.8 The synthesis of semi-peptide 2 (WHFSYN-, (3.15) 100
3.3.9 The synthesis of semi-peptide 2 (WHFSYN-, 3.15) using the oxime resin 103
3.3.10 The synthesis of semi-peptide 2 (WHFSYNP-) using 2-chlorotrityl resin..... 104
3.3.11 Small molecule fragments functionalised with an amine 111
3.4 Conclusion..... 113
3.5 Experimental 115
3.5.1 Materials and solvents..... 115
3.5.1 Instrumental techniques 115
3.5.2 Semi-peptide synthesis..... 116
3.5.1 PD-1/PD-L1 HTRF binding assay 129
3.6 References 130
Chapter 4 The Synthesis of 1,2,4,5-Tetrazine Derivatives and iEDDA Click Chemistry for use in Peptide-Directed Binding 134
4.1 Introduction 135
4.1.1 Click chemistry 135
4.1.2 Click chemistry as a turn-inducing motif..... 137
4.1.3 Inverse electron demand Diels-Alder 138
4.1.4 Factors that affect iEDDA reactivity..... 139
4.1.5 iEDDA in peptides 143
4.1.1 Previous syntheses of 1,2,4,5-tetrazines suitable for addition to peptides..... 144
4.2 Chapter Aims..... 147
4.3 Results and Discussion..... 148
4.3.1 Synthesis of 1,2,4,5-tetrazine..... 148
4.3.2 iEDDA clicks with di-substituted tetrazine..... 152
4.3.3 Mono-substituted 1,2,4,5-tetrazine synthesis..... 154
4.3.4 iEDDA clicks with mono-substituted tetrazines 157
4.3.5 Work towards better dienophiles..... 158
4.4 Conclusion..... 159
4.5 General procedures..... 160
4.5.1 Materials and solvents..... 160
4.5.2 Instrumental techniques 160
4.5.3 Synthesis 1,2,4,5-tetrazines..... 161
4.5.4 iEDDA click reactions 167
4.6 References 168

Chapter 5 Cyclic Peptides to Inhibit PD-1/PD-L1 171
5.1 Introduction 172
5.1.1 Cyclic peptides 172
5.1.2 Cyclic peptides that target PD-1 or PD-L1 173
5.1.1 Previous *N*-methylated peptide syntheses 174
5.1.2 Bristol Myers Squibb Peptides 175
5.1.3 BMS peptide-57, peptide-71 and peptide-101 177
5.2 Chapter Aims 181
5.3 Results and Discussion 181
5.3.1 P71 and p57 synthesis 181
5.3.2 Capping the peptide with a chloroacetyl group 187
5.3.3 P101 synthesis 190
5.4 Conclusion 193
5.5 Experimental 195
5.5.1 Materials and solvents 195
5.5.2 Instrumental techniques 195
5.5.3 Solid phase peptide synthesis 195
5.5.4 Synthesis of linear p57 (5.10) 196
5.5.5 Synthesis of p101 (5.11) 196
5.6 References 196
Chapter 6 Conclusion 199
6.1 Summary 200
6.2 Conclusion 204
6.3 References 204

Abbreviations

AMPP	3-(3-aminomethylphenylazo)phenylacetic acid
Cl-(Trt) resin	2-chlorotrityl resin
DCM	Dichloromethane
DIC	*N*,*N*'-diisopropylcarbodiimide
DIPEA	*N*,*N*-Diisopropylethylamine
DMAP	4-dimethylaminopyridine
DME	Dimethoxyethane
DMF	Dimethylformamide
EDC	1-ethyl-3-(3-dimethylaminopropyl)carbodiimide hydrochloride
ESI-QQQ	Electron spray ionisation-triple quadrupole
EtOAc	Ethyl Acetate
Fmoc	Fluorenylmethyloxycarbonyl
HATU	*N*-[(Dimethylamino)-1*H*-1,2,3-triazolo-[4,5-b]pyridin-1-ylmethylene]- *N*-methylmethanaminium hexafluorophosphate *N*-oxide
HBTU	*N,N,N',N'*-Tetramethyl-O-(1*H*-benzotriazol-1-yl)uronium hexafluorophosphate
HFIP	Hexafluoroisopropanol
HOBt	1-hydroxybenzotriazole hydrate
HPLC	High-performance liquid chromatography
HTRF Assay	Homologous time resolved fluorescence assay
iEDDA	Inverse electron demand Diels-Alder
LC-MS	Liquid chromatography-mass spectrometry
mAbs	Monoclonal antibodies
MALDI	Matrix-assisted laser desorption/ionisation
NHS	*N*-hydroxysuccinimide
NMM	*N*-methylmorpholine
NMP	*N*-methyl-2-pyrrolidone
PD-1	Programmed cell death 1
PD-L1	Programmed cell death ligand 1

PIDA	Phenyliodine(III) diacetate
PPI	Protein-protein interaction
TFA	Trifluoroacetic acid
THF	Tetrahydrofuran
TIPS	Triisopropylsilane

Acknowledgements

Firstly, I would like to thank my supervisors Dr Andrew Beekman and Prof. Mark Searcey for giving me this opportunity, I will be forever grateful. Thank you for all the guidance and support throughout my PhD, for answering my one thousand questions, and for always believing in me. I also would like to thank the Big C for funding my PhD and allowing me the opportunity to present my work internationally.

A massive thank you must go to the Beekman and Searcey groups for making the lab a wonderful place to work and for all their advice over the past three years. You all are a special bunch of goofballs. A special thank you to Zoë Goddard and Marco Cominetti. Zoë, for her day-to-day help in the lab, her advice and her support have been invaluable for completing this thesis. And to Marco for all his help and teachings, never stop rock and rolling!

My family and friends outside of the lab have also played a massive role in supporting me over the past three years. Thank you to my mum and step-dad, Marianne and Rob, for their continuous, never-wavering love and support (although sometimes strained). I would not be where I am today without both of you and there are not words to tell you how grateful I am. And of course, not forgetting Izzy and Juno, the two best support dogs that any person could ask for!

Last but no means least, to my partner, Trent. I could never thank you enough for the endless support you've given me. On every challenging day you've managed to somehow put a smile back on my face. Thank you for always being there for me, and for making my days infinitely better.

Chapter 1
Literature Review

1.1 Programmed cell death 1 and programmed cell death ligand 1

The immune system plays a crucial role in the surveillance against cancer within the body. While conventional therapies such as chemotherapy treat tumours as a whole population of cells without specificity, immunotherapy uses the body's own tumour-specific immune response to identify tumours and eliminate them.[1,2] Within the immune system, immune checkpoints protect healthy cells by regulating the immune response through immune checkpoint proteins.[2] Effective immunotherapy drugs are immune checkpoint inhibitors. In 2018, the Nobel Prize in Physiology or Medicine was awarded to Tauku Honjo and James Allison for their findings in cancer immunology based on the immune checkpoint proteins – cytotoxic T-lymphocyte associated protein (CTLA-4) and programmed cell death protein 1 (PD-1).[3] Since their discovery, the focus around these proteins has drastically increased and their importance within immunotherapy has become evident.

The protein-protein interaction (PPI) between programmed cell death 1 (PD-1) and its ligand programmed cell death ligand 1 (PD-L1) is now a well-established target for immunotherapy.[4] Under normal physiological conditions, PD-L1 binds to PD-1 on activated T-cells to negatively regulate the immune response preventing autoimmune disease.[5] However, PD-L1 is often expressed on various tumours, handicapping the immune system and preventing the production of T-cells.[6] This triggers the sequential release of cytokines and leads to cell exhaustion and apoptosis of tumour specific T-cells.[7] This mechanism is one of the ways cancer cells evade the immune response. To reverse these immunosuppressive conditions, monoclonal antibodies (mAbs) have shown success at blocking the interaction between PD-1 and PD-L1 (**Figure 1-1**).[8] Following the first clinical trial in 2010, the FDA has approved seven mAbs that target PD-1 (nivolumab, pembrolizumab, cemiplimab, and dostarlimab) and PD-L1 (atezolizumab, durvalumab and avelumab) for a variety of cancers including melanoma and non-small cell lung cancers.[9,10]

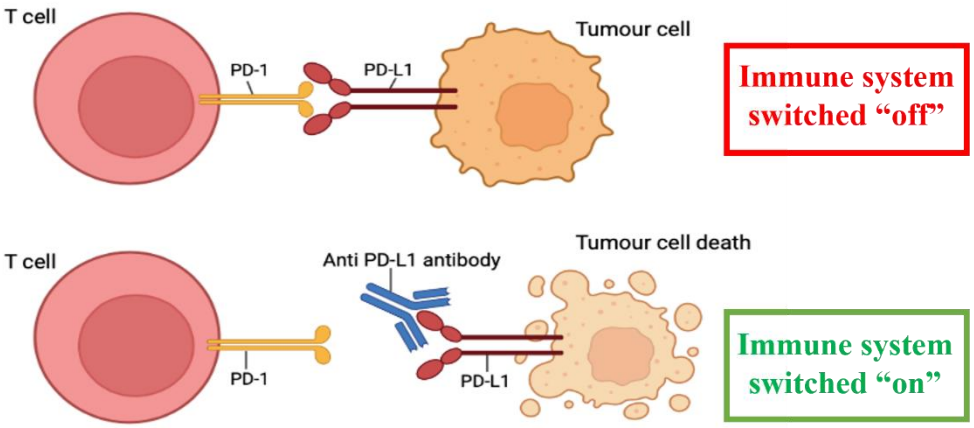


Figure 1-1 *Schematic drawing of the PD-1/PD-L1 interaction being inhibited leading to tumour cell death.*

1.1.1 Drawbacks of antibody treatment

Despite the longevity of the response to anti-PD-1/PD-L1 therapy, the response rate is only 20-30% in patients.[11] This sub optimal response could be due to the size of the antibodies (ca. 150 kDa).[12] PD-1 expressing T-cells are often found within solid tissue of PD-L1 expressing tumours, and due to the size of antibodies deep tissue penetration could be problematic.[12] Currently the mAbs available have half-lives of 2-3 weeks.[13] This prolonged activity has the potential to result in off-target T-cell activation resulting in autoimmunity.[14] In addition, clinical data suggests that long term immune checkpoint inhibition is the main contributor to immune related adverse events.[15] Lastly, mAbs lack oral bioavailability and are a costly treatment with anti-PD-1 treatment costing around £84,000 per patient on the NHS.[16,17] To bridge this gap, small molecules and peptides open an avenue that retains the benefits of mAbs while overcoming these short falls. A small molecule or peptide inhibitor could be more cost effective, have less off target effects, and have possible enhanced tumour penetration. However, as discussed in chapter 3 section 3.1.2, there are fewer small molecules that are currently in clinical trial, and none yet that have been clinically approved.[18–22] Due to the side effects of these small molecules stunting their progression to market, an alternative inhibitor that could present less adverse immune related events is crucial.

1.1.2 PD-1/PD-L1 structure

1.1.2.1 PD-1 and its ligand PD-L1

PD-1 is a type 1 transmembrane glycoprotein with two immunoreceptor-based tyrosine motifs.[23] These are specific amino acid sequences that are involved in regulating immune cell activation and signalling. The membrane proximal sequence is an immunoreceptor tyrosine-based inhibitory motif (ITIM) while the immunoreceptor tyrosine-based switch motif (ITSM) is found in the C-terminus and is likely responsible for PD-1 signalling.[24] PD-1 consists of two β-sheets that adopt a β-sandwich fold stabilized by the conical IgV disulfide bond .[25,26] PD-1 has two ligands, PD-L1 and PD-L2. PD-L2 also plays a role in regulating the immune response.[25] Unlike PD-L1 that is found expressed on a variety of tissues, PD-L2 is restricted to expression on immune cells at comparatively low levels.[27] While there is ongoing research into PD-L2 inhibitors and their potential as a cancer treatment, PD-L1 has taken the forefront in initial research leading to clinical trials and approved FDA treatments. PD-L1 is also a type 1 transmembrane glycoprotein.[25] PD-L1 is not anticipated to function as a signalling protein as it lacks the signalling motif.[23] Recent findings shows that PD-L1 contains conserved motifs in the cytolytic region that serves as protection against the immune system, aiding in immune evasion.[28] The PD-1/PD-L1 pathway has been talked about in length alongside many reviews of extensive research into the inner workings within cancer.[29–31]

1.1.2.2 Binding interface of PD-1/PD-L1

The crystal structures of PD-1 and PD-L1 show that the binding interface is defined by several β-strand and β-turn motifs (**Figure 1-2B**).[25] PD-1 interacts with PD-L1 with 1:1 stoichiometry through polar interactions and the hydrophobic effect *via* its CC'FG β-sheet.[25] The interface is mostly flat and makes up a surface area of 1970 $Å^2$.[32] The amino acids on PD-1 that are essential for binding PD-L1 are hydrophobic residues V64, I126, L128, A132, and I134, these are surrounded by a polar network.[25] Upon binding to PD-L1, PD-1 under goes a conformational change as the CC' loop transitions from an open conformation seen in **Figure 1-2A** to a closed one in the C β-strand seen in **Figure 1-2B**.[25] This change causes four additional hydrogen bonds between $_{PD\text{-}1}$Gln75 to $_{PD\text{-}L1}$D26 and $_{PD\text{-}1}$T76 to $_{PD\text{-}L1}$Y123 (**Figure 1-2B**).[33] A

further conformational change is found at E136 and Y68 of PD-1, this results in the formation of a pocket in the middle of the PD-1 interaction (**Figure 1-2C**).[25]

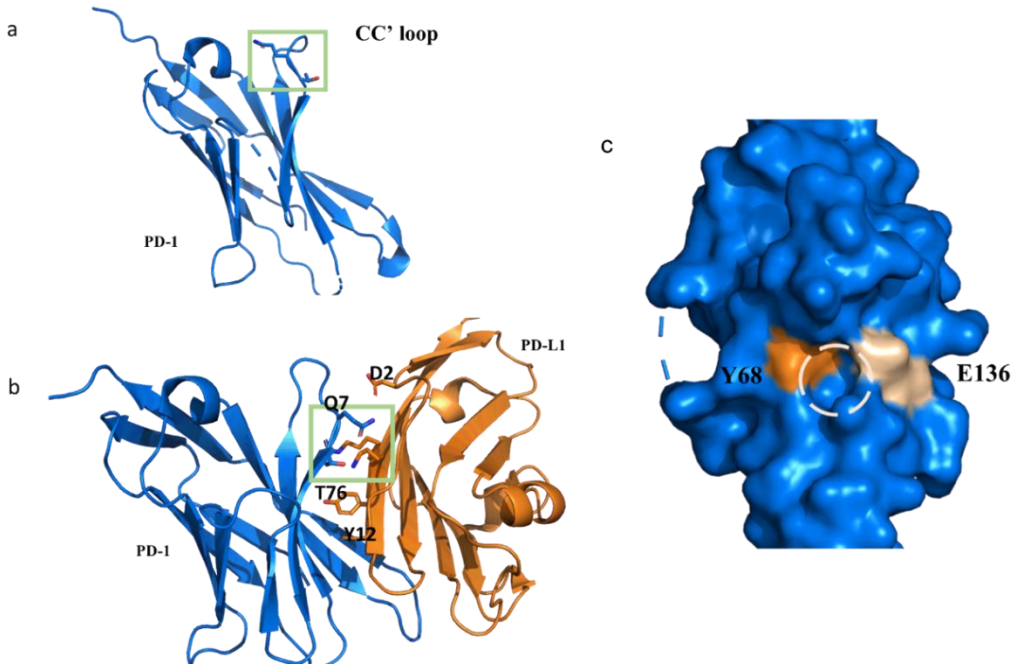


Figure 1-2 *a) PD-1 (blue) without PDL-1 in an open conformation b) PD-1 (blue) binding to PD-L1 (orange) showing the conformational change upon binding to closed (PDB: 3RRQ) c) PD-1 (blue) with a binding pocket (circled) formed by residues Y68 (orange) and E136 (cream) (PBD: 5C3T).*

Three binding hotspots have been identified on PD-L1 as seen in **Figure 1-3**.[25] The deepest hotspot is formed by Y56, E58, R113, Y123 and M115, binding $_{PD\text{-}1}$I134 (cyan).[25] The second is formed by M115, A121 and Y123, binding $_{PD\text{-}1}$I126.[25] Finally, the third hotspot comprises D122-R125 and D26, binding $_{PD\text{-}1}$Y68, T76, and Q75.[25] As Y123 is contained within two of these hot spots it is often considered to be the main residue for targeting when considering small molecule inhibitors for the PD-1/PD-L1 interaction.[25]

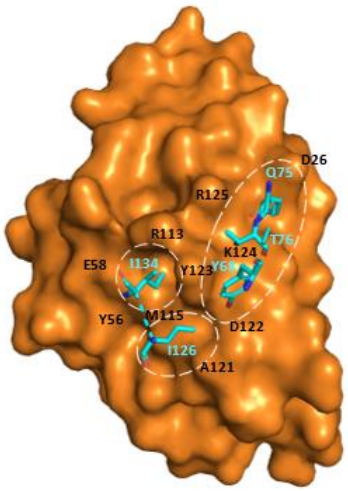


Figure 1-3 *Three hotspots identified on PD-L1 (orange) shown with the residues from PD-1 (cyan) that bind within those hotspots (PBD: 4ZQK).*

When choosing which protein to target there has been some research to suggest targeting PD-L1 over PD-1 would be more effective.[13] Antibodies that target PD-1 can potentially inhibit the interaction between PD-L1 and PD-L2 that possibly could lead to autoimmunity.[13] Clinical trial data highlights that targeting PD-1 in comparison to PD-L1 showed a higher case of immune-related adverse events reinforcing PD-L1 as the preferential target.[34]

Although there are approved, effective antibodies available that inhibit PD-1/PD-L1, the negative drawbacks that face these treatments leaves an avenue open for improvement. Due to the large, flat nature of the PPI interaction, targeting this area with a small molecule is challenging. With their larger more variable structure, peptides offer a foundation in the design of small molecules. Furthermore, due to the β-strands and β-sheets of PD-1 and PD-L1 studies have highlighted that designing a peptide with a turn structure is important for binding, covering a large percentage of the interaction surface area.[35] Binding peptides allow us to determine important characteristics that are necessary for inhibition, that can then be applied to small molecules, creating a novel small molecule inhibitor.

1.2 Using cyclic peptides to target PPIs

Proteins are the elementary unit to life with nearly all cellular functions being controlled *via* PPIs.[36] The release of human genome sequences catapulted PPI targeting to the forefront of chemical biology by providing a comprehensive map of our genes, and subsequently protein interactions suitable for drug development.[37]

The genome sequencing provided information on the amino acid sequences found in proteins involved in PPIs. These specific binding sites found in the interaction site were highlighted as the starting point to develop PPI inhibitors.[37] Although plentiful in interactions, PPIs were largely deemed "undruggable" owing to the difficulty to control large interfaces that are flat, hydrophobic, and absent of binding pockets.[38]

Peptide-based therapeutics combat these challenges and target PPIs with remarkable potency, selectivity, and low toxicity.[39] Peptides are larger than conventional small molecule binders and more structurally flexible, so cover a larger surface area of the PPI interface. The area of the protein that is involved in the interaction is often localised to small, preorganized, structurally defined regions recognized by a binding partner. Their structurally diverse peptide chain with various amino acids also encourages extensive hydrogen bonding and electrostatic interactions, contributing to the stability of the peptide-protein complex.

Linear peptides however, commonly demonstrate low oral bioavailability, poor metabolic stability, and short circulation times.[40] Cyclic peptides, due to their more rigid conformation can overcome these limitations. The ring structure of the cyclic peptide allows for preorganization and the restricted conformation lowers the entropic cost upon binding, resulting in increased binding affinity and specificity (**Figure 1-4**).[41]

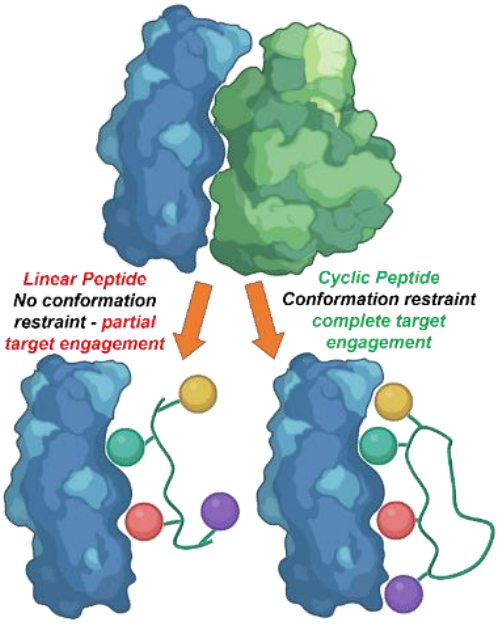


Figure 1-4 *The rigid conformation of cyclic peptides increases peptide-protein interaction in comparison to linear peptides.*

Cyclic peptides often lack amino and carboxyl termini, resulting in increased resistance to proteolysis. These features may also increase the ability to cross the cell membrane due to intramolecular hydrogen bonding within the ring.[42] Cyclic peptides have the potential to mimic biologically relevant secondary structures of protein interactions (β-turns, α-helices etc.) functioning as an inhibitor by mimicking and displaying these motifs.[41] Pre-organization of these secondary structures can result in increased binding affinity.[43]

Despite no peptides that target PPI's being FDA approved there are many in clinical trials such BBT-401 that is an orally available Pellino-1 PPI inhibitor to treat ulcerative colitis.[44] BNZ132-1-40 is another peptide found in clinical trials that belongs to the anticytokine peptide family. This peptide is found active selectively on IL-15, IL-2 and IL-9, these are found to drive T-cell mediated diseases.[45]

1.2.1.1 Cyclisation methods

Cyclisation of peptides is categorized into four classes: side chain to side chain, head to tail, head to side chain, and side chain to tail (**Figure 1-5A**).[46] Head to tail cyclisation only allows for one variant and forms an amide bond between the amino and carboxyl termini. Several cyclic peptides found in nature that are biologically active are cyclised this way such as gramicidin S and tyrocidines.[47] Other methods allow for bi- and tricyclic peptides through chemically stable bonds such as oximes, thioether and disulfides (**Figure 1-5B**).[48–51]

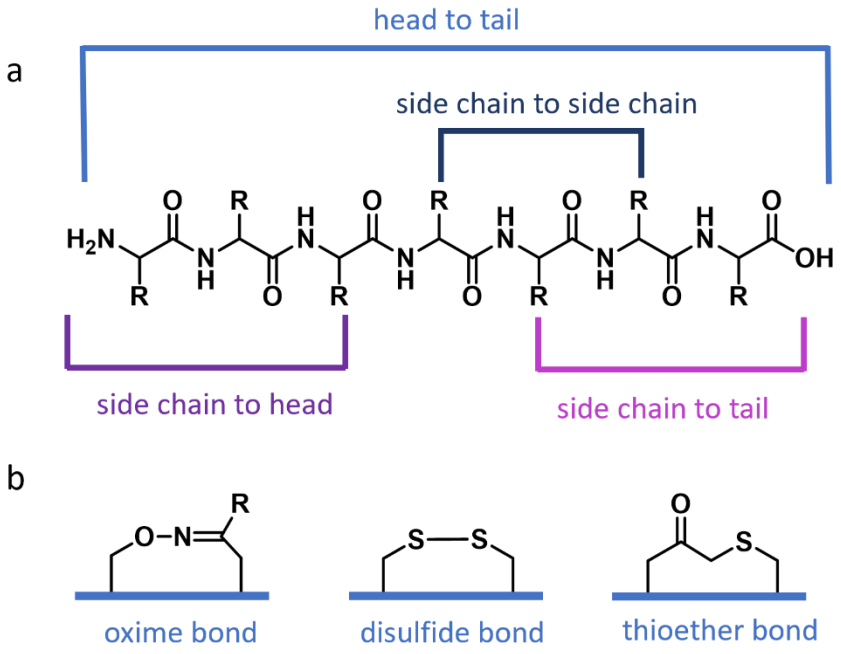


Figure 1-5 *a) cyclisation strategies showing head to tail, side chain to head, and side chain to tail b) bonds featured in cyclic peptides.*

The point of cyclisation relates directly to the conformational constraint, influencing flexibility, secondary structure display and binding.[52–54] Bicyclic peptides have shown improved cell membrane penetration compared to linear or monocyclic counterparts, while for some proteins higher-order structures such as tricyclic peptides demonstrate enhanced activity levels.[55–57]

Over the past two decades, 18 cyclic peptides have been successfully approved for clinical use cementing their importance within the pharmaceutical sector.[58] Common approaches to identify cyclic peptides include natural product elucidation, protein sequence-based drug design, and display technologies. Isolating natural cyclic peptides as scaffolds for affinity development is promising due to their likelihood for biological activity. Difficulties in purification are common with natural isolation, often leading to analogues being optimised and prepared using solid phase peptide synthesis (SPPS).[59] Peptides designed from amino acid sequences extracted from the interface of protein partners highlights “hotspot” sequences that often occur in the same secondary structure. To optimize potency and selectivity cyclisation techniques are utilized on these linear peptides.[60]

1.2.2 Methods for discovering novel cyclic peptides

Several display techniques have been developed to discover cyclic peptides including phage display, split-intein circuit ligation of peptides and proteins (SICLOPPS), and random nonstandard peptides integrated discovery (RaPiD) system.[61–63] Phage display is one of the most effective technologies to generate large libraries of peptides, proteins and antibodies based on the phage phenotype and genotype being physically connected. The cyclic peptide sequence is displayed on the phage coat protein and screened against target proteins to detect interactions. Recent developments have reported bicyclic peptides prepared by phage display.[64] SICLOPPS utilizes ribosomal protein synthesis and separates the C-terminal intein domain from the N-terminal intein domain with cyclic peptide sequences. The first amino acid is required to be a nucleophilic cysteine or serine, while there is no limit on the number of amino acids in the target peptide. The intein domains come together, resulting in splicing of the cyclic peptide.[65] Similarly to phage display in the genotype-phenotype linkage, the RaPiD system uses mRNA encoded libraries of peptides, with an additional custom-reconstituted translation system known as flexible *in vitro* translation (FIT) system enabling reprogramming of the genetic code with unnatural amino acids.[63,66]

Although peptides have opened an avenue into targeting and inhibiting PPI's, small molecules are still the leading compounds found on the drug market.[67] The development of small molecules to target PPIs remains a critical task. Commonly, small molecule design approaches tend to focus on structure activity relationships (SAR) of large libraries of compounds based on computational modelling and refining the structures until optimum affinity is achieved. The functionality of using peptides as valuable starting points for drug development could make this process more efficient due to their modular structure, variable functional groups and ease of preparation.[68]

Despite the rapid rise in effective cyclic peptide identification techniques for controlling PPIs, methods to transfer these characteristics to small molecules are limited. There are few studies that have optimised the structural data found about the superior binding of cyclic peptides (or turn motifs) to PPIs, analysed the essential amino acid side chain properties that create binding, and applied that knowledge to a

small molecule structure, avoiding the laborious journey of SAR or expense and time of testing large libraries. However, when applied there have been several successful technologies capable of transferring the characteristics of peptide binders to non-peptidic small molecules.[67,69–71]

When developing a peptidic inhibitor for a PPI, structural biology is pivotal. Commonly, these projects are supported by X-ray crystallography, protein-based nuclear magnetic resonance (NMR) spectroscopy and cryogenic electron microscopy.[72] Further information can be obtained through ongoing monitoring with lead compounds revealing any conformational changes that may occur upon binding. It is important to note that not all interactions drive the affinity of the PPI, and determining which interactions are essential for binding or inhibition is invaluable information.

When structural information is absent interactions can be investigated experimentally using an alanine scan, a process which takes a peptide sequence of interest and sequentially mutates each amino acid residue with alanine.[73] Alanine is chosen due to its small, non-reactive state minimizing the chance of the overall structure of the peptide being altered, isolating the effects of the singular residue.[74] Depending on whether inhibition is lost or remains, determines which amino acid residue or residues are key for this interaction to take place, leading to the identification of targetable "hotspots". Once key fragments for binding are identified, the conformation of the peptide can be investigated by introducing constraints at various positions to decrease conformational flexibility.

In this chapter, small molecules that have been designed and modified using structure activity relationship information from cyclic or turn based peptides will be discussed. Three strategies have emerged for the transfer of binding interactions of peptides to small molecules. 1) The decoration of small molecule scaffolds with amino acid side chain functionality. This method sees the direct addition of amino acid side chains to non-peptidic skeletons, and subsequent refinement for ideal functional group placement. 2) The enhancement of current small molecule protein binders using structure activity relationship information from peptide binders. This approach modifies known small molecule binders with the amino acid side chain functionality. 3) The mimicking of peptide side chain interactions with similar functionality. This

method applies the addition of functional groups which can emulate amino acid side chain interactions to more synthetically accessible small molecules.

1.2.3 Transferring peptide side chain functionality to small molecule scaffolds

Following the identification of peptide sequences capable of controlling the targeted interaction, the essential amino acid side chains can be extracted. These side chain functionalities can form part of very short peptides or can be placed on non-peptide skeletons (Figure 1-6). Small molecule scaffolds should be small and rigid, aiding in preorganization of side chains that are important for activity.

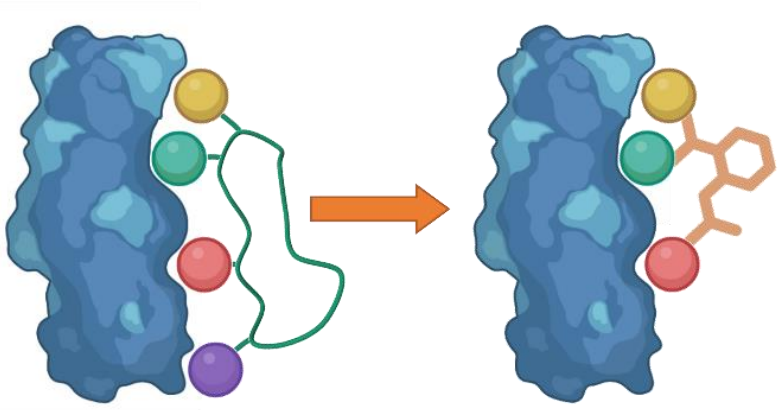


Figure 1-6 *A schematic diagram of taking the side chain functionalities of the peptide and applying them to design small molecule skeletons.*

Perhaps conceptually the simplest method for mimicking cyclic peptide residues for binding is to create di- or tri-peptides of the key amino acids identified. From here, further SAR may be applied, modifying the side chains of the amino acids to enhance binding affinity. The Tavassoli group demonstrated this approach using a cyclic peptide (CRYFNV, **1**, **Figure 1-7**) inhibitor of ATIC (Aminoimidazole carboxamide ribonucleotide transformylase/inosine monophosphate cyclohydrolase) homodimerization, a key interaction in *de novo* purine biosynthesis. This cyclic peptide, identified using a combination of SICLOPPS technology with bacterial reverse two-hybrid system (RTHS), was found to be a potent inhibitor (K_i = 17±4 μM) of homodimerization.[75,76] An alanine scan of the cyclic peptide identified the arginine and tyrosine residues as significant for inhibition. This resulted in dipeptide **2** (K_i = 84±7 μM), which mimics the active RY motif of the cyclo-CRYFNV. Further structural modifications culminated in the addition of the electron withdrawing nitro group, resulting in a 120-fold improvement in activity with a K_i value of 685±35 nM (**Figure 1-7**). **3** maintained inhibition of ATIC

homodimerization in the presence of bovine serum albumin (BSA), suggesting specificity as a cyclic peptide mimic.[70] Despite the risks of the nitro group being highly susceptible to metabolism, compound **3** shows potential as a lead compound with the nitro group acting as a potential improved hydrogen acceptor in comparison to **2**. However, without structural data identifying the binding sites of these compounds the reasons for the difference in activity is uncertain.

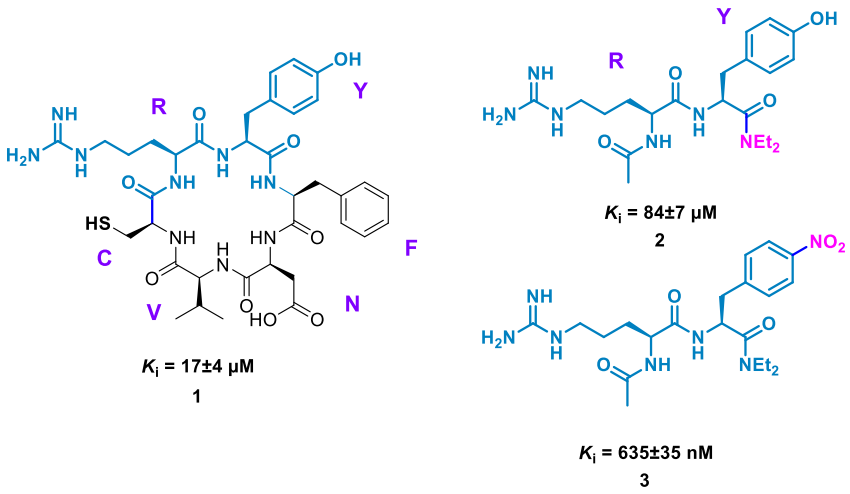


Figure 1-7 *Structures of cyclic peptide **1**, di-peptide **2** and small molecule **3**.*

The cyclic peptide C4m-3127 H10V (MHPFLPIVSVHF) **4** (**Figure 1-8**) inhibits the interaction between Cytotoxic T-lymphocyte-associated protein 4 (CTLA-4) and B7-1 (IC_{50} = 11.5 µM) and was identified using protein synthesis using recombinant elements (PURE).[77] CTLA-4 is expressed on the surface of activated T-cells and binds with ligands B7-1 and B7-2, suppressing T-cell activation.[77] Alanine scan mutagenesis highlighted eight mutants (H2, P3, L5, P6, I7, S9, H11, and F12) that led to a decrease in binding with CTLA-4. In the absence of structural data, the team computationally modelled consecutive trimers of amino acid side chains onto 40 virtual scaffolds and performed molecular docking of these compounds to CTLA-4. Several compounds were highlighted for synthesis, leading to compound PGF00432 **5** (IC_{50} of 294 µM) which mimicked residues V10, H11 and F12 (**Figure 1-8**, blue). Structure based drug design, complemented by the docking pose of **5** suggested the replacement of histidine with arginine, the replacement of valine with a cyclohexylmethyl group, and the replacement of phenylalanine by 3,3-diphenylpropyl, resulting in compound PGF00506 **6** with an IC_{50} of 6.8 µM (**Figure 1-8**).[67] Competitive ELISA was performed on **6** and peptide **4** to confirm **6** binds to

CTLA-4 on the same binding surface as **4**. **6** is a successful small molecule that is a direct mimic of cyclic peptide **4** with an increased inhibitory activity.

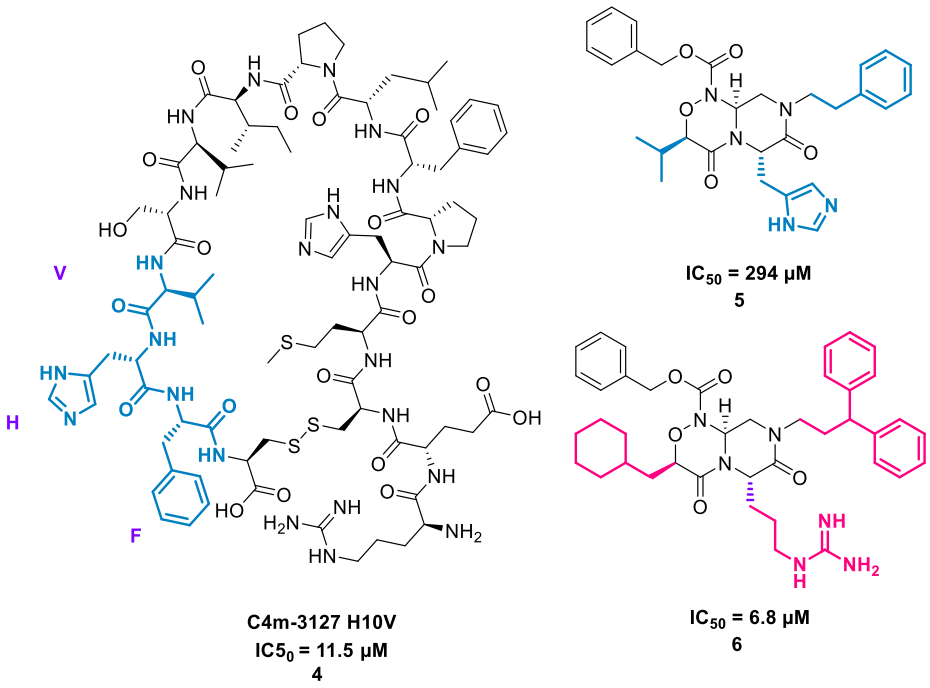


Figure 1-8 *Structures of cyclic peptide **4** and small molecules **5** and **6**.*

The turn-motif peptide PVKRRLFG **7** (**Figure 1-9**) is a Cyclin A binder that was derived from the crystal structures of the protein-protein interactions of Cyclin A and a variety of protein partners, including E2F1, p27, p53, and p101.[78,79] An alanine scan highlighted the essential residues, R4, L6 and F7 which informed truncated peptide design. Investigation of the crystal structure of a related peptide (KPSAC**R**N**LF**GP) highlighted structural modifications for further investigation.[80] To mimic the preorganization of peptide **7**, modifications began by focusing on the turn conformation of the RNLF motif upon binding, leading to **8** as a starting tetra-peptide (**Figure 1-9**). Structure activity relationship (SAR) studies highlighted **9** which was 500-fold more potent, contains fewer rotational bonds and is neutral at physiological pH. However, the peptidic nature of **9** was susceptible to metabolism and offered poor oral absorption. Therefore, the N-terminal amide (**Figure 1-9**, purple) was replaced by a ketone to exploit a key H-bond with the protein, resulting in **10** with an IC_{50} of 40 nM.[81] **10** showed moderate inhibition of cyclin A and when modelled onto a crystal structure of the peptide fragment RNFL showed the ketone to accept the hydrogen bond similarly to the N-terminal amide carbonyl.

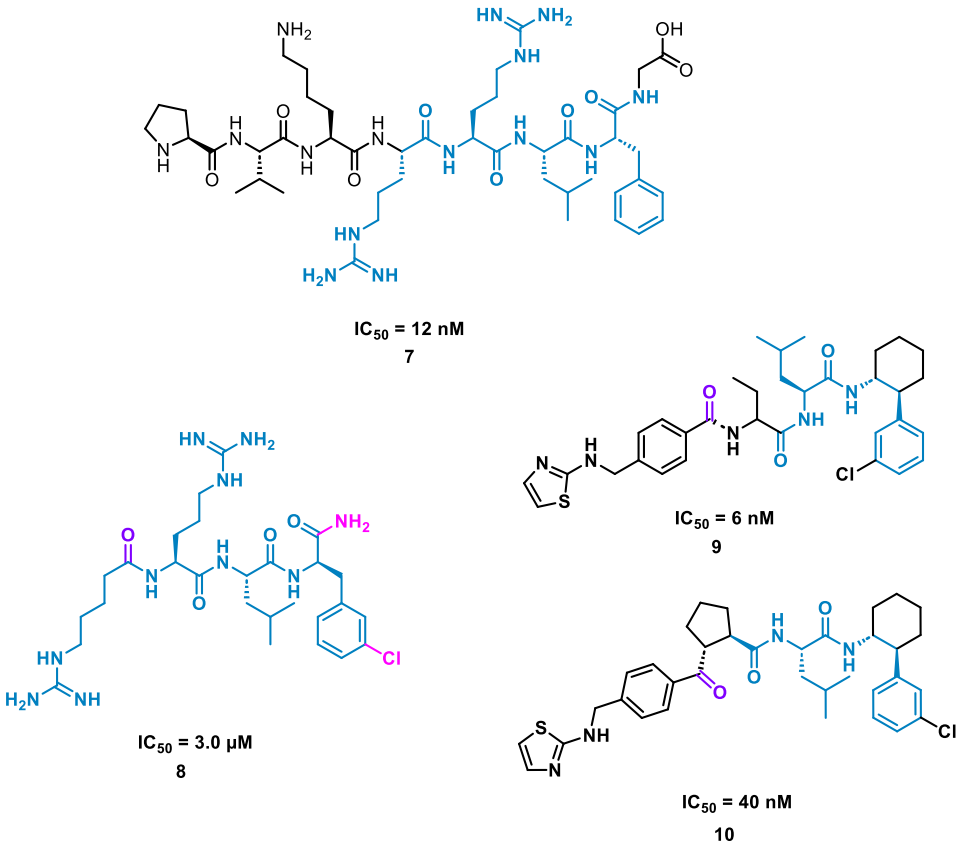


Figure 1-9 *Structures of turn-motif peptides* ***7*** *and* ***8****, and small molecules* ***9*** *and* ***10.***

A high-profile example of this method is the development of CA-170, derived from peptide AUNP-12 (H-SNTSESFK(SNTSESF)FRVTQLAPKAQIKE-NH_2).[82] AUNP-12 was identified as a PD-1/PD-L1 inhibitor through the synthesis of a series of loops and strands from PD-1 at the PD-L1 interface. AUNP-12 was found to rescue T-cells from inhibitory activity of PD-L1 in a mouse splenocyte assay to 100% at 100 nM. Truncation experiments highlighted the SNTSESF sequence as the source of activity (EC_{50} = 81 nM), despite not being present at the PD-L1 interface (**Figure 1-10**, purple). This peptide demonstrated poor stability in plasma, but head-to-tail cyclisation resulted in **11** (**Figure 1-11**), demonstrating similar activity (EC_{50} = 55 nM) and stability in mouse, rat, and human plasma.

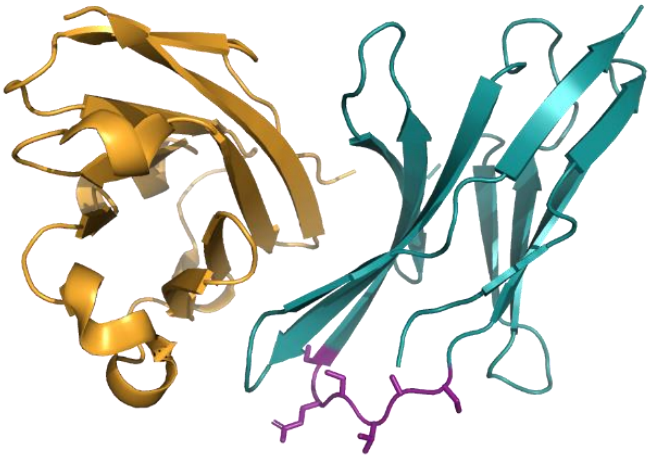


Figure 1-10 *The PD-1/PD-L1 interaction highlighting the SNTSESF sequence in purple.*

The tri-peptide **12** SNT retained activity (EC50 = 6 nM), but again was highly unstable in plasma. CA-170, **13**, was the culmination of several strategies to stabilise the peptidic backbone, incorporating a urea moiety, and a fused 1,2,4-oxadiazole heterocyclic backbone. **13** maintained activity (EC50 = 15.4 ± 1.3 nM) while restoring stability in plasma, and went on to face clinical trials as an inhibitor of the immune checkpoint proteins PD-1/PD-L1.[71]

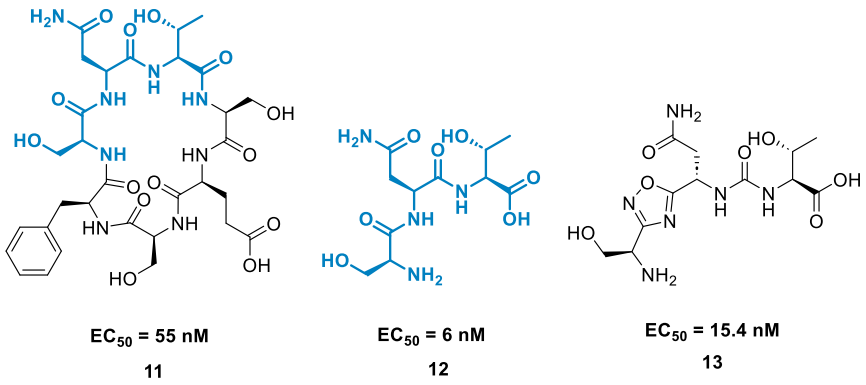


Figure 1-11 *Structures of cyclic peptide **11**, tri-peptide **12**, and small molecule **13**.*

Extensive research has taken place on peptides that modulate human melanocortin receptors (hMCRs) for various potential therapeutic values. Peptidic agonists of hMCRs all possess the sequence HFRW.[83,84] Hruby *et al.* virtually screened a library of bespoke pyrrolopiperazines, decorated with functionality based on known peptide and small molecule ligands. Comparable to the HFRW sequence, previous small molecules required two hydrophobic aromatic groups and a basic nitrogen for activity. By overlapping the proposed compounds and MT-II, **14** (**Figure 1-12**) the structures that best aligned with **14** were selected for synthesis and biological evaluation.[85] Biological competition assays using hMCRs expressed in cells

confirmed displacement comparable to **14** treatment. Each small molecule showed binding to one or more of the receptors (MC1-MC5) with most having high selectivity. Notably, five new antagonists with sub-molar IC_{50} values were identified for the relatively unexplored MC-5 receptor, including **15** and **16** (**Figure 1-12**).[86]

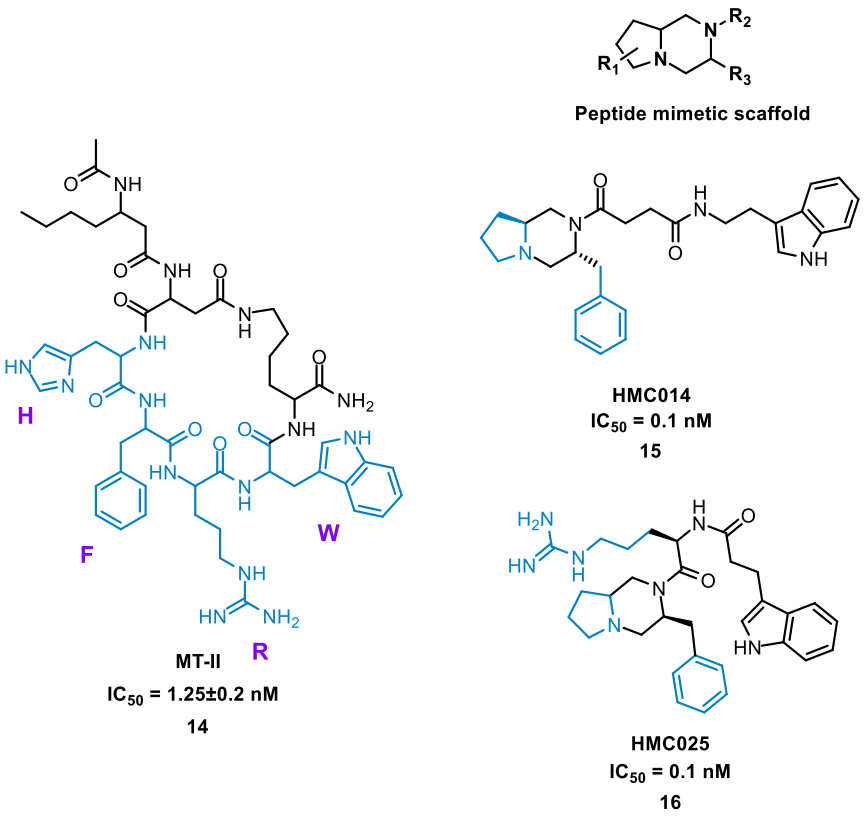


Figure 1-12 *Structure of cyclic peptide* ***14****, and small molecules* ***15*** *and* ***16.***

Inhibition of the interaction between receptor neuropilin (NRP1) and vascular endothelial growth factor (VEGF-A) impacts tumour growth, and has been shown to synergistically enhance VEGF-A inhibitors.[87] Using the crystal structures of NRP1/VEGF-A and an alanine scan of the identified binding site, the VEGF-A amino acids Tyr297, Trp301, Thr316, D320, S346, T349, Y353, K351 and Trp411 were highlighted as essential for binding. The turn motif peptide KPAR **17** (**Figure 1-13**) was shown to bind VEGF-A and inhibit NRP1 interaction, with Arg and Lys essential for activity.[88,89] Using modelling, a series of scaffolds to connect the terminal arginine to the lysine were screened (**18**). The best scaffold identified was thiophene-based, exemplified by **19** with an IC_{50} of 13 μM, culminating in a benzothiadiazole heteroaryl improved **20** (IC_{50} = 8 ± 0.02 μM) (**Figure 1-13**). X-ray crystallography showed, importantly, the arginine residue fits almost perfectly into

the binding pocket, and a critical intramolecular bond between the carbonyl amide NH and the sulfonamide nitrogen aided in compound stability. **20** showed inhibition of VEGF-A/NRP1 but not to VEGFR2 expressing cells, and also showed inhibition of VEGF-A binding to lung carcinoma and prostate carcinoma cells both which express NRP1. **20** is a successful mimicked structure of a turn motif peptide **17**, with the ability to inhibit VEGF-A binding in carcinoma cells, providing a small molecule for potential anti-NRP1 drug.[90]

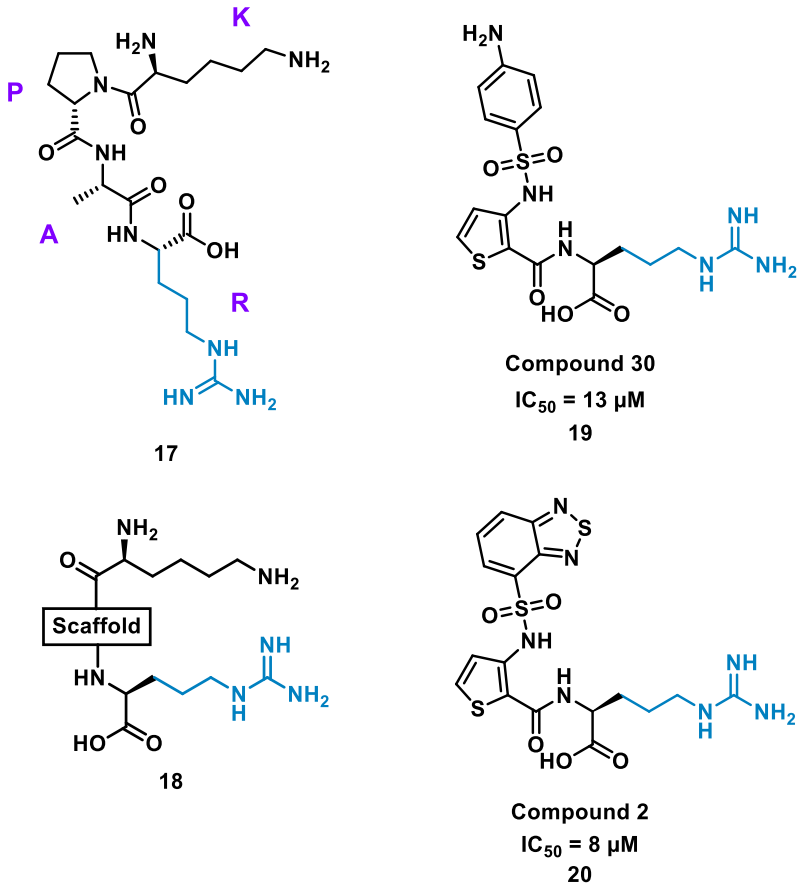
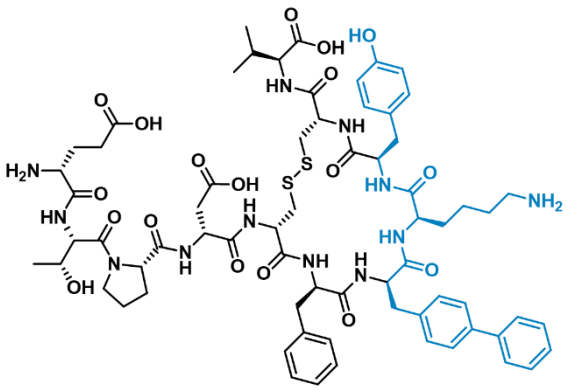


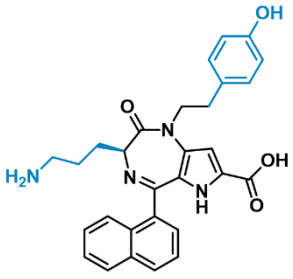
Figure 1-13 *Structure of turn-motif peptide* ***17****, and small molecules* ***18****,* ***19****, and* ***20.***

The urotensin II receptor (UT) binds two endogenous cyclic peptide ligands, urotensin II (UII, ETPD-*c*[CFWKYC]-V) and urotensin II-related peptide (URP, A-*c*[CFWKYC]-V). The urotensinergic system regulates various organs and tissue and has shown to be a promising target for cardiovascular diseases. The WKY residues are important for binding in both UII and URP, but URP lacks the N-terminal and therefore likely binds differently.[91–93] Currently the market lacks any agonist or antagonist for this interaction with the ability to discriminate between UII or URP activity. Previous SAR modelling suggested that Trp interacts with the UT receptor

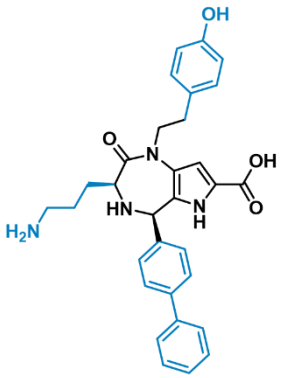
via polar interactions rather than hydrophobic interaction. Most recently, the inversion of the Trp configuration resulted in a partial agonist capable of inhibiting UII associated aortic ring contraction.[92] By replacing Trp for a biphenylalanine, resulting in urocontrin, **21** (**Figure 1-14**), the peptide is more potent and selective to inhibit the response of UII with no effect on URP induced vasoconstriction.[93] Dufour-Gallant and co-workers sought to combine this selective cyclic peptide characteristics onto a small molecule scaffold, pyrrolodiazepinones.[94,95] X-ray crystallography confirmed pyrrolodiazepinones have the ability to adopt the inverse γ-turn found in the binding motif of **21**.[96] A library of small molecule UT ligands were designed based of this concept and tested *in vitro* using a competitive binding assay, resulting in **21** and **22**. **21** can selectively inhibit the vasoconstrictive effects of UII, while having little effect on URP-induced vasoconstriction. **22** shows the opposite effect, selectively inhibiting vasoconstrictive effects of URP, while having little effect on UII induced vasoconstriction. Despite the low potency, the development of these non-peptide inhibitors mimicked from the original cyclic peptide have shown that **21** and **22** have different mechanisms of action with specific targeting to either UII or URP.[97]



Urocontrin
21



1b
22



***R*-4a**
23

Figure 1-14 *Structures of cyclic peptide* ***21****, and small molecules* ***22*** *and* ***23.***

1.2.4 Mimicking peptide side chain interactions to enhance small molecule binders

One of the main challenges faced by small molecules in targeting a PPI is controlling the large interface. Often interfaces have "hotspots" which can be identified when analysing how a peptide binds to the protein via crystal structures or modelling. The peptide SAR offers valuable information about what interactions can be modified and then applied directly to a small molecule inhibitor design (**Figure 1-15**).

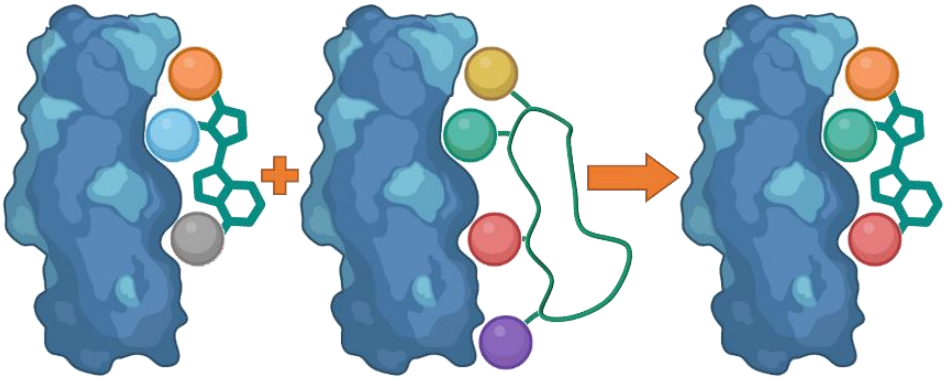


Figure 1-15 *Using peptide side-chain interactions to improve affinity of known small molecule binders.*

This can inform new compound design or allow for improvements on known binders. This allows for SAR studies to be performed on the synthetically accessible peptides, and then applied to the synthetically challenging small molecules.

Harper *et al.* demonstrated this approach when altering known small molecule inhibitor of the Nrf2/KEAP1 interaction, tetrahydroisoquinoline **25** (IC_{50} = 2.3 μM) into a non-acidic entity.[98] Acid containing compounds have poor blood – brain barrier (BBB) penetration, undesirable for reaching the central nervous system. Recent developments have shown replacing the acidic groups with primary amides can form a non-acid inhibitor of Nrf2/KEAP1.[99,100]

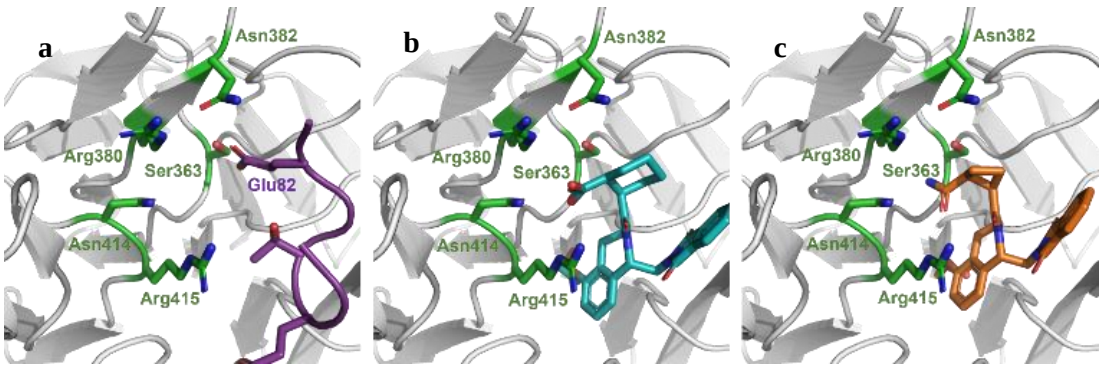


Figure 1-16 *Structure of a)* ***24*** *(purple) b)* ***25*** *(cyan), and c)* ***26*** *(orange) interacting with KEAP1.*

The 9mer peptide LDEETGEFL (**Figure 1-17**, **24)** is a high affinity KEAP1 binder, derived from the NRF2 binding interface. The turn sequence $_{79}$ETGE$_{82}$ is key for binding, and Glu82 make key interactions into the P2 pocket of KEAP1 (**Figure 1-16A**).[101] This pocket is defined by the residues Ser363, Asn382, Arg380, Asn414, and Arg415. This site is also where the carboxylic acid of **25** is known to bind, interacting with Arg415 (**Figure 1-16B**).[98] To explore the necessity for an acidic functional group in this pocket, peptide analogues were tested with Glu82 replaced with alkyl, aromatic and amide side chains. The SAR discovered that substitution with cyclobutylalanine produced an active peptide only 10-fold weaker than the original peptide despite lacking the acidic side chain functionality. When docking these peptides, superimposed images with **25** showed the cyclobutyl group of the peptide occupied the same region as the cyclohexyl region of the **25**. Based on these observations, a series of 5-substituted tetrahydroisoquinolines containing carboxamide substituted cyclobutylamides resulted in **26** showing IC_{50} of 2.5 µM, proving an alternative binding mode at the P2 pocket (**Figure 1-16C**), engaging Asn414 and Ser36. This non-acidic analogue **26** can inhibit the PPI between Nrf2 and KEAP1 in the low micromolar range.

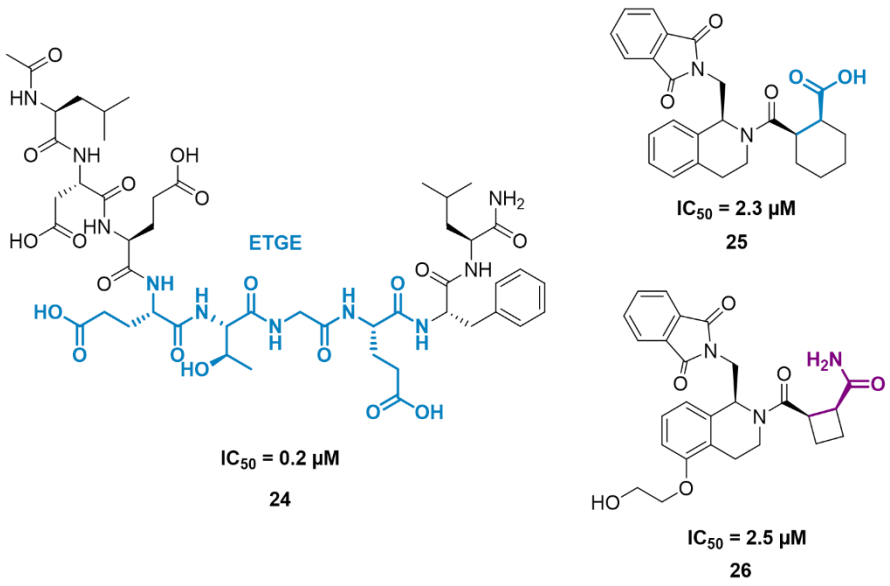


Figure 1-17 *Structures of turn-motif peptide* ***24***, ***25***, *and* ***26.***

Takahashi *et al.* described a method of applying overlapping and non-overlapping sections of peptide and small molecule binders to improve small molecules, demonstrated with the platelet receptor glycoprotein VI (GPVI) and collagen.[102] Using an NMR technique termed INPHARMA (Protein-Mediated Interligand NOEs

for Pharmacophore Mapping)[103], they identified the common pharmacophore of a peptide and small molecule that compete for the same binding site.[103–105] Peptide pep10L **27** (**Figure 1-18**) was identified through phage display to inhibit the GPVI-collagen interaction (K_D = 57 µM), binding to GPVI with a turn motif.[106] The side chains of Trp6, Leu7, and Phe9 formed a hydrophobic cluster and are key to GPVI binding.[106] The binding site of peptide **27** overlaps with the binding site of losartan, a small molecule inhibitor of aggregation of platelets, which relies on the phenyltetrazole for binding.[107] Using the INPHARMA method the overlapping sections of peptide **27** and losartan **28** were identified, showing the phenyl group in losartan corresponded to the centre of the hydrophobic cluster in **27**. The hydrogen atoms on the phenyltetrazole moiety occupied the same site as the hydrogen atoms on Trp6 and Leu7 (**Figure 1-18**, blue). The hydrogen atoms on the central phenyl ring overlapped with hydrogen atoms on Trp6, Leu7, Tyr8, Phe9 and Ser10 (**Figure 1-18**, pink).[103] Notably, there were no INPHARMA peaks for the aromatic ring of Phe9 of **27** and **28**. Addition of a phenyl ring to **28** to mimic Phe9 (**Figure 1-18**, green) resulted in **29** (K_D = 52 ± 4 µM).[106] The INPHARMA experiments confirmed that the new phenyl ring of **29** mimics Phe9 while retaining previous overlapping of the phenyltetrazole moiety and Trp6 and Leu7. This novel ligand based strategy has proven a successful way to modify pharmacophores using peptide structural binding information.[108]

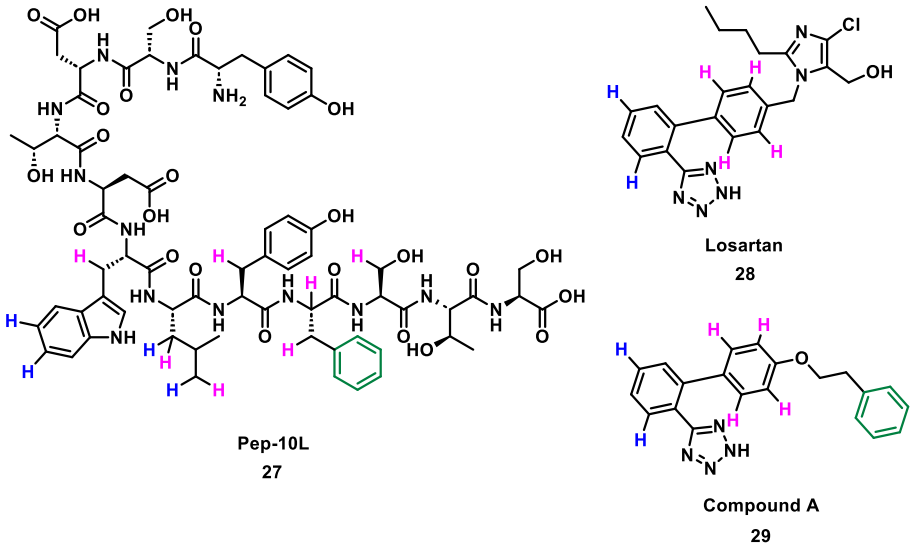


Figure 1-18 *Structure of turn-motif peptide **27**, and small molecule **28** and **29**. Hydrogen atoms highlighted blue occupy the same site, and those highlighted pink occupy the same site. The phenyl ring (green) was not accounded for in **28**.*

1.2.5 Using peptide side-chain functionality to inspire small molecule design

The analysis of a peptide can also be used to influence the design of small molecules through important properties rather than direct structure mimicking. This is used when there is bountiful knowledge about peptides that bind to the PPI but maybe no known small molecule that has shown promise. Characteristics including sterics, hydrogen bonding and lipophilic nature are analysed and applied when designing the small molecule (**Figure 1-19**).

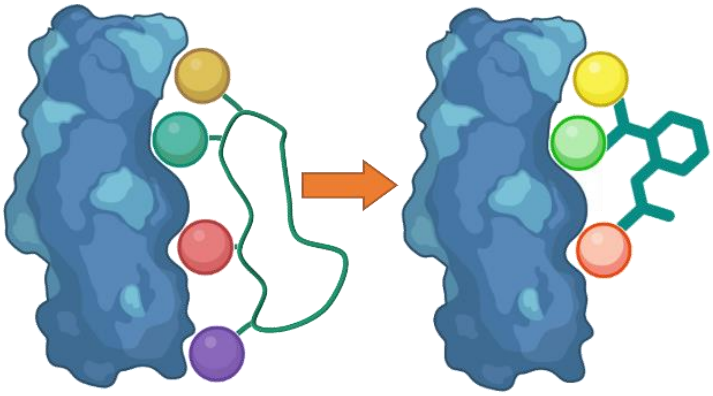


Figure 1-19 *Designing small molecules that mimic side-chain properties of peptides.*

Nicotinamide N-methyltransferase (NNMT) is an intracellular enzyme over-expressed in many diseases such as obesity, diabetes, and alcohol related liver diseases.[109–113] Identified using RaPiD, **30** (macrocyclic peptide) exhibited good inhibitory activity for NNMT with an IC_{50} = 0.1 µM but lacked cellular potency. An alanine scan of peptide **30** showed the side chains of R, G, HxG (N-hexyl-glycine) and W were essential and located at two crucial binding pockets (**Figure 1-20**). Arg picks up electrostatic interactions with NNMT while HxG and Trp sits in the hydrophobic pocket of NNMT, suggesting two lipophilic side chains are important for strong binding. HxG alongside Gly were also indicated to act as hydrogen bond acceptors to displace entropically unfavoured water molecules and restore electrostatic interactions with NNMT. These four key pharmacophore characteristics matching the four functional groups were carried forward into virtual screening to identify small molecules that possessed all key traits.

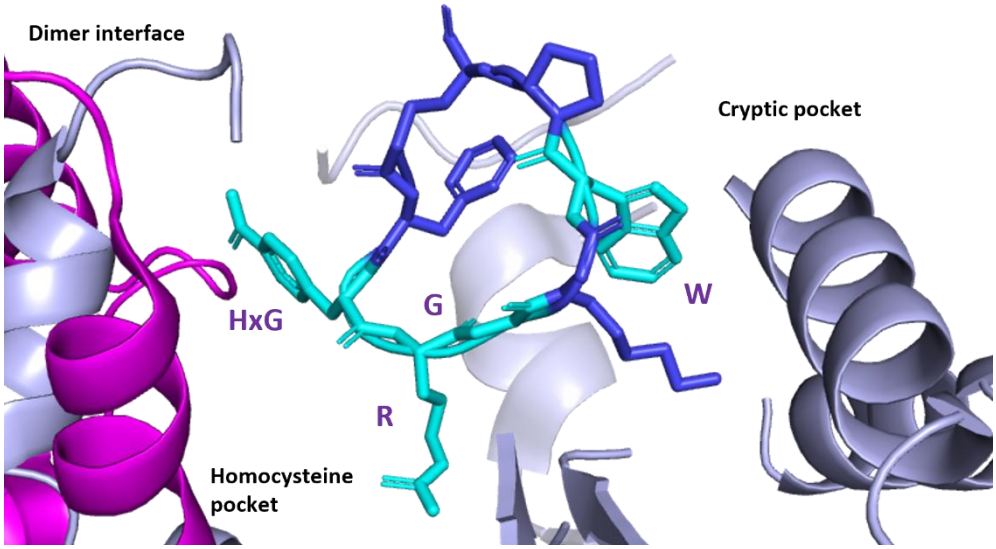


Figure 1-20 *Peptide* ***30*** *highlighting residues R, HxG, G, and W as important residues that bind at two crucial pockets in NNMT.*

Unfortunately, there were no compound hits that incorporated all four binding elements, therefore three features were chosen, two hydrogen bond acceptors and the hydrophobic properties to give virtual hit **31** (**Figure 1-21**). To mimic the Arg electrostatic interactions, an imidazole with an amine functional group was introduced (**Figure 1-21**, blue). A phenyl group was added to the benzimidazole for interactions with the hydrophobic pocket (**Figure 1-21**, green). Addition of an azaindole group to form a polar interaction (**Figure 1-21**, pink) resulted in **32** (**Figure 1-21**). **32** showed weak inhibitory activity and NMR experiments confirmed binding to NNMT. The addition of methyl groups on the benzimidazole and azaindole rings yielded 33 showing a potent inhibitory activity (IC_{50} = 0.0011 µM) and promising cell based activity without toxicity (IC_{50} = 0.40 µM).[114] Through peptide mimicking, a novel cell potent and selective small molecule was identified to inhibit NNMT without conventional library screening.

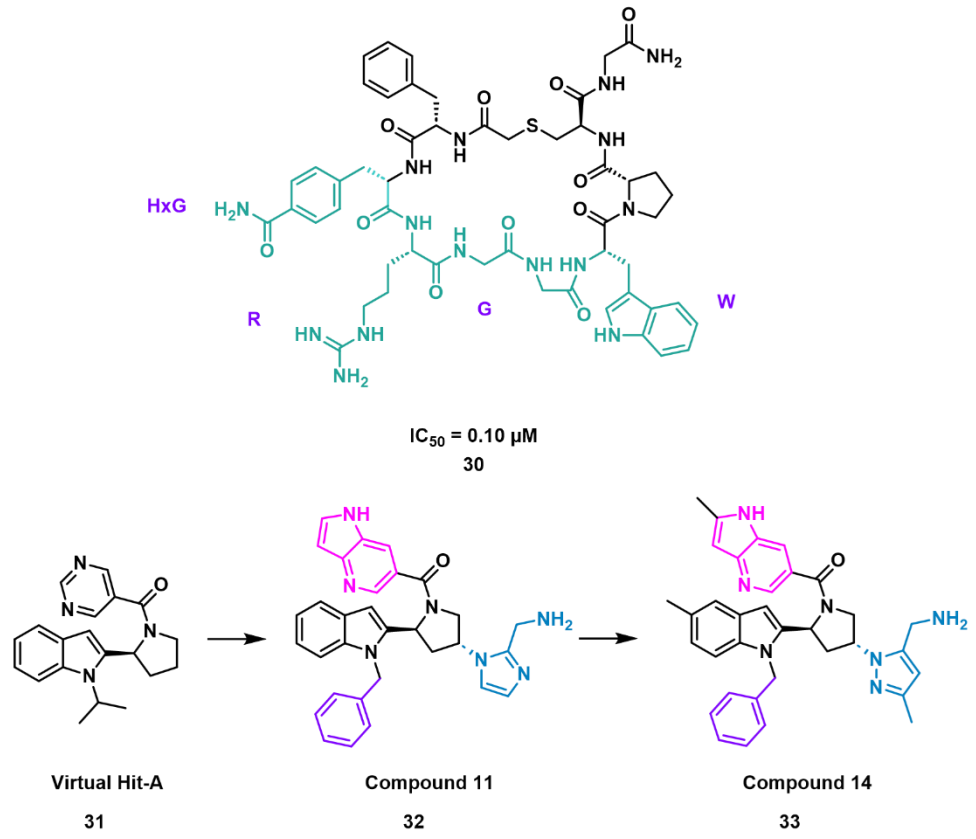


Figure 1-21 *Structures of cyclic peptide* ***30****, inspired hit* ***31****, and subsequent small molecules* ***32*** *and* ***33.***

The turn motif peptide L803F **34** (KEAPPSPPQS(p)PF) (**Figure 1-22**) inhibits GSK-3β, an isozyme of the serine-threonine kinase GSK-3 targeted in diabetes, neuronal development and neurodegenerative diseases.[115,116] The peptide was based on the interacting section of heat shock factor-1 (HSF-1) and GSK-3. GSK-3 and GSK-3β recognise a phosphorylated residue, usually serine, in the sequence of SXXXS(p), that is docked in a positively charged binding pocket.[115] Modelling also highlighted key hydrophobic interactions of F12 in **34** (**Figure 1-22**, pink) and proline residues (**Figure 1-22**, green) engaging F93 of GSK-3β.[115] Pharmacophore based virtual screening identified 137 hits using the highlighted properties of the L803F peptide. By using an *in vitro* GSK-3 kinase assay, six compounds were identified as GSK-3β inhibitors with IC_{50} values ranging from 1-20 µM in an *in vitro* GSK-3 kinase assay.

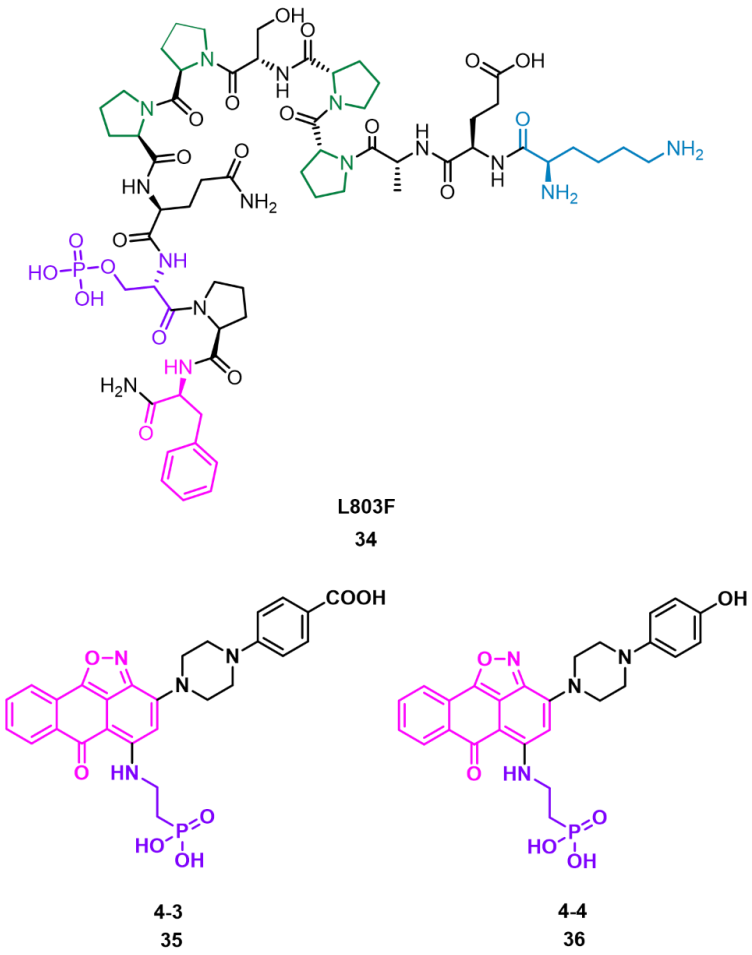


Figure 1-22 *Structures of turn-motif peptide* ***34*** *and small molecules* ***35*** *and* ***36.***

Molecular docking of these compounds showed overlapping with the original peptide including the anthracenone-isoxazole core forming π-π interactions with F93 in GSK-3β. Interestingly, the carboxylic acid of **35**, and the phenol of **36** were predicted to engage the positively charged binding pocket normally occupied for the phosphorylated amide, with the phosphoric acid group interacting with a second polar binding site (**Figure 1-22**). Compound **36** was shown to inhibit cellular GSK-3, demonstrating the rational design of small molecules from protein binding models.[117]

1.3 Conclusion

The development of small molecules that can mimic the inhibitory effects of cyclic peptides and turn motif peptides on protein-protein interactions holds great promise. The literature describes three common approaches for the transfer of the characteristics of cyclic or turn peptides to small molecules. The most used technique is the decoration of small molecule scaffolds with peptide functionality. This offers several advantages. Conceptually, this is the most straightforward, particularly when

structural information is available. The small molecule scaffold can be selected to balance any physicochemical properties of the side chain functionality. The use of computational modelling and SAR has enabled the creation of small molecules with similar or enhanced pharmacological properties. The hits that are generated with this method can then be optimised with classical small molecule medicinal chemistry approaches. This method has yielded several examples of compounds that surpass the peptide that inspired them.

Recent advances in techniques offers promise for an increase in the design of small molecules from cyclic peptide starting points. Cyclic peptide development techniques, including phage display and mRNA display allow for rapid identification of peptides able to control a target protein. The development of analytical NMR techniques, including STD NMR and INPHARMA, allow the collection of structural information for more protein targets in a timely manner. These analytical techniques identify pharmacophores from multiple binding molecules and identify the key binding motifs to be included in small molecules.

The field of small molecule peptide mimetics is rapidly evolving, and we can expect to see further advances in the design and synthesis of small molecules that can mimic the biological activities of cyclic peptides and turn motif peptides.

1.4 Thesis outline

The research in this thesis investigates alternative inhibitors for the immune checkpoint pathway PD-1/PD-L1. In chapter 2, a light activated peptide was investigated for selective inhibition of PD-1/PD-L1. A linear peptide that was known to inhibit PD-1/PD-L1 was analysed and modified with a photo-switchable compound. This led to the exploration of selectivity based on the conformation of the photo-switchable peptide. The effectiveness and selectivity of the successful photo-switchable peptides as an inhibitor for PD-1/PD-L1 was determined.

Chapter 3 investigates the development of small molecule-peptide hybrid inhibitors for PD-1/PD-L1. The characteristics of a known peptide inhibitor for PD-1/PD-L1 were mimicked to develop smaller inhibitors using peptide directed binding creating small molecule-peptide hybrids. The inhibitory and biological activity of these compounds was then explored.

PD-1/PD-L1 inhibitors often have a turn structure for effective inhibition and in chapter 4 a possible turn structure is discussed. An investigation into whether the inverse electron demand Diels Alder reaction between an alkene or alkyne and a 1,2,4,5-tetrazine could produce a turn structure was carried out. Finally, chapter 5 describes the investigation of cyclic peptides that inhibit PD-1/PD-L1. This led to the exploration of optimum synthetic conditions for three cyclic peptide inhibitors of PD-1/PD-L1.

1.5 References

1 A. Salmaninejad, S. F. Valilou, A. G. Shabgah, S. Aslani, M. Alimardani, A. Pasdar and A. Sahebkar, *J. Cell. Physiol.*, 2019, **234**, 16824–16837.

2 J. Wang, N. Seebacher, H. Shi, Q. Kan and Z. Duan, *Oncotarget*, 2017, **8**, 84559–84571.

3 H.-G. Ljunggren, R. Jonsson and P. Höglund, *Scand. J. Immunol.*, 2018, **88**, e12731.

4 G. J. Freeman, A. J. Long, Y. Iwai, K. Bourque, T. Chernova, H. Nishimura, L. J. Fitz, N. Malenkovich, T. Okazaki, M. C. Byrne, H. F. Horton, L. Fouser, L. Carter, V. Ling, M. R. Bowman, B. M. Carreno, M. Collins, C. R. Wood and T. Honjo, *J. Exp. Med.*, 2000, **192**, 1027–1034.

5 A. A. Davis and V. G. Patel, *J. Immunother. Cancer.*, 2019, **7**, 278.

6 Q. Wang, F. Liu and L. Liu, *Medicine (Baltimore)*, 2017, **96**, e6369.

7 H. Dong, S. E. Strome, D. R. Salomao, H. Tamura, F. Hirano, D. B. Flies, P. C. Roche, J. Lu, G. Zhu, K. Tamada, V. A. Lennon, E. Celis and L. Chen, *Nat. Med.*, 2002, **8**, 793–800.

8 S. L. Topalian, C. G. Drake and D. M. Pardoll, *Cancer Cell*, 2015, **27**, 450–461.

9 J. Liu, Z. Chen, Y. Li, W. Zhao, J. Wu and Z. Zhang, *Front. Pharmacol.*, 2021, **12,** 731798.

10 S. Upadhaya, S. T. Neftelinov, J. Hodge and J. Campbell, *Nat. Rev. Drug. Discov.*, 2022, **21**, 482–483.

11 S. Maleki Vareki, C. Garrigós and I. Duran, *Crit. Rev. Oncol. Hematol.*, 2017, **116**, 116–124.

12 R. L. Maute, S. R. Gordon, A. T. Mayer, M. N. McCracken, A. Natarajan, N. G. Ring, R. Kimura, J. M. Tsai, A. Manglik, A. C. Kruse, S. S. Gambhir, I. L. Weissman and A. M. Ring, *Proc. Natl. Acad. Sci. U.S.A.*, 2015, **112**, E6506-E6514.

13 A. De Sousa Linhares, C. Battin, S. Jutz, J. Leitner, C. Hafner, J. Tobias, U. Wiedermann, M. Kundi, G. J. Zlabinger, K. Grabmeier-Pfistershammer and P. Steinberger, *Sci. Rep.*, 2019, **9**, 11472.

14 S. Fukushima, *Nihon. Rinsho. Meneki. Gakkai. Kaishi.*, 2016, **39**, 30–36.

15 A. Patnaik, S. P. Kang, D. Rasco, K. P. Papadopoulos, J. Elassaiss-Schaap, M. Beeram, R. Drengler, C. Chen, L. Smith, G. Espino, K. Gergich, L. Delgado, A. Daud, J. A. Lindia, X. N. Li, R. H. Pierce, J. H. Yearley, D. Wu, O. Laterza, M. Lehnert, R. Iannone and A. W. Tolcher, *Clin. Cancer. Res.*, 2015, **21**, 4286–4293.

16 M. L. dos Santos, W. Quintilio, T. M. Manieri, L. R. Tsuruta and A. M. Moro, *Braz. J. Pharm. Sci.*, 2018, **54**, e01007.

17 NHS England » NHS England strikes deal on new NICE recommended lung cancer immunotherapy drug, https://www.england.nhs.uk/2018/06/nhs-england-strikes-deal-on-new-nice-recommended-lung-cancer-immunotherapy-drug/, (accessed 21 May 2023).
18 Y. Wang, X. Liu, X. Zou, S. Wang, L. Luo, Y. Liu, K. Dong, X. Yao, Y. Li, X. Chen and L. Sheng, *Pharmaceutics*, 2021, **13**, 598.
19 Curis, Inc., *A Phase 1, Open-Label, Dose Escalation and Dose Expansion Trial Evaluating the Safety, Pharmacokinetics, Pharmacodynamics, and Clinical Effects of Orally Administered CA-170 in Patients With Advanced Tumors and Lymphomas*, NCT02812875, clinicaltrials.gov, 2020.
20 E. V. Cutsem, H. Prenen, B. Delafontaine, K. Spencer, T. Mitchell, H. Burris, N. Kotecki, R. Kristeleit, D. Pinato, S. Sahebjam, D. Graham, T. Karasic, J. Daniel, K. O'Hayer, R. Geschwindt and S. Piha-Paul, *J. Immunother. Cancer.*, 2021, **9**, A559–A560.
21 Incyte Corporation, *A Phase 2 Study of INCB086550 (Oral PD-L1 Inhibitor) in Participants Who Are Immune Checkpoint Inhibitor-Naïve With Selected Solid Tumors*, NCT04629339, clinicaltrials.gov, 2023.
22 Maxinovel Pty., Ltd., *A Phase I Study of MAX-10181 Given Orally to Patients With Advanced Solid Tumor*, NCT04122339, clinicaltrials.gov, 2022.
23 X. Zhang, J.-C. D. Schwartz, X. Guo, S. Bhatia, E. Cao, M. Lorenz, M. Cammer, L. Chen, Z.-Y. Zhang, M. A. Edidin, S. G. Nathenson and S. C. Almo, *Immunity*, 2004, **20**, 337–347.
24 E. O. Long, *Annu. Rev. Immunol.*, 1999, **17**, 875–904.
25 K. M. Zak, R. Kitel, S. Przetocka, P. Golik, K. Guzik, B. Musielak, A. Dömling, G. Dubin and T. A. Holak, *Structure*, 2015, **23**, 2341–2348.
26 X. Cheng, V. Veverka, A. Radhakrishnan, L. C. Waters, F. W. Muskett, S. H. Morgan, J. Huo, C. Yu, E. J. Evans, A. J. Leslie, M. Griffiths, C. Stubberfield, R. Griffin, A. J. Henry, A. Jansson, J. E. Ladbury, S. Ikemizu, M. D. Carr and S. J. Davis, *J. Bio. Chem.*, 2013, **288**, 11771–11785.
27 L. Jimbu, O. Mesaros, A. Neaga, A. M. Nanut, C. Tomuleasa, D. Dima, C. Bocsan and M. Zdrenghea, *Pharmaceuticals (Basel)*, 2021, **14**, 1105.
28 M. Gato-Cañas, M. Zuazo, H. Arasanz, M. Ibañez-Vea, L. Lorenzo, G. Fernandez-Hinojal, R. Vera, C. Smerdou, E. Martisova, I. Arozarena, C. Wellbrock, D. Llopiz, M. Ruiz, P. Sarobe, K. Breckpot, G. Kochan and D. Escors, *Cell. Rep.*, 2017, **20**, 1818–1829.
29 C. Ghosh, G. Luong and Y. Sun, *J. Cancer*, 2021, **12**, 2735–2746.
30 M. Yi, M. Niu, L. Xu, S. Luo and K. Wu, *J. Hematol. Oncol.*, 2021, **14**, 10.
31 H. O. Alsaab, S. Sau, R. Alzhrani, K. Tatiparti, K. Bhise, S. K. Kashaw and A. K. Iyer, *Front. Pharmacol.*, 2017, **8**, 561.
32 S. Yin, Z. Chen, D. Chen and D. Yan, *Theranostics*, 2023, **13**, 1520–1544.
33 D. Shi, S. Zhou, X. Liu, C. Zhao, H. Liu and X. Yao, *Biochim. Biophys. Acta. Subj.*, 2018, **1862**, 576–588.
34 T. Okazaki and T. Honjo, *Int. Immunol.*, 2007, **19**, 813–824.
35 K. Wang, Y. Song, Y. Su, Y. Liang and L. Wang, *Biochem. Biophys. Res. Commun.*, 2020, **527**, 453–457.
36 R. Sable and S. Jois, *Molecules*, 2015, **20**, 11569–11603.
37 S. Sato, Y. Shimoda, A. Muraki, M. Kohara, Y. Nakamura and S. Tabata, *DNA Res.*, 2007, **14**, 207–216.
38 H. Lu, Q. Zhou, J. He, Z. Jiang, C. Peng, R. Tong and J. Shi, *Sig. Transduct. Target. Ther.*, 2020, **5**, 213.

39 R. J. Boohaker, M. W. Lee, P. Vishnubhotla, J. L. M. Perez and A. R. Khaled, *Comput. Mater. Contin.*, 2012, **19**, 3794–3804.
40 S.-H. Joo, *Biomol. Ther.*, 2012, **20**, 19–26.
41 D. A. Horton, G. T. Bourne and M. L. Smythe, *Chem. Rev.*, 2003, **103**, 893-930.
42 L. Gentilucci, R. De Marco and L. Cerisoli, *Curr. Pharm. Des.*, 2010, **16**, 3185–3203.
43 H. Wang, R. S. Dawber, P. Zhang, M. Walko, A. J. Wilson and X. Wang, *Chem. Sci.*, **12**, 5977–5993.
44 Bridge Biotherapeutics, Inc., *Efficacy and Safety of Orally Administered BBT-401-1S in Subjects With Ulcerative Colitis*, NCT04596293, clinicaltrials.gov, 2023.
45 Bioniz Therapeutics, Inc., *A Multiple-Dose Study of Intravenous BNZ123-1-40 in Healthy Adult Subjects*, NCT03239379, clinicaltrials.gov, 2018
46 A. D. Foster, J. D. Ingram, E. K. Leitch, K. R. Lennard, E. L. Osher and A. Tavassoli, *J. Biomol. Screen.*, 2015, **20**, 563–576.
47 W. Danders, M. A. Marahiel, M. Krause, N. Kosui, T. Kato, N. Izumiya and H. Kleinkauf, *Antimicrob. Agents. Chemother.*, 1982, **22**, 785–790.
48 J. N. Lambert, J. P. Mitchell and K. D. Roberts, *J. Chem. Soc., Perkin Trans. 1*, 2001, 471–484.
49 K. D. Roberts, J. N. Lambert, N. J. Ede and A. M. Bray, *J. Pept. Sci.*, 2004, **10**, 659–665.
50 M. Góngora-Benítez, J. Tulla-Puche and F. Albericio, *Chem. Rev.*, 2014, **114**, 901–926.
51 A. A. Golosov, A. N. Flyer, J. Amin, C. Babu, C. Gampe, J. Li, E. Liu, K. Nakajima, D. Nettleton, T. J. Patel, P. C. Reid, L. Yang and L. G. Monovich, *J. Med. Chem.*, 2021, **64**, 2622–2633.
52 Z. Fang, Y. Song, P. Zhan, Q. Zhang and X. Liu, *Future Med. Chem.*, 2014, **6**, 885–901.
53 C. A. Chang, W. Chen and M. K. Gilson, *Proc. Natl. Acad. Sci.*, 2007, **104**, 1534–1539.
54 L. K. Henchey, A. L. Jochim and P. S. Arora, *Curr. Opin. Chem. Biol.*, 2008, **12**, 692–697.
55 C. A. Rhodes, P. G. Dougherty, J. K. Cooper, Z. Qian, S. Lindert, Q.-E. Wang and D. Pei, *J. Am. Chem. Soc.*, 2018, **140**, 12102–12110.
56 O. Tietz, F. Corteson-Tamarit, R. Chalk, S. Able and K.A. Vallis, *Nautre*, 2022, **14**, 284-293.
57 G. J. J. Richelle, S. Ori, H. Hiemstra, J. H. van Maarseveen and P. Timmerman, *Angew. Chem. Int. Ed.*, 2018, **57**, 501–505.
58 H. Zhang and S. Chen, *RSC Chem. Biol.*, 2022, **3**, 18–31.
59 M. Gao, K. Cheng and H. Yin, *Biopolymers*, 2015, **104**, 310–316.
60 A. Tapeinou, M.-T. Matsoukas, C. Simal and T. Tselios, *Biopolymers*, 2015, **104**, 453–461.
61 G. P. Smith, *Science*, 1985, **228**, 1315–1317.
62 C. P. Scott, E. Abel-Santos, M. Wall, D. C. Wahnon and S. J. Benkovic, *Proc. Natl. Acad. Sci. U.S.A.*, 1999, **96**, 13638–13643.
63 Y. Goto and H. Suga, *Acc. Chem. Res.*, 2021, **54**, 3604–3617.
64 K. Deyle, X.-D. Kong and C. Heinis, *Acc. Chem. Res.*, 2017, **50**, 1866–1874.
65 A. Tavassoli, *Curr. Opin. Chem. Biol.*, 2017, **38**, 30–35.
66 M. S. Newton, Y. Cabezas-Perusse, C. L. Tong and B. Seelig, *ACS Synth. Biol.*, 2020, **9**, 181–190.

67 K. Tsuihiji, E. Honda, K. Kojoh, S. Katoh, T. Taguri, A. Yoshimori and H. Takashima, *Pharmaceuticals*, 2022, **15**, 1506.
68 G. Hummel, U. Reineke and U. Reimer, *Mol. BioSyst.*, 2006, **2**, 499.
69 A. M. Beekman, M. A. O'Connell and L. A. Howell, *Angew. Chem. Int. Ed.*, 2017, **56**, 10446–10450.
70 I. B. Spurr, C. N. Birts, F. Cuda, S. J. Benkovic, J. P. Blaydes and A. Tavassoli, *Chembiochem*, 2012, **13**, 1628–1634.
71 P. G. Sasikumar, R. K. Ramachandra, S. Adurthi, A. A. Dhudashiya, S. Vadlamani, K. Vemula, S. Vunnum, L. K. Satyam, D. S. Samiulla, K. Subbarao, R. Nair, R. Shrimali, N. Gowda and M. Ramachandra, *Mol. Cancer Ther.*, 2019, **18**, 1081–1091.
72 D. E. Scott, A. R. Bayly, C. Abell and J. Skidmore, *Nat. Rev. Drug Discov.*, 2016, **15**, 533–550.
73 A. A. Bogan and K. S. Thorn, *J. Mol. Biol.*, 1998, **280**, 1–9.
74 B. C. Cunningham and J. A. Wells, *Science*, 1989, **244**, 1081–1085.
75 K. R. Lennard and A. Tavassoli, *Chem. Eur. J.*, 2014, **20**, 10608–10614.
76 A. Tavassoli and S. J. Benkovic, *Angew. Chem. Int. Ed.*, 2005, **44**, 2760–2763.
77 Y. Shimizu, A. Inoue, Y. Tomari, T. Suzuki, T. Yokogawa, K. Nishikawa and T. Ueda, *Nat. Biotechnol.*, 2001, **19**, 751–755.
78 D. Y. Takeda, J. A. Wohlschlegel and A. Dutta, *J. Biol. Chem.*, 2001, **276**, 1993–1997.
79 J. A. Wohlschlegel, B. T. Dwyer, D. Y. Takeda and A. Dutta, *Mol. Cell. Biol.*, 2001, **21**, 4868–4874.
80 G. Kontopidis, M. J. I. Andrews, C. McInnes, A. Cowan, H. Powers, L. Innes, A. Plater, G. Griffiths, D. Paterson, D. I. Zheleva, D. P. Lane, S. Green, M. D. Walkinshaw and P. M. Fischer, *Structure*, 2003, **11**, 1537–1546.
81 G. Castanedo, K. Clark, S. Wang, V. Tsui, M. Wong, J. Nicholas, D. Wickramasinghe, J. C. Marsters and D. Sutherlin, *Bioorg. Med. Chem. Lett.*, 2006, **16**, 1716–1720.
82 B. Musielak, J. Kocik, L. Skalniak, K. Magiera-Mularz, D. Sala, M. Czub, M. Stec, M. Siedlar, T. A. Holak and J. Plewka, *Molecules*, 2019, **24**, 2804.
83 A. M. L. Castrucci, M. E. Hadley, T. K. Sawyer, B. C. Wilkes, F. Al-Obeidi, D. J. Staples, A. E. de Vaux, O. Dym, M. F. Hintz, J. P. Riehm, K. R. Rao and V. J. Hruby, *Gen. Comp. Endocrinol.*, 1989, **73**, 157–163.
84 V. J. Hruby, B. C. Wilkes, M. E. Hadley, F. Al-Obeidi, T. K. Sawyer, D. J. Staples, A. E. DeVaux, O. Dym and A. M. de L. Castrucci, *J. Med. Chem.*, 1987, **30**, 2126–2130.
85 F. Al-Obeidi, M. E. Hadley, B. M. Pettitt and V. J. Hruby, *J. Am. Chem. Soc.*, 1989, **111**, 3413–3416.
86 J. P. Cain, A. V. Mayorov, M. Cai, H. Wang, B. Tan, K. Chandler, Y. Lee, R. R. Petrov, D. Trivedi and V. J. Hruby, *Bioorg. Med. Chem. Lett*, 2006, **16**, 5462–5467.
87 M. Fridkin and V. A. Najjar, *Crit. Rev. Biochem. Mol. Biol.*, 1989, **24**, 1–40.
88 C. C. Lee, A. Kreusch, D. McMullan, K. Ng and G. Spraggon, *Structure*, 2003, **11**, 99–108.
89 J. Shang, G. Ye, K. Shi, Y. Wan, C. Luo, H. Aihara, Q. Geng, A. Auerbach and F. Li, *Nature*, 2020, **581**, 221–224.
90 A. Jarvis, C. K. Allerston, H. Jia, B. Herzog, A. Garza-Garcia, N. Winfield, K. Ellard, R. Aqil, R. Lynch, C. Chapman, B. Hartzoulakis, J. Nally, M. Stewart, L.

Cheng, M. Menon, M. Tickner, S. Djordjevic, P. C. Driscoll, I. Zachary and D. L. Selwood, *J. Med. Chem.*, 2010, **53**, 2215–2226.
91 E. Lescot, J. Sopkova-de Oliveira Santos, C. Dubessy, H. Oulyadi, A. Lesnard, H. Vaudry, R. Bureau and S. Rault, *J. Chem. Inf. Model.*, 2007, **47**, 602–612.
92 D. Chatenet, C. Dubessy, J. Leprince, C. Boularan, L. Carlier, I. Ségalas-Milazzo, L. Guilhaudis, H. Oulyadi, D. Davoust, E. Scalbert, B. Pfeiffer, P. Renard, M.-C. Tonon, I. Lihrmann, P. Pacaud and H. Vaudry, *Peptides*, 2004, **25**, 1819–1830.
93 D. Chatenet, M. Létourneau, Q. Nguyen, N. Doan, J. Dupuis and A. Fournier, *Br. J. Pharmacol.*, 2013, **168**, 807–821.
94 S. Neidle and M. J. Waring, *Br. J. Clin. Pharmacol.*, 1993, **37**, 54–88.
95 D. Pearson, J. E. Shively, B. R. Clark, I. I. Geschwind, M. Barkley, R. S. Nishioka and H. A. Bern, *Proc. Natl. Acad. Sci. U.S.A.*, 1980, **77**, 5021–5024.
96 P. Deaudelin and W. D. Lubell, *Org. Lett.*, 2008, **10**, 2841–2844.
97 J. Dufour-Gallant, D. Chatenet and W. D. Lubell, *J. Med. Chem.*, 2015, **58**, 4624–4637.
98 L. Hu, S. Magesh, L. Chen, L. Wang, T. A. Lewis, Y. Chen, C. Khodier, D. Inoyama, L. J. Beamer, T. J. Emge, J. Shen, J. E. Kerrigan, A.-N. T. Kong, S. Dandapani, M. Palmer, S. L. Schreiber and B. Munoz, *Bio. Med. Chem. Lett.*, 2013, **23**, 3039–3043.
99 A. D. Jain, H. Potteti, B. G. Richardson, L. Kingsley, J. P. Luciano, A. F. Ryuzoji, H. Lee, A. Krunic, A. D. Mesecar, S. P. Reddy and T. W. Moore, *Eur. J. Med. Chem.*, 2015, **103**, 252–268.
100 J. S. Pallesen, K. T. Tran and A. Bach, *J. Med. Chem.*, 2018, **61**, 8088–8103.
101 Y. Chen, D. Inoyama, A.-N. T. Kong, L. J. Beamer and L. Hu, *Chem. Biol. Drug Des.*, 2011, **78**, 1014–1021.
102 K. Kato-Takagaki, Y. Mizukoshi, Y. Yoshizawa, D. Akazawa, Y. Torii, K. Ono, R. Tanimura, I. Shimada and H. Takahashi, *J. Biol.Chem.*, 2009, **284**, 10720–10727.
103 V. M. Sánchez-Pedregal, M. Reese, J. Meiler, M. J. J. Blommers, C. Griesinger and T. Carlomagno, *Angew. Chem. Int. Ed.*, 2005, **44**, 4172–4175.
104 J. Orts, C. Griesinger and T. Carlomagno, *J. Magn. Reason.*, 2009, **200**, 64–73.
105 V. M. Sánchez-Pedregal, M. Reese, J. Meiler, M. J. J. Blommers, C. Griesinger and T. Carlomagno, *Angew. Chem. Int. Ed.*, 2005, **117**, 4244–4247.
106 K. Kato-Takagaki, Y. Mizukoshi, Y. Yoshizawa, D. Akazawa, Y. Torii, K. Ono, R. Tanimura, I. Shimada and H. Takahashi, *J. Biol. Chem.*, 2009, **284**, 10720–10727.
107 M.-B. Onselaer, M. Nagy, C. Pallini, J. A. Pike, G. Perrella, L. G. Quintanilla, J. A. Eble, N. S. Poulter, J. W. M. Heemskerk and S. P. Watson, *Platelets*, 2020, **31**, 187–197.
108 K. Ono, K. Takeuchi, H. Ueda, Y. Morita, R. Tanimura, I. Shimada and H. Takahashi, *Angew. Chem. Int. Ed.*, 2014, **53**, 2597–2601.
109 Q. Song, Y. Chen, J. Wang, L. Hao, C. Huang, A. Griffiths, Z. Sun, Z. Zhou and Z. Song, *J. Hepatol.*, 2020, **73**, 783–793.
110 H. Neelakantan, C. R. Brightwell, T. G. Graber, R. Maroto, H.-Y. L. Wang, S. F. McHardy, J. Papaconstantinou, C. S. Fry and S. J. Watowich, *Biochem. Pharmacol.*, 2019, **163**, 481–492.
111 M. A. Eckert, F. Coscia, A. Chryplewicz, J. W. Chang, K. M. Hernandez, S. Pan, S. M. Tienda, D. A. Nahotko, G. Li, I. Blaženović, R. R. Lastra, M. Curtis, S. D.

Yamada, R. Perets, S. M. McGregor, J. Andrade, O. Fiehn, R. E. Moellering, M. Mann and E. Lengyel, *Nature*, 2019, **569**, 723–728.
112 A. Kannt, A. Pfenninger, L. Teichert, A. Tönjes, A. Dietrich, M. R. Schön, N. Klöting and M. Blüher, *Diabetologia*, 2015, **58**, 799–808.
113 D. Kraus, Q. Yang, D. Kong, A. S. Banks, L. Zhang, J. T. Rodgers, E. Pirinen, T. C. Pulinilkunnil, F. Gong, Y. Wang, Y. Cen, A. A. Sauve, J. M. Asara, O. D. Peroni, B. P. Monia, S. Bhanot, L. Alhonen, P. Puigserver and B. B. Kahn, *Nature*, 2014, **508**, 258–262.
114 S. Yoshida, S. Uehara, N. Kondo, Y. Takahashi, S. Yamamoto, A. Kameda, S. Kawagoe, N. Inoue, M. Yamada, N. Yoshimura and Y. Tachibana, *J. Med. Chem.*, 2022, **65**, 10655–10673.
115 A. Licht-Murava, B. Plotkin, M. Eisenstein and H. Eldar-Finkelman, *J. Mol. Biol.*, 2011, **408**, 366–378.
116 B. Plotkin, O. Kaidanovich, I. Talior and H. Eldar-Finkelman, *J. Pharmacol. Exp. Ther.*, 2003, **305**, 974–980.
117 I. Rippin, N. Khazanov, S. Ben Joseph, T. Kudinov, E. Berent, S. M. Arciniegas Ruiz, D. Marciano, L. Levy, A. Gruzman, H. Senderowitz and H. Eldar-Finkelman, *Int. J. Mol. Sci.*, 2020, **21**, 8709.

Chapter 2

The Design, Synthesis and Biological Evaluation of Photo-switchable Peptide Inhibitors of PD-1/PD-L1

2.1 Introduction

2.1.1 Restricting peptide secondary structure

Modulators of protein-protein interactions (PPIs) are considered promising candidates in drug development. Peptides represent ideal scaffolds for developing novel inhibitors due to their modular assembly, biorecognition ability, and affordable synthetic options.[1] In particular, cyclic or looped peptides often feature superior affinity, selectivity and stability due to their constrained conformation.[2,3] Often, novel peptide inhibitors are designed by extracting hot spot sequences from within the protein interaction site.[4] However, these binding sites are defined by their secondary structure that aligns the amino acids to their preferential position to ensure tight binding within the PPI.[3] The secondary structures can be β-strands, α-helices and irregular turn structures or loops.[5–9] When these binding peptide sequences are removed from the protein, the peptides tend to lose their secondary structure as they are no longer stabilized by the protein domain and therefore exist in greater conformational freedom. This structural flexibility can make the peptide prone to proteolytic degradation and results in low target affinity due to entropic penalties when binding.[10] Peptide mimics of secondary structures can be a promising strategy to design PPI inhibitors.[11] Structural stability can lead to increased binding affinity through displaying hot-spot residues in their bioactive orientation and preventing proteolytic degradation. Methods such as macrocyclization and introducing turn-inducing amino acids modify the backbone of peptides to incorporate a turn structure, forcing molecular pre-arrangement (**Figure 2-1**).[5,6,12]

Another strategy is to incorporate a small molecule into the backbone of the peptide to align the peptide residues for optimal binding. One example of this is the use of the photo-controlled molecules known as photo-switches.[13] Photochromic switches, such as azobenzenes, can reconfigure the entire peptide upon photo-isomerisation allowing for remote control over target-binding affinity, independent from environmental conditions.[14]

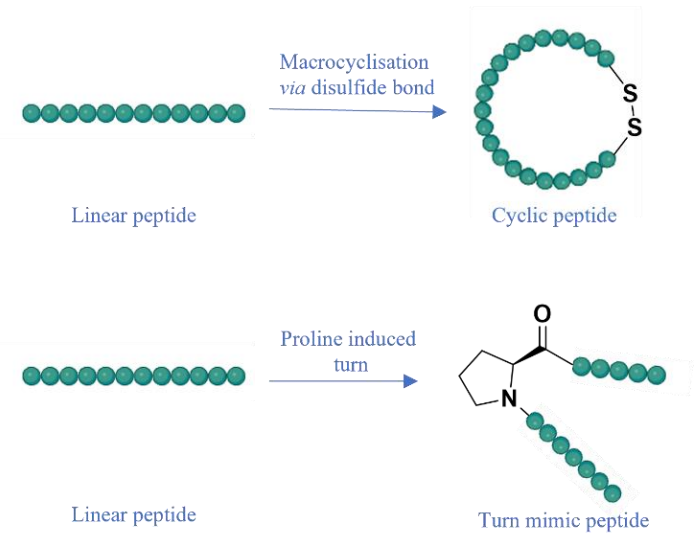
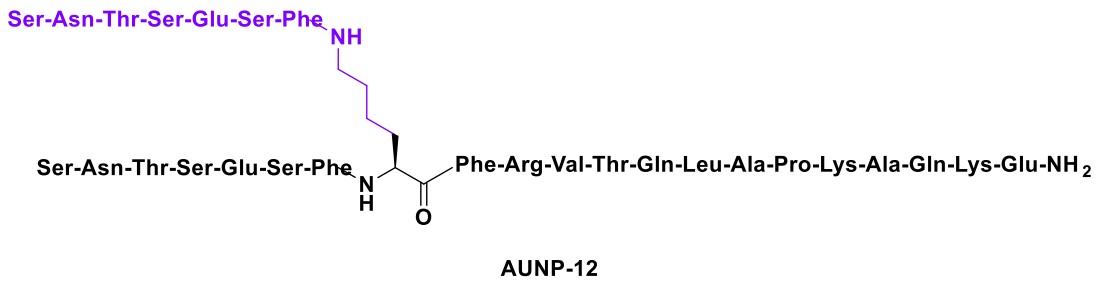


Figure 2-1 *Schematic illustration of macrocyclisation and introducing a turn inducing amino acid such as proline.*

2.1.2 Peptide inhibitors of PD-1/PD-L1

Among the reported peptide inhibitors for PD-1/PD-L1, the most well-known peptide is AUNP-12 (EC_{50} = 0.72 nM) identified by Aurigene Discovery Technologies and Laboratoires Pierre Fabre (**Figure 2-2**).[15] Sequences taken from the PD-1 extracellular domains were the starting point to design peptide derivatives with a non-linear peptide. AUNP-12 was one of the most active peptides and progressed onto pre-clinical trials where it exhibited impressive biological results including a 44% inhibited growth of mouse melanoma cells.[15] As seen by the structure in **Figure 2-2**, the linear peptide has a branched section (purple) that forms a turn like structure linked to the peptides high binding affinity and capabilities of blocking PD-1/PD-L1.



AUNP-12

Figure 2-2 *The structure of peptide inhibitor AUNP-12 branched section highlighted in purple.*

Li *et al.* designed linear peptide inhibitors that binds to PD-1 based on the residues Y56, R113, A121, D122 and Y123 found on the PD-1 binding interface of PD-L1. Through virtual high throughput screening, the most potent peptides were selected. Among these peptides was the linear peptide **2.1** with a K_D value of 1.38 ± 039 μM, validated using surface plasmon resonance (SPR) (**Figure 2-3A**).[16] The peptide was also found to block the PD-1/PD-L1 interaction at the cellular level. **Figure 2-3B** shows the predicted modelling of **2.1** binding to PD-1. From this it can be seen that the peptide adopts a looped structure upon binding.[16] Importantly, within those turns five anchor residues (**Figure 2-3B**, yellow) were identified *via* an alanine scan whereby replacement of this amino acids resulted in reduced binding affinity demonstrating the importance of the turn structure.

a

GN**WDY**NSQ**R**AQL**Y**NQ

K_D = 1.38 ± 039 μM

2.1

b

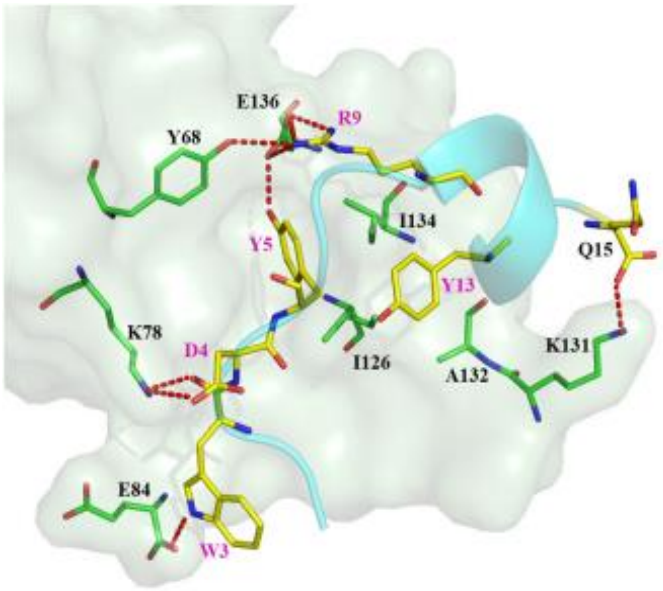


Figure 2-3 *a) the structure of* ***2.1****, a linear peptide inhibitor of PD-1/PD-L1 b)* ***2.1*** *binding to PD-1 exhibiting a turn structure. Image reproduced from ref. 15.*

Another example isolated peptides from the surface of PD-1 and optimised the structure to give the linear peptide **2.2** that exhibited high affinity for PD-L1 (**Figure 2-3A**).[17] When removed from the PD-1 protein, these isolated peptides became unstructured and to re-establish the turn structure necessary for binding to PD-L1, the peptides were conjugated to a dendrimer to aid peptide folding (**Figure 2-3C**).[17] When comparing the unstructured isolated peptide to the peptide tethered to the dendrimer using SPR, a 5 fold increase in affinity was seen for PD-L1. Furthermore, the tethered peptide could block the PD-1/PD-L1 interaction *in vitro*, measured through the production of cytokine, interleukin-2 (IL-2). In comparison to non-treated cancer cells, the tethered peptide showed a 1.5-fold increase in IL-2 secretion from the T-cells besting the control antibody that showed a 1.3-fold enhancement and the free peptides that showed no noticeable IL-2 production.[17] These results reiterate that the turn in the peptide structure is crucial for increased affinity (**Figure 2-3B**).

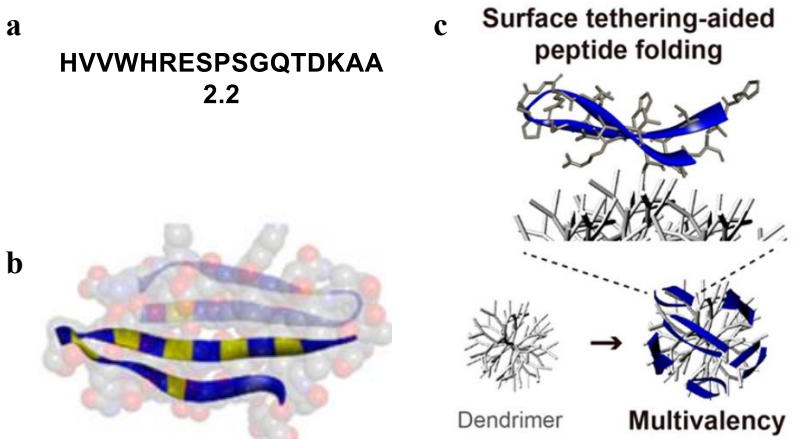


Figure 2-4 *a) The structure of the modified sequence from PD-1,* ***2.2*** *b) 3D structure of* ***2.2*** *binding to PD-L1 c) the schematic illustration of the process of developing a multivalent dendrimer-peptide conjugate using a PD-L1 peptide inhibitor. Images reproduced from ref. 16.*

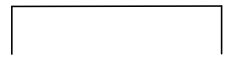
Four linear low molecular weight peptides (12 aa, ~1.6 kDa) were discovered *via* phage display to bind to PD-L1 in the nanomolar range.[18] Of these, two peptides, CLP002, **2.3** and CLP003, **2.4**, were highlighted for their ability to effectively block the PD-1/PD-L1 interaction at the cellular level, showing IC_{50} of 1.43 μM and 2.22 μM respectively (**Figure 2-5**).[18] Both peptides also showed inhibition of tumour growth using mouse models resulting in increased survival. Molecular docking of these peptides showed that, upon binding to PD-L1, both peptides adopted a turn like structure within the interaction site of PD-1/PD-L1.

WHRSYYTWNLNT
CLP002
K_D = 366 nM
2.3

WHFSYNWRWLPP
CLP003
K_D = 117 nM
2.4

Figure 2-5 *The sequences for CLP002 (**2.3**) and CLP003 (**2.4**) and their binding affinity for PD-L1 as determined by SPR.*

Furthermore, Cheng *et al.* enhanced the binding of **2.3** through cyclisation using a di-sulfide bond to create the cyclic peptide **2.5** (**Figure 2-6**). This limited the high degree of conformational flexibility found in the linear peptide and offered molecular pre-arrangement into a turn mimic (**Figure 2-7**).



CHRSYYTWNLNC
K_D = 119 nM
2.5

Figure 2-6 *The sequence for the modified CLP002 (**2.3**) using a disulfide bond to create the cyclic peptide **2.5.***

After cyclisation, **2.5** demonstrated a 34-fold improvement in comparison to **2.3** in the PD-1/PD-L1 blocking activity and *in vivo* anti-tumour activity.[19] Previously, **2.3** had shown anti-tumour activity at a dose of 2 mg/kg. After cyclisation, efficacy was enhanced using **2.5**, with anti-tumour activity seen at a low dose of 0.5 mg/kg to significantly reduce the tumour volume.[19]

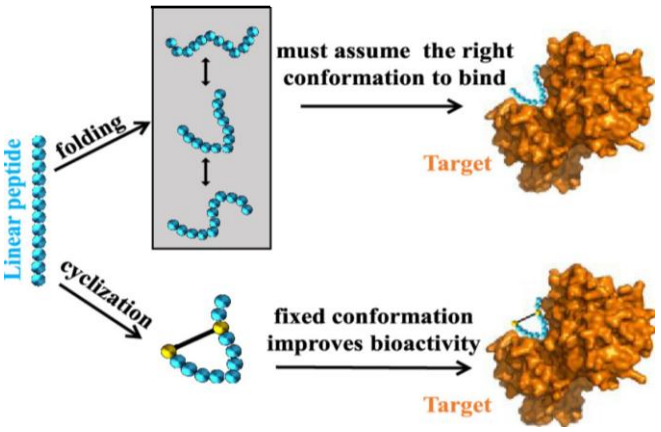


Figure 2-7 *Schematic illustration showing how conformational restriction improves the binding affinity of CLP003 (**2.4**) for PD-L1 to show superior blocking ability of PD-1/PD-L1. Image reproduced from ref. 17.*

These examples show that inducing a turn structure within linear peptides is advantageous when inhibiting PD-1/PD-L1. As linear peptides are generally conformationally flexible, this allows them to adopt many conformations in solution. This flexibility can be disadvantageous as there is a risk of off-target binding that could

lead to low efficacy and increased side effects. By introducing a turn structure, this allows for molecular pre-arrangement, lowering the entropic cost of binding and resulting in a higher binding affinity.

To date there are no peptide photo-switches in clinical trials. The UV light used to trigger isomerisation of photo-switches like azobenzenes limits the application of these compounds as UV light penetrates the skin poorly while also potentially causing damage to biological tissue.[20] There is ongoing work into compounds with the ability to isomerise under red-light to account for a deeper skin penetration possibility. Furthermore, the difference in activity must be significant between the active and inactive isomer. These contributing factors have limited the progression of photo-switchable peptides. However, Kiora Pharmaceuticals have entered clinical trials for a light-sensing small molecule, KIO-301, to restore sight with promising early results.

2.2 Photo-switchable molecules

Light provides the ability to regulate biological systems in a non-invasive and non-contaminating manner.[14,22] Furthermore, it allows for the timing, location and intensity of irradiation to be specifically attuned to individual targets. By incorporating a photo-switch into a molecule it allows for reversible switching between isomeric forms. Within these two forms, one configuration would ideally be active through high affinity for the target, while inactive in the other with low affinity. [14,22] This effectively creates an "on" and "off" switch, ideally with the compound existing in its inactive isomeric form until specifically activated through irradiation with light. Through this mechanism, photo-pharmacology aims to prevent off-target activity that leads to severe side effects by establishing remote control over action of the compound.[14] The structural advantages of peptides discussed above present them as ideal compounds to modify with a photo-switch. There have been several photo-switch molecules applied to peptides each with advantages and disadvantages. Stilbenes can be isomerised from the *trans* isomer, **2.6**, to the *cis* isomer, **2.7**, through UV light (300 nm), with the *trans* isomer being more stable (**Figure 2-8**).[23]

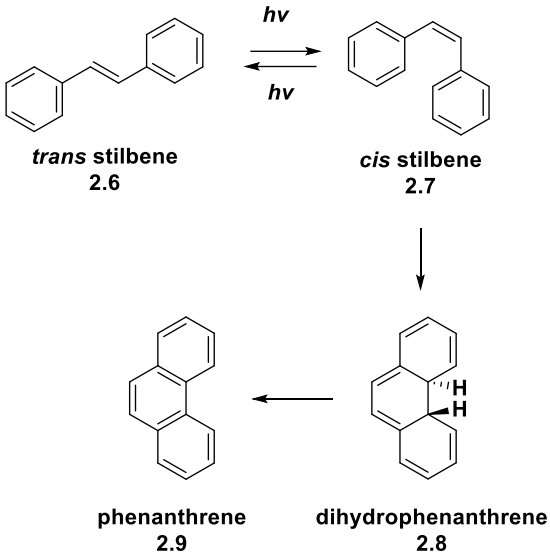


Figure 2-8 *The structure of trans stilbene(**2.6**) isomerised to the cis stilbene (**2.7**) upon irradiation. This can undergo irreversible cyclisation to form the dihydrophenanthrene (**2.8**) that can oxidise to phenanthrene(**2.9**).*

Stilbenes generally do not experience thermal *cis-trans* isomerisation at room temperature due to the large energy barrier between configurations (41-46 kcal/mol). Therefore, the isomers can be separated easily resulting in 100% isomerisation.[24] However, the *cis* isomer can undergo irreversible cyclisation to form a dihydrophenanthrene, **2.8**, that is oxidised to phenanthrene, **2.9**, limiting stilbene as a photo-switch (**Figure 2-8**).[25] The modification of stilbene led to a hemithioindigo photoswitch (**Figure 2-9**).[26,27]

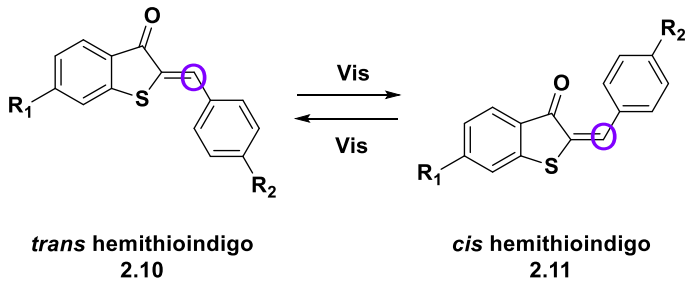


Figure 2-9 *The structures of trans hemithioindigo (**2.10**) and the cis hemithioindigo (**2.11**), the central carbon is circled in purple.*

The isomerisation properties are found on the central carbon double bond with the *cis* isomer, **2.11**, being more thermodynamically favourable than the *trans* isomer, **2.10** (**Figure 2-9**, circled). The hemithioindigo has picosecond switching in both directions, irradiation at 400 nm switches *cis* to *trans*, while 480 nm reverts the isomer back to *cis*.[26,27] Furthermore, due to the *cis*/*trans* isomerisation energy barrier, the thermal isomerisation is very slow resulting in a very bistable switching system.[28,29] Despite

having high fatigue resistance to cycles of photo-switching, hemithioindigo containing compounds often have low water solubility resulting in biological studies to nearly always be performed in DMSO.[30,31] Moreover, the switch is unstable in basic conditions and in SPPS, limiting the incorporation into peptides.[32]

Diarylethenes are controlled by a light activated reversible pericyclic reaction that switches the structure between an open ring isomer, **2.12**, to a closed ring isomer, **2.13**, through UV light (**Figure 2-10**).[33]

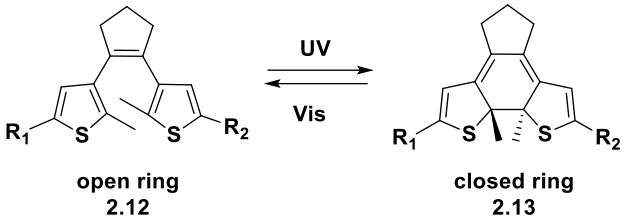


Figure 2-10 *The structure of a diarylethene in the open ring isomer(**2.12**) and the closed ring isomer (**2.13**).*

They are thermally irreversible therefore irradiation with visible light reverts diarylethenes back to the open isomer.[33,34] The isomerisation process happens in a picosecond time frame and has been shown to be resistant to degradation during photo-cycling, with no degradation occurring in one study for 10,000 switching cycles. [34] However, despite these impressive benefits, the synthesis of these compounds can be highly complicated.[34]

The spiropyran (SP) photoswitch, **2.14**, isomerises upon UV irradiation by undergoing heterolytic cleavage of the C_{spiro}-O bond (**Figure 2-11**, purple).[35]

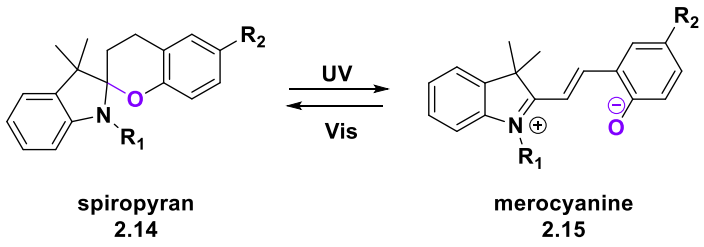


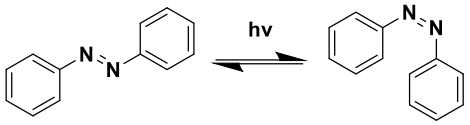
Figure 2-11 *The structure of the spiropyran (**2.14**) and the open ring isomer, merocyanine (**2.15**).*

This results in the open ring isomer, merocyanine (MC), **2.15**. Interestingly, SP to MC isomerisation can also be achieved using near infrared radiation, that has been found more beneficial when performing isomerisation in biological samples.[35] Furthermore, in highly polar biological environments, it is found in its MC form without the need for irradiation.[36] While this can be an advantage where UV light can be harmful for

biological samples, it removes the potential to control the isomerisation. Moreover, the MC isomer is prone to aggregation, blocking the ring closing reaction to form the SP isomer. There has also been degradation reported when repeating switching cycles that leads to non-photo responsive side products.[36]

2.2.1 Azobenzenes

The mostly widely used photo-switches are the azobenzenes due to their fast switching, low photobleaching rate, and straight forward synthesis.[37] The photochromic molecule is comprises of two phenyl rings connected by an azo group, **2.16**.



2.16 ***trans*** **2.17** ***cis***

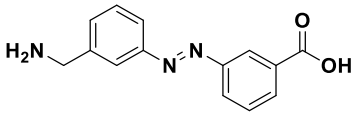
Figure 2-12 *The structure of azobenzene in the trans isomer (**2.16**) and the cis isomer (**2.17**).*

Upon UV light irradiation (365 nm) the azobenzene will undergo *trans*, **2.16**, to *cis*, **2.17**, isomerization while relaxing back to the more thermodynamically stable *trans* position or upon exposure at 450 nm (**Figure 2-12**).[38,39] In the dark at equilibrium, the *trans* conformation of azobenzene is the dominant isomer (>99.99%).[39,40] While full conversion to the *cis* isomer is unlikely, a substantial amount can be produced through irradiation with 365 nm light.[39,40] Furthermore, the photostationary state and stability of the *cis* isomer is highly dependent on the substituents of the azobenzene.[20]

2.2.2 Azobenzene modified peptides

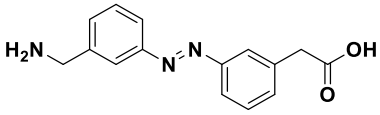
Photo-controlled peptide switches have been developed with both linear and cyclic peptides with backbone and side-chain incorporation explored.[41–43] A notable example of this was modelled after the discovery of β-hairpins mimicked from the tryptophan zipper motif.[44] Through backbone modification, a photo-switch β-hairpin peptide was designed that was stable in both isomers.[45] While in the *trans* state, the structure was disordered and extended but once irradiated into the *cis* isomer, the ends were forced closer together, inducing a β-hairpin.[46] The azobenzene moiety has also found success in α-helix stabilization, protein binding and activation, cell-mediated binding and within DNA.[47–49] Recently, Vázquez *et al*. reported photo-switchable azobenzene

containing peptides that disrupt the PPI MLL1-WDR5 affecting leukemic cell proliferation.[50] An azobenzene was inserted into the backbone of the WDR5-interacting peptide sequence (SARAXVHLRKS, X = AMPB, **2.18**) (**Figure 2-13**). While in the *trans* isomer the PPI was blocked, inhibiting the activity of MLL1 and cell proliferation of leukaemia cells, once isomerised to the *cis* isomer, WDR5 was free to interact with MLL1, exhibiting activity control through the photoswitch.[50] This was further shown through the IC_{50} values of 60 nM and 147 nM for the *trans* and *cis* isomers respectively. While this probe demonstrates that azobenzenes within a peptide can be used as a photo-switch, when considering developing an inhibitor for a PPI, ideally the *cis* isomer would be the active form with high affinity for the target. This would provide the active form only when needed, and in the desired location which is exposed to light. This is opposed to the scenario where the *trans* isomer is active, and so you would need to shine light everywhere you did not want biological activity. Trauner and Hoffmann-Röder reported a cyclic AMPP (**Figure 2-13**, **2.19**) peptide to achieve optical control of atrial natriuretic peptide (ANP)-based guanosine monophosphate (GMP) production. The most promising compound saw four amino acids of the ANP C-terminus replaced by AMPP and exhibited a 4-fold higher potency in cGMP production in the *cis* isomer (EC_{50} = 127 nM) compared to the *trans* isomer (EC_{50} = 468 nM).[51] These few examples highlight the practical use of azobenzenes as a photo-switch within peptides to allow for remote control over the structure of peptide inhibitors.



2.18

3-(3-aminomethylphenylazo)-benzoic acid (AMPB)



2.19

3-(3-aminomethylphenylazo)phenylacetic acid (AMPP)

Figure 2-13 *The structures of AMPB (**2.18**) and AMPP (**2.19**).*

2.3 Chapter aims

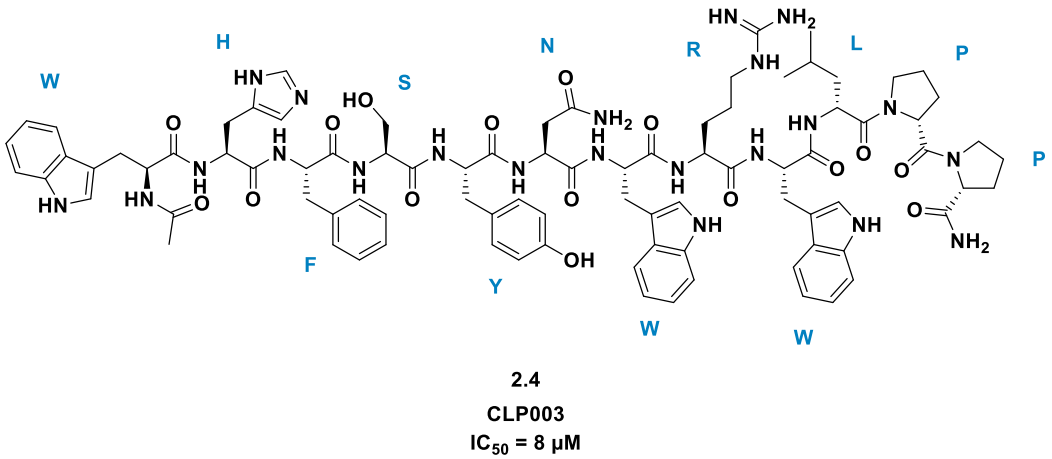
In this chapter, the modification of a linear peptide that is a known inhibitor of PD-1/PD-L1 was investigated to create a novel photo-switchable inhibitor. An alanine scan was used to determine which amino acids within the PD-L1 sequence were essential for the inhibition of PD-1/PD-L1. Once the important residues were determined, AMPP was inserted into the backbone of the linear, flexible peptide to create a turn

structure upon irradiation. The inclusion of this photo-switchable molecule was hypothesized to mimic the conformational strain found in cyclic peptides favourable for effective inhibition of PD-1/PD-L1.[18] Furthermore, the structural remote control of the peptide between the *cis* and *trans* isomer using light would create controlled inhibitor for PD-1/PD-L1.

2.4 Results and Discussion

2.4.1 Structural investigation of CLP003

Discovered using phage display, CLP003 (**Figure 2-14**, **2.4**) was selected as a linear peptide that inhibits the interaction of PD-1/PD-L1 by binding to PD-L1.[18] A total of 57 single phage colonies were randomly selected to be sequenced, and CLP003 was found to have 32 repeats. SPR analysis demonstrated the high binding affinity for PD-L1 showing a K_D of 117±80 nM.[18] Furthermore, it showed high blocking efficiency of 56% against PD-L1 expressing cancer cells.[18] These promising properties of CLP003 made it an ideal candidate to investigate light controlled conformational restraints.



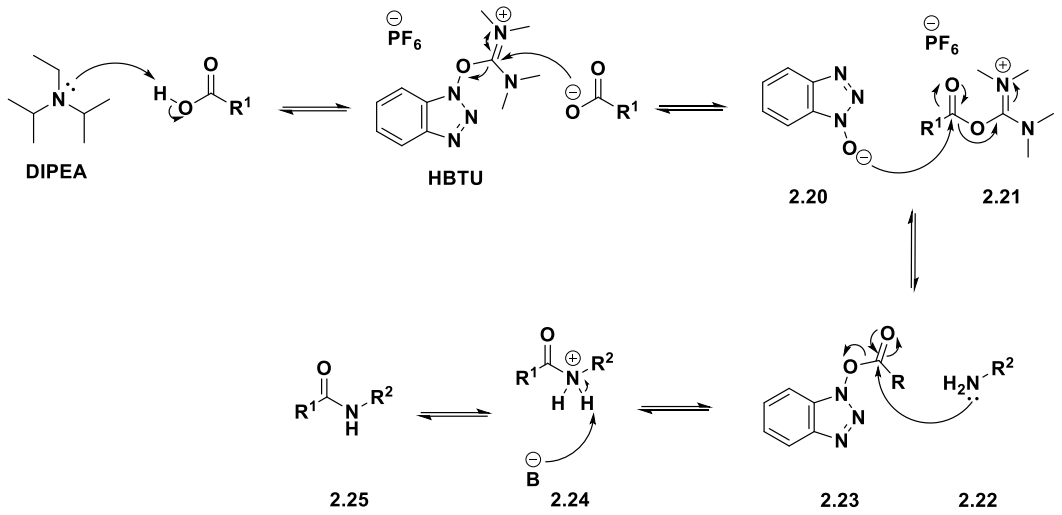
2.4
CLP003
IC_{50} = 8 μM

Figure 2-14 *The structure of CLP003 (**2.4**).*

To determine which amino acids were essential for inhibiting PD-1/PD-L1, an alanine scan of the peptide was performed. This method sequentially replaces every amino acid within the sequence with an alanine and then tests to see if the peptide retains the ability to inhibit PD-1/PD-L1. If inhibition is lost, the amino acid is deemed essential for binding. Alanine is used due its small size and non-polar methyl group to not cause drastic changes to the overall structure or polarity of the peptide.[52]

To synthesize the alanine scan peptides, fluorenylmethyloxycarbonyl (Fmoc) solid phase peptide synthesis (SPPS) was used. SPPS uses a solid support or resin to

facilitate the growing peptide chain through cycles of addition. The resin allows for excess of reagents to be used to ensure successful coupling and for the waste reagents to be washed away, this results in an efficient and clean synthesis of peptides. Most resins are polystyrene beads functionalized by a linker. For the synthesis of CLP003, TentaGel S RAM resin was used. This resin is functionalised with an acid labile Rink amide linker that upon cleavage forms a terminal amide on the C-terminus. The linker is protected via an Fmoc protecting group on the amine that is base labile and can be removed upon treatment with the base piperidine. Amino acids used in SPPS are also Fmoc protected, this prevents the formation of polymers of the same amino acid. Amino acids are Fmoc protected on the backbone nitrogen with any side chain functionalities protected with acid labile protecting groups such as tert-butyl (*t*Bu) for alcohols and both trityl (trt) and tert-butyloxycarbonyl (Boc) for amines. These orthogonal protecting groups allow the side chains to remain protected throughout the peptide synthesis, avoiding unwanted side reactions and to be easily removed during the final cleavage. After Fmoc deprotection of the resin, four equivalents of the next amino acid were added to the resin alongside four equivalents of both coupling agents *N,N,N',N'*-tetramethyl-*O*-(1H-benzotriazol-1-yl)uranium hexafluorophosphate (HBTU) and 1-hydroxybenzotriazole hydrate (HOBt) and eight equivalents of the base *N*,*N*-diisopropylethylamine (DIPEA). HBTU was used alongside HOBt to prevent racemisation of amino acids.[53,54] Due to the basicity of HBTU it can deprotonate the α-position of amino acids. When used in conjunction with HOBt, it forms an equilibrium to limit the concentration of free active HBTU.[53,54] Furthermore, HBTU is highly stable in DMF so it is ideal for automatic peptide synthesis where coupling agents are prepared for use over long periods of time.[33] The mechanism of the coupling reaction begins with the deprotonation of the carboxylic acid of an amino acid with DIPEA, a non-nucleophilic base (**Scheme 2-1**).



Scheme 2-1 *The general mechanism for amide bond formation in SPPS using HBTU, HOBt and DIPEA.*

This allows for nucleophilic attack of the iminium ion of HBTU leading to the elimination of the azabenzotriazole **2.20**. This sequentially attacks the electrophilic carbonyl centre of **2.21** to give an activated ester. The nucleophilic amine, **2.22**, on the terminal amino acid of the peptide chain can now attack the activated ester, **2.23**, releasing the azabenzotriazole to form an amide bond, **2.25**.

Once the peptide synthesis was complete, the peptide was acetylated on the N-terminus to prevent protonation at physiological pH. Acetic anhydride was used with DIPEA to react with the free amino group on the N-terminus to form an amide bond and releases acetic acid as a by-product. Acetylation of the N-terminus can improve the stability of the peptides and enhance their resistance to enzymatic degradation.[55]

The peptide was then removed from the resin using the cleavage cocktail of 95% trifluoroacetic acid (TFA), 2.5% water, and 2.5% triisopropylsilane (TIPS). The high concentration of acid also removed the protecting groups from the side chains of the amino acids, while the TIPS and water act as scavengers to prevent unwanted side reactions.

After cleavage, each peptide was purified using reverse-phase preparative HPLC and the purity of the peptide was confirmed using reverse-phase analytical HPLC with all peptides showing >98% purity (**Figure 2-15**). The successful synthesis was confirmed using MALDI to find the desired *m/z* (**Table 1**).

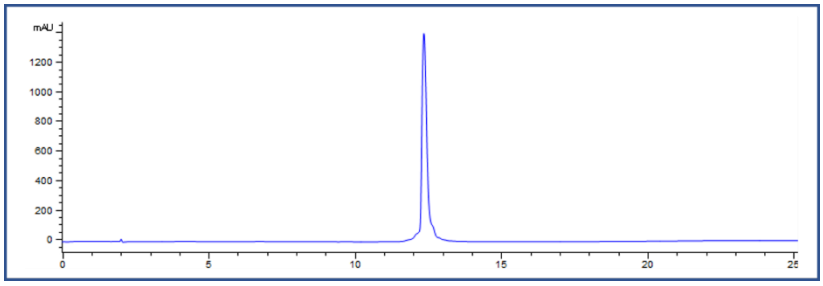


Figure 2-15 *The analytical HPLC traces of* ***2.32*** *reading at 214 nm a) after irradiation at 365 nm showing predominantly the cis isomer b) after being exposed for 20 minutes of ambient light showing predominantly the trans isomer* ***(****Agilent eclipse XDB-C18 column (4.6 x 150 mm, 5 µm) and a flow rate of 1 mL/min. Spectra were run with a solvent gradient of 0-100% B over 20 min. Solvent A: H_2O, 0.05% TFA, solvent B: MeCN, 0.05% TFA).*

Table 1 *CLP003 and the alanine scan mutation peptides showing the molecular weight, the observed mass and the percentage yield.*

	Peptide	Molecular weight (Da)	Observed mass (*m/z*)	Yield
(**2.4**)	Ac-WHFSYNWRWLPP-NH_2	1729.83	1729.09	9%
(**2.26**)	Ac-AHFSYNWRWLPP-NH_2	1614.78	1614.83	4%
(**2.27**)	Ac-WAFSYNWRWLPP-NH_2	1662.81	1663.55	7%
(**2.28**)	Ac-WHASYNWRWLPP-NH_2	1652.80	1653.87	7%
(**2.29**)	Ac-WHFAYNWRWLPP-NH_2	1711.84	1712.64	7%
(**2.30**)	Ac-WHFSANWRWLPP-NH_2	1635.81	1636.54	8%
(**2.31**)	Ac-WHFSYAWRWLPP-NH_2	1686.83	1686.38	11%
(**2.32**)	Ac-WHFSYNARWLPP-NH_2	1613.78	1613.30	7%
(**2.33**)	Ac-WHFSYNWAWLPP-NH_2	1643.77	1643.73	4%
(**2.34**)	Ac-WHFSYNWRALPP-NH_2	1613.78	1613.60	6%
(**2.35**)	Ac-WHFSYNWRWAPP-NH_2	1687.78	1687.75	5%
(**2.36**)	Ac-WHFSYNWRWLAP-NH_2	1703.81	1703.28	6%
(**2.37**)	Ac-WHFSYNWRWLPA-NH_2	1703.81	1703.11	8%

2.4.2 Protein interaction of alanine scan peptides

To determine if each peptide retained the ability to inhibit the interaction between PD-1/PD-L1 ultimately confirming which amino acids were essential for inhibition, a homogeneous time-resolved fluorescence (HTRF) PD-1/PD-L1 binding assay was used. The benefit of this assay is that it combines fluorescence resonance energy transfer (FRET) technology with time-resolved measurement to reduce any background fluorescence, this also eliminates buffers and proteins from influencing the results with a negative background.[56–58] The time delay of 150 µs between excitation and measurement allows for the clearance of all unspecific short-lived emissions, with acceptors emitting long lived fluorescence.[56–58] Furthermore, the assay is homogenous meaning the donor-acceptor complex can be detected without the need

of separation from the unbound components. The assay is designed to measure the interaction between PD-1 and PD-L1 by tagging the proteins with antibodies. The PD-L1 binding antibody is tagged with europium and acts as a HTRF donor, whilst the PD-1 binding antibody is tagged with XL665, a HTRF acceptor. When PD-1 and PD-L1 bind and are therefore in proximity of one another, the HTRF donor antibody initiates FRET towards the HTRF acceptor antibody, that emits at 665 nm (**Figure 2-16**). However, if the interaction is blocked and no FRET can occur, the europium tagged antibody emits at 625 nm. The intensity of the PD-1/PD-L1 interaction is directly proportional to this specific signal. If there is a reduction in the HTRF ratio this means PD-1/PD-L1 is being inhibited. For each sample, a positive control that contains both tagged proteins, a negative control that contains only tagged PD-L1 and a buffer control is included.

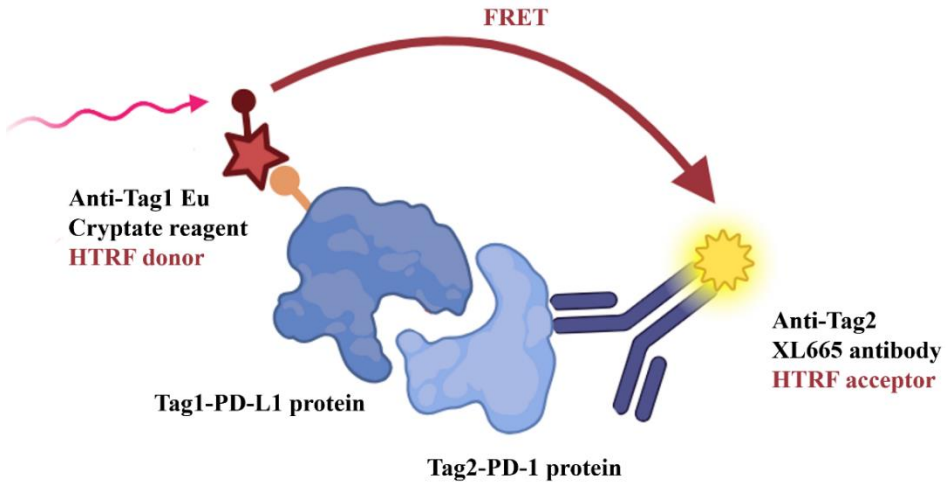


Figure 2-16 *A schematic illustration of the HTRF PD-1/PD-L1 assay.*

The parent peptide, CLP003, and each of the alanine scan peptides were initially screened in this assay at 1 mM concentration in PPI-Europium detection buffer. The reported data was performed in triplicate, twice. For use as a control, BMS-1 was purchased and used at 10 µM concentration. This is a known potent small molecule inhibitor of PD-1/PD-L1 with an IC_{50} of 6 nM.[59] Using the positive control as a guide, peptides **2.27**, **2.28**, **2.29**, **2.31**, **2.34**, and **2.37** showed a near complete loss in the ability to inhibit the HTRF signal, suggesting no binding to PD-L1. Peptides **2.26**, **2.33**, **2.35** and **2.36** showed moderate ability to inhibit HTRF signal but weaker than the parent peptide. Interestingly, peptides **2.30** and **2.32** showed inhibitory activity equal to or better than CLP003, **2.4**.

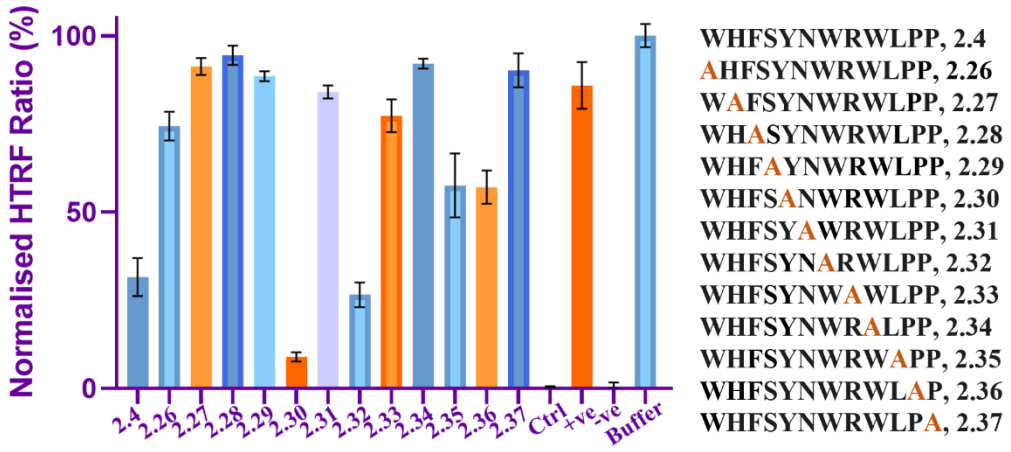


Figure 2-17 *The HTRF assay data for alanine screen of CLP003 showing* ***2.30*** *and* ***2.32*** *inhibiting PD-1/PD-L1 demonstrating that Tyr5 and Trp7are not important for binding. All peptides were screened at 1 mM (n/N = 2/6), BMS 1 (10 µM) was the control (Ctrl), the positive control contained tagged PD-L1 and tagged PD-1, the negative control contained tagged PD-L1 only. Errors are SEM..*

The reduced signal shown for the replacement of amino acids Tyr5 and Trp7 correlates to no loss of inhibition when replaced by alanine therefore they are not essential for binding as shown by **Figure 2-17**. Peptides **2.30** and **2.32** were then assayed over 20 µM to 1 nM to determine the IC_{50} of each peptide. The alanine screened peptides showed better inhibition of PD-1/PD-L1 using the HTRF assay than CLP003 (IC_{50} = 8 µM [7.12, 11.27]), with **2.30** having an IC_{50} of 0.052 µM [0.028, 0.10] and **2.32** having an IC_{50} of 0.025 µM [0.013, 0.052] (**Figure 2-18**).

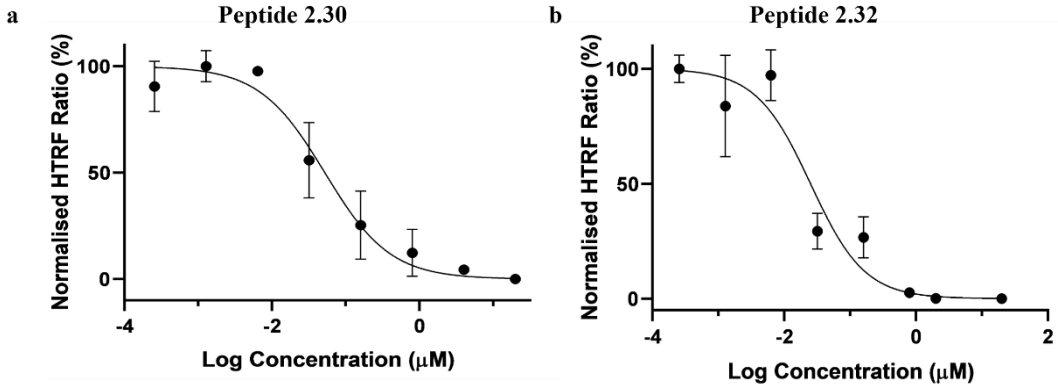


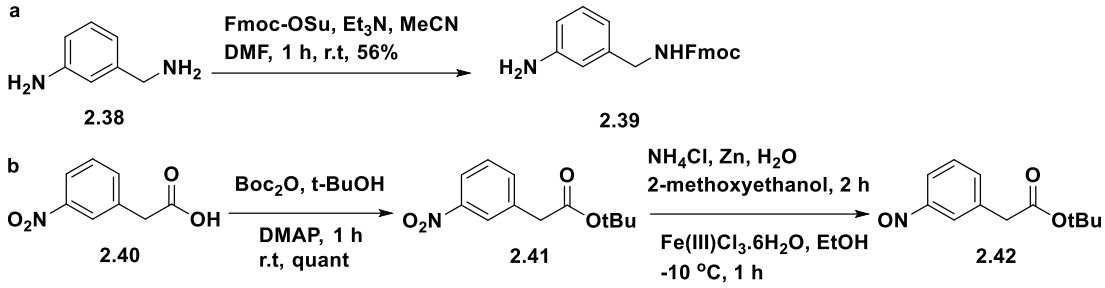
Figure 2-18 *The dose dependent curves of a) peptide* ***2.30*** *with an IC_{50} =0.052 µM [0.028,0.10] b) peptide* ***2.32*** *with an IC_{50} = 0.025 µM [0.013, 0.052]. IC_{50} +/- 95% confidence interval (n/N = 2/6).*

HTRF false positives within this assay could be due to auto-fluorescence, the peptides acting as fluorescence donors, and tag/antibody binders. To identify any false positives, the emission wavelength for each compound would be tested to ensure that there was no interference. Another method was to set up the HTRF assay with the tagged PD-1/PD-L1 as the procedure states and add the compounds, the inhibitory

effect would then measured at 0 min and 60 mins where initial compounds binding to PD-1/PD-L1 should show little to no activity.

2.4.3 Synthesis of AMPP

Once the important residues of CLP003, **2.4**, had been highlighted, the next step was to synthesise the azobenzene that would be inserted into the backbone of the peptide. The azobenzene chosen was AMPP, **2.19**, due to its easy synthesis and the structure being suitable for SPPS as the amine can be Fmoc protected. AMPP was synthesised as previously reported with the overall pathway being shown in **Scheme 2-2**.[60]

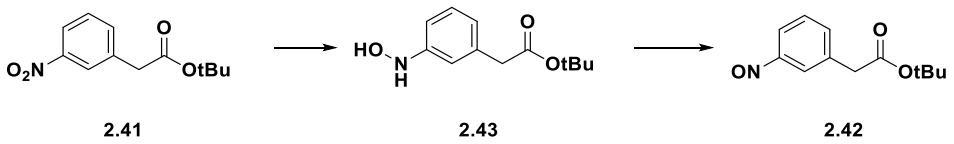


Scheme 2-2 *a) The Fmoc protection of 3-aminobenzylamine (**2.38**) to give **2.39** b) The tert-butyl protection of 3-nitrophenylacetic acid to give **2.41**, followed by the the reduction of the nitro group to a nitroso group to give the product **2.42**.*

The synthesis began by Fmoc protecting 3-aminobenzylamine, **2.38**, using Fmoc-OSu and triethylamine as shown in **Scheme 2-2A**. The amine is more nucleophilic than the aniline and therefore more readily reacts with Fmoc-OSu. By Fmoc protecting this amine, **2.39**, the aniline amine is free to react to form the N=N azobenzene bond. Further, by being Fmoc protected this is ideal for being use SPPS, as Fmoc protected amino acids are used. After filtration and product drying, **2.39** was obtained as a white solid (56%). The compound was confirmed using ^{1}H NMR where the methylene protons shifted from 3.75 ppm to 4.04 ppm corresponding to the successful protection of the amine.

To form the second precursor for the AMPP synthesis, **2.42**, a second benzyl ring with a carboxylic acid functional group was used. Initially, 3-nitrophenylacetic acid, **2.40**, was used without the carboxylic acid group protected but this caused poor yields when forming the azobenzene. To improve the yield, Boc anhydride and DMAP in *tert*-butanol was used to *tert*-butyl protect **2.41** (**Scheme 2-2B**).[60] The product was purified by flash column chromatography to give **2.41** in quantitative yield. ^{1}H NMR confirmed a successful protection, showing a singlet integrating for nine protons at 1.45 ppm corresponding to the *tert*-butyl group.

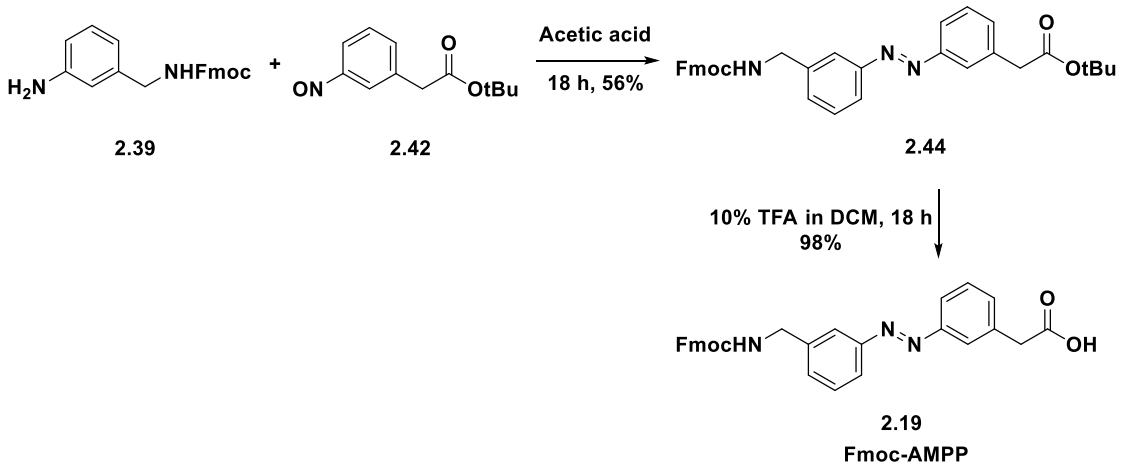
The next step was to reduce the nitro group to a nitroso. Zinc and ammonium chloride were used to reduce the nitro group to a hydroxylamine (**Scheme 2-3, 2.43**) where iron (III) chloride hexahydrate oxidises the arylazanol to a nitroso compound, **2.42**. This was confirmed using high resolution LCMS with a *m/z* of 222.1096 being observed, corresponding to the calculated $[M+H]^+$ of calculated as 222.1052.



2.41 2.43 2.42

Scheme 2-3 *The reduction of the nitro group on **2.41** through the intermediate of the reaction shown in **2.43** to give a nitroso group found on **2.42**.*

With both azobenzene precursors **2.39** and **2.42** synthesised, the final steps were the formation of the azobenzene N=N bond and the deprotection of the *tert*-butyl group. **2.39** and **2.42** were stirred in acetic acid overnight, the brown-orange oil was then purified using flash column chromatography to give **2.44** as an orange oil with a 56% yield. The mass obtained showed an *m/z* of 548.40, corresponding to the $[M+H]^+$ of 548.25. This product was then stirred in 10% TFA in DCM overnight to give a burnt orange solid as the final product, Fmoc protected AMPP, **2.19** (**Scheme 2-4**). The ^1H NMR showed a broad peak at 12.47 ppm corresponding to the unprotected carboxylic acid. Fmoc-AMPP, **2.19**, was further confirmed to have a *m/z* of 492.2 that corresponded to a $[M+H]^+$ of 492.2. The data matched the literature reported.[60]



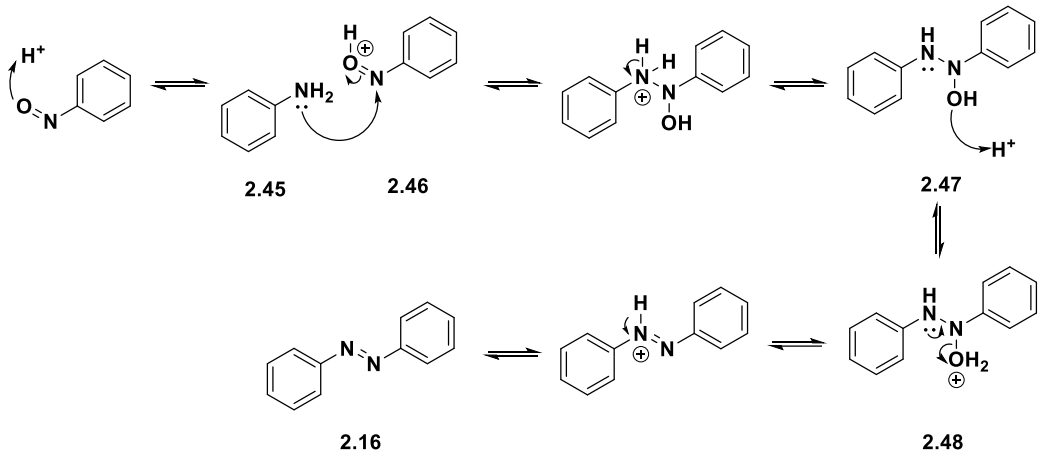
2.39 2.42 2.44

2.19
Fmoc-AMPP

Scheme 2-4 *The formation of the azobenzene bond through **2.39** and **2.42** being stirred in acetic acid overnight. This was followed by the tert-butyl deprotection to give the Fmoc protected AMPP (**2.19**).*

The mechanism of azobenzene formation through the condensation of nitrosobenzene with anilines is acid catalysed (**Scheme 2-5**).[61,62] The aniline, **2.45**, acts as a

nucleophile to attack the protonated nitrosobenzene, **2.46**. The hydroxylamine, **2.47**, is then protonated, and the loss of water forms the characteristic N=N bond, **2.48**.[61,62]



Scheme 2-5 *The proposed mechanism for the formation of the azobenzene (**2.16**).*

2.4.4 The design of azobenzene peptides

The HTRF assay data of the alanine scan of CLP003, **2.4**, was the foundation of the design of azobenzene peptides **2.51**-**2.56** found in **Table 2**. Due to both Trp7 and Tyr5 being unimportant for inhibition, for **2.51** Trp7 was replaced by AMPP. Similarly, for **2.52** Tyr5 was replaced by AMPP. To counteract the size of AMPP, **2.53** and **2.54** had the Trp7 replaced with AMPP and the Tyr5 removed from the sequence resulting in a peptide of similar size to the parent peptide. Another consideration was the changing stereochemistry of Asn due to the removal of amino acids and the insertion of AMPP. To determine whether the orientation preferential for inhibiting PD-1/PD-L1, L-Asn was replaced with the isomer, D-Asn in **2.55** and **2.56**.

Table 2 *The designed azobenzene substituted peptides.*

	Peptide	Molecular weight	Observed mass	Yield
(**2.51**)	Ac-WHFSYN-AMPP-RWLPP-NH_2	1794.85	1794.53	22%
(**2.52**)	Ac-WHFS-AMPP-NWRWLPP-NH_2	1817.87	1817.62	17%
(**2.53**)	Ac-WHFSN-AMPP-RWLPP-NH_2	1631.79	1631.50	16%
(**2.54**)	Ac-WHFS-AMPP-NRWLPP-NH_2	1630.79	1631.23	18%
(**2.55**)	Ac-WHFSn-AMPP-RWLPP-NH_2	1630.79	1631.84	11%
(**2.56**)	Ac-WHFS-AMPP-nRWLPP-NH_2	1630.79	1631.34	10%

All peptides shown in **Table 2** were synthesised using SPPS and purified to >97%. Fmoc-AMPP, **2.19**, was coupled identically to the other Fmoc amino acids. Once peptide synthesis was complete, the peptides were acetylated and cleaved. However,

the cleavage of TFA:TIPS:H_2O 94:2.5:2.5 was shaken for 2 hours instead of 3 due to degradation occurring in the AMPP, **2.19**, unit when shaken for 3 hours.

2.4.5 Photo-switching peptides

The photo-switching behaviour of azobenzene substituted peptides was first analysed to assess suitability as a photo-switch. Peptides **2.51**-**2.56** were dissolved 1 mg/mL in 1:1 MeCN/H_2O and exposed to visible light (~ 425-500 nm). As shown in **Figure 2-19B** using **2.51**, the analytical HPLC showed **2.51** was predominantly in the *trans* isomer over the *cis* isomer (70:30). After irradiation for 20 minutes at 365 nm, the analytical HPLC showed predominantly the *cis* isomer (68:32) (**Figure 2-19A**). A similar trend was observed for peptides **2.51**-**2.56**. The isomeric ratio of the *cis* and *trans* could possibly be due to the steric hinderance and interactions introduced by the surrounding amino acids. While 100% conversion from *trans* to *cis* would be preferable for continuing with biological work, for the instance of this study to identify a lead compound the ratio was sufficient.

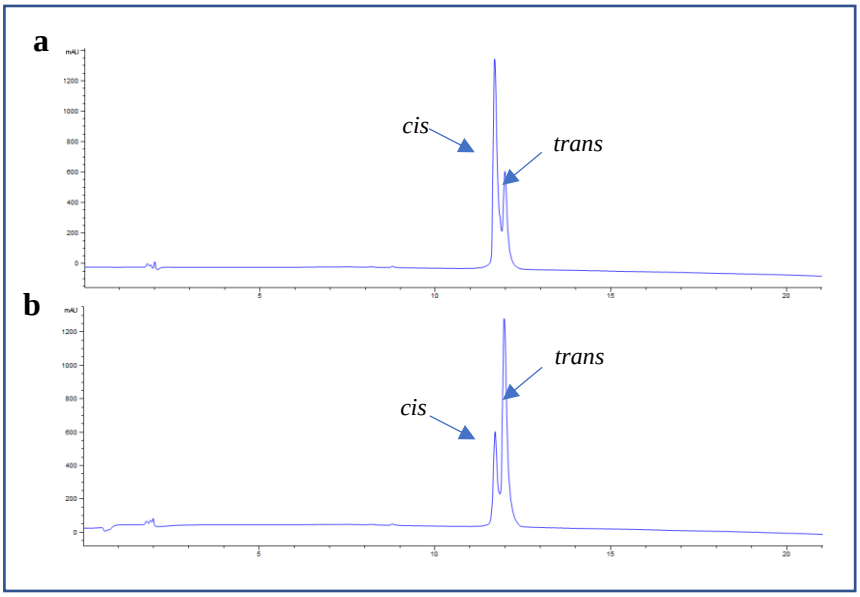


Figure 2-19 *The analytical HPLC traces of* ***2.51*** *reading at 214 nm a) after irradiation at 365 nm showing predominantly the cis isomer b) after being exposed for 20 minutes of ambient light showing predominantly the trans isomer* ***(****Agilent eclipse XDB-C18 column (4.6 x 150 mm, 5 µm) and a flow rate of 1 mL/min. Spectra were run with a solvent gradient of 0-100% B over 20 min. Solvent A: H_2O, 0.05% TFA, solvent B: MeCN, 0.05% TFA).*

After confirming the photo-switching ability, determining how stable the peptides **2.51**-**2.56** were in the *cis* isomer was essential as this isomer would be the turn mimic for inhibition of PD-1/PD-L1. UV/visible absorption spectroscopy was utilized to measure this stability as the characteristic bands of absorption are in the visible and UV region. The *trans* isomer absorbs in the UV region around 320 nm, corresponding

to the asymmetry allowed π → π* transition.[20] After irradiation the *cis* isomer is in abundance, the π → π* band is reduced followed by the appearance of a second absorption band at 450 nm corresponding to the symmetry forbidden n → π* transition (**Figure 2-20**).[20] Peptides **2.51**-**2.56** were dissolved in methanol at 1 µg/mL and measured at time intervals starting with the unirradiated peptide.

As expected, the unirradiated **2.51** showed two absorption bands as it is found in a mixture of *cis* and *trans* isomers, a dominant one around 330 nm and a weaker band around 430 nm corresponding to the π→π* electronic transition found in the *trans* isomer and n→π* electronic transition found in the *cis* isomer. Upon irradiation for 20 mins at 365 nm, the increase of *cis* isomer was observed by a decrease in intensity of the band at 330 nm and an increase at band 430 nm (**Figure 2-20**).

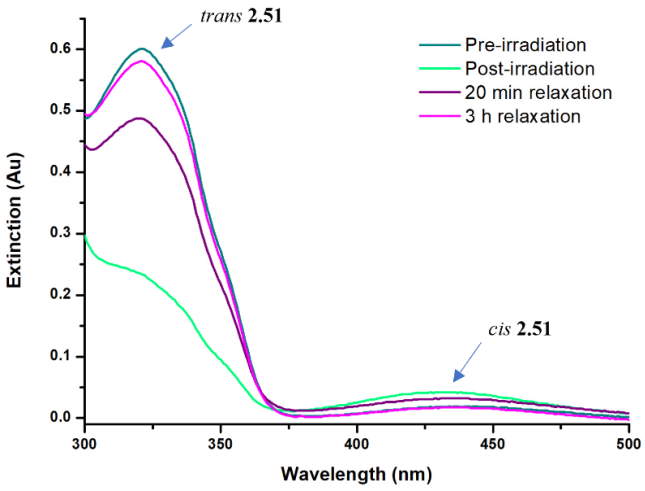


Figure 2-20 *UV/Vis spectra for* ***2.51*** *after being irradiated for 20 minutes and being kept in ambient light while taking time interval readings showing that after 3 hours* ***2.51*** *had relaxed back to the trans isomer.*

Initially, the relaxation of **2.51** after irradiation in ambient light was recorded at 20 minutes (**Figure 2-20**, purple) and again at 3 hours (**Figure 2-20**, pink). After 3 hours, **2.53** was showing the *trans* isomer being more abundant with almost complete relaxation back to pre-irradiated levels (**Figure 2-20**). This process was repeated this time keeping **2.51** in the dark after irradiation. When kept in the dark, the *cis* isomer remained much more stable showing that after 24 hours **2.51** had still not relaxed back to where the *trans* isomer was most abundant as shown in **Figure 2-21**. Most importantly, after 6 hours, there was negligible change in the UV-Vis spectrum, highlighting the stability of the *cis* isomer over this period of time. These UV-Vis results demonstrated that peptides **2.51**-**2.56** were sufficiently stable in the *cis* isomer

for PD-1/PD-L1 inhibition assaying which in this case was one hour of incubation time.

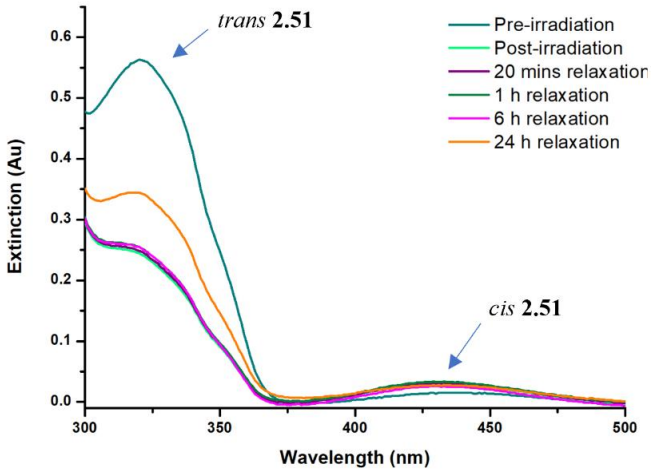


Figure 2-21 *UV/Vis spectra for* ***2.51*** *after being irradiated for 20 minutes and being kept in the dark while taking time interval readings showing that after 24 hours* ***2.51*** *remained predominantly in the cis isomer.*

2.4.6 Photo stability of azobenzene peptides

The photo-stability of AP1-6 to repeated light exposures, known as photo-cycling, is essential for potential application as a controllable inhibitor of PD-1/PD-L1. Repeated cycles of illumination have the potential to cause degradation of the azobenzene compound. To ensure peptides **2.51**-**2.56** were stable through repeated irradiation cycles, they were repeatedly illuminated at 365 nm and 465 nm under continuous monitoring of UV absorbance band at 330 nm. All peptides yielded a consistent absorbance at 330 nm over 10 cycles, demonstrating photostability as seen with AP1 in **Figure 2-22**.

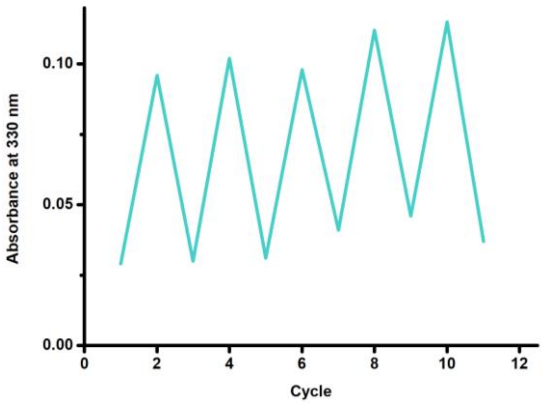


Figure 2-22 *UV-Vis showing* ***2.53*** *absorbance at 330 nm over 10 cycles after 20 min irradiation at 365 nm, and then isomerisation for 20 min exposed to white light to demonstrate photo-stability.*

2.4.7 Peptides 2.51-2.56's ability to inhibit PD-1/PD-L1

To determine the ability of peptides **2.51**-**2.56** to inhibit the interaction between PD-1/PD-L1 the HTRF assay was used (**Figure 2-16**). Each peptide was dissolved in PPI-Europium detection buffer with 5% DMSO at a concentration of 100 µM and irradiated separately at 365 nm for 30 mins to obtain the respective *cis* isomer. Of the six peptides that were tested in the assay, only **2.51** showed the ability to inhibit the interaction. A dose response curve determined an IC_{50} of 0.3 µM [0.15, 0.56], while showing limited inhibition in the unirradiated sample at various concentrations (**Figure 2-23**). This assay data demonstrates that **2.51** inhibits the PD-1/PD-L1 interaction and a similar IC_{50} to CLP003, while the unirradiated sample showed no inhibition. Due to the *trans:cis* isomer ratio it would have been expected to see some inhibition when testing *trans* **2.51**. This suggests that perhaps there was solubility issues at higher concentrations that led to no activity being seen, or variations in light source quality when assaying compared to evaluation of isomerisation. Further investigation is underway to determine this unexpected result.

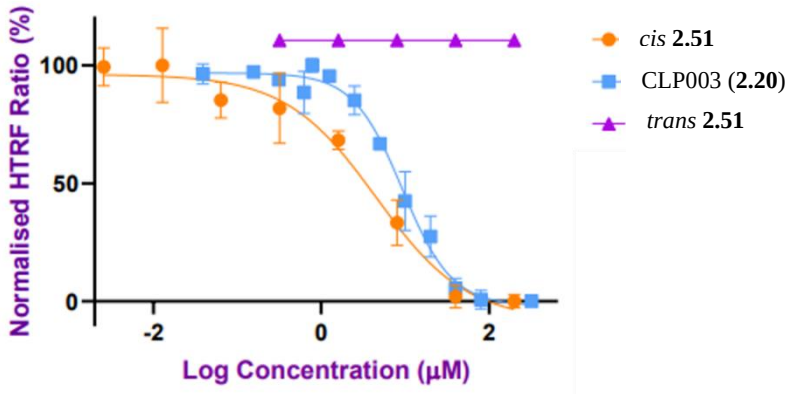


Figure 2-23 *Dose dependent curve of cis* ***2.51*** *(IC_{50} of 0.3 µM [0.15,0.56]) (orange), trans* ***2.51*** *(purple) and CLP003 (IC_{50} = 8 µM [0.72,0.11] (blue). Errors are SEM, n/N = 2/6.*

2.4.8 Thermal stability of 2.51

As the *trans* isomer is the more thermally stable configuration, there was concern that during the cellular assay incubation at 37 °C would cause the azobenzene modified peptide to relax back to be predominantly in the *trans* isomer. To determine whether **2.51** was thermally stable to continue with cellular assays, **2.51** was incubated at 37 °C over 8 hours after irradiation at 365 nm for 15 minutes in PPI-Europium detection

buffer. The peptide was monitored every hour *via* analytical HPLC and showed no degradation while remaining 65:25 majority *cis* isomer throughout the whole 8 hours.

2.4.9 The cellular inhibition of PD-1/PD-L1 by 2.51

Due to the low micromolar IC_{50} of the *cis* isomer of **2.51**, it was hypothesized that this compound should be active at the cellular level. To test this, **2.51** was tested in a PD-1/PD-L1 cell-based assay purchased from InvivoGen. This assay relies on Jurkat T-cells that are engineered to express luciferase *via* T-cell receptor (TCR) signalling and Raji cells engineered to express PD-L1 on the cell surface. The luciferase reporter gene is controlled under NFAT response elements that enables the monitoring of T-cell activation when PD-1/PD-L1 is inhibited. If PD-L1 is bound to PD-1, the luciferase expression is inhibited. If the interaction is inhibited, TCR signalling causes luciferase expression. Luciferase activity is then measured by measuring luminescence after the addition of luciferase substrate. Due to this, the assay readout is indirect and as such any unintended side effects that results in NFAT activation may produce a luminescent response.

As shown in **Figure 2-24**, at the higher concentrations the *cis* isomer of **2.51** (purple) exhibits greater inhibitory activity of PD-1/PD-L1 than the *trans* isomer (pink), most strikingly at 100 μM and 10 μM. Pleasingly, the *cis* isomer of **2.51** demonstrates a greater inhibitory effect than the parent peptide CLP003, **2.20**. These results suggest that by incorporating a turn mimic into the structure of the linear peptide, this can increase inhibition and thereby the binding affinity. Furthermore, they prove that upon irradiation, the *cis* isomer inhibits PD-1/PD-L1 more effectively than the *trans* isomer providing a photo-controlled inhibitor for PD-1/PD-L1.

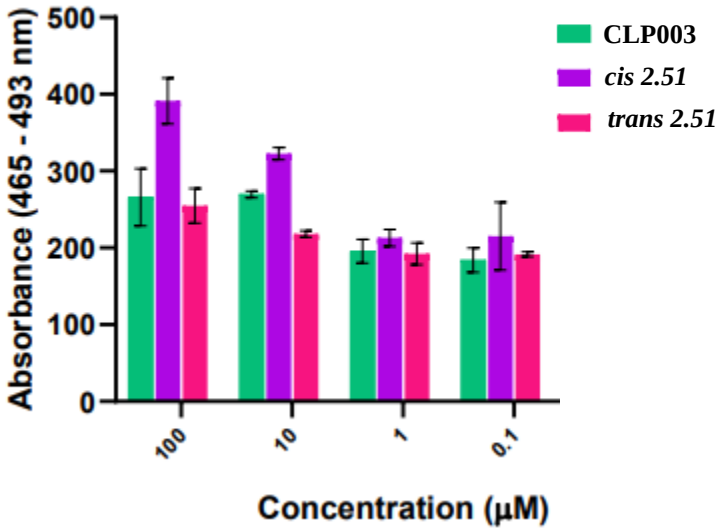


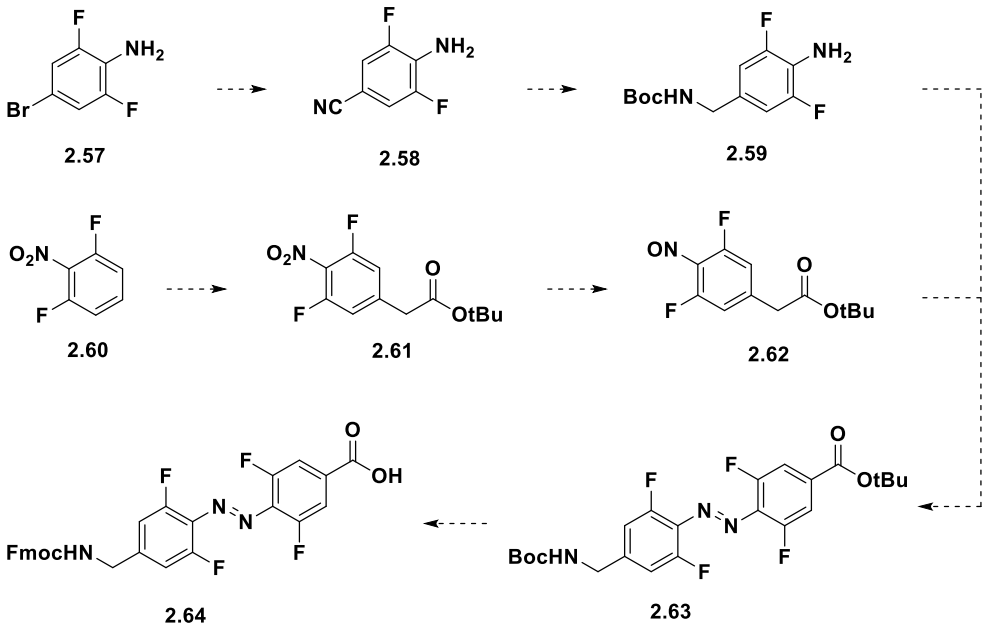
Figure 2-24 *PD-1/PD-L1 cell-based assay results showing the cis isomer of* ***2.51*** *being more a more effective inhibitor than trans isomer of* ***2.51****. Errors are SEM, n/N = 2/6.*

2.5 Work towards red-light photo-switches

While AMPP is controlled *via* UV light, photo-control of biological systems is more efficient with visible wavelengths.[63] Particularly photo-switches that are triggered between 600-900 nm, known as the "therapeutic window".[64] These wavelengths allow for deeper tissue penetration of the soft tissues in humans.[64] In an effort to make an azobenzene peptide that is switchable within this range, the synthesis of an azobenzene derivative modified with fluorine atoms was attempted. While adding fluorine atoms to an azobenzene is not uncommon, creating a compound that could be used in the backbone of a peptide in conjugation with SPPS with an Fmoc protected amine functional group on one side and a carboxylic acid on the other has yet to be reported.[65,66]

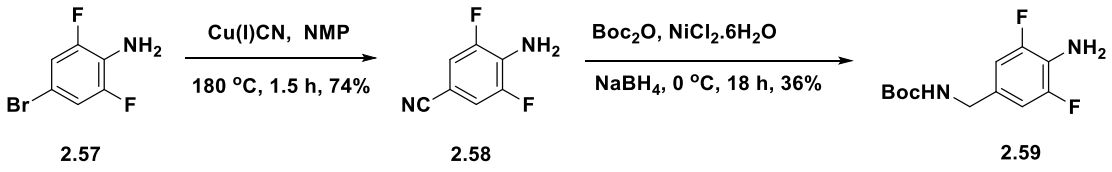
Initially a similar synthetic pathway as AMPP, **2.20**, was proposed whereby two precursors would be made (**Scheme 2-6**). One precursor would be functionalised with a nitroso group **2.62** and one with an amine group **2.59** that could form the azobenzene bond under acidic conditions. To synthesise **2.59,** cyanation of the aryl bromide will be utilised.[67] Once the nitrile is established it will be reduced catalysed by nickel chloride, and protected using a tert-butyloxycarbonyl (Boc) group.[68] For the second precursor, **2.61** will be synthesised from **2.60** *via* vicarious nucleophilic substitution to give a tert-butyl protected carboxylic acid.[69–71] **2.61** will then undergo reduction of the nitro group to form a nitroso functional group, **2.62**. After the synthesis of **2.59** and

2.62, these will then be stirred in acetic acid to form the azobenzene as previously discussed through the mechanism shown in **Scheme 2-5**. As both the amine and the carboxylic acid will be functionalised with acid labile groups, they will be deprotected at the same time and the amine will undergo Fmoc protection for suitability to be used in SPPS.



Scheme 2-6 *The proposed pathway to synthesise a fluorinated azobenzene suitable for SPPS.*

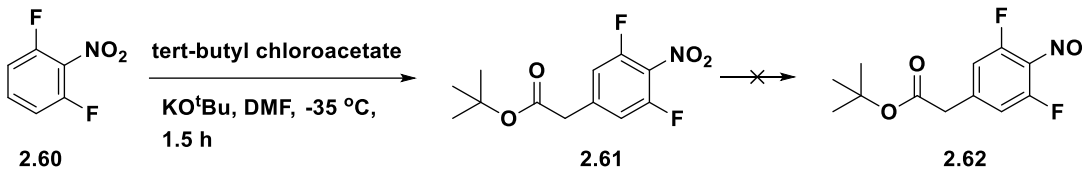
To form the amine derivative precursor **2.59**, 4-bromo-2,4-difluoroaniline, **2.57**, was refluxed with copper (I) cyanide in NMP. This reaction is known as the Rosenmund-von Braun reaction and it prepares the aryl nitrile **2.58** through the cyanation of the aryl bromide **2.57** with an excess of copper (I) cyanide in a polar high-boiling solvent, NMP.[67,72] The next step was to reduce the nitrile to an amine using nickel chloride hexahydrate, Boc anhydride, and sodium borohydride to give a light brown solid with a yield of 36%.[68]



*Scheme 2-7 The Rosenmund-von Braun reaction using copper(I) cyanide to form the nitrile product **2.58**, this was then further reduced using nickel chloride hexahydrate and Boc protected to give the product **2.58**.*

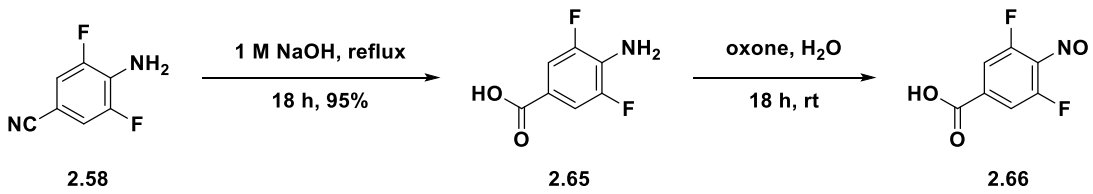
When attempting to synthesise the nitroso functionalised precursor **2.62** there were some challenges. The first step was adding a *tert*-butyl protected carboxylic ester to

2,6-difluoronitrobenzene, **2.60**. Potassium *tert*-butoxide was added to 2,6-difluoronitrobenzene and *tert*-butyl chloroacetate resulting in vicarious nucleophilic substitution of the chlorine to give **2.61** (**Scheme 2-8**).[69–71] However, after purification the yield was less than 15% and impurities remained as seen by ^{1}H NMR. As fluorine is *ortho/para* directing, this could impact the product formation in the *meta* position and potentially could account for this low yield. Due to this and success found in an alternative method, the reduction to the nitroso was not attempted using this method.



Scheme 2-8 *The vicarious nucleophilic substitution of tert-butyl chloroacetate to give the product **2.61**.*

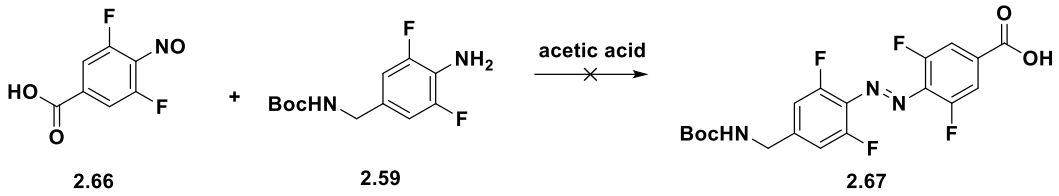
The alternative approach utilised the already synthesised 4-amino-3,5-difluorobenzonitrile **2.58**. The hydrolysis of the nitrile was achieved by refluxing **2.58** in NaOH overnight to give **2.65** as a white solid with a 95% yield (**Scheme 2-9**).[73] The carboxylic acid functional group was confirmed using ^{1}H NMR showing a singlet at 12.69 ppm. **2.65** was then oxidised to form the nitroso group **2.66** using oxone in water overnight (**Scheme 2-9**).[74] There were some solubility issues with the starting material, so a minimal amount of DCM was added. The reaction was monitored *via* TLC and confirmed using high resolution mass spectrometry showing a *m/z* of 188.0158, corresponding to $[M+H]^+$ of 188.0159. This compound proved not stable and needed to be kept under argon and at −20°C to prevent degradation.



Scheme 2-9 *Alternative approach to form the nitroso product with an carboxylic acid functional group **2.67**. The hydrolysis of **2.58** with sodium hydroxide to give the product **2.65**, this underwent oxidation of the amine to form a nitroso in **2.66**.*

With both starting materials in hand, **2.66** and **2.59** were stirred in acetic acid overnight under N_2 to form a brown solid (**Scheme 2-10**). However, upon analysis there was no evidence to suggest that the azobenzene had formed. This could be due to the electron withdrawing fluorine atoms affecting the nucleophilic ability of the amine effecting

the formation of the azobenzene. Furthermore, the stability of **2.66** could also impact the formation of the product.



Scheme 2-10 *The proposed reaction between* ***2.66*** *and* ***2.59*** *to form the azobenzene* ***2.67****.*

2.6 Conclusion

In the search for an improved novel inhibitor for PD-1/PD-L1, including a turn structure has shown to be advantageous when targeting PD-1/PD-L1 due to their β-strand and β-sheet structures.[75] One such turn inducing method is the inclusion of an azobenzene into a peptide structure. In determining a design for the insertion of the azobenzene, an alanine scan of the peptide CLP003, **2.4**, revealed that residues Tyr5, peptide **2.30**, and Trp7, peptide **2.32**, were not essential for inhibiting PD-1/PD-L1. Furthermore, both peptides showed better inhibition of PD-1/PD-L1 using the HTRF assay than CLP003 (IC_{50} = 8 μM [0.72, 0.11]), with **2.30** having an IC_{50} of 0.052 μM [0.028, 0.016] and **2.32** having an IC_{50} of 0.025 μM [0.013, 0.052] (**Figure 2-18**). Six peptides in total were designed and synthesised based on the alanine scan results. The azobenzene peptide **2.51** showed photo-controllable inhibition of PD-1/PD-L1 through the induction of a turn mimic *via* irradiation. In a dose dependent curve of the irradiated **2.51**, an IC_{50} of 0.3 μM [0.15, 0.56] was concluded with the *trans* isomer showing limited inhibition at various concentrations. However, due to the ratio of the *cis:trans* isomer some inhibition should be expected and as such the *trans* isomer should be retested at lower concentrations to confirm the difference in inhibition between the isomers. To determine the effectiveness of **2.51** in cells, a PD-1/PD-L1 cell-based assay was used. The results from the HTRF assay were replicated where after irradiation, **2.51** in the *cis* isomer showed greater inhibition of PD-1/PD-L1 than the *trans* isomer. Not only did **2.51** show selective inhibition through photo-switching behaviour, the *cis* isomer of **2.51** pleasingly showed better inhibition than the original peptide CLP003, **2.4**. To date, there have been no published photo-switchable inhibitors for PD-1/PD-L1. In comparison to the previously mentioned peptide inhibitors of PD-1/PD-L1 in section 2.1.2, **2.51** stands as a good starting compound for further modifications to improve the binding affinity. Further biorthogonal assays

are required to prove *cis* **2.51** binds to PD-L1 while the *trans* isomer shows limited activity. Incomplete SPR work due to time constraints requires optimisation of the method and would be a good indicator of **2.51**'s affinity for PD-L1.

The future work following on from this research could include obtaining a crystal structure of both CLP003, **2.4**, and **2.51**. The direct comparison of these compounds and how the amino acids interact with PD-L1 could provide a clearer picture for further modifications to improve the inhibitory activity. Testing both **2.30** and **2.32** in the cell-based assay described in section 2.4.9 would also be interesting by determining whether the improved potency from the HTRF assay would translate at the cellular level. To combat potential false positives found within the cell-based assay, further screening within a T-cell based assay for evaluating biological functions could be included. To improve **2.51**, this could include the incorporation of a photo-switch that is within the "therapeutic window", 400-600 nm. The fluorinated azobenzene synthesis in section 2.5 could be continued to create a compound suitable for SPPS. A strategy to improve the synthesis could be to attach the precursor **2.58** to the peptide and then form the azobenzene bond, potentially increasing the stability.[67] Other fluorinated compounds have also been reported and could possibly be used to insert into the backbone of CLP003 to create a red-light photo-switchable peptide.[66,67]

2.7 Experimental

2.7.1 Materials and solvents

All chemicals were purchased from Sigma Aldrich, Fisher Scientific or Fluorochem unless otherwise specified. Fmoc-amino acids and coupling agents were purchased from Novabiochem, Fluorochem or AGTC Bioproducts.

2.7.2 Instrumental techniques

^{1}H-, ^{13}C-NMR, ^{19}F- were collected using a Bruker spectrometer operating at 400 MHz (^{1}H), 101 MHz (^{13}C) or 376 MHz (^{19}F) using the specified deuterated solvent. The chemical shifts were recorded in ppm and were referenced to the residual solvent peak of DMSO (2.50 ppm) or chloroform (7.26 ppm). Multiplicities in the NMR spectra are described as s = singlet, d = doublet, t = triplet, q = quartet, m = multiplet, and combinations thereof. Coupling constants are reported in Hz.

High resolution masses were recorded using Waters Synapt XS QTOF under electrospray ionisation. Low resolution mass was recorded using an Agilent 1200 Series equipped with a 6460 triple quadrupole. MALDI-MS was performed on a Kratos Analytical Axima-CFR MALDI ToF, using cyano-4-hydroxycinnamic as the matrix.

Analytical RP-HPLC was performed using an Agilent 1200 HPLC, fitted with an Agilent eclipse XDB-C18 column (4.6 x 150 mm, 5 μm) and a flow rate of 1 mL/min. Spectra were run with a solvent gradient of 0-100% B over 20 min. Solvent A: H_2O, 0.05% TFA, solvent B: MeCN, 0.05% TFA. Detection wavelengths were 214 nm and 254 nm. Preparative RP-HPLC was performed using an Agilent 1200 HPLC, fitted with an Agilent eclipse XDB-C18 column (21.2 x 150 mm, 5 μM) and a flow rate 20 mL/min. Spectra were run with a solvent gradient of 0-100% B over 15 min. Solvent A: 95% H_2O, 5% MeCN, 0.05% TFA, solvent B: 95% MeCN, 5% H_2O, 0.05% TFA. Detection wavelengths were 214 nm and 254 nm.

Automated peptide synthesis was performed using a Biotage I.

UV-vis spectra were recorded on an Agilent Cary 60 spectrometer, using quartz cuvettes with 1 cm pathlength. Fluorescence spectra were recorded on a Horiba Jobin Yvon Fluorolog spectrometer, using quartz cuvettes with a 1 cm pathlength. Infrared spectra were recorded on a PerkinElmer BX with an ATR attachment.

Human PD-1/PD-L1 biochemical binding assay was purchased from Revvity. Anti-PD-1/PD-L1 cell-based assay was purchased from InvivoGen. Microplate spectral scans were recorded on a CLARIOstar (BMG Labtech) microplate reader and used following manufacturer's protocols.

2.7.3 Solid phase peptide synthesis

The twelve amino acid CLP003 peptide, **2.4**, (Ac-WHFSYNWRWLPP-NH_2) and the azobenzene substituted peptides (**2.51**-**2.56**) were synthesised on TentaGel S RAM resin (resin loading 0.23 mmol/g) using an automated peptide synthesiser. The AMPP unit was coupled identically as other amino acids. 100 mg of Tentagel resin (0.023 mmol) was suspended in DMF (2 mL) and allowed to swell for 20 minutes. The DMF was drained from the peptide vessel and Fmoc deprotection was carried out by addition of 2 x 2 mL of 20% piperidine in DMF, which was shaken for 10 minutes. This was

removed and the resin was washed with DMF (3 x 2 mL). The resin was then treated with a solution of Fmoc-Pro-OH (4 equiv. compared to resin loading), to which HBTU (3.9 equiv.) and HOBt (4 equiv.) and DIPEA (8 equiv.) in DMF were added. The mixture was then shaken for 30 min. The vessel was drained and the resin washed with DMF (3 x 2 mL). The coupling reaction was then repeated followed by Fmoc deprotection (2 x 2 mL 20% piperidine in DMF, 10 min) and finally the resin was washed with DMF. Subsequent amino acids were coupled in an identical fashion. After the final amino acid coupling reaction (tryptophan) and Fmoc deprotection, the resin was treated with acetic anhydride (4 equiv.) and DIPEA (3.9 equiv.) in DMF and reacted for 45 minutes. The resin was washed with DCM (x 3) and MeOH (x 3) to remove any residual DMF.

2.7.3.1 CLP003 and alanine substituted peptides

The general procedure above was followed. Once synthesised the peptide was cleaved from the resin using 95:2.5:2.5 TFA:H_2O:TIPS (5 mL) and shaken for three hours. The resulting solution was extracted and the resin was washed with TFA (3 x 1 mL), the solutions were combined and concentrated under vacuum. The peptide was precipitated using cold diethyl ether and filtered. The peptide was purified to >98% purity using preparative RP-HPLC and concentrated under vacuum to yield a white solid (3.6 mg, 2.1 µmol, 9%). RP-HPLC: t_R = 11.98 min. MALDI-ToF $[M+H]^+$ *m/z* calcd. for $[C_{88}H_{109}N_{22}O_{16}]^+$ 1729.83, found 1729.09.

This was repeated for the twelve alanine scanned peptides:

2.26: Ac-AHFSYNWRWLPP-NH_2 (1.7 mg, 1.1 µmol, 4%). RP-HPLC: t_R = 11.27 min. MALDI-ToF $[M+H]^+$ *m/z* calcd. for $[C_{80}H_{105}N_{21}O_{16}]^+$ 1614.78, found 1614.83.

2.27: Ac-WAFSYNWRWLPP-NH_2 (2.9 mg, 1.7 µmol, 7%). RP-HPLC: t_R = 11.33 min. MALDI-ToF $[M+H]^+$ *m/z* calcd. for $[C_{86}H_{108}N_{19}O_{16}]^+$ 1662.81, found 1663.55

2.28: Ac-WHASYNWRWLPP-NH_2 (2.6 mg, 1.6 µmol, 7%). RP-HPLC: t_R = 11.33 min. MALDI-ToF $[M+H]^+$ *m/z* calcd. for $[C_{83}H_{105}N_{21}O_{16}]^+$ 1652.80, found 1653.87

2.29: Ac-WHFAYNWRWLPP-NH_2 (2.7 mg, 1.6 µmol, 7%). RP-HPLC: t_R = 11.08 min. MALDI-ToF $[M+H]^+$ *m/z* calcd. for $[C_{89}H_{110}N_{21}O_{15}]^+$ 1711.84, found 1712.64.

2.30: Ac-WHFSANWRWLPP-NH_2 (3 mg, 1.3 µmol, 8%). RP-HPLC: t_R = 11.84 min. MALDI-ToF $[M+H]^+$ *m/z* calcd. for $[C_{83}H_{106}N_{21}O_{15}]^+$ 1635.81, found 1636.54.

2.31: Ac-WHFSYAWRWLPP-NH_2 (4.2 mg, 2.5 µmol, 11%). RP-HPLC: t_R = 11.82 min. MALDI-ToF $[M+H]^+$ *m/z* calcd. for $[C_{87}H_{108}N_{21}O_{15}]^+$ 1686.83, found 1686.38.

2.32: Ac-WHFSYNARWLPP-NH_2 (2.7 mg, 1.7 µmol, 7%). RP-HPLC: t_R = 12.33 min. MALDI-ToF $[M-H]^+$ *m/z* calcd. for $[C_{80}H_{104}N_{21}O_{16}]^-$ 1613.78, found 1613.30.

2.33: Ac-WHFSYNWAWLPP-NH_2 (1.3 mg, 0.79 µmol, 4%). RP-HPLC: t_R = 12.38 min. MALDI-ToF $[M-H]^+$ *m/z* calcd. for $[C_{85}H_{101}N_{19}O_{16}]^-$ 1643.77, found 1643.73.

2.34: Ac-WHFSYNWRALPP-NH_2 (2.3 mg, 1.4 µmol, 6%). RP-HPLC: t_R = 11.21 min. MALDI-ToF $[M-H]^+$ *m/z* calcd. for $[C_{80}H_{104}N_{21}O_{16}]^-$ 1613.78, found 1613.60.

2.35: Ac-WHFSYNWRWAPP-NH_2 (1.9 mg, 1.1 µmol, 5%). RP-HPLC: t_R = 11.46 min. MALDI-ToF $[M+H]^+$ *m/z* calcd. for $[C_{85}H_{103}N_{22}O_{16}]^+$ 1687.78, found 1687.75.

2.36: Ac-WHFSYNWRWLAP-NH_2 (2.6 mg, 1.5 µmol, 6%). RP-HPLC: t_R = 11.86 min. MALDI-ToF $[M+H]^+$ *m/z* calcd. for $[C_{88}H_{108}N_{22}O_{16}]^+$ 1703.81, found 1703.28.

2.37: Ac-WHFSYNWRWLPA-NH_2 (3.1 mg, 1.3 µmol, 8%). RP-HPLC: t_R = 11.89 min. MALDI-ToF $[M+H]^+$ *m/z* calcd. for $[C_{88}H_{108}N_{22}O_{16}]^+$ 1703.81, found 1703.11.

*2.7.3.2 Peptides **2.51-2.56***

The general procedure above was followed. Once synthesised the peptide was cleaved from the resin using 95:2.5:2.5 TFA:H_2O:TIPS (5 mL) and shaken for 2 h after which the cleavage cocktail was drained into a round bottom flask. The resin was washed with TFA (3 x 1 mL) and the solutions combined and concentrated in vacuo. The peptide was precipitated using cold diethyl ether and filtered. The peptide was purified using RP-preparative HPLC.

2.51: *trans*-Ac-WHFSYN-AMPP-RWLPP-NH_2 (9.4 mg, 5.2 µmol, 22%). RP-HPLC: t_R = 12.50 min. MALDI-ToF $[M+H]^+$ *m/z* calcd. for $[C_{80}H_{105}N_{21}O_{16}]^+$ 1794.85, found 1794.53.

2.52: *trans*-Ac-WHFS-AMPP-NWRWLPP-NH_2 (7.5 mg, 4.5 µmol, 17%). RP-HPLC: t_R = 11.36 min. MALDI-ToF $[M+H]^+$ *m/z* calcd. for $[C_{80}H_{105}N_{21}O_{16}]^+$ 1817.87, found 1817.62.

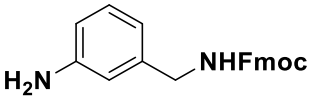
2.53: *trans*-Ac-WHFSN-AMPP-RWLPP-NH_2 (6.2 mg, 3.3 µmol, 16%). RP-HPLC: t_R = 12.50 min. MALDI-ToF $[M+H]^+$ *m/z* calcd. for $[C_{80}H_{105}N_{21}O_{16}]^+$ 1631.79, found 1631.50.

2.54: *trans*-Ac-WHFS-AMPP-NRWLPP-NH_2 (6.9 mg, 4.2 µmol, 18%). RP-HPLC: t_R = 12 min. MALDI-ToF $[M+H]^+$ *m/z* calcd. for $[C_{80}H_{105}N_{21}O_{16}]^+$ 1631.79, found 1631.23.

2.55: *trans*-Ac-WHFSn-AMPP-RWLPP-NH_2 (4.3 mg, 2.6 µmol 11%). RP-HPLC: t_R = 11.5 min. MALDI-ToF $[M+H]^+$ *m/z* calcd. for $[C_{80}H_{105}N_{21}O_{16}]^+$ 1631.79, found 1631.84.

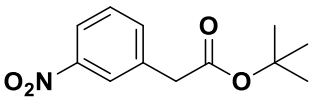
2.56: *trans*-Ac-WHFS-AMPP-nRWLPP-NH_2 (3.8 mg, 2.3 µmol, 10%). RP-HPLC: t_R = 11.4 min. MALDI-ToF $[M+H]^+$ *m/z* calcd. for $[C_{80}H_{105}N_{21}O_{16}]^+$ 1631.79, found 1631.34.

2.7.4 Synthesis of AMPP



2.43

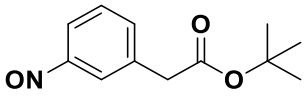
Compound **2.43** was prepared following a published protocol.[60] A solution of Fmoc-OSu (3.4 g, 10 mmol) in acetonitrile (25 mL) was added dropwise to a mixture of 3-aminobenzylamine (1.2 g, 10 mmol) and triethylamine (1.4 mL/1.0 g, 10 mmol) in acetonitrile/DMF (10:1, 22 mL). After 1 h of stirring at room temperature, the reaction mixture was precipitated with water to form a white solid. The precipitant was filtered and washed with diethyl ether/trifluoroethanol (1:1, 30 mL) to form a white solid (1.92 g, 5.57 mmol, 56%). The data matched that observed in the literature.[60] Mp: 142-143 °C. ^{1}H NMR (400 MHz, DMSO-d_6) δ 7.89 (d, *J* = 7.5 Hz, 2H), 7.76 (t, *J* = 6.2 Hz, 1H), 7.71 (d, *J* = 7.4 Hz, 2H), 7.42 (t, *J* = 7.4 Hz, 2H), 7.33 (t, *J* = 7.5 Hz, 2H), 6.94 (t, *J* = 7.7 Hz, 1H), 6.46 (m, 1H), 6.42 (d, *J* = 8.1, 1H), 6.38 (d, *J* = 7.5 Hz, 1H), 5.01 (s, 2H), 4.30 (d, *J* = 7.0 Hz, 2H), 4.22 (t, *J* = 6.9 Hz, 1H), 4.04 (d, *J* = 6.1 Hz, 2H).^{13}C NMR (101 MHz, DMSO) δ 157.0, 148.6, 144.0, 140.8, 140.3, 128.8, 127.7, 127.1, 125.3, 120.1, 114.6, 112.6, 112.5, 65.5, 46.8, 44.1. ESI-QQQ $[M+H]^+$ *m/z* calc. for $[C_{22}H_{21}N_2O_2]^+$ 345.15; found 345.30.



2.42

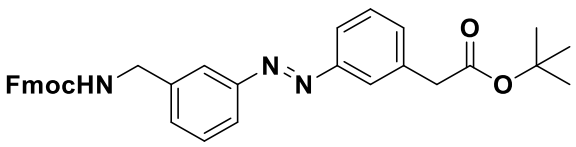
Compound **2.42** was prepared following a published protocol.[60] To a solution of 3-nitrophenylacetic acid (2 g, 10 mmol) in *tert*-butanol (50 mL) was added Boc_2O (4.8 g, 22 mmol) and DMAP (0.4 g, 0.003 mmol). After 1 hour, the solvent was removed under vacuum leaving a dark brown oil. The crude product was redissolved in DCM and purified using a silica plug with 10% ethyl acetate in hexane to yield a yellow oil (quant.). The data matched that observed in the literature.[60] ^{1}H NMR (400 MHz, Chloroform-*d*) δ 8.13 (s, 1H), 8.09 (t, *J* = 8.2 Hz, 1H), 7.59 (d, *J* = 7.6, 1H), 7.47 (t, 7.8 Hz, 1H), 3.62 (s, 2H), 1.43 (s, 9H). ^{13}C NMR (101 MHz, $CDCl_3$) δ 169.7, 148.3,

136.6, 135.7, 129.4, 124.4, 122.1, 81.7, 42.0, 28.0. ESI-QQQ $[M+H]^+$ *m/z* calc. for $[C_{12}H_{16}NO_4]^+$ 237.1; found 238.2.



2.43

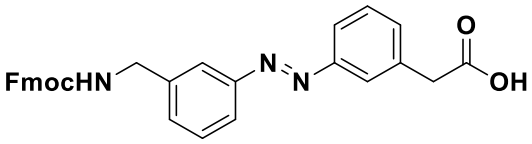
Compound **2.43** was prepared following a published protocol.[60] **2.42** (2.50 g, 10.5 mmol) was dissolved in 2-methoxyethanol (60 mL) and NH_4Cl (0.85 g, 16 mmol) in 20 mL of H_2O was added. The resulting solution was degassed with argon for 1 h. With vigorous stirring, zinc (2.0 g, 31 mmol) was added over the course of 1 h. The reaction was monitored by TLC (25% ethyl acetate in hexane). After the starting material had disappeared, the reaction was filtered over celite and washed with methoxyethanol (2 x 10 mL). The filtrate was then added dropwise to iron (III) chloride hexahydrate (5.7 g, 21 mmol) in 80 mL of H_2O/EtOH (2:1 vol/vol) cooled to -10 °C. After stirring for 1 h, the reaction was poured into ice cold water with vigorous stirring and extracted with ethyl acetate (x 3). The collected organic layers were dried with Na_2SO_4 and concentrated under vacuum to give a green oil that was continued to the next step without purification. The data matched that observed in the literature.[60] Rf 0.23 (25% ethyl acetate in hexane). HRMS (ESI-) $[M+H]^+$ *m/z* calc. for $[C_{12}H_{15}NO_3]^+$ 222.1052; found 222.1096.



2.45

Compound **2.45** was prepared following a published protocol.[60] To a solution of **2.40** (2.25 g, 10.18 mmol) in acetic acid (50 mL), **2.43** (3.5 g, 10.2 mmol) in acetic acid (50 mL) was added dropwise under N_2 and left to stir overnight. The solvent was removed and purified using a silica gel column chromatography (25% ethyl acetate in hexane) to give an orange oil (3.12 g, 5.70 mmol, 56%). The data matched that observed in the literature.[60] Rf 0.25 (30% ethyl acetate in hexane). ^{1}H NMR (400 MHz, Chloroform-*d*) δ 7.87 – 7.81 (m, 4H), 7.76 (d, *J* = 7.6 Hz, 2H), 7.61 (d, *J* = 7.5 Hz, 2H), 7.53 – 7.44 (m, 3H), 7.44 – 7.37 (m, 4H), 7.31 (t, *J* = 7.5 Hz, 2H), 5.24 (bs, 1H), 4.56 – 4.33 (m, 4H), 4.25 (t, *J* = 6.8 Hz, 1H), 3.64 (s, 2H), 1.46 (s, 9H). ^{13}C NMR (101 MHz, $CDCl_3$)

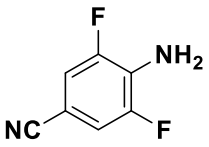
δ 170.7, 156.6, 153.0, 152.8, 144.0, 141.5, 140.0, 136.0, 132.1, 130.2, 129.6, 129.3, 127.8, 127.2, 125.2, 123.6, 122.5, 122.0, 121.5, 120.1, 81.3, 66.9, 47.4, 45.0, 42.5, 28.2, 28.0. ESI-QQQ $[M+H]^+$ *m/z* calc. for $[C_{34}H_{34}N_3O_4]^+$ 548.3; found 548.4.



2.19

Fmoc-AMPP, **2.19**, (3.12 g, 5.70 mmol) was prepared following a published protocol.[60] Compound **2.45** was dissolved in DCM (40 mL) and treated with TFA (10 mL) dropwise. The reaction mixture was left to stir overnight under N_2. The mixture was then washed with water until pH was neutral, then washed with brine and dried with Na_2SO_4 before being concentrated under vacuum to give an orange solid (2.7 g, 5.5 mmol, 98%). The data matched that observed in the literature.[60] ^{1}H NMR (400 MHz, DMSO-d_6) δ 12.45 (bs, 1H), 8.00 (t, *J* = 6.2 Hz, 1H), 7.89 (d, *J* = 7.4 Hz, 2H), 7.81-7.75 (m, 4H), 7.71 (d, *J* = 7.5 Hz, 2H), 7.58-7.53 (m, 2H), 7.48-7.37 (m, 4H), 7.31 (t, *J* = 7.5 Hz, 2H), 4.37 (d, *J* = 6.6 Hz, 2H), 4.32 (d, *J* = 6.1 Hz, 2H), 4.25 (t, *J* = 7 Hz, 1H), 3.74 (s, 2H). ^{13}C NMR (101 MHz, DMSO) δ 172.5, 156.4, 152.0, 151.9, 143.9, 141.4, 140.8, 136.6, 132.7, 130.2, 129.4, 129.3, 127.6, 127.1, 125.2, 123.1, 121.6, 121.4, 120.5, 120.1, 65.4, 46.8, 43.5. ESI-QQQ $[M+H]^+$ *m/z* calc. for $[C_{30}H_{26}N_3O_4]^+$ 492.2; found 492.2.

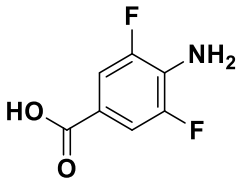
2.7.5 Synthesis of fluorinated AMPP



2.58

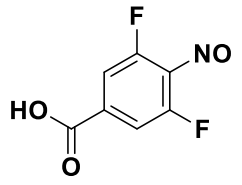
Compound **2.58** was prepared following a published protocol.[76] 4-bromo-2,6-difluoroaniline (10 g, 48 mmol) and copper (I) cyanide (6.7 g, 75 mmol) were suspended in NMP and refluxed for 1.5 h. Once cooled to room temperature, 1,2-diaminoethane (50 mL) was added and the mixture was poured into water (200 mL). The mixture was extracted with ethyl acetate (x 3). The collected organic layers were washed with 10% wt 1,2-diaminoethane in water (x 2), water (x 1) and dried with

Na_2SO_4 before being concentrated under vacuum. The crude product was purified *via* flash column chromatography with 10% ethyl acetate in hexane to give a pale yellow-brown solid (5.48 g, 35.6 mmol, 74%). Rf 0.38 (DCM/hexane 2:1). The data matched that observed in the literature.[76] ^{1}H NMR (400 MHz, DMSO-d_6) δ 7.48 (dd, J = 6.6, 2.6 Hz, 2H), 6.34 (s, 2H). ^{19}F NMR (376 MHz, DMSO-d_6) δ -131.41. ESI-QQQ $[M-H]^-$ *m/z* calcd. for $[C_7H_4F_2N_2]^+$ 154.0, found 154.6.



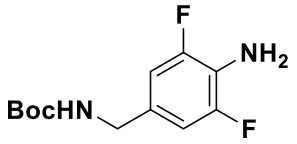
2.65

Compound **2.65** was prepared following a published protocol.[73] The 4-amino-3,5-difluorobenzonitrile **2.58** (100 mg, 0.600 mmol) was suspended in 1 M NaOH (3.2 mL) was refluxed overnight. The reaction mixture was cooled to room temperature and acidified with 1 M HCl. The resulting precipitant was filtered, washed with water and dried to give a white solid (94 mg, 0.54 mmol, 92%). Rf 0.36 (30% acetone in hexane on silica). The data matched that observed in the literature.[73] ^{1}H NMR (400 MHz, DMSO-d_6) δ 12.70 (s, 1H), 7.39 (dd, J = 7.2, 2.6 Hz, 2H), 6.06 (s, 2H). ^{13}C NMR (101 MHz, DMSO) δ 166.0 (t, J = 3.2 Hz, 1C), 151.0 (d, J = 9.6 Hz, 1C), 148.6 (d, J = 9.6 Hz, 1C), 130.6 (t, J = 16.9 Hz, 1C), 115.6 (t, J = 8 Hz, 1C), 112.4 (m, 2C), 59.7 (s, 1C), 14.1 (s, 1C). ESI-QQQ $[M+H]^+$ *m/z* calcd. for $[C_7H_6F_2NO_3]^+$ 174.0, found 174.2.



2.66

Compound **2.66** was prepared following a published protocol.[74] **2.65** (100 mg, 0.6 mmol) was added to an aqueous solution of oxone (178 mg, 0.78 mmol) alongside a minimal amount of DCM (2 µL). The reaction was stirred vigorously and monitored *via* TLC (30% acetone in hexane). Once the reaction had gone to completion, the resulting precipitant was filtered, washed with water and dried to give a white solid. Rf 0.19 (30% acetone in hexane). HRMS (ESI-) $[M+H]^+$ *m/z* calcd. for $[C_7H_4F_2NO_3]$ 188.0159, found 188.0158.



2.59

Compound **2.59** was prepared following a published protocol.[68] 4-amino-3,5-fluorobenzonitrile **2.58** (200 mg, 1.86 mmol) was dissolved in anhydrous methanol (12 mL) and cooled to 0 °C in an ice bath. Nickel(II) chloride hexahydrate (0.035 mg, 2.17 mmol) and di-tert-butyl dicarbonate (378 µL, 355 mg, 1.63 mmol) were both added, followed by sodium borohydride (288 mg, 7.60 mmol) over 15 mins. The reaction was allowed to come to room temperature and stirred overnight. Diethylenetriamine (117 µL, 1.08 mmol) was then added and stirred for 2 hours. The reaction was filtered over celite and concentrated under vacuum. The crude product was redissolved in ethyl acetate and washed with Na_2CO_3 and brine before being dried with Na_2SO_4 and concentrated under vacuum. The product was purified using flash column chromatography with 1% ethyl acetate in petroleum ether to give a white solid (576 mg, 2.2 mmol, 36%). Rf 0.25 (DCM/hexane 1:1). ^{1}H NMR (400 MHz, DMSO-d_6) δ 7.29 (t, J = 6.3 Hz, 1H), 6.76 (dd, J = 7.4, 2.1 Hz, 2H), 5.03 (s, 2H), 3.97 (d, J = 6.2 Hz, 2H), 1.38 (s, 9H). ^{19}F NMR (376 MHz, DMSO) δ -131.39, -131.42. ESI-QQQ $[M+H]^+$ *m/z* calcd. for $[C_{12}H_{16}F_2N_2O_2]^+$ 259.1, found 259.2.

2.7.6 Photo-switching of peptides 2.51-2.56

The peptides **2.51-2.56** were dissolved in methanol at 1 µg/mL. UV-Vis spectra was recorded between 300-500 nm. Samples were exposed to 15 mins irradiation at 365 nm and kept in the dark. UV-Vis spectra was recorded at 20 mins, 1 hour, 3 hours, 6 hours and 24 hours.

2.7.7 Thermal stability of 2.51

The peptide was dissolved in PPI-Europium detection buffer to 1 mg/mL and incubated at 37 °C for 8 hours. The analytical HPLC trace was recorded every hour.

2.7.8 PD-1/PD-L1 HTRF binding assay

The assay was performed following the manufacturer's protocol. Tag1-PD-L1 and Tag2-PD-1 was diluted 40-fold from the stock solution with PPI-Europium detection buffer. Anti-Tag1 Eu Cryptate reagent and Anti-Tag2 XL665 antibody was diluted 50-

fold from the stock solution with PPI-Europium detection buffer. HTRF 96-well low volume white plate was used. The samples were made to the desired concentration and 2 µL was pipetted into the well. The 4 µL of the diluted Tag-1-PD-L1 solution was added, followed by 4 µL of the diluted Tag2-PD-1 solution. Anti-Tag1 Eu Cryptate reagent solution and Anti-Tag2 XL665 antibody solution were pre-mixed prior to dispensing 10 µL into the well, for a total volume of 20 µL. The plate was sealed and incubated for 1 hour at room temperature. Samples were analysed in triplicate. Once incubated, the plate was read using a CLARIOstar (BMG Labtech) microplate reader following manufacturer's protocols for time resolved fluorescence (excitation filter EX-TR, emission filters 620 (10) nm, 665 (10) nm, dichoric mirror LP-TR, integration delay (lag time) 60 µs, integration time 400 µs, number of flashes 200, gain for white plate 2500).

The emission ratio was calculated for each well was calculated with the following equation:

$$Ratio = \frac{665\ nm\ Intensity}{620\ nm\ Intensity} \times 10^4$$

The "specific signal" (ΔR) is obtained by subtracting the background from the signal of each sample ratio

$$\Delta R = Ratio_{Sample} - Ratio_{background}$$

An decreased ΔR suggests an decreased FRET signal, suggesting a decrease in PD-1/PD-L1 interaction.

2.7.9 PD-1/PD-L1 cell-based assay

The assay was performed following the manufacturer's protocol. Jurkat-Lucia TCR-hPD-1 cells were cultured in IMDM (ThermoFisher) with 10% FBS, Pen-Strep (100 µg/mL) and Normocin (100 µg/mL). Cells were passaged every 4 days to a seeding density of 300,00 cells/mL. Every other passage Blasticidin (10 µg/mL), Zeocin (100 µg/mL), Hygromycin (100 µg/mL) and Geneticin (250 µg/mL) were added to maintain selection pressure. Raji-APC-nPD-L1 cells were cultured in IMDM (ThermoFisher) with 10% FBS, Pen-Strep (100 µg/mL) and Normocin (100 µg/mL). Cells were passaged every 4 days to a seeding density of 300,00 cells/mL. Every other passage Blasticidin (10 µg/mL) and Geneticin (250 µg/mL) were added to maintain selection

pressure. 2 days before analysis Jurkat-Lucia TCR-hPD-1 cells were seeded at 50,000 cells/mL and Raji-APC-nPD-L1 cells were seeded at 40,000 cells/mL in media absent of antibiotics. On the day of analysis Raji-APC-nPD-L1 cell suspension ~100,000 (90 µL) was added to a 96 well plate containing test sample (1.8 µL), followed by Jurkat-Lucia TCR-hPD-1 cell suspension of ~200,000 (90 µL). The plate was incubated at 37 °C in a CO_2 incubator for 6 hours. The co-cultured supernatant was transferred to 96-well clear bottomed white plate. QUANTI-Luc 4 reagent was diluted 20X from the stock solution and 50 µL was added per well. The plate was read using a CLARIOstar (BMG Labtech) microplate reader and used following manufacturer's protocols, reading luminescence at a 4 s start time and 0.1 s reading time. Increased luminescence suggests increased luciferase activity, implying PD-1/PD-L1 inhibition.

2.8 References

1 R. J. Boohaker, M. W. Lee, P. Vishnubhotla, J. L. M. Perez and A. R. Khaled, *Comput. Mater. Contin.*, 2012, **19**, 3794–3804.
2 C. Heinis and G. Winter, *Curr. Opin. Chem. Biol.*, 2015, **26**, 89–98.
3 A. Zorzi, K. Deyle and C. Heinis, *Cur. Opin. Chem. Biol.*, 2017, **38**, 24–29.
4 A. L. Jochim and P. S. Arora, *ACS Chem. Biol.*, 2010, **5**, 919–923.
5 O. Koch and G. Klebe, *Proteins*, 2009, **74**, 353–367.
6 P. Y. Chou and G. D. Fasman, *J. Mol. Biol.*, 1977, **115**, 135–175.
7 G. N. Ramachandran, C. Ramakrishnan and V. Sasisekharan, *J. Mol. Biol.*, 1963, **7**, 95–99.
8 L. Pauling and R. B. Corey, *Proc. Natl. Acad. Sci. U.S.A.*, 1951, **37**, 251–256.
9 L. Pauling, R. B. Corey and H. R. Branson, *Proc. Natl. Acad. Sci. U.S.A.*, 1951, **37**, 205–211.
10 K. N. Houk, A. G. Leach, S. P. Kim and X. Zhang, *Angew. Chem. Int. Ed.*, 2003, **42**, 4872–4897.
11 N. Sawyer, A. M. Watkins and P. S. Arora, *Acc. Chem. Res.*, 2017, **50**, 1313–1322.
12 F. Siedler, D. Quarzago, S. Rudolph-Böhner and L. Moroder, *Biopolymers*, 1994, **34**, 1563–1572.
13 V. Peddie and A. D. Abell, *J. Photochem. Photobiol. C: Photochem. Rev.*, 2019, **40**, 1–20.
14 M. M. Lerch, M. J. Hansen, G. M. van Dam, W. Szymanski and B. L. Feringa, *Angew. Chem. Int. Ed.*, 2016, **55**, 10978–10999.
15 K. Guzik, M. Tomala, D. Muszak, M. Konieczny, A. Hec, U. Błaszkiewicz, M. Pustuła, R. Butera, A. Dömling and T. A. Holak, *Molecules*, 2019, **24**, 2071.
16 Q. Li, L. Quan, J. Lyu, Z. He, X. Wang, J. Meng, Z. Zhao, L. Zhu, X. Liu and H. Li, *Oncotarget*, 2016, **7**, 64967–64976.
17 W. Jeong, J. Bu, Y. Han, A. J. Drelich, A. Nair, P. Král and S. Hong, *J. Am. Chem. Soc.*, 2020, **142**, 1832–1837.
18 H. Liu, Z. Zhao, L. Zhang, Y. Li, A. Jain, A. Barve, W. Jin, Y. Liu, J. Fetse and K. Cheng, *J. Immunother. Cancer*, 2019, **7**, 270.

19 J. Fetse, Z. Zhao, H. Liu, U.-F. Mamani, B. Mustafa, P. Adhikary, M. Ibrahim, Y. Liu, P. Patel, M. Nakhjiri, M. Alahmari, G. Li and K. Cheng, *J. Med. Chem.*, 2022, **65**, 12002–12013.
20 M. Gao, D. Kwaria, Y. Norikane and Y. Yue, *Nat. Sci.*, 2023, **3**, e220020.
21 Kiora Pharmaceuticals, Inc. *A Phase I/II Dose-escalating Study of the Safety, Tolerability and Efficacy of KIO-301 Administered Intravitreally to Patients with Retinitis Pigmentosa and Choroideremia,* NCT05282953, clinicaltrials.gov, 2023.
22 W. A. Velema, W. Szymanski and B. L. Feringa, *J. Am. Chem. Soc.*, 2014, **136**, 2178–2191.
23 D. H. Waldeck, *Chem. Rev.*, 1991, **91**, 415–436.
24 H. K. Cammenga, V. N. Emel'yanenko and S. P. Verevkin, *Ind. Eng. Chem. Res.*, 2009, **48**, 10120–10128.
25 F. B. Mallory and C. W. Mallory, in *Organic Reactions*, ed. S. E. Denmark, Wiley, 1st edn., 1984, pp. 1–456.
26 T. Cordes, C. Elsner, T. T. Herzog, C. Hoppmann, T. Schadendorf, W. Summerer, K. Rück-Braun and W. Zinth, *Chemical Physics*, 2009, **358**, 103–110.
27 B. Maerz, S. Wiedbrauk, S. Oesterling, E. Samoylova, A. Nenov, P. Mayer, R. de Vivie-Riedle, W. Zinth and H. Dube, *Chem. Eur. J.*, 2014, **20**, 13984–13992.
28 S. Wiedbrauk and H. Dube, *Tetrahedron Lett.*, 2015, **56**, 4266–4274.
29 S. Kitzig, M. Thilemann, T. Cordes and K. Rück-Braun, *ChemPhysChem*, 2016, **17**, 1252–1263.
30 T. Yamaguchi, T. Seki, T. Tamaki and K. Ichimura, *Bull. Chem. Soc. Jpn.*, 1992, **65**, 649–656.
31 T. Lougheed, V. Borisenko, T. Hennig, K. Rück-Braun and G. A. Woolley, *Org. Biomol. Chem.*, 2004, **2**, 2798–2801.
32 M. Varedian, V. Langer, J. Bergquist and A. Gogoll, *Tetrahedron Lett.*, 2008, **49**, 6033–6035.
33 K. Matsuda and M. Irie, *J. Photochem. Photobiol. C*, 2004, **5**, 169–182.
34 M. Irie, T. Fukaminato, K. Matsuda and S. Kobatake, *Chem. Rev.*, 2014, **114**, 12174–12277.
35 O. Ivashenko, J. T. Van Herpt, B. L. Feringa, P. Rudolf and W. R. Browne, *Langmuir*, 2013, **29**, 4290–4297.
36 R. Klajn, *Chem. Soc. Rev.*, 2014, **43**, 148–184.
37 A. S. Lubbe, W. Szymanski and B. L. Feringa, *Chem. Soc. Rev.*, 2017, **46**, 1052–1079.
38 K. Hüll, J. Morstein and D. Trauner, *Chem. Rev.*, 2018, **118**, 10710–10747.
39 H. Fliegl, A. Köhn, C. Hättig and R. Ahlrichs, *J. Am. Chem. Soc.*, 2003, **125**, 9821–9827.
40 H. Rau, *Angew. Chem. Int. Ed. Engl.*, 1973, **12**, 224–235.
41 C. Johnson, J. S. Harwood, M. Lipton and J. Chmielewski, *Peptide Sci.*, 2022, **114**, e24265.
42 S.-L. Dong, M. Löweneck, T. E. Schrader, W. J. Schreier, W. Zinth, L. Moroder and C. Renner, *Chem. Eur. J.*, 2006, **12**, 1114–1120.
43 S. Samanta and G. A. Woolley, *ChemBioChem*, 2011, **12**, 1712–1723.
44 A. G. Cochran, N. J. Skelton and M. A. Starovasnik, *Proc. Natl. Acad. Sci. U.S.A.*, 2001, **98**, 5578–5583.
45 L. Ulysse, J. Cubillos and J. Chmielewski, *J. Am. Chem. Soc.*, 1995, **117**, 8466–8467.

46 Y. Q. Yeoh, J. Yu, S. W. Polyak, J. R. Horsley and A. D. Abell, *ChemBioChem*, 2018, **19**, 2591–2597.
47 K. Day, J. D. Schneible, A. T. Young, V. A. Pozdin, G. Van Den Driessche, L. A. Gaffney, R. Prodromou, D. O. Freytes, D. Fourches, M. Daniele and S. Menegatti, *J. Mater. Chem. B.*, 2020, **8**, 7413–7427.
48 D. G. Flint, J. R. Kumita, O. S. Smart and G. A. Woolley, *Chem. Biol.*, 2002, **9**, 391–397.
49 H. Asanuma, X. Liang, H. Nishioka, D. Matsunaga, M. Liu and M. Komiyama, *Nat. Protoc.*, 2007, **2**, 203–212.
50 L. Albert, J. Xu, R. Wan, V. Srinivasan, Y. Dou and O. Vázquez, *Chem. Sci.*, 2017, **8**, 4612–4618.
51 T. Podewin, J. Broichhagen, C. Frost, D. Groneberg, J. Ast, H. Meyer-Berg, N. H. F. Fine, A. Friebe, M. Zacharias, D. J. Hodson, D. Trauner and A. Hoffmann-Röder, *Chem. Sci.*, 2017, **8**, 4644–4653.
52 F. Lefevre, *Nucleic Acids Res.*, 1997, **25**, 447–448.
53 V. Dourtoglou, J.-C. Ziegler and B. Gross, *Tetrahedron Lett.*, 1978, **19**, 1269–1272.
54 W. C. Chan and P. D. White, *Fmoc Solid Phase Peptide Synthesis*, Oxford University Press, Oxford, 2000.
55 R. B. Merrifield, *J. Am. Chem. Soc.*, 1963, **85**, 2149–2154.
56 L. Hong, C. M. Quinn and Y. Jia, *Anal. Biochem.*, 2009, **391**, 31–38.
57 F. Degorce, A. Card, S. Soh, E. Trinquet, G. P. Knapik and B. Xie, *Curr. Chem. Genomics*, 2009, **3**, 22–32.
58 L. Einhorn and K. Krapfenbauer, *EPMA Journal*, 2015, **6**, 23.
59 K. Bräutigam, E. Kabore-Wolff, A. F. Hussain, S. Polack, A. Rody, L. Hanker and F. Köster, *J. Cancer Res. Clin. Onco.l*, 2021, **147**, 2923–2933.
60 A. Aemissegger and D. Hilvert, *Nat. Protoc.*, 2007, **2**, 161–167.
61 Y. Ogata and Y. Takagi, *J. Am. Chem. Soc.*, 1958, **80**, 3591–3595.
62 K. Ueno and S. Akiyoshi, *J. Am. Chem. Soc.*, 1954, **76**, 3670–3672.
63 A. A. Beharry, O. Sadovski and G. A. Woolley, *J. Am. Chem. Soc.*, 2011, **133**, 19684–19687.
64 M. Wegener, M. J. Hansen, A. J. M. Driessen, W. Szymanski and B. L. Feringa, *J. Am. Chem. Soc.*, 2017, **139**, 17979–17986.
65 E. Cataldi, M. Raschig, M. Gutmann, P. T. Geppert, M. Ruopp, M. Schock, H. Gerwe, R. Bertermann, L. Meinel, M. Finze, A. Nowak-Król, M. Decker and T. Lühmann, *ChemBioChem*, 2023, **24**, e202200570.
66 D. Bléger, J. Schwarz, A. M. Brouwer and S. Hecht, *J. Am. Chem. Soc.*, 2012, **134**, 20597–20600.
67 A.-L. Leistner, S. Kirchner, J. Karcher, T. Bantle, M. L. Schulte, P. Gödtel, C. Fengler and Z. L. Pianowski, *Chem. Eur. J.*, 2021, **27**, 8094–8099.
68 US. Pat., 102052 Al, 2020.
69 UK. Pat., 043389, 2019.
70 G. P. Stahly, B. C. Stahly and K. C. Lilje, *J. Org. Chem.*, 1984, **49**, 578–579.
71 M. Makosza and K. Sienkiewicz, *J. Org. Chem.*, 1998, **63**, 4199–4208.
72 K. W. Rosenmund and E. Struck, *Ber. dtsch. Chem. Ges.*, 1919, **52**, 1749–1756.
73 L. Albert, A. Peñalver, N. Djokovic, L. Werel, M. Hoffarth, D. Ruzic, J. Xu, L. Essen, K. Nikolic, Y. Dou and O. Vázquez, *ChemBioChem*, 2019, **20**, 1417–1429.
74 B. Priewisch and K. Rück-Braun, *J. Org. Chem.*, 2005, **70**, 2350–2352.

75 K. M. Zak, R. Kitel, S. Przetocka, P. Golik, K. Guzik, B. Musielak, A. Dömling, G. Dubin and T. A. Holak, *Structure*, 2015, **23**, 2341–2348.
76 K. Negoro, Y. Yonetoku, H. Misawa-Mukai, W. Hamaguchi, T. Maruyama, S. Yoshida, M. Takeuchi and M. Ohta, *Bioorg. Med. Chem.*, 2012, **20**, 5235-5246.

Chapter 3

Peptide-Directed Binding to Identify Peptide-Small Molecule Hybrids that Inhibit PD-1/PD-L1

3.1 Introduction

3.1.1 Small molecules can control protein-protein interactions

Small molecules are mainly used for targeting protein-ligand interactions. This is typically because they contain a well-defined binding site for the small molecule to easily interact with.[1] Due to protein-protein interactions (PPIs) often being large, flat surfaces, the modulation of PPIs is considered difficult and often regarded as "undruggable" when using small molecules.[2] The degree of difficulty in targeting PPIs with small molecules is dependent on the structural complexity of the PPI interaction. Despite these obstacles there are many small molecules that are successful drugs that target PPIs.[3] The breakthrough in targeting PPIs was the discovery of "hotspot" residues whereby selective residues are responsible for most of the binding energy at an interface.[3,4] Hotspots are often clustered in the centre of the interaction interface and cover an area comparable in size to a small molecule. Furthermore, they are often found to be hydrophobic and show the ability to be conformationally adaptive. These characteristics demonstrate that some of the PPI surface may have pockets that could bind a drug-like small molecule.[5]

3.1.2 Small molecules that target PD-1/PD-L1

The PD-1/PD-L1 immune checkpoint pathway is currently successfully targeted using monoclonal antibodies (mAbs). The shortfalls of using mAbs includes limited permeability, immune-related adverse events, immunogenicity, and high cost.[6] Small molecule inhibitors typically have fewer side effects due to having a shorter half-life, they are less expensive, and often are suitable for oral administration.[7] Further, current preclinical studies have shown that small molecule compounds are advantageous over mAbs to supress tumour growth and migration with favourable biosafety.[8] Despite the development of small molecule inhibitors lagging behind the progress of mAbs, the beneficial characteristics that overcome the shortcomings of mAbs demonstrates there is an urgent need to develop small molecule inhibitors that target PD-1/PD-L1 signalling pathway.

In 2015, the Bristol Myers Squibb (BMS) company released the first patent on biphenyl-type immunomodulators and has disclosed many other small molecule inhibitors since.[9,10] The structures of two groups of small molecule inhibitors have

been revealed: one structure is the 3-(2,3-dihydro-1,4-benzodioxan-6-yl)-2-methylphenyl methanol (BMS-200) scaffold (**Figure 3-1**, **3.1**), and the other is based on the 2-methyl-3-biphenyl methanol (BMS-202) scaffold (**Figure 3-1**, **3.2**).[9] Both were found to inhibit the PD-1/PD-L1 interaction with an IC_{50} of 80 nM and 18 nM respectively, determined using a homologous time resolved fluorescence (HTRF) assay.[11]

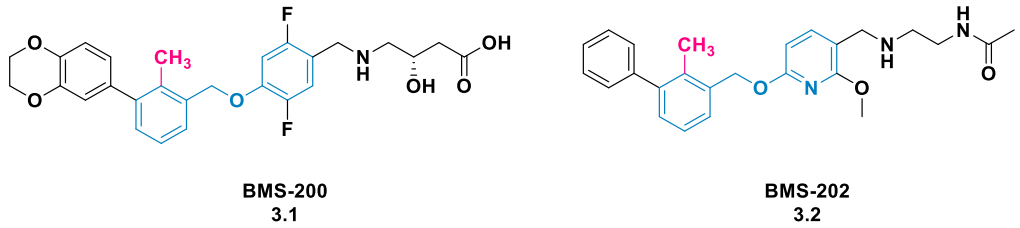


Figure 3-1 *3-(2,3-dihydro-1,4-benzodioxan-6-yl)-2-methylphenyl methanol (BMS-200),* ***3.1,*** *and 2-methyl-3-biphenyl methanol (BMS-202),* ***3.2*** *highlighting the similarity in structure in blue*

Subsequent research reported the crystal structures of the BMS compounds bound to PD-L1.[12] The small molecule inhibitors bind on the C'CFG strands of PD-L1, blocking the interaction between PD-1/PD-L1 by inducing dimerization of PD-L1 (**Figure 3-2**).[12] As shown in **Figure 3-2**, the residue that contributed the most significant binding for the **3.1** inhibitor was Met115, while for **3.2** it differed to Tyr56. Furthermore, it was shown that Ala121 had a negative effective on binding affinity for **3.1** but was key residue for **3.2**.[12]

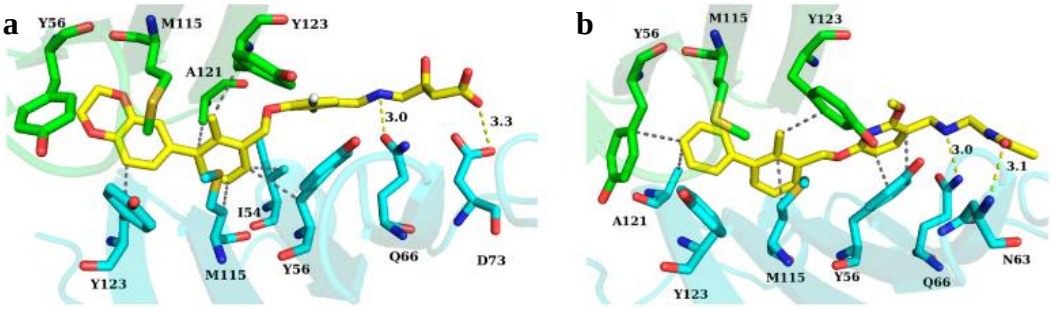


Figure 3-2 *The interaction of a) BMS-200,* ***3.1*** *(yellow) and b) BMS-202,* ***3.2*** *(yellow) showing important interactions with the residues of PD-L1 dimer (green and blue).*

Despite the low nanomolar IC_{50} of **3.1** reported using the HTRF assay, the compound reported weak cell-based PD-1/PD-L1 inhibitory activity and high cytotoxic activity.[13] When administered to humanized NOG-dKO mice, **3.2** showed depleted tumour-infiltrating lymphocytes and substantial weight loss.[14] These observations demonstrate

that **3.1** is unlikely to become a lead compound due to its poor drug-like qualities. **3.2** also reports a nanomolar IC_{50} with the ability to block the PD-1/PD-L1 interaction *in vitro*. *In vivo* studies revealed **3.2** was capable of inhibiting tumour growth.[15] Furthermore, it was reported that tumour-bearing mice were administered 60 mg/kg of **3.2** showing easy absorption and distribution to the tumours producing the blockade effects against PD-1/PD-L1.[15] These traits provide the pharmacological basis to potentially use **3.2** as a lead compound. However, when comparing the IC_{50} to a known monoclonal antibody inhibitor, pembrolizumab, that reports an IC_{50} of ~0.1-0.3 nM there is still an area for improvement of this molecule.[16]

Feng's research group released a patent disclosing bromobenzyl ether derivatives that inhibit the interaction of PD-1/PD-L1 (**Figure 3-3**). The structure is similar to the BMS compounds, replacing the methyl group with bromine (**Figure 3-3**, pink). The IC_{50}'s were measured by HTRF assay to give impressive numbers in the picomolar range.[17,18] These scaffolds show potent blocking of PD-1/PD-L1 at the biochemical level with a salt formulation of the test compound dosing at 15 mg/kg to displayed antitumour activity.[17,18] IMMH-010, **3.4**, was approved for trial in April 2020 but has yet to recruit patients. **3.4** is an ester prodrug that is catalysed to become an active metabolite by the enzyme carboxylesterase 1 (CES), mainly in the human liver.[19]

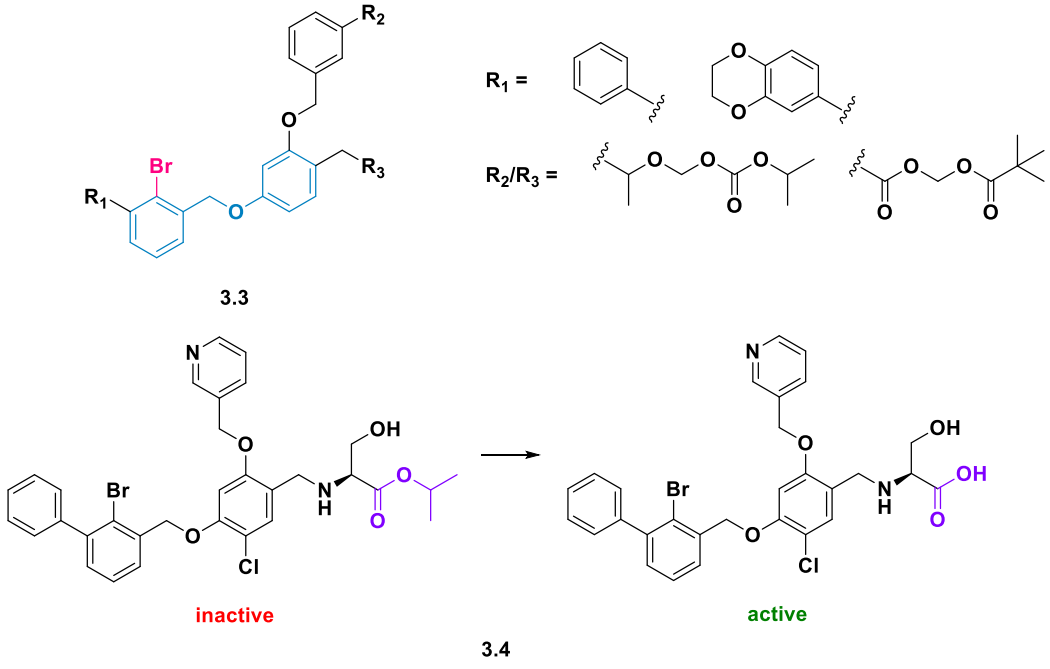
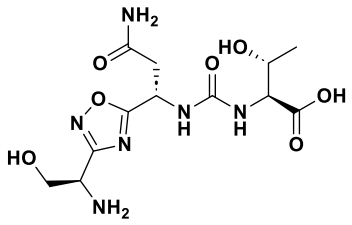


Figure 3-3 *The structure of the bromobenzyl derivatives found in the patent by Feng (**3.3**) and the structure of IMMH-010 (**3.4**) in the inactive and active form with the ester being hydrolysed to an acid (purple).*

When tested against melanoma and colon carcinoma cells **3.4** showed remarkable antitumour efficacy.[19] While the main metabolite found was the active compound as seen in **Figure 3-3**, three other metabolites were seen.[19] Furthermore, this compound would be limited to the production of where CES was found.

The first small molecule to enter clinical trial was CA-170 developed by Curis Pharmaceuticals and Aurigene Pharmaceuticals (**Figure 3-4**).[20–22] It is a dual inhibitor of oral anti-V-domain immunoglobulin suppressor of T-cell activation (VISTA) and PD-1. VISTA is another checkpoint that negatively regulates T-cell function.[23] It has been reported that CA-170 binds to PD-L1 but that it does not block the assembly of PD-1/PD-L1 complex suggesting a defective ternary complex as the mechanism of action.[24] From the clinical data from the on-going phase 1 trial, it has the best effect on non-small-cell lung cancer (NSCLC) and Hodgkin's lymphoma with its overall clinical benefit rate (CBR) being 70% and 78%.[25,26] The maximum dose considered well tolerated was 1200 mg/d. Overall, CA-170, **3.5**, demonstrated rapid absorption, good bioavailability, and a short half-life.[26,27] This short half-life has led to the ability to control drug exposure and manage immune related side effects. Of the 30 patients tested, 2 reported severe adverse events possibly related to the treatment. [26,27] The phase 2 study of CA-170, **3.5**, is on-going with preliminary reports showing a better efficacy was found at a lower dosage of 400 mg, but also demonstrated a high number of patients developed immune related adverse events. Currently the dosing regimen is being optimised for various tumour types to achieve the maximum response.[28]



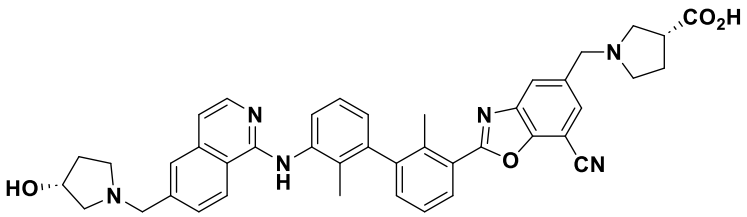
EC_{50} = 15.4 nM

3.5

Figure 3-4 *The structure of CA-170 (**3.5**).*

Another small molecule that has entered phase 2 clinical trials is INCB086550 (**Figure 3-5**, **3.6)**. **3.6** is a potent small-molecule inhibitor of PD-L1 with an IC_{50} value of 3.1 nM in humans.[29] The inhibitor binds to PD-L1 and blocks the interaction between PD-1 and PD-L1, inducing dimerization and internalisation of PD-L1 that in turns removes

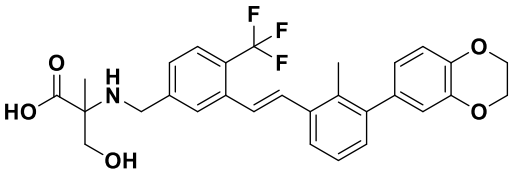
the ability of the tumour cell to initiate immunosuppressive conditions.[29] Further investigations showed that **3.6** binds to PD-L1 at a site that overlaps with the anti-PD-L1 monoclonal antibodies, atezolizumub and durvalumab. The phase 1 clinical trial results showed over 20% of patients were affected by treatment-emergent adverse events with 36% of patients experiencing severe adverse events.[30–32] Two patients (1.4%) had a complete response for squamous cell anal cancer and colorectal cancer with a 400 mg dose daily respectively and 10 patients (7.2%) showed a partial response.[30–32] There were no dose-limiting toxicities observed. Despite the high levels of treatment-emergent adverse events the promising anti-tumour activity is advantageous, and the phase 2 clinical trial for **3.6** has begun to evaluate efficacy and safety.[30–32]



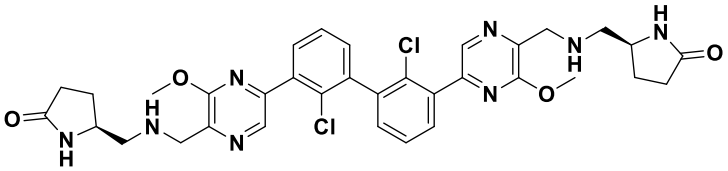
3.6

Figure 3-5 *The structure of INCB086550 (**3.6**).*

MAX-10181 **(Figure 3-6**, **3.7**) was granted trial approval for advanced solid tumours in early 2021.[33] The most recent release suggests that **3.7** could be used in combination with an PD-1/CTLA-4 bispecific antibody. GS-4224 (**Figure 3-6**, **3.8**) was also approved for advanced solid tumours but a percentage of patients experienced dose limiting toxicity during the dose escalation phase.[34] As of March 2021, this clinical trial has been terminated to re-evaluate the safety and tolerability of **3.8**.[34] Similarly to **3.6**, **3.8** was also found to induce dimerization of PD-L1 and the *in vitro* studies found enhanced antiviral functions comparable to anti-PD-L1 mAbs. The *in vivo* activity was assessed using assessed using mouse tumour models determining that **3.8** can block the interaction of PD-1/PD-L1 with a potency of < 0.75 nM and further investigation showed a greater than 90% target occupancy on the tumours 24 hours post dosing comparable to PD-L1 antibodies.[35]



3.7



3.8

Figure 3-6 *The structures of MAX-10181 (**3.7**) and GS-4224 (**3.8**).*

While these small molecules have made it to clinical trials, few drugs make it past the phase 1 of the clinical trial, such as **3.8**, and of those which have, many suffer from immune related adverse events. This highlights a need for the development of alternative small molecule inhibitors for PD-1/PD-L1 with a greater affinity and specificity to avoid off target effects.

3.1.3 Methods to identify novel small molecules for PPIs

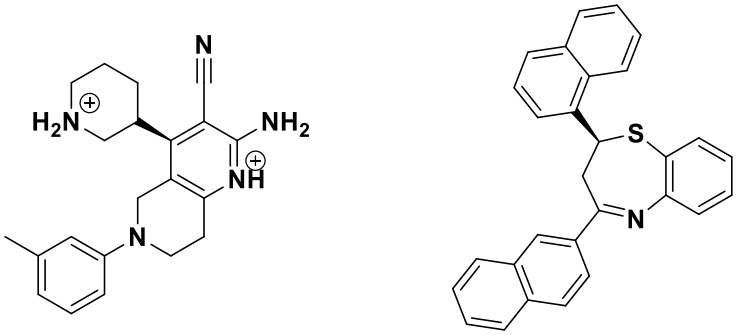
The interface of PPIs tend to be large and flat making classical medicinal chemistry methods less effective in discovering PPI modulators, in comparison to conventional targets that are found to have binding pockets. Computational and chemical strategies have been developed to identify hits and lead to novel small molecule PPI modulators.

3.1.3.1 High throughput screening and virtual screening

High throughput screening (HTS) is one strategy that is used to discover starting compounds for small molecule drug design. Large libraries of compounds compiled of small molecules or peptides are screened to identify compounds with biological activity against targets.[36] The HTS techniques for PPIs include the two-hybrid assay, affinity purification, fluorescence polarization and fluorescence resonance energy transfer.[37–39] Within the pharmaceutical industry, libraries of millions of compounds can be screened.[36] Virtual screening is a complementary method to HTS to lighten the burden of screening a multitude of compounds experimentally.[40] It is a computational approach of *in silico* screening of a compound library. Molecular docking is one

example of virtual screening. This is the technique of placing compounds into the binding site of the virtual receptor and evaluating the binding affinity through energy scoring.[41] When modelling induced fit effects, the two limitations noted are the comprehensive sampling techniques and the accuracy of scoring.[42]

Two inhibitors for PD-1/PD-L1 discovered *via* HTS can be seen in **Figure 3-7**.[43] Virtual HTS was used to screen ~3.7 million lead-like compounds and ~87,000 National Cancer Institute (NCI) compounds. The lead-like compounds were screened against both PD-1 and PD-L1, and the NCI compounds only against PD-1. From this, the top 4000 hits were selected, ~0.1% of the original compounds.[43] Computational methods were used to explore the binding interactions leading to a total of 35 compounds being shortlisted. Following biological activity testing, the lead compound was **3.9** with an IC_{50} = 200 µM and from the NCI compounds, **3.10** with an IC_{50} = 15 µM.[43]



IC_{50} = 200 µM
3.9

IC_{50} = 15 µM
3.10

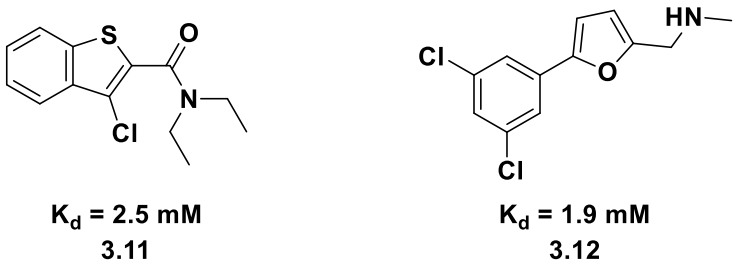
Figure 3-7 *The structures of* ***3.9*** *and* ***3.10*** *identified using HTS.*

As shown, when applying HTS to PPIs the hit rate is exceeding low. In a study identifying JIP-JNK inhibitors, it was reported the hit rate was as low as 0.00001%.[44] This limitation is often due to incompatible libraries and false positive results.

3.1.3.2 Fragment based drug design

Another approach is fragment-based drug design (FBDD). FBDD usually starts by identifying a low complexity chemical structure that may only have low binding affinity to the target. This compound can then be optimised *via* fragment linking, fragment evolution, fragment modification, and fragment self-assembly to result in a hit with an increased binding affinity.[45,46] The validity of the fragments can be

measured using multiple techniques including NMR, X-ray crystallography, surface plasmon resonance (SPR) and isothermal calorimetry.[46] Despite having a higher hit rate in comparison to HTS, the demand for detection equipment and focused expertise limits FBDD.[47] Furthermore, the structure of the protein must also be known limiting the development of inhibitors for unknown targets. Fesik *et al.* reported a fragment-based screen of PD-L1 using NMR spectroscopy.[48] Multiple novel chemotypes were discovered that were capable of displacing PD-1 such as **3.11** and **3.12** (**Figure 3-8**). Furthermore, X-ray crystallography of these compounds with PD-L1 serves as a starting point for further modification and optimization of these compounds.



K_d = 2.5 mM
3.11

K_d = 1.9 mM
3.12

Figure 3-8 *The structures of* ***3.11*** *and* ***3.12*** *discovered using FBDD.*

3.1.4 Peptide-directed binding

As discussed in chapter one, peptides are an invaluable starting point in the design of small molecule inhibitors. Their larger structure and further interactions being possible through contacts formed by multiple residues offers advantages in structural relationship not available initially to small molecules.

Peptide directed binding is one approach that utilizes the peptide's ability to bind tightly and selectively to PPIs to develop novel small molecule inhibitors.[49] Firstly, the amino acids that are essential for the interaction are determined. The parent peptide is then divided into two smaller semi peptides with the key amino acids distributed evenly, losing the ability to bind to the PPI. The other half of the peptides are replaced with reactive terminals to undergo click reactions with small molecule fragments to form a peptide-small molecule hybrid. These hybrids are then tested for binding and inhibition, if successful it can be assumed the small molecule fragment emulates the binding capabilities of the original peptide (**Figure 3-9**).

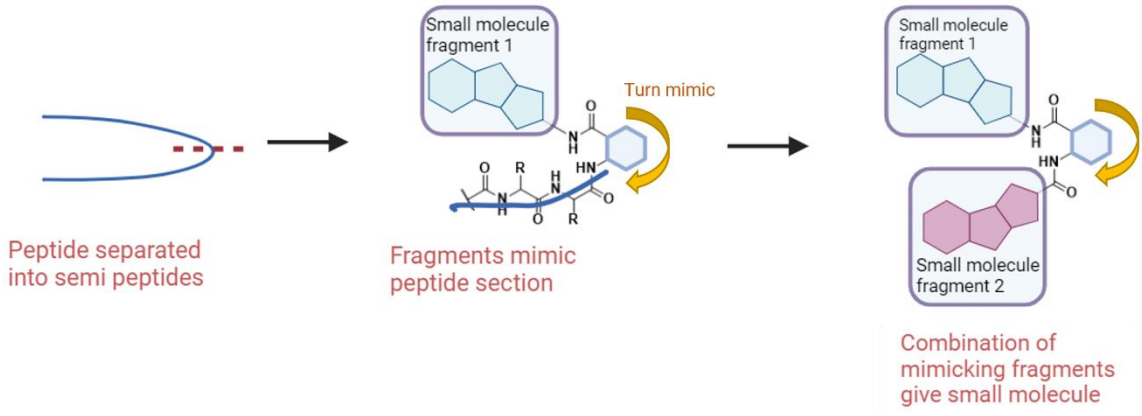


Figure 3-9 *Schematic illustration of peptide-directed binding.*

The sequential replacement of the peptide sections with small molecule fragments results in a novel more drug like molecule that can mimic the binding of the original peptide. Beekman *et al.* used the NOXA peptide as a small molecule mimic, replacing the ends of the peptide with an azide and alkyne to undergo cooper catalysed azide-alkyne cycloaddition (CuAAC) click reaction to develop novel small molecules *via* small molecule-peptide hybrids.[49] The small molecule fragments chosen to be conjugated to the peptides were determined by *in silico* modelling. They also applied peptide-directed binding to the PPIs of hDM2/hDMX and p53.[50] However, in this instance they mitigated the small molecule-peptide step, applying a fully computational peptide-directed ligand design whereby *in silico* covalent docking was used to identify fragments likely to restore binding of the semi-peptides. Instead of experimentally testing the peptide-small molecule hybrids, the top 10 azide and alkyne fragments were combined virtually. This chosen library was then redocked and the top 10 results were chosen to be synthesised and tested. When compared, both techniques previously demonstrated 50% or higher hit rates in contrast to the hit rate of 0.0001% found in a study using HTS to identify inhibitors for an α-helical interaction.[44] Despite experimental peptide-directed binding requiring more synthesis and consequently a higher cost, this technique has the added benefits of identifying peptide-small molecule hybrids that can be leads in their own right. Also, it provides an opportunity for greater structural diversity.

As a well-known immunotherapy target with limited small molecule inhibitors that have successfully made it to the clinical trial stage, PD-1/PD-L1 is an exciting

interaction to which peptide-directed binding can be applied. The application of the intermediate peptide-small molecule hybrids highlights this technique to be used with or without a known crystal structure of the known peptide and protein interaction. This opens the door to the choice of peptide to be the starting point to apply peptide-directed binding to. Furthermore, there is room for development into a turn mimic to complement the structure of the interaction of PD-1/PD-L1, replacing the chemistry previously used for α-helices.

3.2 Chapter Aims

To address the remaining need for small molecules capable of controlling PD-1/PD-L1, this chapter aims to do serendipitous drug discovery using the information obtained from the alanine scan in chapter two to develop peptide-small molecule hybrids that block the interaction of PD-1/PD-L1. The development of these peptide-small molecule hybrids for peptide-directed binding will be for the purpose of mimicking turn motif peptides to bind to the β-sheet mediated protein interactions. A small library of reactive fragments that represent a wide chemical space will be curated for attachment to the semi-peptides for the synthesis of peptide-small molecule hybrids.

3.3 Results and Discussion

3.3.1 Semi peptides

As previously discussed in chapter two, CLP003, **3.13**, was discovered *via* phage display and inhibits PD-1/PD-L1 by binding to PD-L1. An alanine scan of CLP003 revealed that Tyr5 and Trp7 (**Figure 3-10**, purple) were not essential for inhibition, as demonstrated using a HTRF binding assay.

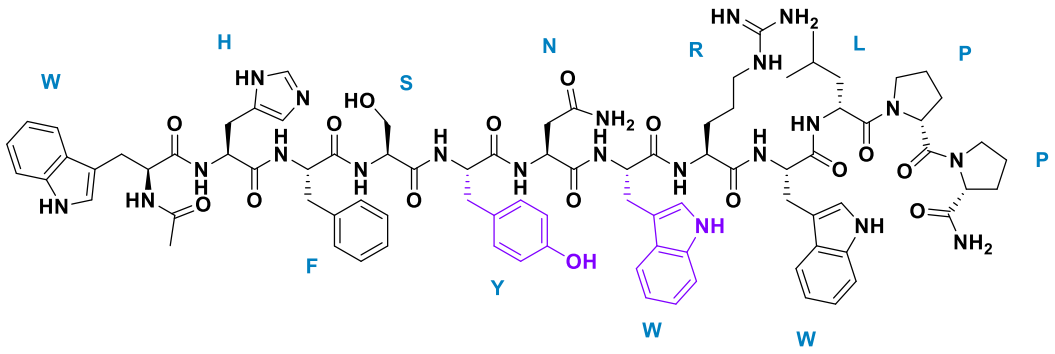
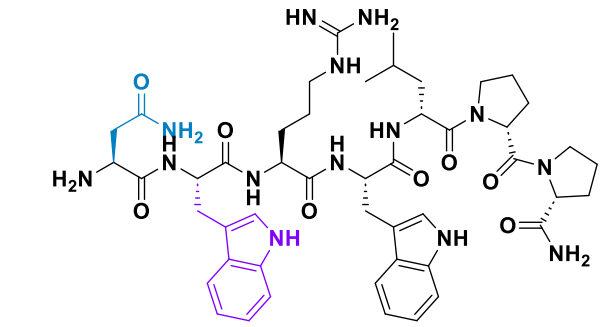
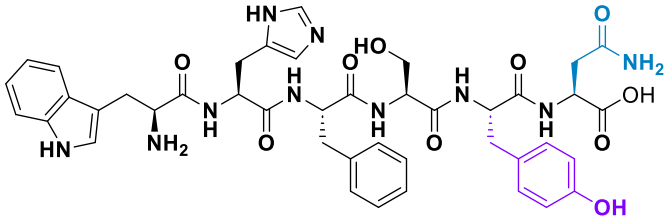


Figure 3-10 *The structure of CLP003 (**3.13**) highlighting Tyr5 and Trp7 (purple) as they are not important for inhibiting PD-1/PD-L1.*

Following the alanine scan results, the next step to apply peptide-directed binding to CLP003 was to split the peptide in half to create semi-peptides. CLP003 was split in two and the non-essential residues for inhibition were distributed evenly. Semi-peptide 1 was the seven residues found at the N-terminus, -NWRWLPP (**Figure 3-11**, Trp7 purple) and semi-peptide 2 was the six residues found at the C-terminus, WHFSYN- (**Figure 3-11**, Tyr5 purple). The alanine scan HTRF assay data showed that Asn6 was essential for inhibiting the PD-1/PD-L1 interaction and therefore was kept in both semi peptides (**Figure 3-11**, blue).



3.14



3.15

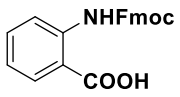
Figure 3-11 *The structure of semi peptide 1 (-NWRWLPP,* ***3.14****) highlighting Trp7 (purple) and Ash6 (blue) and semi peptide 2 (WHFSYN-,* ***3.15****) highlighting Tyr5 (purple) and Asn6 (blue).*

The interaction between PD-1/PD-L1 contains β-sheets and β-strands, suggesting that inhibition of this PPI was more effective if the inhibitor contained a turn like structure.[51] Due to this, it was important to incorporate a turn like structure to which the respective acid or amine small molecule would be coupled to as shown in **Figure 3-9**.

3.3.2 The synthesis of semi-peptide 1 (-NWRWLPP, 3.14)

Semi-peptide 1 (**Figure 3-11**, **3.14**) was synthesised with Fmoc SPPS as described previously in chapter two in section 2.4.1. Using an automated peptide synthesiser and the TentaGel S RAM resin, SPPS was utilized with the coupling agents HBTU and HOBt. Once the peptide was synthesised, the turn mimic was added to the C-terminus of the semi-peptide *via* an amide bond.

To mimic the turn necessary for binding, Fmoc-2-aminobenzoic acid (Abz) (**Figure 3-12**, **3.16**) was utilised. Abz is classified as an aromatic cyclic $\beta^{2,3}$-amino acid due its constrained cyclic structure. The benzene ring of Abz had been proposed as an isosteric replacement to enforce a turn through hydrogen bonding that results in peptide folding.[52–56]

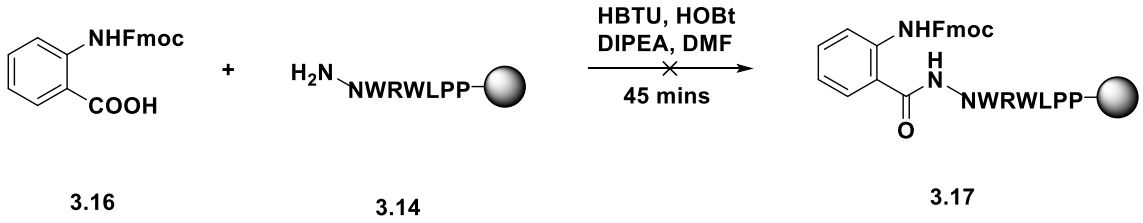


3.16

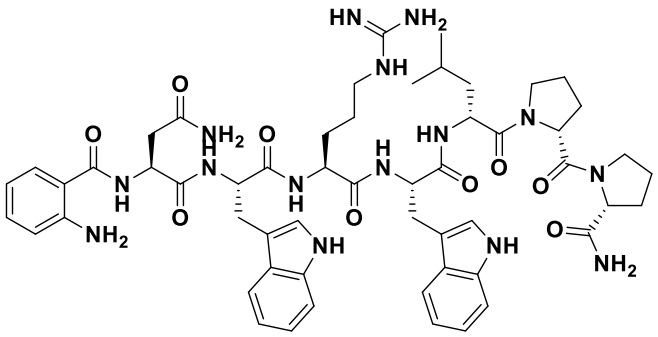
Figure 3-12 *The structure of Fmoc-2-aminobenzoic acid (**3.16**).*

3.3.3 The synthesis of semi-peptide 1 (-NWRWLPP, 3.14) with the turn mimic Fmoc-2-aminobenzoic acid (3.16)

To synthesise the peptide-small molecule hybrids using semi-peptide 1, **3.14**, the peptide would be built on resin and the turn mimic would be coupled to the N-terminus followed by the small molecule fragment that was functionalised with an acid. The resulting compound would then be cleaved from the resin to give the peptide-small molecule hybrid. Initially, **3.16** was coupled using SPPS with the coupling agent HBTU and HOBT with DIPEA for 45 minutes following the synthesis of semi-peptide 1, **3.14** (**Scheme 3-1**).



3.16 3.14 3.17

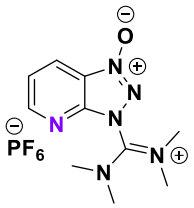


3.18

Scheme 3-1 *The coupling between Fmoc-Abz (**3.16**) and semi-peptide 1 (**3.14**) using HBTU, HOBt and DIPEA in DMF for 45 mins at room temperature to give **3.17** on resin. After cleavage for 3 hours using TFA:TIPS:H_2O (95:2.5:2.5), the product would be **3.18.***

However, after cleavage using TFA:TIPS:H_2O (95:2.5:2.5) for 3 hours, it was clear that **3.18** had not been formed and **3.16** had not coupled to semi-peptide **3.14.** This was

confirmed as only the mass of the semi-peptide H-NWRWLPP-NH_2 was seen with an *m/z* of 966.27 corresponding to an $[M-H]^-$ of 966.51. Concluding that perhaps the acid being directly attached to the aromatic ring was affecting reactivity, the coupling agent was changed *N*-[(Dimethylamino)-1*H*-1,2,3-triazolo-[4,5-b]pyridin-1-ylmethylene]-*N*-methylmethanaminium hexafluorophosphate *N*-oxide (HATU) (**3.19**).



3.19

Figure 3-13 *The structure of N-[(Dimethylamino)-1H-1,2,3-triazolo-[4,5-b]pyridin-1-ylmethylene]-N-methylmethanaminium hexafluorophosphate N-oxide (HATU) (**3.19**).*

HATU, **3.19**, is utilized for difficult couplings as it is found to be more reactive than HBTU.[57] The structure of HATU differs from HBTU through an additional nitrogen giving a triazolopyridine derivative containing a guanidine (**Figure 3-13**, purple).[57] Due to being more reactive it was hoped that HATU would be able to activate the carboxylic acid on **3.16**. The mechanism of action for forming an amide is much the same as HBTU (**Figure 3-14**).

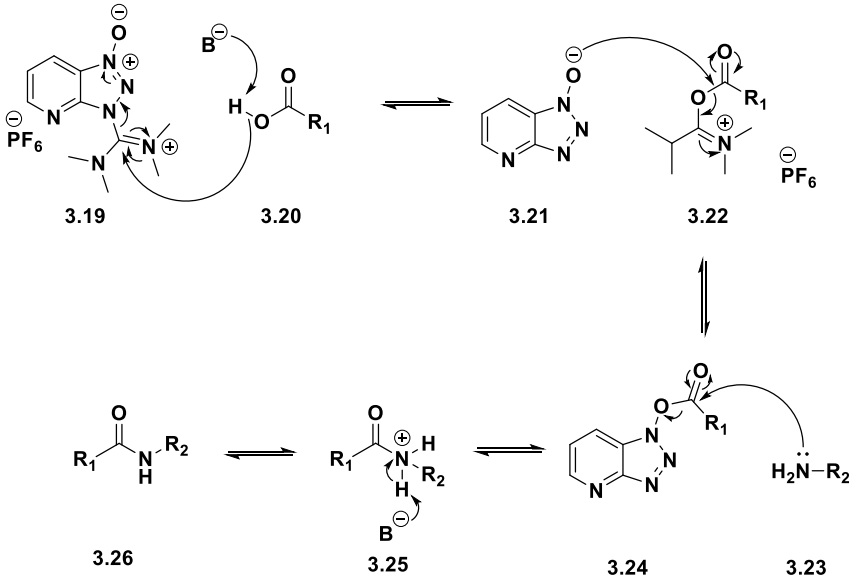


Figure 3-14 *The mechanism for amide bond formation using HATU.*

The carboxylic acid of the amino acid is deprotonated by DIPEA leading to a nucleophilic attack on the iminium ion **3.19**. This attack results in the elimination of azabenzotriazole **3.21** that can attack the electrophilic carbonyl centre of **3.22**, releasing tetramethylguanidine. The ester **3.24** is now activated and is attacked by the amine nucleophile on the amino acid of the growing peptide chain **3.23,** forming an amide bond and eliminating azabenzotriazole. Once the semi-peptide **3.14** was synthesised, the coupling between Asn, the N-terminal amino acid, and **3.16** was proceeded with for 15 minutes at 75 °C, followed by Fmoc deprotection using piperidine in DMF. Upon cleavage of the peptide from the resin using TFA:TIPS:H_2O (95:2.5:2.5) for 3 hours, both masses were seen for **3.14** (H-NWRWLPP-NH_2) and **3.18** with an *m/z* of 966.73 and 1086.67 matching the $[M-H]^-$ of 966.51 and $[M+H]^+$ and 1086.56 respectively. When analysing these the analytical HPLC peaks it was found that the coupling was not going to completion, with the major peak corresponding to the semi-peptide H-NWRWLPP-NH_2 without **3.16** (**Figure 3-15**). This showed little change when the coupling for **3.16** was performed twice. Due to time constraints, it was concluded to move forward without using **3.16** as a turn mimic option.

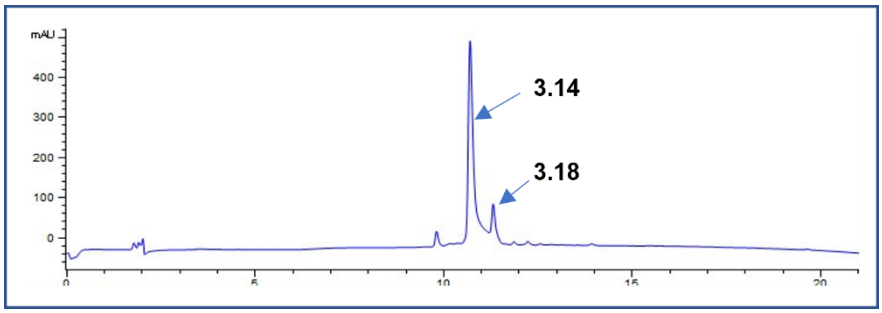
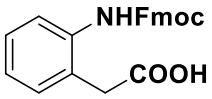


Figure 3-15 *The analytical HPLC trace recorded at 214 nm showing semi-peptide H-NWRWLPP-NH_2 and* ***3.18*** *after 15 mins at 75°C (Agilent eclipse XDB-C18 column (4.6 x 150 mm, 5 µm) and a flow rate of 1 mL/min. Spectra were run with a solvent gradient of 0-100% B over 20 min. Solvent A: H_2O, 0.05% TFA, solvent B: MeCN, 0.05% TFA).*

3.3.4 The synthesis of semi-peptide 1(-NWRWLP, 3.14) with turn mimic Fmoc-2-aminophenylacetic acid (3.27)

Due to **3.16** not being reactive enough under conditions that we would have expected, possibly because the carbonyl was too electron rich as a result of being *ortho* to the electron donating amine. Therefore, Fmoc-2-aminophenylacetic acid was considered as a turn mimic. By using Fmoc-2-aminophenylacetic acid (**Figure 3-16**, **3.27**) this will reduce the electron density on the carboxylic acid and therefore improve

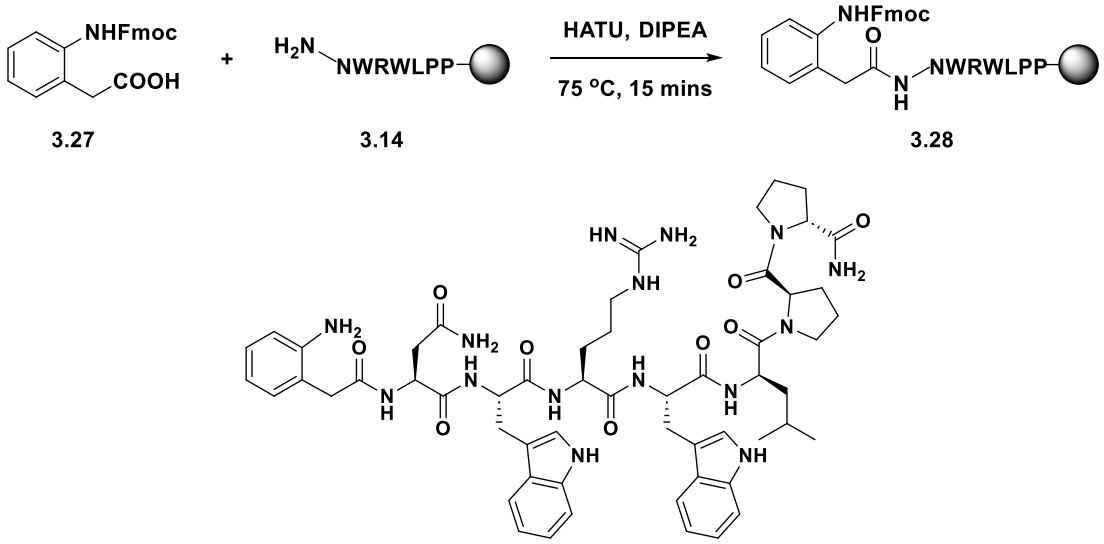
reactivity. Furthermore, with the added methylene this will become less sterically hindered also improving reactivity.



3.27

Figure 3-16 *The structure of Fmoc-2-aminophenylacetic acid (**3.27**).*

The coupling was attempted using HATU and DIPEA at 75°C for 15 minutes (**Scheme 3-2**). The successful coupling was confirmed showing an *m/z* of 1099.90 corresponding to $[M-H]^-$ of 1099.57. However, when analysing the analytical HPLC, it was seen that some of the peptide without the turn, H-NWRWLPP-NH_2, remained and degradation was occurring.



Scheme 3-2 *The coupling between Fmoc-2-aminophenylacetic acid (**3.27**) and semi-peptide 1 (**3.14**) using HATU and DIPEA in DMF for 15 mins at 75 °C to give **3.28** on resin. After cleavage for 3 hours using TFA:TIPS:H_2O (95:2.5:2.5), the product **3.29** was formed.*

Despite trialling additional couplings and an increase in temperature, these attempts only led to degradation. Oxyma and DIC were used as alternative coupling agents in an attempt to decrease degradation resulting in a clean analytical HPLC, but **3.29** was unconfirmed *via* mass and analytical HPLC suggesting coupling did not occur (**Figure 3-17**).

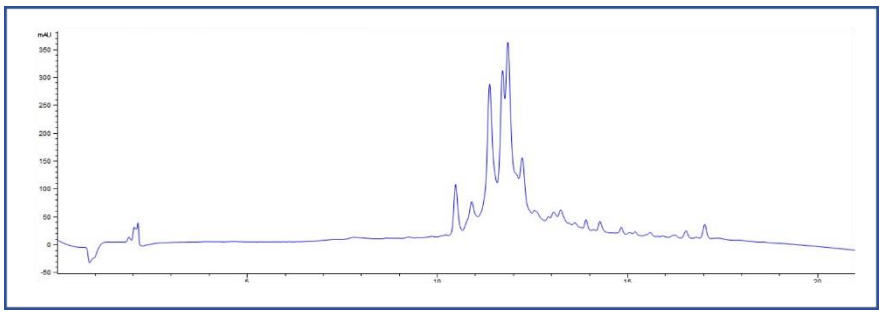


Figure 3-17 *The analytical HPLC trace recorded at 214 nm showing* ***3.28*** *after coupling 4-fluorobenzoic acid once using DIC and Oxyma at 75 °C for 10 mins and cleavage using TFA:TIPS:H_2O (95:2.5:2.5) for 3 hours (Agilent eclipse XDB-C18 column (4.6 x 150 mm, 5 μm) and a flow rate of 1 mL/min. Spectra were run with a solvent gradient of 0-100% B over 20 min. Solvent A: H_2O, 0.05% TFA, solvent B: MeCN, 0.05% TFA).*

Despite the incomplete conversion, it was decided to continue to couple the small molecule fragments to the free amine using the conditions noted in **Scheme 3-2**. For initial screening of these hybrids the yield was not a priority. After Fmoc deprotection, the same conditions were used to couple an initial small molecule fragment, 4-fluoro-benzoic acid, with HATU and DIPEA at 75 °C for 15 minutes.

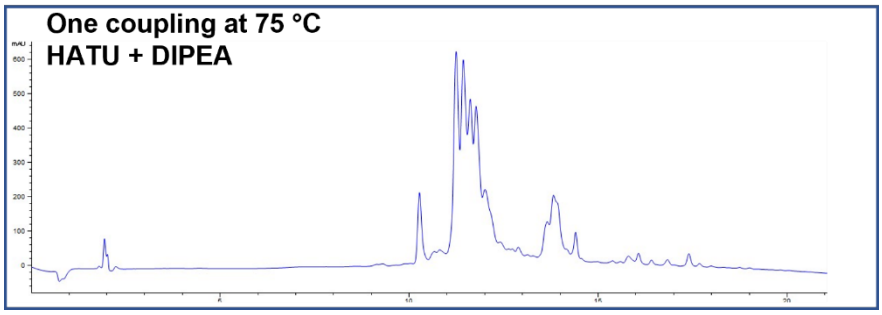


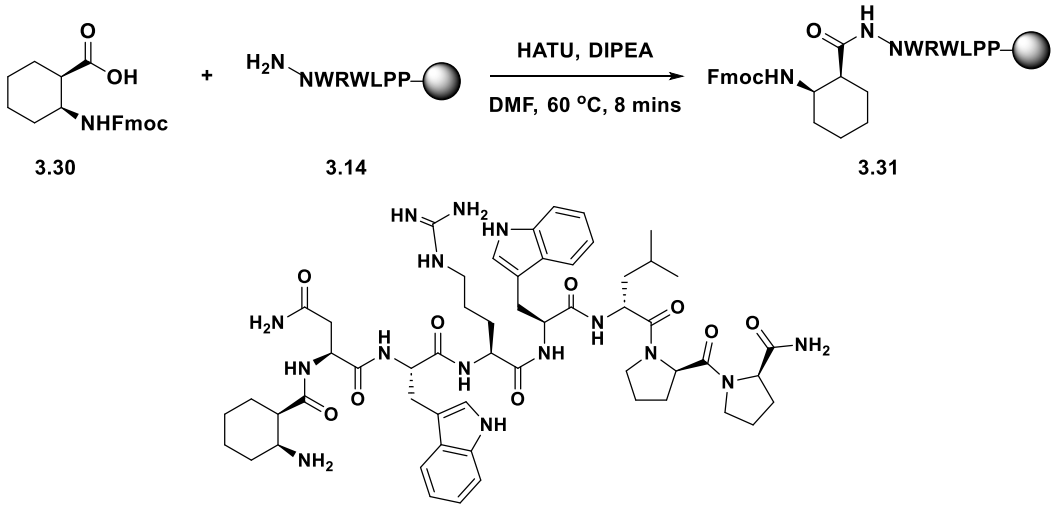
Figure 3-18 *The analytical HPLC trace recorded at 214 nm showing* ***3.28*** *after coupling 4-fluorobenzoic acid once using HATU and DIPEA at 75 °C for 10 mins and cleavage using TFA:TIPS:H_2O (95:2.5:2.5) for 3 hours (Agilent eclipse XDB-C18 column (4.6 x 150 mm, 5 μm) and a flow rate of 1 mL/min. Spectra were run with a solvent gradient of 0-100% B over 20 min. Solvent A: H_2O, 0.05% TFA, solvent B: MeCN, 0.05% TFA).*

When analysing the analytical HPLC it was seen to have multiple peaks all within proximity of one another making purification challenging (**Figure 3-18**). Furthermore, the MALDI results confirmed the semi-peptide without the turn, H-NWRWLPP-NH_2, with an *m/z* of 989.10 corresponding to $[H+Na]^+$ of 988.52, the peptide with the turn, **3.29**, with an *m/z* of 1099.90 matching $[H-M]^-$ of 1099.57, and the peptide with the turn and the 4-fluorobenzoic acid that had coupled twice to the peptide with an *m/z* of 1343.55 corresponding to $[M-H]^-$ of 1343.61. To make the conditions milder to prevent the 4-fluorobenzoic acid from coupling to the peptide twice, the coupling was trialled

at room temperature, 40 °C, 50 °C and 60 °C degrees. However, no mass was confirmed for the single addition of 4-fluorobenzoic acid. It was apparent that the phenylacetic acid linker, **3.27** was in some way unstable and not amenable to the synthesis of a library of peptide-small molecule hybrids, as such alternatives were investigated.

3.3.5 The synthesis of semi-peptide 1(-NWRWLPP, 3.14) with the turn mimic cis-2-Fmoc-aminocyclohexanecarboxylic acid (3.30)

Another turn mimic approach considered was *cis*-2-Fmoc-aminocyclohexanecarboxylic acid, **3.30**. The structure of **3.30** is similar to **3.16**, but crucially is not aromatic and therefore the amine is not feeding electron density to the carboxylic acid, increasing reactivity towards the nucleophiles. 2-Fmoc-aminocyclohexanecarboxylic acid is available for purchase as either the *cis* or *trans* enantiomeric mixtures. It is important to note that the use of *cis*-2-Fmoc-aminocyclohexanecarboxylic acid, **3.30**, will make two compounds in the peptide-small molecule hybrids, but for the identification of binding fragments this shortcoming was considered acceptable. Initially **3.30** and **3.14** were coupled with HBTU and HOBt for 45 mins twice at room temperature, identical to other Fmoc-protected amino acids (**Scheme 3-3**).



Scheme 3-3 *The coupling between Cis-2-Fmoc-aminocyclohexanecarboxylic acid (**3.30**) and semi-peptide 1 (**3.14**) using HATU and DIPEA in DMF for 8 mins at 60 °C to give **3.31** on resin. After cleavage for 3 hours using TFA:TIPS:H_2O (95:2.5:2.5), the product **3.32** was formed.*

Cis-2-Fmoc-aminocyclohexanecarboxylic acid, **3.30** showed incomplete coupling with the analytical HPLC showing a peak for the semi peptide H-NWRWLPP-NH_2. To optimize the coupling, the coupling agents were kept the same and the coupling temperature was increased to 60 °C for 8 minutes.[58] After purification *via* preparative HPLC, the successful coupling between the semi-peptide, **3.14**, and **3.30** to give the product **3.32** was confirmed by the analytical HPLC showing a peak at 13.25 min, and no peak of the original peptide for H-NWRWLPP-NH_2. This was further confirmed by mass spectrometry where the mass of 1130.0 was found, corresponding to $[M+K]^+$ of 1130.6.

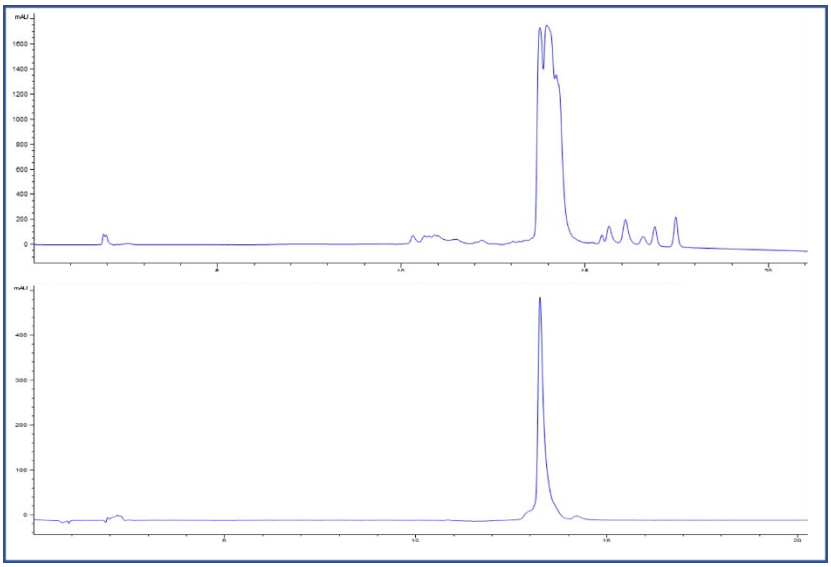
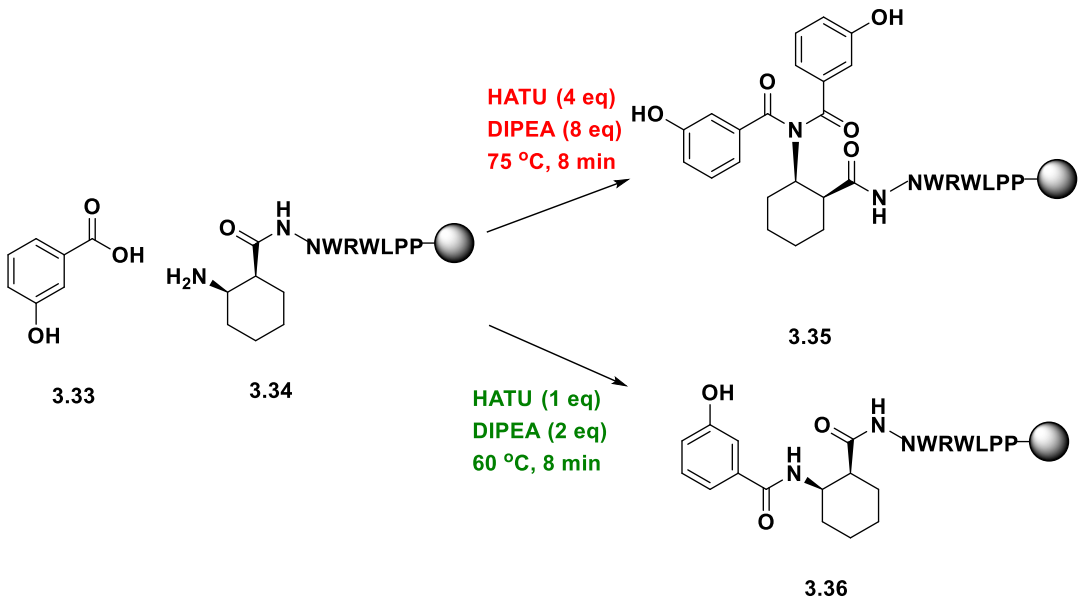


Figure 3-19 *The analytical trace of the semi-peptide with the turn,* ***3.32****. The top trace showing the crude trace, the bottom trace showing* ***3.32*** *after purification. (Agilent eclipse XDB-C18 column (4.6 x 150 mm, 5 μm) and a flow rate of 1 mL/min. Spectra were run with a solvent gradient of 0-100% B over 20 min. Solvent A: H_2O, 0.05% TFA, solvent B: MeCN, 0.05% TFA).*

Once the turn unit coupling was confirmed, the Fmoc was deprotected using 20% piperidine in DMF for 10 minutes twice. The small molecule fragment functionalised with a carboxylic acid, 3-hydroxybenzoic acid, **3.30**, was then coupled. The curation of the library of compounds is described in section 3.3.1.3.1. The reaction proved sensitive to equivalents of reagents and heat as when too much of either was used, a di-substitution was taking place with the mass of the acid derivative adding twice being seen (**Scheme 3-4**).



Scheme 3-4 *The coupling conditions using HATU and DIPEA for the addition of* ***3.33*** *to* ***3.34*** *(****3.31*** *Fmoc deprotected). The coupling at 75 °C resulted in di-substitution of the carboxylic acid (****3.35****) while the coupling at 60 °C gave the desired compound* ***3.36.***

The coupling agent HATU and DIPEA were used with one equivalent of the small molecule acid derivative. For the small molecule **3.33** this was successfully coupled at 60 °C for 8 minutes. Optimisation of the method was performed to allow for coupling of a library of small molecule fragments. Optimisation treaded a fine line of di-substitution or no substitution, successful conditions employed were HATU (4 eq) and DIPEA (4 eq) at 70 °C for 8 minutes with 2 equivalents of the small molecule fragment. Once the small molecule coupling was complete, the peptide was removed from the resin using a cleavage cocktail of 95% TFA, 2.5% TIPS and 2.5% water and shaken over 3 hours. The high concentration of acid cleaves the peptide from the resin and removes any acid labile protecting groups on the side chains of the amino acids. Each peptide-small molecule hybrid showed a crude purity of >80% as analysed by analytical HPLC and were confirmed *via* LCMS. Any hybrids that fell under this marker, were purified using semi-preparative HPLC. As seen in **Figure 3-20**, the peaks of the peptide-small molecule hybrids could be seen to have a shoulder peak. This could be due to solubility problems or due to diastereoisomers formed from the racemic c*is*-2-aminocyclohexanecarboxylic acid.

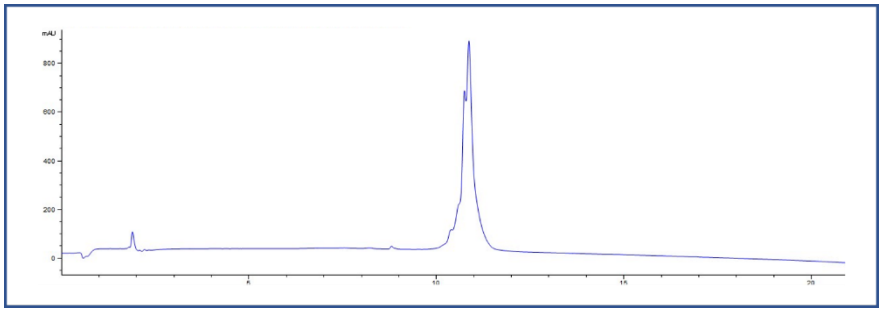


Figure 3-20 *The analytical HPLC trace of 214 nm of the cleaved peptide-small molecule,* ***3.36*** *(Agilent eclipse XDB-C18 column (4.6 x 150 mm, 5 µm) and a flow rate of 1 mL/min. Spectra were run with a solvent gradient of 0-100% B over 20 min. Solvent A: H_2O, 0.05% TFA, solvent B: MeCN, 0.05% TFA).*

3.3.6 Testing peptide-small molecule hybrids

Once the structures were confirmed, the HTRF assay was used to identify activity to inhibit PD-1/PD-L1, as previously described in chapter two, section 2.4.2. The small molecule fragments that were chosen to be coupled to semi-peptide 1(-NWRWLPP, **3.14**) were based on collected fragment-hit data since 2012.[59,60] Cheminformatic analysis of the fragment hits assessed their properties, followed by the interaction with their targets finding the most common successful hits. The library of peptide-small molecule hybrids was tested in the HTRF assay. The semi-peptide with only the turn unit, **3.32**, was tested and showed no ability to inhibit PD-1/PD-L1. Therefore, it can be assumed that the small molecule that was coupled onto the semi-peptide, **3.32**, can act like a mimic of the other half of the peptide. Each peptide-small molecule hybrid was initially screened at 10 µM with several demonstrating a lack of solubility in DMSO buffer mixtures at high concentrations.

3.3.7 Small molecule fragments functionalised with a carboxylic acid

Due to the lack of crystal structure available of CLP003, viable fragments were chosen to cover a good amount of chemical space with a small number of compounds. *Shaw et al*. released a review in 2019 comparing various data sets to highlight the fragment hits that share commonalities such as preferences in structure upon binding, hydrogen bonding, and preferential directional interactions with the protein targets. From their summary, fragments functionalised by acids were selected shown in **Figure 3-21** that showed binding to more than one protein pocket either on different proteins or distinct pockets on the same protein.[60] It was assumed that these "privileged" fragments would

have a higher chance to re-establish inhibitory activity of the peptide-small molecule hybrids to PD-L1 and provide good starting points for compound development.

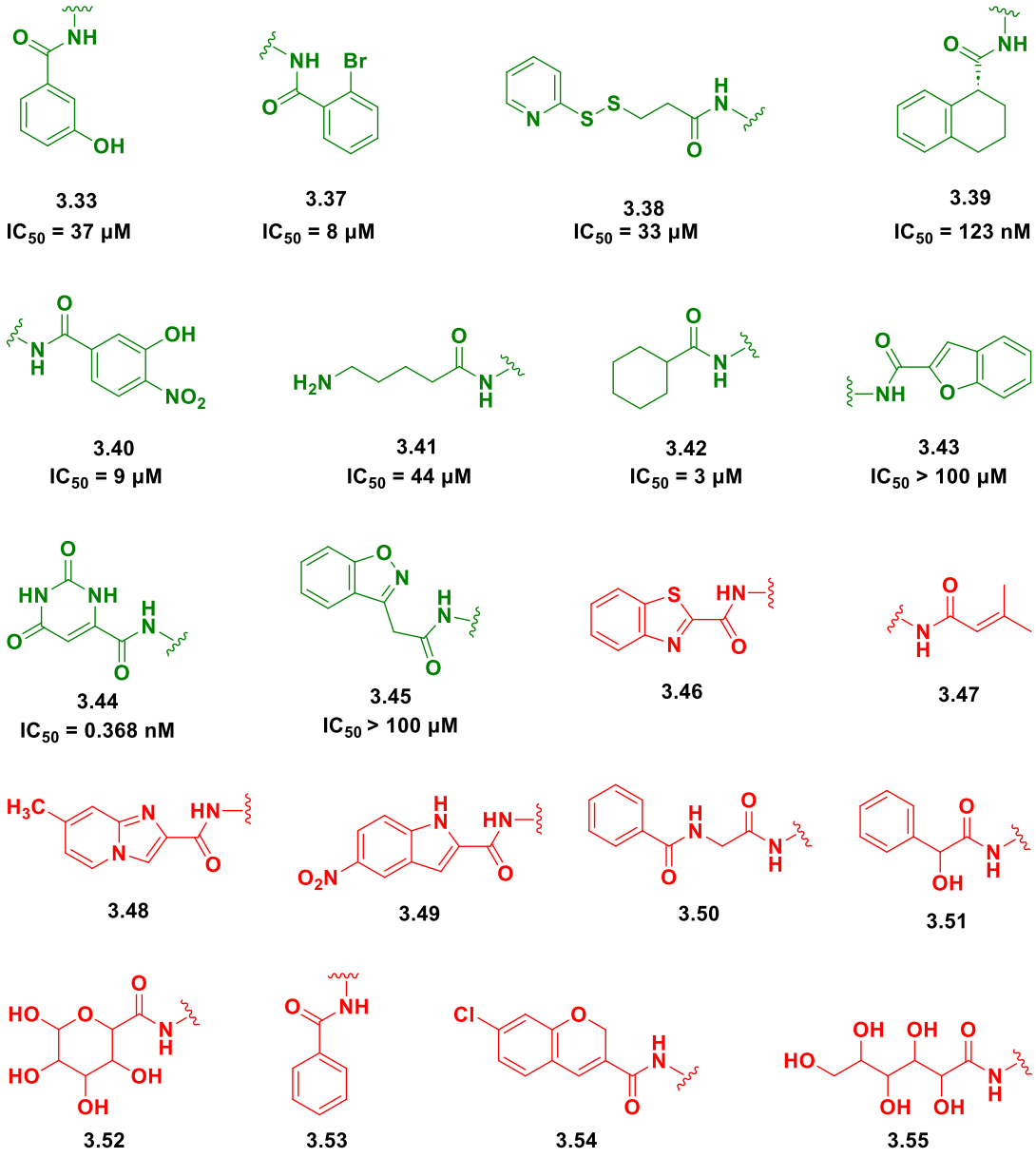


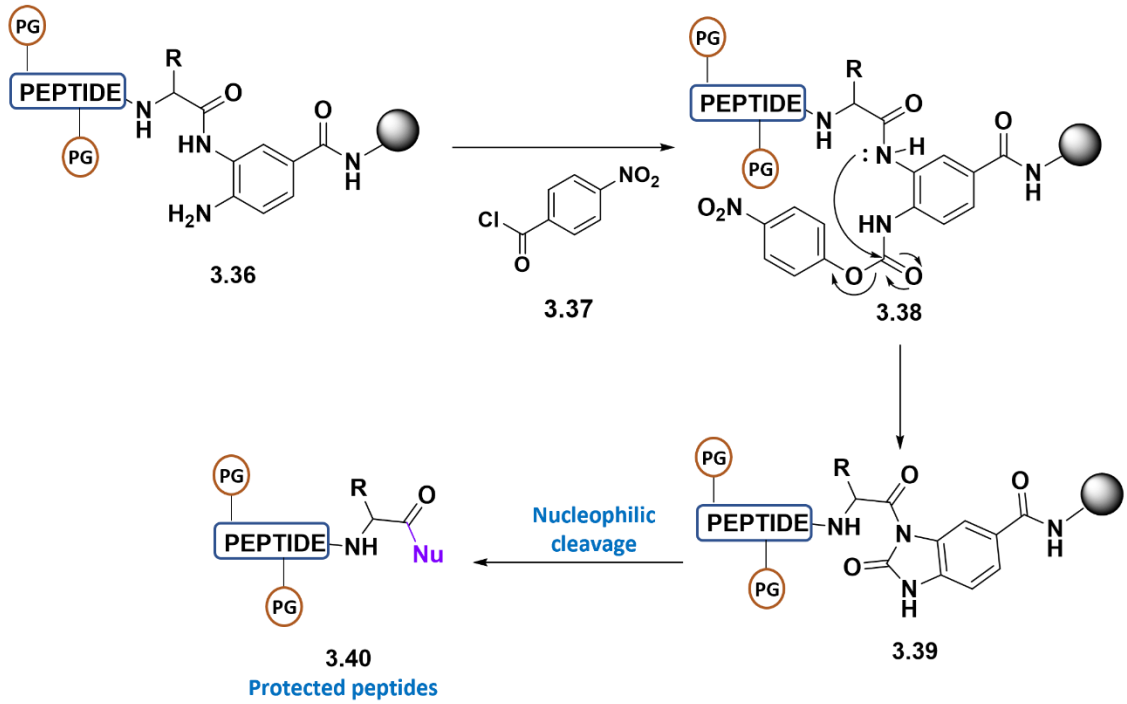
Figure 3-21 *The acid small molecule fragments chosen, successful hits in green, unsuccessful hits in red. IC_{50} values reported* (n/N = 2/6).

Compounds **3.48** and **3.49** proved insoluble in the HTRF buffer including when using DMSO. While compounds **3.52** and **3.55** were unsuccessfully coupled onto the semi-peptide. The successful peptide-small molecule hybrids that showed inhibition of PD-1/PD-L1 were further purified if needed and IC_{50} values were calculated for each small molecule-peptide hybrid. Ten out of the twenty peptide-small molecule hybrids showed inhibition of PD-1/PD-L1 at 10 μM. **3.37**, **3.40**, and **3.42** showed an IC_{50} value

of less than 10 µM while **3.39** and **3.44** showed nanomolar inhibition of PD-1/PD-L1, being exceptional hits. Interestingly, it was seen that while benzoic acid, **3.53**, was not a hit, the substituted benzyl rings showed inhibition, **3.33** and **3.37**. Furthermore, that the fragment hits that contained a non-aromatic moiety also showed strong inhibition in compounds **3.44**, **3.42**, and **3.39**. To confirm that these compounds showed inhibition *via* binding to PD-L1, SPR was attempted but due to time constraints the results were inconclusive as further optimisation was needed.

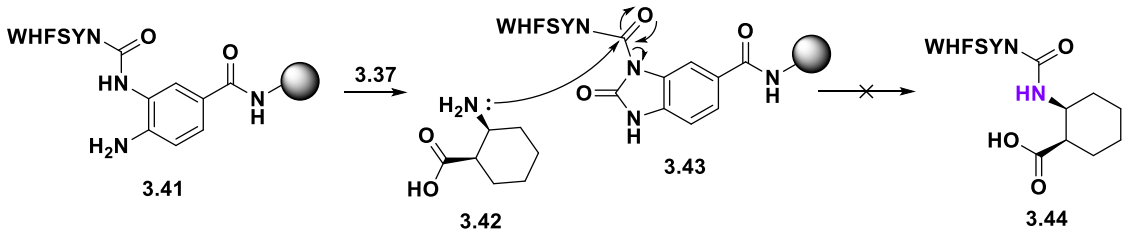
3.3.8 The synthesis of semi-peptide 2 (WHFSYN-, (3.15)

For the other half of the peptide, it was necessary to modify the C-terminus. This presented a challenge as peptides are generally built on the resin from the C-terminus to the N-terminus using excess N-carbamate protected amino acids and condensation reagents to reduce epimerisation.[61] Dawson *et al.* developed an approach for Fmoc SPPS that is based on the formation of a C-terminal *N*-acylurea functionality (**Scheme 3-5, 3.39**). This *N*-acylurea becomes a labile group between the C-terminus and the resin.[62] They found that *o*-aminoanilides are stable intermediates that can be cyclised to form an aromatic *N*-acylurea moiety.[63] This has been harnessed to develop a technique that can cleave the peptide from the resin through a nucleophilic attack of the carbonyl (**Scheme 3-5**, **3.40**). Through this method, the peptide would be cleaved from the peptide with the protecting groups on the amino acids remaining, allowing for modifications without inducing side reactions through unprotected amino acids.



Scheme 3-5 *The formation of the N-acylurea moiety (**3.39**) on the Dawson resin leading to nucleophilic cleavage.*

This was reported using various amines including primary amines, tert-butylamine and 3-azidopropylamine, that showed complete conversion and slightly less nucleophilic amines such as propargylamine that also showed effective displacement.[64] This highlighted the potential of this technique to make peptide-small molecule hybrids using semi-peptide 2, **3.15**. The semi-peptide **3.15** was synthesised on the Dawson Dbz Am resin using HBTU and HOBt, as previously discussed in section 2.4.1, in chapter two. Once the peptide synthesis was complete, 4-nitrophenyl chloroformate (**Scheme 3-5, 3.37)** was added with DIPEA and shaken for 1.5 hours to form the *N*-acylurea moiety with the semi-peptide attached, **3.43**.



Scheme 3-6 *The nucleophilic cleavage of semi-peptide 2 (**3.15**) activated with 4-nitrophenyl chloroformate (**3.37**) to give **3.42** that undergoes nucleophilic attack by **3.30** to give **3.43.***

During this time, *cis*-2-(Fmoc-amino)cyclohexanecarboxylic acid, **3.30**, was Fmoc deprotected in 30% triethylamine in DCM for 30 minutes to give **3.42**. This was used

in replacement of piperidine that is usually used for Fmoc deprotection as it is easy to remove under vacuum.[65] This was then re-dissolved in DCM, and DIPEA was added. The solution was then degassed with nitrogen for 30 minutes. Following the degassing step, this was immediately added to the activated peptide, **3.43**, to cleave from the resin *via* nucleophilic attack resulting in **3.44**. The reaction was tracked using analytical HPLC. However, after leaving the reaction overnight at room temperature, only the *cis*-2-aminocyclohexanecarboxylic acid, **3.42**, was recovered (**Figure 3-22A**) with the fluorene by-product also present. The resin was then microwaved at 50 °C for 15 minutes, again reporting no change, and a further 15 minutes at 80 °C, also reporting no change (**Figure 3-22B**).

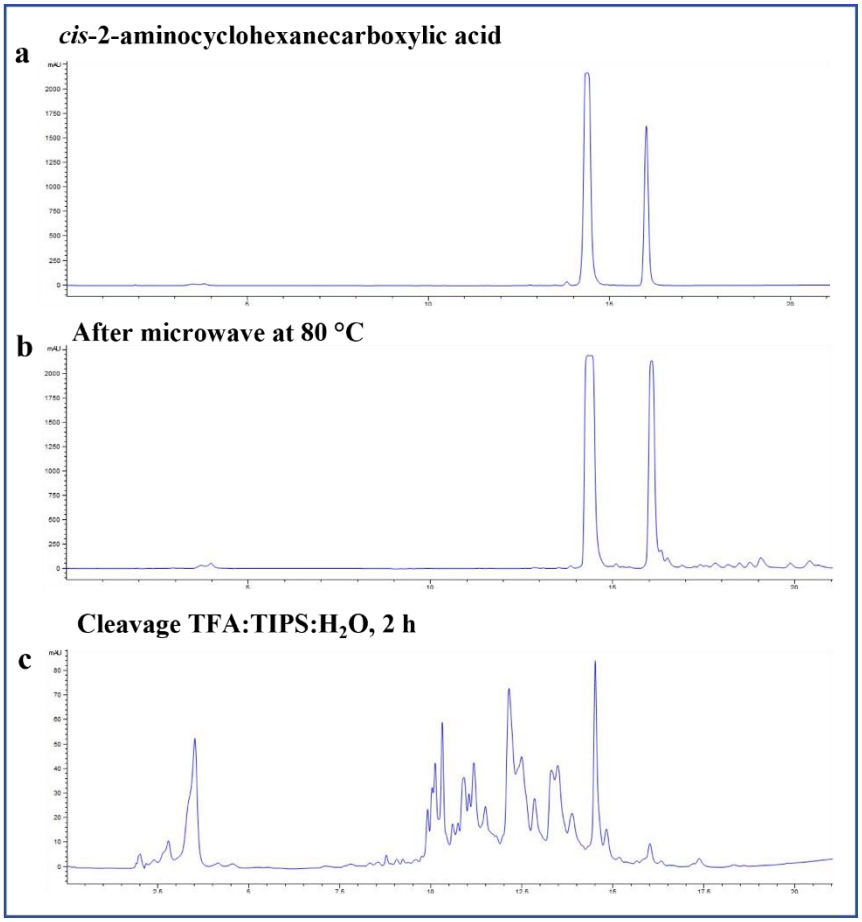
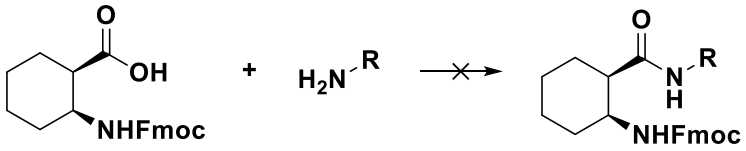


Figure 3-22 *The analytical HPLC trace recorded at 214 nm of a) cis-2-aminocyclohexanecarboxylic acid (**3.42**) and the fluorene by-product b) after attempting nucleophilic cleavage after overnight shaking, 15 minutes at 50 °C and 15 minutes at 80 °C showing only recovered cis-2-aminocyclohexanecarboxylic acid (**3.42**) c) the cleaved semi-peptide with the N-arcyluea activating group **3.43** from the Dawson resin (Agilent eclipse XDB-C18 column (4.6 x 150 mm, 5 μm) and a flow rate of 1 mL/min. Spectra were run with a solvent gradient of 0-100% B over 20 min. Solvent A: H_2O, 0.05% TFA, solvent B: MeCN, 0.05% TFA).*

When the peptide was then cleaved from the resin using TFA:TIPS:H_2O for 2 hours, what was seen in the analytical HPLC suggested synthesis of the peptide chain was in some way hindered (**Figure 3-22C**). The mass confirmed that only the activated peptide with the *N*-acylurea, **3.43**, was present showing an *m/z* of 1012.5 corresponding to $[M+H]^+$ of 1012.4.

To use the *cis*-2-(Fmoc-amino)cyclohexanecarboxylic acid as a nucleophilic cleavage unit it was thought to pre-couple this to the amine small molecule fragments. The was attempted using EDC, NHS and DIPEA at 50 °C overnight to recover only Fmoc deprotected starting material. It was also trialled using EDC, HOBt and EDC and DMAP with similar unsuccessful results.

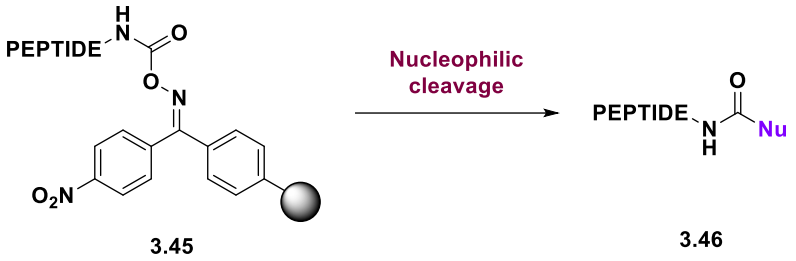


Scheme 3-7 *The scheme of forming an amide bond with cis-2-(Fmoc-amino)cyclohexanecarboxylic acid(**3.30**)*

As this coupling was proving challenging, instead of using the *cis*-2-(Fmoc-amino)cyclohexanecarboxylic acid as the nucleophilic cleavage component, this was coupled to the Dawson resin as the first amino acid. However, when attempting the nucleophilic cleavage with the amine, the same results as seen in **Scheme 3-6** was seen as the peptide was unable to be cleaved from the resin.

3.3.9 The synthesis of semi-peptide 2 (WHFSYN-, 3.15) using the oxime resin

A resin with similar nucleophilic cleavage traits was also trialled, the oxime resin (**Scheme 3-8**).[66] This approach was chosen as it showed a different mechanism than the Dawson's resin with a similar principle. There was also the question of whether this would work with Fmoc chemistry in SPPS as it is base labile and is often used in Boc chemistry.[66,67] The synthesis of semi-peptide with the turn, **3.32**, was attempted using the oxime resin with the coupling agents HOBt and HBTU as discussed in section 2.4.1 in chapter two. However, upon cleavage to confirm the synthesis of **3.32** no mass was found.



3.45 3.46

Scheme 3-8 *The structure of the oxime resin* ***3.45*** *and the ability to undergo nucleophilic cleavage to give an N-terminally modified peptide with a nucleophile* ***3.46.***

Due to steric hinderance of the aminooxy-function of the oxime resin, loading the first amino acid can cause difficulty. To ensure the first amino acid, c*is*-2-(Fmoc-amino)cyclohexanecarboxylic acid, **3.30**, was loaded to the oxime resin some coupling procedures were trialled and cleaved with TFA:TIPS:H_2O (95:2.5:2.5) for 3 hours. The initial trial was to elongate the coupling time with HOBt and HBTU to 1.5 hours, but this showed no addition of **3.30** to the resin. Another approach was trialled using HATU and DIPEA for 15 minutes at 75 °C with **3.30**. However, as seen in **Figure 3-23**, the analytical HPLC showed degradation potentially because of the cleavage conditions. Furthermore, no mass was confirmed for the successful coupling. Due to the degradation seen and the difficulty loading the oxime resin with the initial amino acid, **3.30**, it was decided to try an alternative approach.

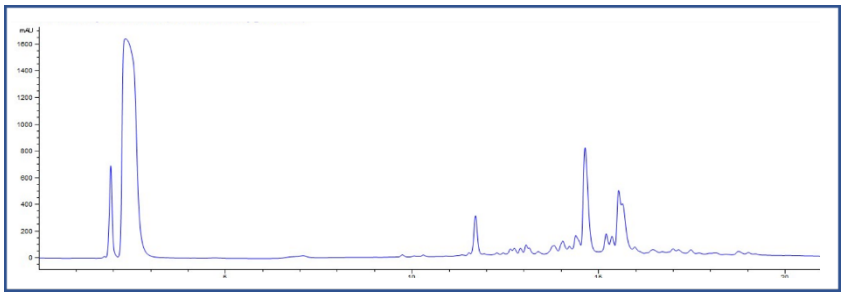
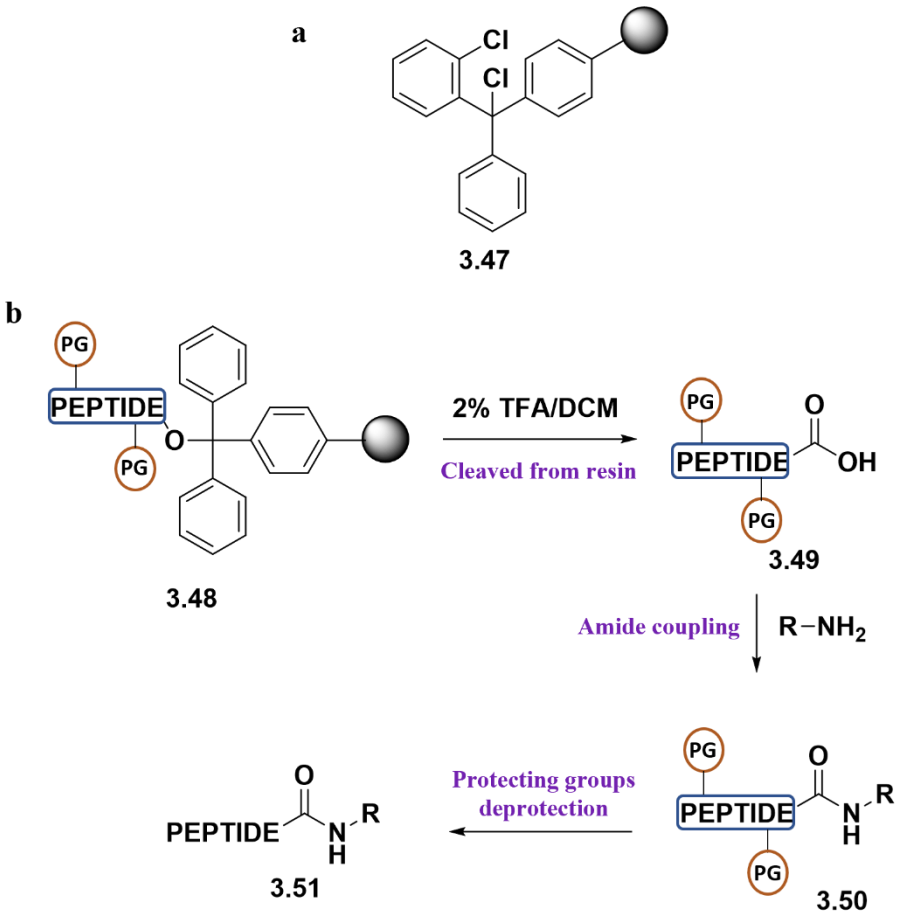


Figure 3-23 *The analytical HPLC trace recorded at 214 nm of the oxime resin after coupling with cis-2-(Fmoc-amino)cyclohexanecarboxylic (**3.30**) using HATU and DIPEA for 75°C for 15 minutes (Agilent eclipse XDB-C18 column (4.6 x 150 mm, 5 µm) and a flow rate of 1 mL/min. Spectra were run with a solvent gradient of 0-100% B over 20 min. Solvent A: H_2O, 0.05% TFA, solvent B: MeCN, 0.05% TFA).*

3.3.10 The synthesis of semi-peptide 2 (WHFSYNP-) using 2-chlorotrityl resin

Due to the difficulties faced when trying to modify the C-terminus on resin, an alternative approach to try achieve the C-terminal modification in solution was tried. The 2-chorotrityl (Cl-Trt) resin (**Scheme 3-9A**, **3.47**) is a sensitive acid labile resin

that can be cleaved with low percentages of TFA. This gives the advantage of leaving residues with their side chain protecting groups, leaving the C-terminus open to modifications without causing unwanted side reactions (**Scheme 3-9B**). It is important to note that the N-terminal amino acid must be Boc protected rather than Fmoc protected, due to Fmoc being labile using a base and the amide coupling requiring a base to proceed.



Scheme 3-9 *a) The structure of 2-chlorotrityl resin (**3.47**) b) Schematic illustration of cleaving a peptide with protecting groups (**3.49**) from 2-chlorotrityl resin, amide coupling in solution to give **3.50**, followed by deprotection for the final product **3.51***

Despite having this advantageous strategy, loading the Cl-Trt resin with c*is*-2-(Fmoc-amino)cyclohexanecarboxylic acid, **3.30**, proved challenging. Initially, automated SPPS with DIC and oxyma was trialled. However, when analysing the cleaved peptide there was no conclusive mass found for the semi-peptide with the c*is*-2-(Fmoc-amino)cyclohexanecarboxylic acid turn, **3.44.** Other coupling agents including HATU and HOBt were attempted and showed the same result. The combination of the bulky phenyl groups causing steric hindrance, the sterically hindered carboxylic acid and the

weak nucleophilic properties of the carboxylate could have affected the loading. Therefore, Cl-Trt resin pre-loaded with proline was used to build the peptide. Proline offers a turn like structure similar to *cis*-2-aminocyclohexanecarboxylic acid, **3.42**, and the use of a pre-loaded resin would allow the rapid preparation of a large enough quantity of semi-peptide to screen a fragment library (**Figure 3-24**, blue).



3.44 **3.52**

Figure 3-24 *The structures of semi-peptide 2 (WHFSYN-, **3.15**) coupled to the turn mimic cis-2-aminocyclohexanecarboxylic acid (blue) to give **3.44** and couple to proline (blue) to give **3.52***

By using a pre-loaded resin with proline, the peptide, **3.52**, was able to be successfully synthesised (**Figure 3-25**).

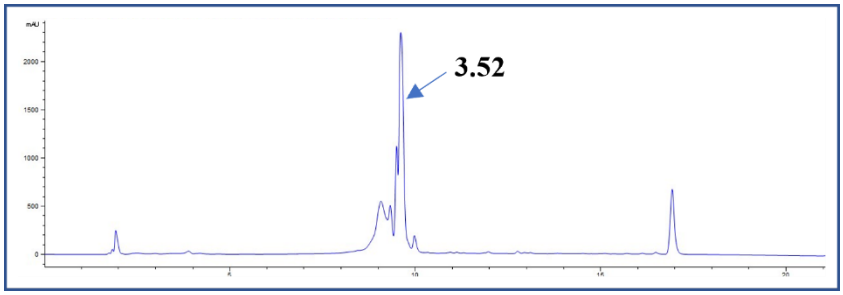
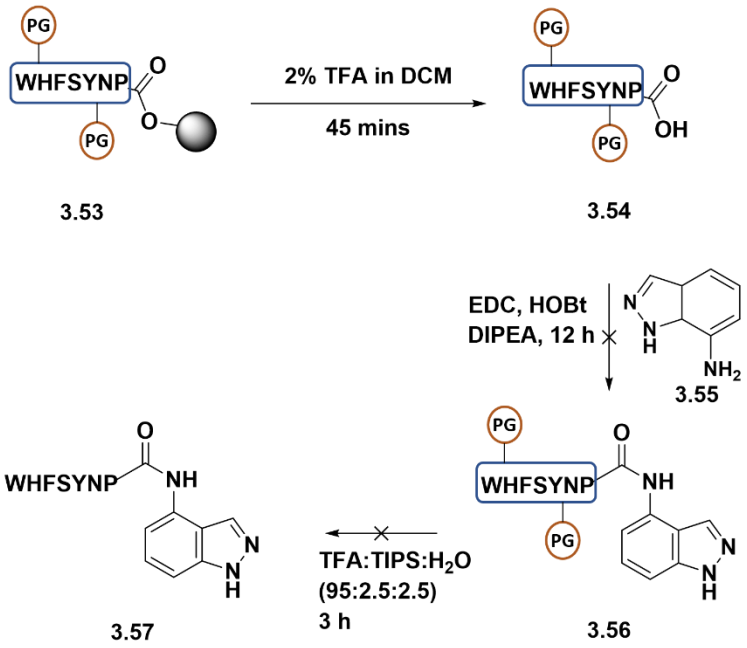


Figure 3-25 *The analytical HPLC trace recorded at 214 nm of **3.52** (Agilent eclipse XDB-C18 column (4.6 x 150 mm, 5 µm) and a flow rate of 1 mL/min. Spectra were run with a solvent gradient of 0-100% B over 20 min. Solvent A: H_2O, 0.05% TFA, solvent B: MeCN, 0.05% TFA).*

To couple the amine small molecules to the proline, following the completed semi-peptide synthesis, the peptide was cleaved with 2% TFA in DCM for 45 minutes. This allowed for the protecting groups of the amino acids to remain. 1-Ethyl-3-(3-dimethylaminopropyl)carbodiimide (EDC) and HOBt with DIPEA were first trialled to form the amide bond using 7 amino-1H-indazole, **3.55** (**Scheme 3-10**). However, when analysed through analytical HPLC the main peak that can be seen is the semi-peptide without 7 amino-1H-indazole as seen in **Figure 3-26**. This was confirmed showing an *m/z* of 950.5 matching the semi-peptide **3.52** $[M+H]^+$ of 950.5.



Scheme 3-10 *The semi-peptide WHFSYNP was built on Cl-Trt (**3.53**) that was cleaved in 2% TFA in DCM to give **3.54**, the amide bond was then attempted using EDC, HOBt and DIPEA for 12 h to give **3.56** and the protecting groups were then removed using the cleavage cocktail TFA:TIPS:H_2O for 3 h to give **3.57.***

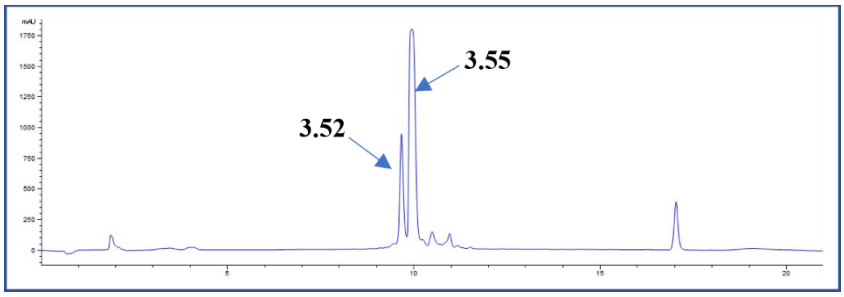
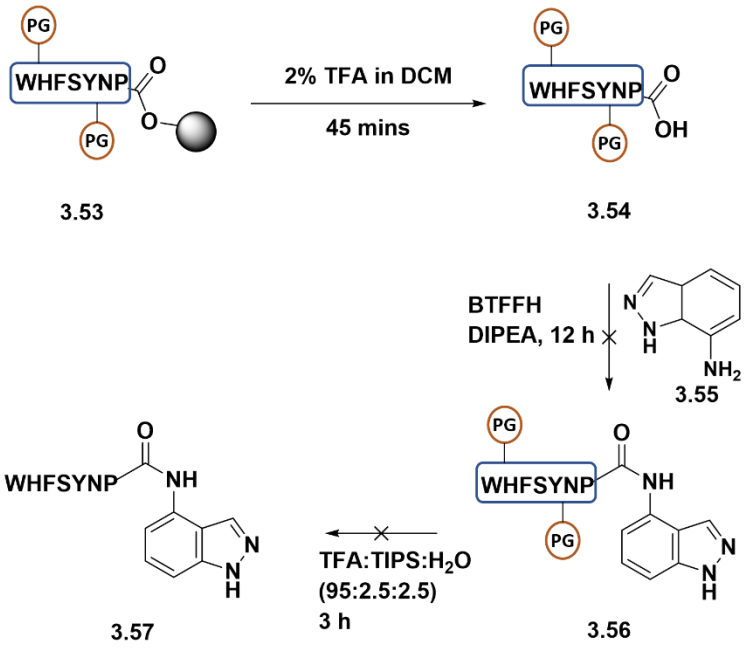


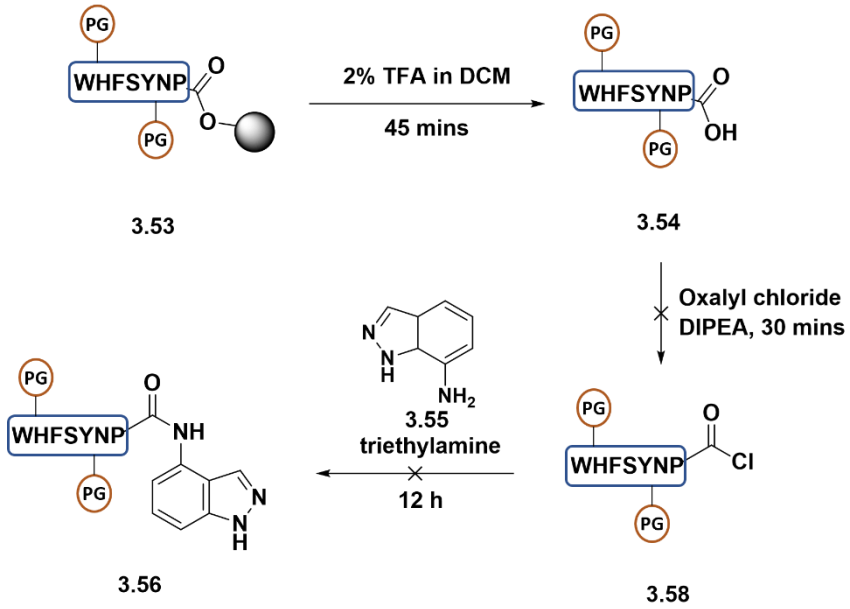
Figure 3-26 *The analytical HPLC trace recorded at 214 nm after EDC, HOBt coupling with 7 amino-1H-indazole showing the product of **3.52** (Agilent eclipse XDB-C18 column (4.6 x 150 mm, 5 μm) and a flow rate of 1 mL/min. Spectra were run with a solvent gradient of 0-100% B over 20 min. Solvent A: H_2O, 0.05% TFA, solvent B: MeCN, 0.05% TFA).*

Due to the steric hinderance at the proline carbonyl and perhaps the amines selected being electron deficient, we sought to make the proline more active by creating a better leaving group. Ulven *et al*. reported using the fluorouronium reagents, Fluoro-*N,N,N',N'*-bis(tetramethylene)formamidinium hexafluorophosphate (BTFFH) to couple sterically hindered amino acids.[68] This strategy converts carboxylic acids into acyl fluorides. The protected semi-peptide was stirred with BTFFH (1.5 eq) and DIPEA (4.5 eq) in DCM before the amine small molecule fragment was added and left to stir overnight (**Scheme 3-11**).



Scheme 3-11 *The semi-peptide WHFSYNP was built on Cl-Trt (**3.53**) that was cleaved in 2% TFA in DCM to give **3.54**, the amide bond was then attempted using BTFFH and DIPEA for 12 h to give **3.56** and the protecting groups were then removed using the cleavage cocktail TFA:TIPS:H_2O for 3 h to give **3.57.***

Following this, the peptide was deprotected using TFA:TIPS:H_2O (95:2.5:2.5) for 3 hours and when analysed no mass was confirmed for the coupling of the amine to the proline carboxylic acid, **3.56**. In another approach to activate the proline carbonyl it was attempted to turn the carboxylic acid into an acyl chloride, **3.58** (**Scheme 3-12**).



Scheme 3-12 *The semi-peptide WHFSYNP was built on Cl-Trt (**3.53**) that was cleaved in 2% TFA in DCM to give **3.54**. Oxalyl chloride and DIPEA were used to turn the carboxylic acid to an acyl chloride (**3.58**) the amide bond was then attempted using triethylamine overnight to give **3.56** and the protecting groups were then removed using the cleavage cocktail TFA:TIPS:H_2O for 3 h to give **3.57.***

Oxalyl chloride and DIPEA were stirred with the semi peptide, **3.54**, for 30 minutes, and then amine small molecule and triethylamine were added and left to stir overnight. Similarly, after deprotection no mass was confirmed for a successful amide coupling and the analytical HPLC showed the semi peptide as seen in **Figure 3-27**.

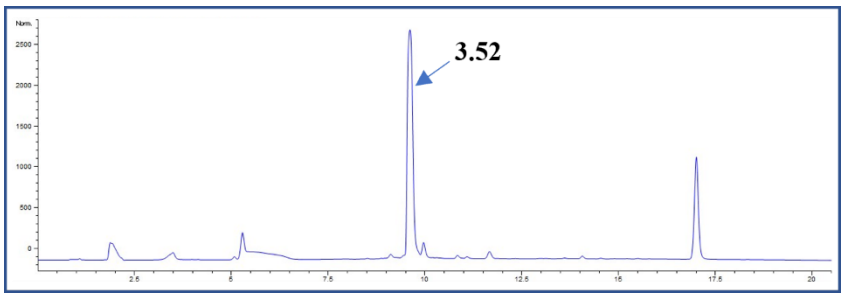
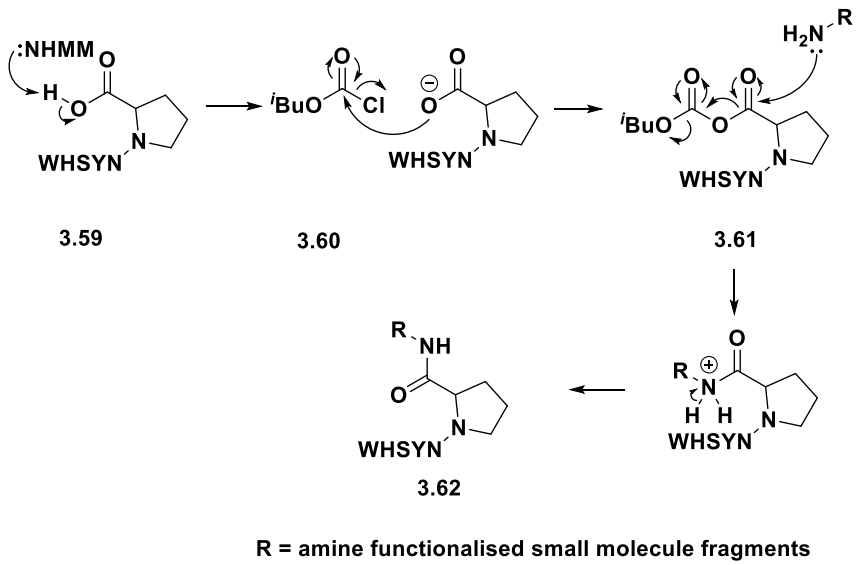


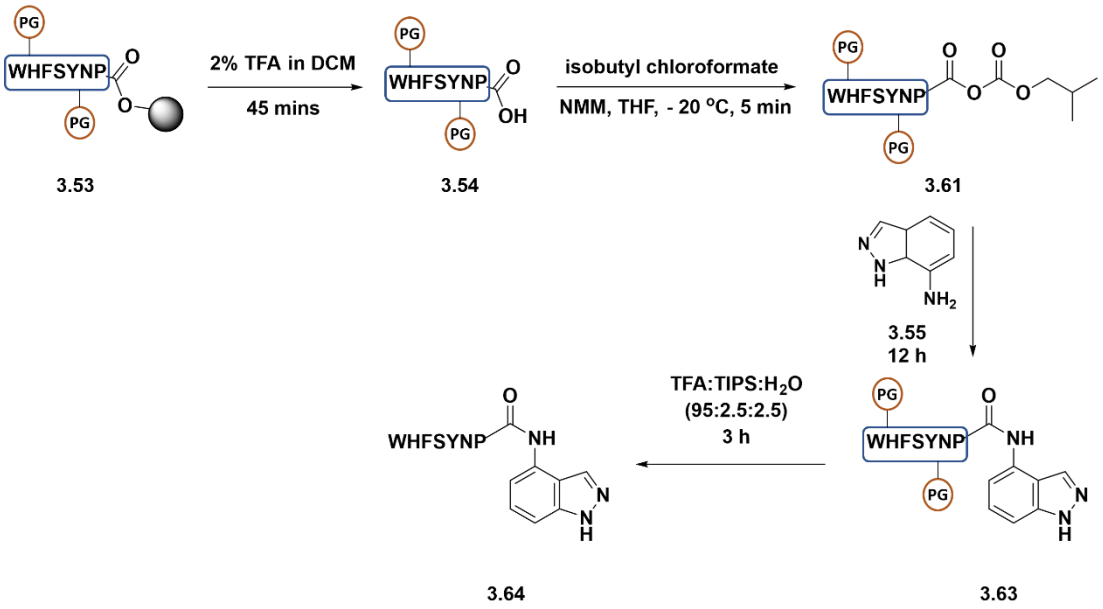
Figure 3-27 *The analytical HPLC trace recorded at 214 nm after oxalyl chloride and DIPEA to form an acyl chloride (Agilent eclipse XDB-C18 column (4.6 x 150 mm, 5 µm) and a flow rate of 1 mL/min. Spectra were run with a solvent gradient of 0-100% B over 20 min. Solvent A: H_2O, 0.05% TFA, solvent B: MeCN, 0.05% TFA).*

It was suggested that the acid chloride may not be forming or may be too unstable to achieve the desired reaction. As such, a strategy was proposed using isobutyl chloroformate with a base to activate the terminal proline as a mixed anhydride, previously reported to be effective.[69,70] The mixed anhydride has a similar reactivity to an acid chloride, but is formed under milder conditions, perhaps prolonging the lifetime of the reactive moiety. The base, N-methylmorpholine, deprotonates the terminal proline on the protected semi-peptide, **3.59**, this causes the nucleophilic attack of the isobutyl chloroformate to activate the carboxylic acid, (**Scheme 3-13**, **3.61**). A second nucleophilic attack by the amine of the activated carboxylic acid leads to the formation of an amide bond.



Scheme 3-13 *The scheme of activating the carboxylic acid of proline on the protected semi peptide* ***3.59****, using isobutyl chloroformate (****3.60****) to give the activated compound* ***3.61*** *that can be attacked by the amine nucleophile (****3.61****) to form the amide bond (****3.62****).*

After semi-peptide synthesis and cleavage from the resin using 2% TFA in DCM for 45 minutes, the protected semi-peptide, **3.54**, was then dissolved in THF and cooled to −10 °C under nitrogen. N-methylmorpholine and isobutyl chloroformate (IBCF) were added and the reaction was cooled to −20 °C. Once cooled, the amine functionalised small molecule fragment, **3.55**, was added and a minimal amount of DMF, for solubility, and the reaction was allowed to come to room temperature. After stirring overnight, THF was removed under vacuum and the cleavage conditions to remove the protecting groups from the amino acids of TFA:TIPS:H_2O (95:2.5:2.5) was added and stirred for 3 hours. The cleavage solution was removed under vacuum and the peptide-small molecule hybrid, **3.64**, was precipitated using diethyl ether.



Scheme 3-14 *The semi-peptide 2 (**3.53**) was built on Cl-Trt (**3.47**) this was cleaved in 2% TFA in DCM to give **3.54**. Isobutryl chloroformate was used to activate the peptide (**3.61**) and the amine **3.55** was added to stir overnight at room temperature. **3.63** was deprotected to give the peptide-small molecule hybrid **3.64.***

This was successfully replicated for eleven amine functionalised small molecule fragments. Each crude hybrid was confirmed using analytical HPLC and mass spectrometry. Purification was performed using semi-preparative HPLC, and purity was confirmed using the analytical HPLC and mass spectrometry (**Figure 3-28**).

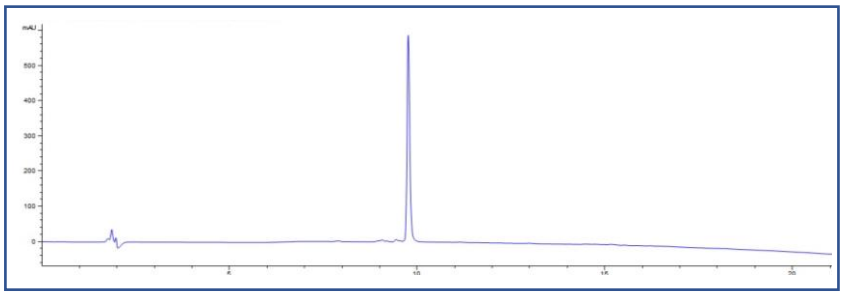


Figure 3-28 *The analytical HPLC trace recorded at 214 nm showing peptide-small molecule hybrid **3.64** (4.6 x 150 mm, 5 µm) and a flow rate of 1 mL/min. Spectra were run with a solvent gradient of 0-100% B over 20 min. Solvent A: H_2O, 0.05% TFA, solvent B: MeCN, 0.05% TFA).*

3.3.11 Small molecule fragments functionalised with an amine

As discussed in section 3.3.1.3.1 when selecting the amine functionalised small molecule fragments, the same considerations were taken when selecting the amine small molecule fragments (**Figure 3-29**). Using a refined search of previous hits that had shown preferential properties, small molecules were chosen to cover a large amount of chemical space.[60] Due to time constraints, eleven small molecule fragments were chosen.

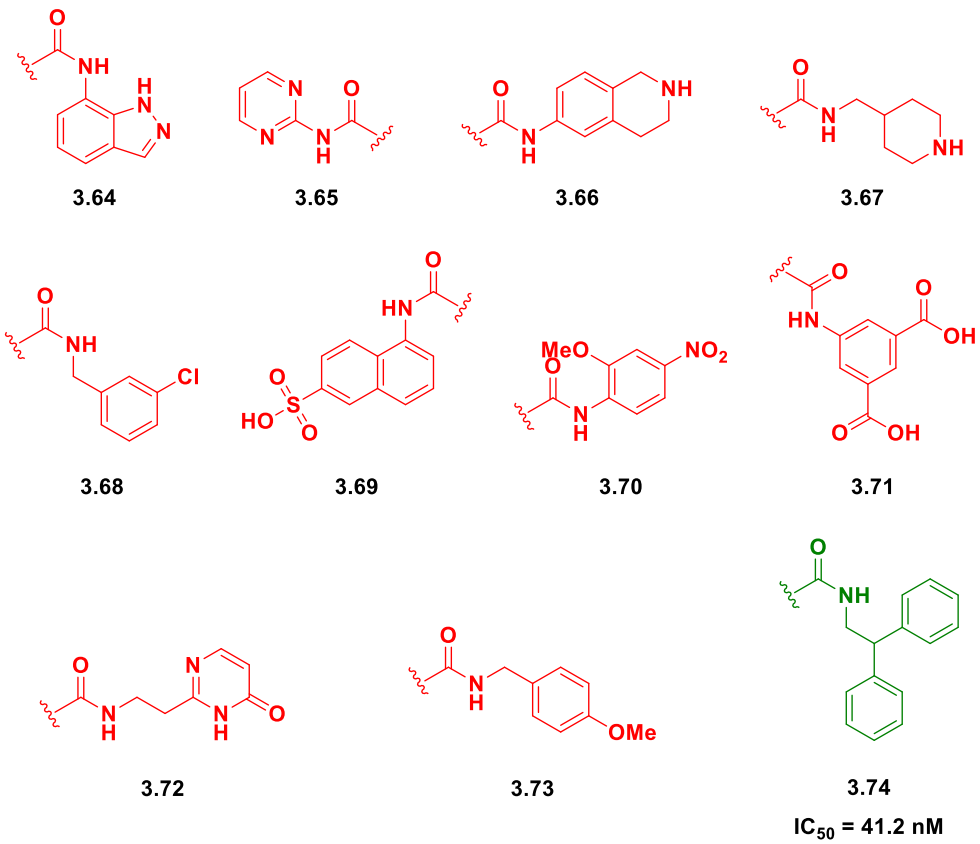


Figure 3-29 *The small molecule fragments selected functionalised with an amine. Hits that retained inhibition of PD-1/PD-L in green, hits that lost the ability to inhibit PD-1/PD-L1 in red.* IC_{50} *values reported (n/N = 2/6).*

When testing the semi-peptide with the turn mimic, **3.52**, it was found to show inhibition of PD-1/PD-L1 with a IC_{50} value of 2.3 nM [1.1, 5] (**Figure 3-29**). This result was somewhat unexpected. The alanine scan had highlighted that the loss of several amino acids in semi-peptide 1 resulted in a complete loss of binding, but this truncated peptide demonstrated inhibition of PD-1/PD-L1 in the HTRF assay superior to the parent CLP003. Further investigation is required to determine if this inhibition is a result of specific binding to the PD-1/PD-L1 interface, but the peptide-small molecule hybrids were investigated nonetheless. When testing the amine small molecule fragments, we were searching for an increased inhibition. It was found that **3.74** was the only peptide-small molecule hybrid that showed inhibition of PD-1/PD-L1, with the remaining 10 losing the ability to inhibit the interaction. The IC_{50} value for **3.74** was 41.2 nM [1.3, 1.18] demonstrating that perhaps hydrophobic effects are required for inhibition of PD-1/PD-L1.

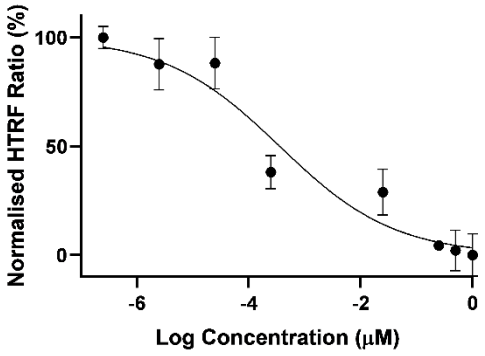


Figure 3-30 *The dose dependent curve of WHFSYNP,* ***3.52****, showing an* IC_{50} *= 0.0023 μM [0.011, 0.005].* IC_{50} *+/- 95% confidence interval (n/N = 2/6).*

3.4 Conclusion

Despite PPIs previously being considered "undruggable" by small molecules, advancements today have repeatedly disproved this.[2] When considering the immune checkpoint PD-1/PD-L1, there is a notable absence of small molecule inhibitors that have progressed into the clinical trial stage. As discussed in chapter one, peptides can offer a valuable starting point in the development of novel small molecules due to their structure benefits. Peptide-directed binding is one approach that capitalises on the peptides ability to bind tightly and selectively to PPIs.[49,50] . There are two methods of this strategy, one that includes the synthesis of the peptide-small molecule hybrids and one that is completely computational, only synthesising the final small molecule mimic. While both techniques have proven to be effective, the process of making the intermediate peptide-small molecule hybrids opens an opportunity for further structural diversity and potential leads.[49,50] The peptide CLP003, **3.13**, was the foundation in the design and synthesis of thirty-one peptide-small molecule hybrids that incorporated a turn mimic within the structure.

The peptide-small molecule hybrids formed of semi-peptide 1, -NWRWLPP, **3.14**, using the turn mimic c*is*-2-(Fmoc-amino)cyclohexanecarboxylic acid, **3.30**, showed ten hits that inhibited PD-1/PD-L1 at 10 μM. **3.34**, **3.40**, and **3.41** showed an IC_{50} value of less than 10 μM and **3.44** and **3.39** showed nanomolar inhibition of PD-1/PD-L1. In comparison to the previously mentioned small molecule inhibitors in section 3.1.2, these hybrids show promising IC_{50} values as potential lead compounds for further investigation.

For semi-peptide 2, **3.16**, proline replaced c*is*-2-(Fmoc-amino)cyclohexanecarboxylic acid, **3.30**, as the turn mimic due to synthesis difficulties. Surprisingly, **3.52** surprisingly showed inhibition of PD-1/PD-L1 with an IC_{50} value of 2.3 nM [1.1, 5], demonstrating superior inhibitory activity in comparison to the parent, CLP003, and comparable to previously mentioned small molecule inhibitors in section 3.1.2. Additional testing such as SPR or using the cell-based assay described in chapter 2 section 2.4.9 could confirm the activity of **3.52**. Similarly, a crystal structure of **3.52** would be interesting in comparison to CLP003 to determine if the binding sites would overlap. Furthermore, when considering the azobenzene peptide **2.51** discussed in chapter 2, out of the six peptides designed this peptide was the only one that contained the sequence WHFSYN-, **3.52**. If potentially this sequence is the cause for successful inhibition, an alanine scan of this shortened peptide would be invaluable to determine which amino acids are essential for binding. With this information, the photo-switchable peptides could be modified and potentially improved to create a smaller PD-1/PD-L1 inhibitor.

When investigating peptide-small molecule hybrids, only **3.74** showed inhibitory activity of the eleven tested resulting in an IC_{50} value of 41 nM [13, 118]. This suggests that hydrophobic effects are required for inhibition of PD-1/PD-L1. Upon returning to this synthesis, building the peptide WHFSYN- on the Cl-Trt resin and upon cleavage adding c*is*-2-(Fmoc-amino)cyclohexanecarboxylic acid using the successful coupling described in section 3.3.10 with ICBF would be interesting to determine if the superior inhibition would remain and as a comparison to semi-peptide 1. The effect of acetylation would also be intriguing as these peptides remained unacetylated, potentially making them susceptible to instability and degradation.

The future work for the positive hits found in section 3.3.7 could include the optimisation of the SPR conditions to confirm binding to PD-L1. Also, further testing using the cell-based assay described in chapter 2 section 2.4.9 to determine activity would confirm the HTRF assay results. While characterisation *via* mass spectrometry and analytical HPLC was sufficient in this study for discovering hits while screening many compounds in a short amount of time, further investigation into characterisation of the most potent hits would be important including determining stereochemistry. Crystal structures of the most potent hits, **3.39** and **3.44**, would be interesting to see in

comparison to CLP003 to determine which interactions between the compounds and PD-L1 potentially overlap or whether new interactions emerge. For the peptide-small molecule hybrids that were successful hits, this could be followed by the sequential replacement of the semi-peptide with the top three hits from each screening to form small-molecule mimics with the turn unit c*is*-2-(Fmoc-amino)cyclohexanecarboxylic acid, **3.30,** acting as a linker between the two fragments.

3.5 Experimental

3.5.1 Materials and solvents

All chemicals were purchased from Sigma Aldrich, Fisher Scientific or Fluorochem. Anhydrous solvents were purchased from Sigma Aldrich, used as purchased and assumed to conform to specification.

3.5.1 Instrumental techniques

^{1}H- and ^{13}C-NMR were collected using a Bruker spectrometer operating at 400 MHz (^{1}H) or 101 MHz (^{13}C) using the specified deuterated solvent. The chemical shifts were recorded in ppm and were referenced to the residual solvent peak of DMSO (2.50 ppm) or chloroform (7.26 ppm). Multiplicities in the NMR spectra are described as s = singlet, d = doublet, t = triplet, q = quartet, m = multiplet, and combinations thereof. Coupling constants are reported in Hz. High resolution masses were recorded using Waters Synapt XS QTOF under electrospray ionisation. Low resolution mass was recorded using an Agilent 1200 Series equipped with a 6460 triple quadrupole.

Analytical RP-HPLC was performed using an Agilent 1200 HPLC using an Agilent eclipse XDB-C18 column (4.6 x 150 mm, 5 μm) and a flow rate of 1 mL/min. Spectra were run with a solvent gradient of 0-100% B over 20 min. Solvent A: H_2O, 0.05% TFA, solvent B: MeCN, 0.05% TFA. Detection wavelengths were 214 nm and 254 nm. . Semi-preparative RP-HPLC was performed using an Agilent 1200 HPLC, fitted with an Agilent eclipse XDB-C18 column (9.4 x 250 mm, 5 μm) and a flow rate of 3 mL/min. Spectra were run with a solvent gradient of 1-100% B over 20 min. Solvents: A = H_2O, 0.05% TFA, B: MeCN, 0.05% TFA. Detection wavelengths were 214 nm and 254 nm. Preparative RP-HPLC was performed on an Agilent 1200 HPLC, fitted with an Agilent eclipse XDB-C18 column (21.2 x 150 mm, 5 μM) and a flow rate of 20 mL/min. Purification was run with a solvent gradient of 0-100% B over 15 min.

Solvent A: 95% H2O, 5% MeCN, 0.05% TFA, solvent B: 95% MeCN, 5% H_2O, 0.05% TFA. Detection wavelengths were 214 nm and 254 nm.

Automated peptide synthesis was performed using a Biotage I. Microwave used was CEM discover.

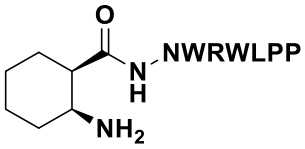
Human PD-1/PD-L1 biochemical binding assay was purchased from Revvity. Microplate spectral scans were recorded on a CLARIOstar (BMG Labtech) microplate reader.

3.5.2 Semi-peptide synthesis

All peptides synthesised in this chapter were synthesised via Fmoc-solid phase peptide synthesis. TentaGel S RAM (resin loading 0.23 mmol/g) or 2-chlorotrityl resin (resin loading 0.1-3.0 mmol/g) was used for this peptide synthesis.

*3.5.2.1 The synthesis of **3.31** (Semi-peptide 1, **3.14**, with the turn mimic Cis-2-aminocyclohexanecarboxylic acid, **3.30** on resin)*

For **3.31**, 50 mg of Tentagel resin (0.023 mmol) was suspended in DMF (2 mL) and allowed to swell for 20 minutes. The DMF was drained from the peptide vessel and Fmoc deprotection was carried out by addition of 2 x 2 mL of 20% piperidine in DMF, which was shaken for 10 minutes. This was removed and the resin was washed with DMF (3 x 2 mL). The resin was then treated with a solution of Fmoc-Pro-OH (4 equiv. compared to resin loading), to which HBTU (3.9 equiv.) and HOBt (4 equiv.) and DIPEA (8 equiv.) in DMF were added. The mixture was then shaken for 30 min. The vessel was drained and the resin washed with DMF (3 x 2 mL). The coupling reaction was then repeated followed by Fmoc deprotection (2 x 2 mL 20% piperidine in DMF, 10 min) and finally the resin was washed with DMF. Subsequent amino acids were coupled in an identical fashion. After the final amino acid coupling reaction (asparagine) the resin was Fmoc protected (2 x 2 mL 20% piperidine in DMF, 10 min) and *cis*-2-(Fmoc-amino)cyclohexanecarboxylic acid, **3.30**, (4 eq) was coupled the peptide chain using HOBt (4 eq), HBTU (4 eq) and DIPEA (8 eq) in DMF for 8 minutes at 70 ℃. The Fmoc was deprotected.

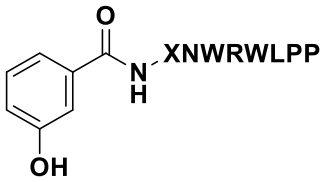


3.32

The general procedure in 3.5.2.1 was followed. The resin was then washed with DCM (x 3) and MeOH (x 3) to remove any residual DMF. The peptide was then cleaved from the resin in TFA:TIPS:H_2O (95:2.5:2.5) and shaken for three hours. The resulting solution was extracted and the resin was washed with TFA (3 x 1 mL), the solutions were combined and concentrated under vacuum. The peptide was precipitated using cold diethyl ether and filtered. The crude peptide was purified by semi-preparative HPLC and their purity confirmed by analytical HPLC. RP-HPLC: t_R = 9.89 min. ESI-QQQ $[M+H]^+$ *m/z* calc. for $[C_{55}H_{77}KN_{15}O_9]^+$ 1130.6; found 1130.0.

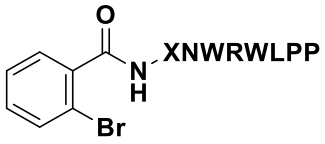
3.5.2.2 The synthesis of the peptide-small molecule hybrids using ***3.31***

X = *cis*-2-aminocyclohexanecarboxylic acid



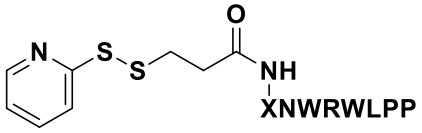
3.33

The general procedure in 3.5.2.1 was followed. 3-hydroxybenzoic acid (1 eq) was coupled with HATU (1 eq) and DIPEA (2 eq) at 60 °C for 8 minutes to the deprotected peptide. The resin was washed with DCM (x 3) and MeOH (x 3) to remove any residual DMF. The peptide was then cleaved from the resin in TFA:TIPS:H_2O (95:2.5:2.5) and shaken for three hours. The resulting solution was extracted and the resin was washed with TFA (3 x 1 mL), the solutions were combined and concentrated under vacuum. The peptide was precipitated using cold diethyl ether and filtered. The crude peptide was purified by semi-preparative HPLC and their purity confirmed by analytical HPLC. RP-HPLC: t_R = 10.86 min. ESI-QQQ $[M+2H]^{2+}$ *m/z* calc. for $[C_{62}H_{82}N_{15}O_{11}]^{2+}$ 606.8; found 606.2



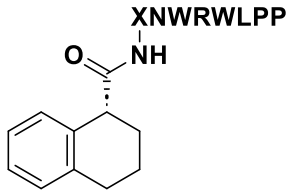
3.37

The general procedure in 3.5.2.1 was followed. 2-bromobenzoic acid (2 eq) was coupled with HATU (2 eq) and DIPEA (4 eq) at 60 ℃ for 8 minutes to the deprotected peptide. The resin was washed with DCM (x 3) and MeOH (x 3) to remove any residual DMF. The peptide was then cleaved from the resin in TFA:TIPS:H_2O (95:2.5:2.5) and shaken for three hours. The resulting solution was extracted and the resin was washed with TFA (3 x 1 mL), the solutions were combined and concentrated under vacuum. The peptide was precipitated using cold diethyl ether and filtered. The crude peptide was purified by semi-preparative HPLC and their purity confirmed by analytical HPLC. RP-HPLC: t_R = 10.87 min. ESI-QQQ $[M+K]^+$ *m/z* calc. for $[C_{62}H_{80}BrKN_{15}NaO_{10}]^+$ 1314.50; found 1314.2



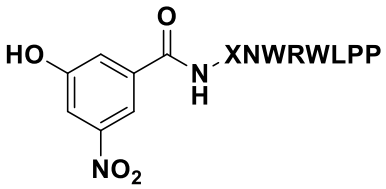
3.38

The general procedure in 3.5.2.1 was followed. 3-(2-pyridylthio)propanoic acid (2 eq) was coupled with HATU (2 eq) and DIPEA (4 eq) at 60 ℃ for 8 minutes to the deprotected peptide. The resin was washed with DCM (x 3) and MeOH (x 3) to remove any residual DMF. The peptide was then cleaved from the resin in TFA:TIPS:H_2O (95:2.5:2.5) and shaken for three hours. The resulting solution was extracted and the resin was washed with TFA (3 x 1 mL), the solutions were combined and concentrated under vacuum. The peptide was precipitated using cold diethyl ether and filtered. The crude peptide was purified by semi-preparative HPLC and their purity confirmed by analytical HPLC. RP-HPLC: t_R= 10.75 min. ESI-QQQ $[M+H]^+$ *m/z* calc. for $[C_{63}H_{85}N_{16}O_{10}S_2]^+$ 1289.6; found 1290.0



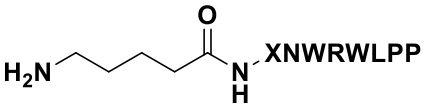
3.39

The general procedure in 3.5.2.1 was followed. *R*-1,2,3,4-tetrazhydronaphthalene-1-carboxylic acid (2 eq) was coupled with HATU (2 eq) and DIPEA (4 eq) at 60 ℃ for 8 minutes to the deprotected peptide. The resin was washed with DCM (x 3) and MeOH (x 3) to remove any residual DMF. The peptide was then cleaved from the resin in TFA:TIPS:H_2O (95:2.5:2.5) and shaken for three hours. The resulting solution was extracted and the resin was washed with TFA (3 x 1 mL), the solutions were combined and concentrated under vacuum. The peptide was precipitated using cold diethyl ether and filtered. The crude peptide was purified by semi-preparative HPLC and their purity confirmed by analytical HPLC. RP-HPLC: t_R= 10.71 min. ESI-QQQ $[M+3H]^{3+}$ *m/z* calc. for $[C_{66}H_{90}N_{15}O_{10}]^{3+}$ 417.9; found 417.3.



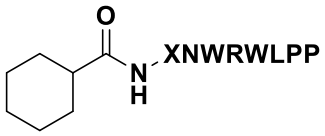
3.40

The general procedure in 3.5.2.1 was followed. 3-hydroxy-5-nitrobenzoic acid (2 eq) was coupled with HATU (2 eq) and DIPEA (4 eq) at 60 ℃ for 8 minutes to the deprotected peptide. The resin was washed with DCM (x 3) and MeOH (x 3) to remove any residual DMF. The peptide was then cleaved from the resin in TFA:TIPS:H_2O (95:2.5:2.5) and shaken for three hours. The resulting solution was extracted and the resin was washed with TFA (3 x 1 mL), the solutions were combined and concentrated under vacuum. The peptide was precipitated using cold diethyl ether and filtered. The crude peptide was purified by semi-preparative HPLC and their purity confirmed by analytical HPLC. RP-HPLC: t_R = 10.74 min. ESI-QQQ $[M-H]^-$ *m/z* calc. for $[C_{62}H_{80}N_{16}O_{13}]^-$ 1256.6; found 1256.6.



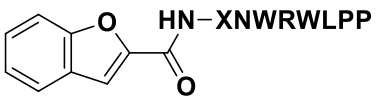
3.41

The general procedure in 3.5.2.1 was followed. 4-aminobutyric acid (2 eq) was coupled with HATU (2 eq) and DIPEA (4 eq) at 60 ℃ for 8 minutes to the deprotected peptide. The resin was washed with DCM (x 3) and MeOH (x 3) to remove any residual DMF. The peptide was then cleaved from the resin in TFA:TIPS:H_2O (95:2.5:2.5) and shaken for three hours. The resulting solution was extracted and the resin was washed with TFA (3 x 1 mL), the solutions were combined and concentrated under vacuum. The peptide was precipitated using cold diethyl ether and filtered. The crude peptide was purified by semi-preparative HPLC and their purity confirmed by analytical HPLC. RP-HPLC: t_R = 10.74 min. ESI-QQQ $[M+H]^+$ *m/z* calc. for $[C_{60}H_{87}N_{16}O_{10}]^+$ 1191.7; found 1191.1



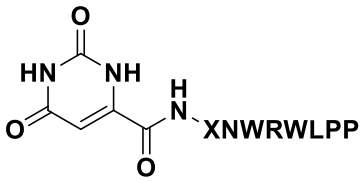
3.42

The general procedure in 3.5.2.1 was followed. Cyclohexanecarboxylic acid (2 eq) was coupled with HATU (2 eq) and DIPEA (4 eq) at 60 ℃ for 8 minutes to the deprotected peptide. The resin was washed with DCM (x 3) and MeOH (x 3) to remove any residual DMF. The peptide was then cleaved from the resin in TFA:TIPS:H_2O (95:2.5:2.5) and shaken for three hours. The resulting solution was extracted and the resin was washed with TFA (3 x 1 mL), the solutions were combined and concentrated under vacuum. The peptide was precipitated using cold diethyl ether and filtered. The crude peptide was purified by semi-preparative HPLC and their purity confirmed by analytical HPLC. RP-HPLC: t_R = 10.81 min. ESI-QQQ $[M+Na]^+$ *m/z* calc. for $[C_{62}H_{87}N_{15}NaO_{10}]^+$ 1224.7; found 1225.3.



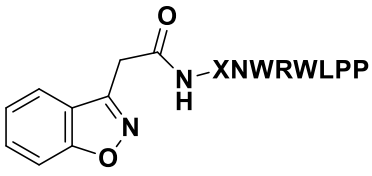
3.43

The general procedure in 3.5.2.1 was followed. Benzo[b]furan-2-carboxylic acid (2 eq) was coupled with HATU (2 eq) and DIPEA (4 eq) at 60 ℃ for 8 minutes to the deprotected peptide. The resin was washed with DCM (x 3) and MeOH (x 3) to remove any residual DMF. The peptide was then cleaved from the resin in TFA:TIPS:H_2O (95:2.5:2.5) and shaken for three hours. The resulting solution was extracted and the resin was washed with TFA (3 x 1 mL), the solutions were combined and concentrated under vacuum. The peptide was precipitated using cold diethyl ether and filtered. The crude peptide was purified by semi-preparative HPLC and their purity confirmed by analytical HPLC. RP-HPLC: t_R = 10.91 min. ESI-QQQ $[M+H]^+$ *m/z* calc. for $[C_{64}H_{81}N_{15}O_{11}]^+$ 1236.6; found 1236.9.



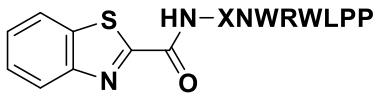
3.44

The general procedure in 3.5.2.1 was followed. Orotic acid (2 eq) was coupled with HATU (2 eq) and DIPEA (4 eq) at 60 ℃ for 8 minutes to the deprotected peptide. The resin was washed with DCM (x 3) and MeOH (x 3) to remove any residual DMF. The peptide was then cleaved from the resin in TFA:TIPS:H_2O (95:2.5:2.5) and shaken for three hours. The resulting solution was extracted and the resin was washed with TFA (3 x 1 mL), the solutions were combined and concentrated under vacuum. The peptide was precipitated using cold diethyl ether and filtered. The crude peptide was purified by semi-preparative HPLC and their purity confirmed by analytical HPLC. RP-HPLC: t_R= 10.79 min. ESI-QQQ $[M+2H]^{2+}$ *m/z* calc. for $[C_{60}H_{81}N_{17}O_{12}]^{2+}$ 615.7; found 615.2.



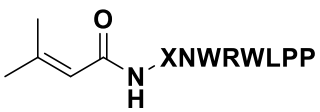
3.45

The general procedure in 3.5.2.1 was followed. 1,2-benzisoxazol-3-ylacetic acid (2 eq) was coupled with HATU (2 eq) and DIPEA (4 eq) at 60 ℃ for 8 minutes to the deprotected peptide. The resin was washed with DCM (x 3) and MeOH (x 3) to remove any residual DMF. The peptide was then cleaved from the resin in TFA:TIPS:H_2O (95:2.5:2.5) and shaken for three hours. The resulting solution was extracted and the resin was washed with TFA (3 x 1 mL), the solutions were combined and concentrated under vacuum. The peptide was precipitated using cold diethyl ether and filtered. The crude peptide was purified by semi-preparative HPLC and their purity confirmed by analytical HPLC. RP-HPLC: t_R = 10.73 min. ESI-QQQ $[M+H]^+$ *m/z* calc. for $[C_{54}H_{60}N_{14}NaO_{10}]^+$ 1087.4; found 1086.9.



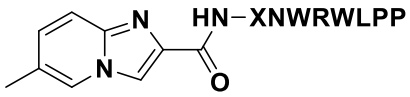
3.46

The general procedure in 3.5.2.1 was followed. 1,3-benzothiazole-2-carboxylic acid (2 eq) was coupled with HATU (2 eq) and DIPEA (4 eq) at 60 ℃ for 8 minutes to the deprotected peptide. The resin was washed with DCM (x 3) and MeOH (x 3) to remove any residual DMF. The peptide was then cleaved from the resin in TFA:TIPS:H_2O (95:2.5:2.5) and shaken for three hours. The resulting solution was extracted and the resin was washed with TFA (3 x 1 mL), the solutions were combined and concentrated under vacuum. The peptide was precipitated using cold diethyl ether and filtered. The crude peptide was purified by semi-preparative HPLC and their purity confirmed by analytical HPLC. RP-HPLC: t_R = 10.80 min. ESI-QQQ $[M+H]^+$ *m/z* calc. for $[C_{63}H_{81}N_{16}O_{10}S]^+$ 1253.6; found 1253.9



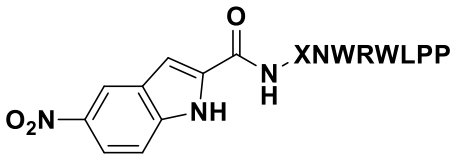
3.47

The general procedure in 3.5.2.1 was followed. 3,3-dimethylacrylic acid (2 eq) was coupled with HATU (2 eq) and DIPEA (4 eq) at 60 ℃ for 8 minutes to the deprotected peptide. The resin was washed with DCM (x 3) and MeOH (x 3) to remove any residual DMF. The peptide was then cleaved from the resin in TFA:TIPS:H_2O (95:2.5:2.5) and shaken for three hours. The resulting solution was extracted and the resin was washed with TFA (3 x 1 mL), the solutions were combined and concentrated under vacuum. The peptide was precipitated using cold diethyl ether and filtered. The crude peptide was purified by semi-preparative HPLC and their purity confirmed by analytical HPLC. RP-HPLC: t_R = 10.72 min. ESI-QQQ $[M+H]^+$ *m/z* calc. for $[C_{60}H_{84}N_{15}O_{10}]^+$ 1174.7; found 1175.0



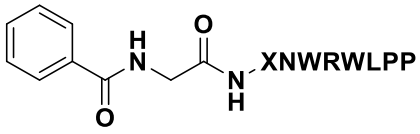
3.48

The general procedure in 3.5.2.1 was followed. 7-methy-imidazo[1,2-α]pyridine-2-carboxylic acid (2 eq) was coupled with HATU (2 eq) and DIPEA (4 eq) at 60 ℃ for 8 minutes to the deprotected peptide. The resin was washed with DCM (x 3) and MeOH (x 3) to remove any residual DMF. The peptide was then cleaved from the resin in TFA:TIPS:H_2O (95:2.5:2.5) and shaken for three hours. The resulting solution was extracted and the resin was washed with TFA (3 x 1 mL), the solutions were combined and concentrated under vacuum. The peptide was precipitated using cold diethyl ether and filtered. The crude peptide was purified by semi-preparative HPLC and their purity confirmed by analytical HPLC. RP-HPLC: t_R= 10.21 min. ESI-QQQ $[M+H]^+$ *m/z* calc. for $[C_{64}H_{84}N_{17}O_{10}]^+$ 1250.7; found 1251.1.



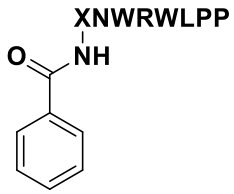
3.49

The general procedure in 3.5.2.1 was followed. 5-nitroindole-2-carboxylic acid (2 eq) was coupled with HATU (2 eq) and DIPEA (4 eq) at 60 ℃ for 8 minutes to the deprotected peptide. The resin was washed with DCM (x 3) and MeOH (x 3) to remove any residual DMF. The peptide was then cleaved from the resin in TFA:TIPS:H_2O (95:2.5:2.5) and shaken for three hours. The resulting solution was extracted and the resin was washed with TFA (3 x 1 mL), the solutions were combined and concentrated under vacuum. The peptide was precipitated using cold diethyl ether and filtered. The crude peptide was purified by semi-preparative HPLC and their purity confirmed by analytical HPLC. RP-HPLC: t_R = 10.79 min. ESI-QQQ $[M-H]^-$ *m/z* calc. for $[C_{64}H_{81}N_{17}O_{12}]^-$ 1279.6; found 1798.9.



3.50

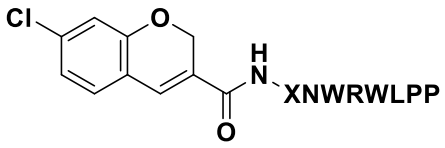
The general procedure in 3.5.2.1 was followed. Hippuric acid (2 eq) was coupled with HATU (2 eq) and DIPEA (4 eq) at 60 ℃ for 8 minutes to the deprotected peptide. The resin was washed with DCM (x 3) and MeOH (x 3) to remove any residual DMF. The peptide was then cleaved from the resin in TFA:TIPS:H_2O (95:2.5:2.5) and shaken for three hours. The resulting solution was extracted and the resin was washed with TFA (3 x 1 mL), the solutions were combined and concentrated under vacuum. The peptide was precipitated using cold diethyl ether and filtered. The crude peptide was purified by semi-preparative HPLC and their purity confirmed by analytical HPLC. RP-HPLC: t_R= 10.91 min. ESI-QQQ $[M+H]^+$ *m/z* calc. for $[C_{64}H_{84}KN_{16}O_{11}]^+$ 1291.61; found 1291.1.



3.53

The general procedure in 3.5.2.1 was followed. Benzoic acid (2 eq) was coupled with HATU (2 eq) and DIPEA (4 eq) at 60 ℃ for 8 minutes to the deprotected peptide. The

resin was washed with DCM (x 3) and MeOH (x 3) to remove any residual DMF. The peptide was then cleaved from the resin in TFA:TIPS:H_2O (95:2.5:2.5) and shaken for three hours. The resulting solution was extracted and the resin was washed with TFA (3 x 1 mL), the solutions were combined and concentrated under vacuum. The peptide was precipitated using cold diethyl ether and filtered. The crude peptide was purified by semi-preparative HPLC and their purity confirmed by analytical HPLC. RP-HPLC: t_R= 10.82 min. ESI-QQQ $[M+H]^+$ *m/z* calc. for $[C_{62}H_{81}KN_{15}O_{10}]^+$ 1234.6; found 1234.2.



3.54

The general procedure in 3.5.2.1 was followed. 6-chloro-2H-chromene-3-carboxylic acid (2 eq) was coupled with HATU (2 eq) and DIPEA (4 eq) at 60 ℃ for 8 minutes to the deprotected peptide. The resin was washed with DCM (x 3) and MeOH (x 3) to remove any residual DMF. The peptide was then cleaved from the resin in TFA:TIPS:H_2O (95:2.5:2.5) and shaken for three hours. The resulting solution was extracted and the resin was washed with TFA (3 x 1 mL), the solutions were combined and concentrated under vacuum. The peptide was precipitated using cold diethyl ether and filtered. The crude peptide was purified by semi-preparative HPLC and their purity confirmed by analytical HPLC. RP-HPLC: t_R = 10.76 min. ESI-QQQ $[M+2H]^{2+}$ *m/z* calc. for $[C_{65}H_{84}ClN_{15}O_{11}]^{2+}$ 642.8; found 624.6.

3.5.2.3 The synthesis of 3.54 (WHFSNP-)

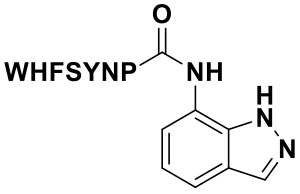
For **3.54**, the N-terminal amino acid was Boc-Trp(Boc)-OH, the remaining amino acids were Fmoc-AA-OH. 100 mg of 2-Chlorotrityl resin was suspended in DMF (2 mL) and allowed to swell for 20 minutes. The DMF was drained from the peptide vessel and Fmoc deprotection was carried out by addition of 2 x 2 mL of 20% piperidine in DMF, which was shaken for 10 minutes. This was removed and the resin was washed with DMF (3 x 2 mL). The resin was then treated with a solution of Fmoc-

Pro-OH (4 equiv. compared to resin loading), to which HBTU (3.9 equiv.) and HOBt (4 equiv.) and DIPEA (8 equiv.) in DMF were added. The mixture was then shaken for 30 min. The vessel was drained and the resin washed with DMF (3 x 2 mL). The coupling reaction was then repeated followed by Fmoc deprotection (2 x 2 mL 20% piperidine in DMF, 10 min) and finally the resin was washed with DMF. Subsequent amino acids were coupled in an identical fashion. The resin was washed with DCM (x 3) and MeOH (x 3) to remove any residual DMF. The peptide was then cleaved from the resin in TFA:TIPS:H_2O (95:2.5:2.5) and shaken for 45 minutes. The resulting solution was extracted and the resin was washed with TFA (3 x 1 mL), the solutions were combined and concentrated under vacuum.

3.52 (WHFSYNP). The general procedure in section 3.5.2.3 was followed. The crude peptide was then deprotected using TFA:TIPS:H_2O 95:2.5:2.5 for 3 hours and concentrated under vacuum. The peptide was precipitated using cold diethyl ether and filtered. RP-HPLC: t_R = 9.85 min. ESI-QQQ $[M+H]^+$ *m/z* calc. for $[C_{54}H_{60}N_{14}NaO_{10}]^+$ 1087.4; found 1086.9

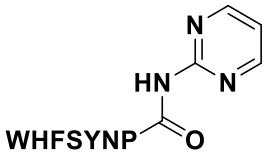
3.5.2.4 The synthesis of peptide-small molecule with amine functionalised small molecules

The general procedure in section 3.5.2.3 was followed. The protected peptide (WHFSYNP, **3.54**) was dissolved in THF and cooled −10 ℃ under N_2. NMM (4 eq) and isobutyl chloroformate (4 eq) was added and after 5 mins cooled to −20 ℃. The amine (4 eq) was added with DMF (2 μL) and stirred at −10 ℃ for 1 hour before stirring at room temperature overnight. The solvent was removed under vacuum and the protecting groups of the peptide were removed using TFA:TIPS:H_2O 95:2.5:2.5 for 3 hours. The small molecule-peptide hybrid was concentrated under vacuum and precipitated with diethyl ether. Crude small molecule-peptide hybrids were purified using semi-preparative HPLC and were confirmed using analytical HPLC and mass spectroscopy.



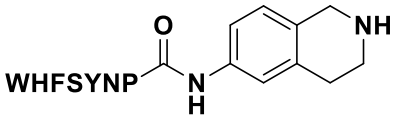
3.54

7 amino-1H-indazole. RP-HPLC: t_R = 9.76 min. ESI-QQQ $[M+H]^+$ *m/z* calc. for $[C_{54}H_{60}N_{14}NaO_{10}]^+$ 1087.4; found 1086.9



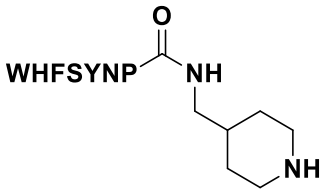
3.65

2-aminopyrimidine. RP-HPLC: t_R = 10.98 min. ESI-QQQ $[M+2H]^{2+}$ *m/z* calc. for $[C_{51}H_{60}N_{14}O_{10}]^{2+}$ 514.2; found 514.2



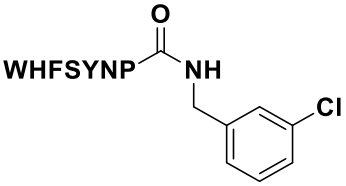
3.66

1,2,3,4-Tetrahydroisoquinolin-7-amine. RP-HPLC: t_R = 11.56 min. ESI-QQQ $[M+2H]^{2+}$ *m/z* calc. for $[C_{56}H_{67}N_{13}O_{10}]^{2+}$ 540.75; found 540.4



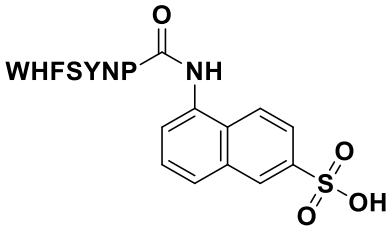
3.67

4-aminomethylpiperidine. RP-HPLC: t_R = 9.70 min. ESI-QQQ $[M+2H]^{2+}$ *m/z* calc. for $[C_{53}H_{69}N_{13}O_{10}]^{2+}$ 523.7; found 523.6



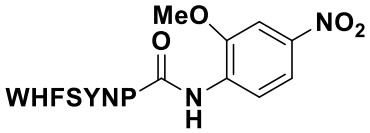
3.68

3-chlorobenzylamine. RP-HPLC: t_R = 9.41 min. ESI-QQQ $[M+K]^+$ *m/z* calc. for $[C_{56}H_{61}ClKN_{12}O_{10}]^+$ 1111.4; found 1111.5.



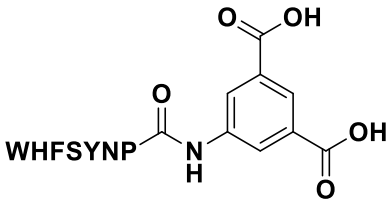
3.69

5-aminonapthaline-2-sulfonic acid. RP-HPLC: t_R = 10.00 min. ESI-QQQ $[M+3H]^{3+}$ *m/z* calc. for $[C_{57}H_{65}N_{12}O_{13}S]^{3+}$ 385.8; found 385.5.



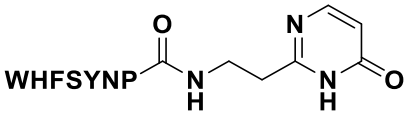
3.70

2-methyoxy-4-nitroaniline. RP-HPLC: t_R = 9.90 min. ESI-QQQ $[M+3H]^{3+}$ *m/z* calc. for $[C_{54}H_{64}N_{13}O_{13}]^{3+}$ 367.5; found 367.4.



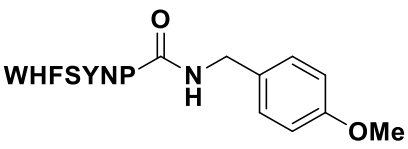
3.71

5-aminoisophthalic acid. RP-HPLC: t_R = 11.21 min. ESI-QQQ $[M+2H]^{2+}$ *m/z* calc. for $[C_{55}H_{62}N_{12}O_{14}]^{2+}$ 557.2; found 556.8



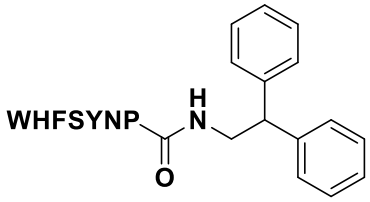
3.72

2-(2-aminoethyl)-3,4-dihydropyrimidin-4-one. RP-HPLC: t_R = 9.38 min. ESI-QQQ $[M+3H]^{3+}$ *m/z* calc. for $[C_{53}H_{65}N_{14}O_{11}]^{3+}$ 357.8; found 357.5.



3.73

4-methoxybenzylamine. RP-HPLC: t_R = 9.65 min. ESI-QQQ $[M+H]^+$ *m/z* calc. for $[C_{55}H_{64}N_{12}O_{11}]^+$ 1069.4; found 1070.0



3.74

2,2-Diphenylethylamine. RP-HPLC: t_R = 10.30 min. ESI-QQQ $[M+2H]^{2+}$ *m/z* calc. for $[C_{53}H_{69}N_{13}O_{10}]^{2+}$ 565.3; found 565.5

3.5.1 PD-1/PD-L1 HTRF binding assay

Tag1-PD-L1 and Tag2-PD-1 was diluted 40-fold from the stock solution with PPI-Europium detection buffer. Anti-Tag1 Eu Cryptate reagent and Anti-Tag2 XL665 antibody was diluted 50-fold from the stock solution with PPI-Europium detection buffer. HTRF 96-well low volume white plate was used. The samples were made to the desired concentration and 2 µL was pipetted into the well. The 4 µL of the diluted Tag-1-PD-L1 solution was added, followed by 4 µL of the diluted Tag2-PD-1 solution. Anti-Tag1 Eu Cryptate reagent solution and Anti-Tag2 XL665 antibody solution were pre-mixed prior to dispensing 10 µL into the well, for a total volume of 20 µL. The plate was sealed and incubated for 1 hour at room temperature. Samples were analysed in triplicate. Once incubated, the plate was read using a CLARIOstar (BMG Labtech) microplate reader following manufacturer's protocols for time resolved fluorescence (excitation filter EX-TR, emission filters 620 (10) nm, 665 (10) nm, dichoric mirror LP-TR, integration delay (lag time) 60 µs, integration time 400 µs, number of flashes 200, gain for white plate 2500).

The emission ratio was calculated for each well was calculated with the following equation:

$$Ratio = \frac{665\ nm\ Intensity}{620\ nm\ Intensity} \times 10^4$$

The “specific signal” (ΔR) is obtained by subtracting the background from the signal of each sample ratio

$$\Delta R = Ratio_{Sample} - Ratio_{background}$$

An decreased ΔR suggests an decreased FRET signal, suggesting a decrease in PD-1/PD-L1 interaction.

3.6 References

1 R. Santos, O. Ursu, A. Gaulton, A. P. Bento, R. S. Donadi, C. G. Bologa, A. Karlsson, B. Al-Lazikani, A. Hersey, T. I. Oprea and J. P. Overington, *Nat. Rev. Drug Discov.*, 2017, **16**, 19–34.
2 A. G. Coyne, D. E. Scott and C. Abell, *Curr. Opin. Chem. Biol.*, 2010, **14**, 299–307.
3 M. R. Arkin, Y. Tang and J. A. Wells, *Chem. Biol.*, 2014, **21**, 1102–1114.
4 T. Clackson and J. A. Wells, *Science*, 1995, **267**, 383–386.
5 M. R. Arkin and J. A. Wells, *Nat. Rev. Drug Discov.*, 2004, **3**, 301–317.
6 B. Baldo, *OncoImmunology*, 2013, **2**, e26333.
7 R. C. Acúrcio, S. Pozzi, B. Carreira, M. Pojo, N. Gómez-Cebrián, S. Casimiro, A. Fernandes, A. Barateiro, V. Farricha, J. Brito, A. P. Leandro, J. A. R. Salvador, L. Graça, L. Puchades-Carrasco, L. Costa, R. Satchi-Fainaro, R. C. Guedes and H. F. Florindo, *J. Immunother. Cancer*, 2022, **10**, e004695.
8 M.-M. Zhan, X.-Q. Hu, X.-X. Liu, B.-F. Ruan, J. Xu and C. Liao, *Drug Discov. Today*, 2016, **21**, 1027–1036.
9 US. Pat., 194307-A1, 2018.
10 US. Pat., 034820 A1, 2015.
11 US. Pat., 160641 A2, 2017.
12 J. Liang, B. Wang, Y. Yang, B. Liu and Y. Jin, *Int. J. Mol. Sci.*, 2023, **24**, 1280.
13 S. Basu, J. Yang, B. Xu, K. Magiera-Mularz, L. Skalniak, B. Musielak, V. Kholodovych, T. A. Holak and L. Hu, *J. Med. Chem.*, 2019, **62**, 7250–7263.
14 T. Ashizawa, A. Iizuka, E. Tanaka, R. Kondou, H. Miyata, C. Maeda, T. Sugino, K. Yamaguchi, T. Ando, Y. Ishikawa, M. Ito and Y. Akiyama, *Biomed. Res.*, 2019, **40**, 243–250.
15 Z. Hu, P. Yu, G. Du, W. Wang, H. Zhu, N. Li, H. Zhao, Z. Dong, L. Ye and J. Tian, *PLoS ONE*, 2020, **15**, e0228339.
16 M. Chatterjee, D. C. Turner, E. Felip, H. Lena, F. Cappuzzo, L. Horn, E. B. Garon, R. Hui, H.-T. Arkenau, M. A. Gubens, M. D. Hellmann, D. Dong, C. Li, K. Mayawala, T. Freshwater, M. Ahamadi, J. Stone, G. M. Lubiniecki, J. Zhang, E. Im, D. P. De Alwis, A. G. Kondic and Ø. Fløtten, *Ann. Oncol.*, 2016, **27**, 1291–1298.
17 CN. Pat., 085417, 2017 .
18 US. Pat., 10975049 B2, 2021.
19 Y. Wang, X. Liu, X. Zou, S. Wang, L. Luo, Y. Liu, K. Dong, X. Yao, Y. Li, X. Chen and L. Sheng, *Pharmaceutics*, 2021, **13**, 598.
20 In. Pat., 142833 A1, 2016.
21 In. Pat., 051343 A1, 2016.
22 US. Pat., 0198219 A1, 2022.

23 J. Liu, Y. Yuan, W. Chen, J. Putra, A. A. Suriawinata, A. D. Schenk, H. E. Miller, I. Guleria, R. J. Barth, Y. H. Huang and L. Wang, *Proc. Natl. Acad. Sci. U.S.A.*, 2015, **112**, 6682–6687.
24 P. G. Sasikumar, N. S. Sudarshan, S. Adurthi, R. K. Ramachandra, D. S. Samiulla, A. Lakshminarasimhan, A. Ramanathan, T. Chandrasekhar, A. A. Dhudashiya, S. R. Talapati, N. Gowda, S. Palakolanu, J. Mani, B. Srinivasrao, D. Joseph, N. Kumar, R. Nair, H. S. Atreya, N. Gowda and M. Ramachandra, *Commun. Biol.*, 2021, **4**, 1–12.
25 A. Carretero-González, D. Lora, I. Ghanem, J. Zugazagoitia, D. Castellano, J. M. Sepúlveda, J. A. López-Martin, L. Paz-Ares and G. de Velasco, *Oncotarget*, 2018, **9**, 8706–8715.
26 Curis, Inc., *A Phase 1, Open-Label, Dose Escalation and Dose Expansion Trial Evaluating the Safety, Pharmacokinetics, Pharmacodynamics, and Clinical Effects of Orally Administered CA-170 in Patients With Advanced Tumors and Lymphomas*, NCT02812875, clinicaltrials.gov, 2020.
27 P. A. Ott, Y. Bang, D. Berton-Rigaud, E. Elez, M. J. Pishvanian, H. S. Rugo, I. Puzanov, J. M. Mehnert, K. L. Aung, J. Lopez, M. Carrigan, S. Saraf, M. Chen, and J. Soria, *J. Clin. Oncol.*, 2017, **35**, 2535-2541.
28 F. Villarroel-Espindola, X. Yu, I. Datar, N. Mani, M. Sanmamed, V. Velcheti, K. Syrigos, M. Toki, H. Zhao, L. Chen, R. S. Herbst, K. A. Schalper. *Clin. Cancer Res.*, 2018, **24**, 1562-1573.
29 H. K. Koblish, L. Wu, L.-C. S. Wang, P. C. C. Liu, R. Wynn, J. Rios-Doria, S. Spitz, H. Liu, A. Volgina, N. Zolotarjova, K. Kapilashrami, E. Behshad, M. Covington, Y. Yang, J. Li, S. Diamond, M. Soloviev, K. O'Hayer, S. Rubin, C. Kanellopoulou, G. Yang, M. Rupar, D. DiMatteo, L. Lin, C. Stevens, Y. Zhang, P. Thekkat, R. Geschwindt, C. Marando, S. Yeleswaram, J. Jackson, P. Scherle, R. Huber, W. Yao and G. Hollis, *Cancer Discov.*, 2022, **12**, 1482–1499.
30 C. L. Tourneau, S. Piha-Paul, H. Prenen, B. Delafontaine, D. Pinato, A. Santoro, R. Kristeleit, K. Spencer, T. Gangadhar, H. Burris, N. Kotecki, B. Basu, D. Graham, A. M. D. Giacomo, S. Sahebjam, M. D. Nicola, C. Gomez-Roca, P. Tomasini, P. Ascierto, G. Curigliano, T. Karasic, R. Geschwindt, J. Daniel and E. V. Cutsem, in *Regular and Young Investigator Award Abstracts*, BMJ Publishing Group Ltd, 2022, pp. A804–A804.
31 E. V. Cutsem, H. Prenen, B. Delafontaine, K. Spencer, T. Mitchell, H. Burris, N. Kotecki, R. Kristeleit, D. Pinato, S. Sahebjam, D. Graham, T. Karasic, J. Daniel, K. O'Hayer, R. Geschwindt and S. Piha-Paul, *J. Immunother. Cancer.*, 2021, **9**, A559–A560.
32 Incyte Corporation, *A Phase 2 Study of INCB086550 (Oral PD-L1 Inhibitor) in Participants Who Are Immune Checkpoint Inhibitor-Naïve With Selected Solid Tumors*, NCT04629339, clinicaltrials.gov, 2023.
33 Maxinovel Pty., Ltd., *A Phase I Study of MAX-10181 Given Orally to Patients With Advanced Solid Tumor*, clinicaltrials.gov, 2022.
34 Gilead Sciences, *A Phase 1b/2 Dose Escalation/Expansion Study to Evaluate the Safety, Tolerability, Pharmacokinetics, and Efficacy of GS-4224 in Subjects With Advanced Solid Tumors*, NCT04049617, clinicaltrials.gov, 2022.
35 US. Pat., 160882A1, 2019.
36 M. S. Attene-Ramos, C. P. Austin and M. Xia, in *Encyclopedia of Toxicology*, Elsevier, 2014, pp. 916–917.
37 X. Li, W. Wang and J. Chen, *Proteomics*, 2015, **15**, 188–202.

38 Y. Du, Z. Nikolovska-Coleska, M. Qui, L. Li, I. Lewis, R. Dingledine, J. A. Stuckey, K. Krajewski, P. P. Roller, S. Wang and H. Fu, *Assay Drug Dev. Technol.*, 2011, **9**, 382–393.
39 J. Mehla, J. H. Caufield and P. Uetz, *Cold Spring Harb. Protoc.*, 2015, pdb.top083345.
40 R. Braga, V. Alves, A. Silva, M. Nascimento, F. Silva, L. Liao and C. Andrade, *Curr. Top. Med. Chem.*, 2014, **14**, 1899–1912.
41 R. Sable and S. Jois, *Molecules*, 2015, **20**, 11569–11603.
42 L. Laraia, G. McKenzie, D. R. Spring, A. R. Venkitaraman and D. J. Huggins, *Chem. Biol.*, 2015, **22**, 689–703.
43 M. DiFrancesco, J. Hofer, A. Aradhya, J. Rufinus, J. Stoddart, S. Finocchiaro, J. Mani, S. Tevis, M. Visconti, G. Walawender, J. DiFlumeri, E. Fattakhova and S. P. Patil, *Comput. Biol. Chem.*, 2023, **102**, 107804.
44 T. Chen, N. Kablaoui, J. Little, S. Timofeevski, W. R. Tschantz, P. Chen, J. Feng, M. Charlton, R. Stanton and P. Bauer, *Biochem. J.*, 2009, **420**, 283–296.
45 E. Valkov, T. Sharpe, M. Marsh, S. Greive and M. Hyvönen, in *Fragment-Based Drug Discovery and X-Ray Crystallography*, eds. T. G. Davies and M. Hyvönen, Springer Berlin Heidelberg, Berlin, Heidelberg, 2011, vol. 317, pp. 145–179.
46 H. Chen, X. Zhou, A. Wang, Y. Zheng, Y. Gao and J. Zhou, *Drug Discov. Today*, 2015, **20**, 105–113.
47 S. Farmer, *J. Comput. Aided Mol. Des.*, 2011, **25**, 599–605.
48 E. Perry, J. J. Mills, B. Zhao, F. Wang, Q. Sun, P. P. Christov, J. C. Tarr, T. A. Rietz, E. T. Olejniczak, T. Lee and S. Fesik, *Bioorg. Med. Chem. Lett.*, 2019, **29**, 786–790.
49 A. M. Beekman, M. A. O'Connell and L. A. Howell, *Angew. Chem. Int. Ed.*, 2017, **56**, 10446–10450.
50 A. M. Beekman, M. M. D. Cominetti, S. J. Walpole, S. Prabhu, M. A. O'Connell, J. Angulo and M. Searcey, *Chem. Sci.*, 2019, **10**, 4502–4508.
51 W. Jeong, J. Bu, Y. Han, A. J. Drelich, A. Nair, P. Král and S. Hong, *J. Am. Chem. Soc.*, 2020, **142**, 1832–1837.
52 Y. Hamuro, S. J. Geib and A. D. Hamilton, *J. Am. Chem. Soc.*, 1996, **118**, 7529–7541.
53 S. Maity, P. Jana, S. K. Maity, P. Kumar and D. Haldar, *Cryst. Growth Des.*, 2012, **12**, 422–428.
54 V. V. E. Ramesh, G. Priya, A. S. Kotmale, R. G. Gonnade, P. R. Rajamohanan and G. J. Sanjayan, *Chem. Commun.*, 2012, **48**, 11205–11207.
55 A. J. Cameron, C. J. Squire, P. J. B. Edwards, E. Harjes and V. Sarojini, *Chem. Asian J.*, 2017, **12**, 3195–3202.
56 M. Goodman, A. Felix, L. Moroder and C. Toniolo, Eds., *Houben-Weyl Methods of Organic Chemistry Vol. E 22c, 4th Edition Supplement*, Georg Thieme Verlag, Stuttgart, 2004.
57 L. A. Carpino, *J. Am. Chem. Soc.*, 1993, **115**, 4397–4398.
58 J. K. Murray, B. Farooqi, J. D. Sadowsky, M. Scalf, W. A. Freund, L. M. Smith, J. Chen and S. H. Gellman, *J. Am. Chem. Soc.*, 2005, **127**, 13271–13280.
59 E. Zartler, C. Swain and S. Pearce, *Drug Discov. World*, 2012, 19–24.
60 F. Giordanetto, C. Jin, L. Willmore, M. Feher and D. E. Shaw, *J. Med. Chem.*, 2019, **62**, 3381–3394.
61 W. C. Chan and P. D. White, *Fmoc Solid Phase Peptide Synthesis*, Oxford University Press, Oxford, 2000.

62 J. B. Blanco-Canosa and P. E. Dawson, *Angew. Chem. Int. Ed.*, 2008, **47**, 6851–6855.
63 C. A. Arbour, H. Y. Saraha, T. F. McMillan and J. L. Stockdill, *Chem. Eur. J.*, 2017, **23**, 12484–12488.
64 A. Selvaraj, H.-T. Chen, A. Ya-Ting Huang and C.-L. Kao, *Chem. Sci.*, 2018, **9**, 345–349.
65 C.-D. Chang, M. Waki, M. Ahmad, J. Meienhofer, E. O. Lundell and J. D. Haug, *Int. J. Pept. Protein Res.*, 2009, **15**, 59–66.
66 C. Bérubé, A. Borgia and N. Voyer, *Org. Biomol. Chem.*, 2018, **16**, 9117–9123.
67 T. Tremblay, G. Robert-Scott, C. Bérubé, A. Carpentier, N. Voyer and D. Giguère, *Chem. Commun.*, 2019, **55**, 13741–13744.
68 M. E. Due-Hansen, S. K. Pandey, E. Christiansen, R. Andersen, S. V. F. Hansen and T. Ulven, *Org. Biomol. Chem.*, 2016, **14**, 430–433.
69 E. Butler, L. Florentino, D. Cornut, G. Gomez-Campillos, H. Liu, A. C. Regan and E. J. Thomas, *Org. Biomol. Chem.*, 2018, **16**, 6935–6960.
70 J. Thierry, C. Grillon, S. Gaudron, P. Potier, A. Riches and J. Wdzieczak-Bakala, *J. Peptide Sci.*, 2001, **7**, 284–293.

Chapter 4

The Synthesis of 1,2,4,5-Tetrazine Derivatives and iEDDA Click Chemistry for use in Peptide-Directed Binding

4.1 Introduction

As discussed in chapter 3, peptide-directed binding is the method of using peptides to identify the key characteristics required for inhibiting a protein-protein interaction (PPI) and applying those characteristics to the development of a novel small molecule. The peptide inhibitor is split in two, with important residues distributed evenly, and one half of the peptide is replaced by a small molecule to form an intermediate peptide-small molecule hybrid. The peptide half is then sequentially replaced to leave a small molecule mimic. Previously, peptide-small molecule hybrids were formed using an azide and an alkyne in copper (I)-catalyzed azide-alkyne cycloaddition (CuAAC) to mimic a linear α-helical peptide.[1] To synthesise a new small molecule inhibitor for PD-1/PD-L1, an alternative click reaction was required that would provide a hybrid that mimicked a peptide with a turn motif. The inverse electron demand Diels Alder reaction (iEDDA) reaction between 1,2,4,5-tetrazine and an alkene or alkyne would potentially provide the turn structure that has been shown to increase binding affinity for PD-1/PD-L1.

4.1.1 Click chemistry

Click chemistry was described by Sharpless *et al.* as reactions that give high yields, generate inoffensive by-products, are stereospecific and have simple reaction conditions.[2] The impact of these reactions was noted in 2022 when Bertozzi, Meldal and Sharpless won a Nobel prize for their discovery surrounding click reactions. They are non-sensitive to oxygen and water, and the products are easily purifiable. The most widely used click chemistry reaction is the 1,3-dipolar cycloaddition taking place between azides and alkynes with copper catalysis.[3,4] This is commonly known as copper (I)-catalyzed azide-alkyne cycloaddition (CuAAC) (**Figure 4-1A**). Alongside click reactions, there are additional approaches including nucleophilic ring opening reactions using epoxides or aziridines (**Figure 4-1B**), non-aldol carbonyl-type reactions to form hydrazones or oximes (**Figure 4-1C**), and specific Michael additions, particularly those that use amine and thiol nucleophiles (**Figure 4-1D**).[5–7]

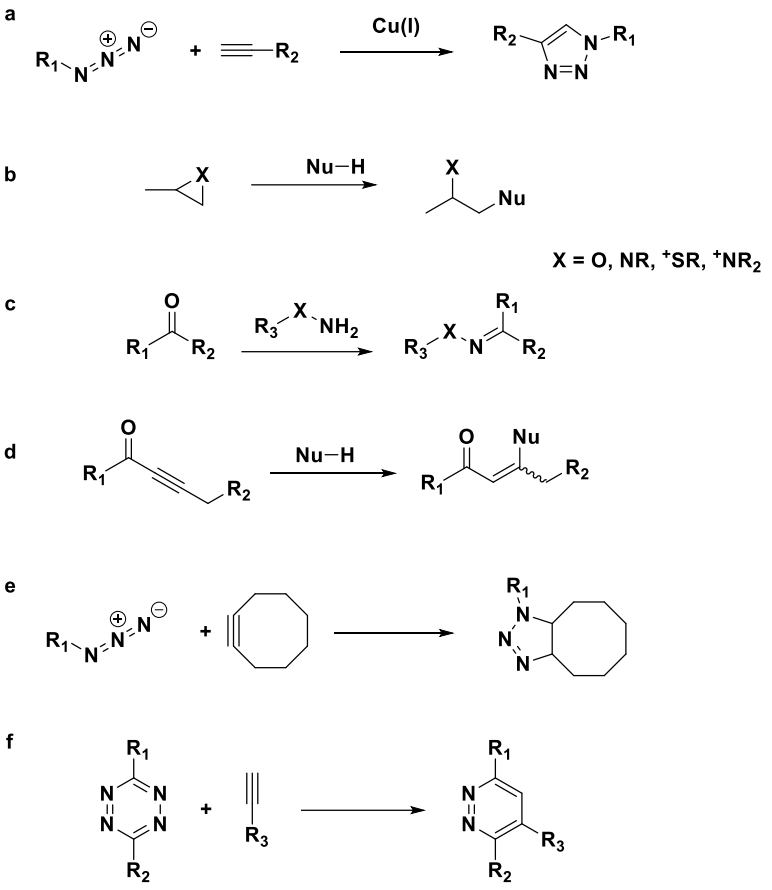


Figure 4-1*a) CuAAC cycloaddition b) Epoxide ring opening c=c bond formation c) hydrazone formation d) Michael addition e) SPAAC cycloaddition f) IEDDA.*

The [3+2] strain-promoted azide-alkyne cycloaddition (SPAAC) as seen in **Figure 4-1E** was developed as a bio-orthogonal alternative to CuAAC. Bio-orthogonal chemistry is characterised by reactions that occur in biological environments without interfering with biomolecules or biochemical processes.[8] Further, they need to react quickly to avoid metabolic processes and must occur in water at physiological temperature.[8] Most importantly, neither the reactants, the products nor the by-products can be toxic. The SPAAC reaction proceeds without the need for the copper catalyst but with slower kinetics in comparison to the CuAAC. It also requires a bulky, strained dienophile for the reaction to proceed. Another click reaction that does not require either metal catalysis or a bulky dienophile is known as inverse electron demand Diels-Alder (iEDDA) (**Figure 4-1F**). The reaction takes place between 1,2,4,5-tetrazine and strained dienophiles with faster kinetics than both SPAAC and CuAAC. The iEDDA reaction has been applied to many avenues within drug discovery, including radiolabelling of antibodies, site-specific release of a drug, fluorescence imaging, and photodynamic therapy.[9–12]

4.1.2 Click chemistry as a turn-inducing motif

PD-1 and PD-L1 are both β-sheet and β-strand proteins. To effectively target this wide and flat surface area it is necessary to include a compound or bond that would enforce a turn and potential pre-arrangement for target specific binding.[13] Previously, the CuAAC click reaction has been utilized within peptide directed binding to mimic an α-helical peptide.[1] However, the resulting 1,4-disubstituted 1,2,3-triazole is orientated in a more linear fashion (**Figure 4-2A)**. Ruthenium is known to catalyse the azide/alkyne reaction to form 1,5-disubstituted triazoles.[14] However, to achieve regioselectivity often the conditions of these reactions require harsh reaction conditions that potentially would not be suitable for peptides.[14] Alternatively, sterically hindered derivatives of Ru catalysts could be used but their sensitive nature would not be suitable for the purpose of this project.[14,15] Both reactions are also limited in dienophile selection to an alkyne compound.

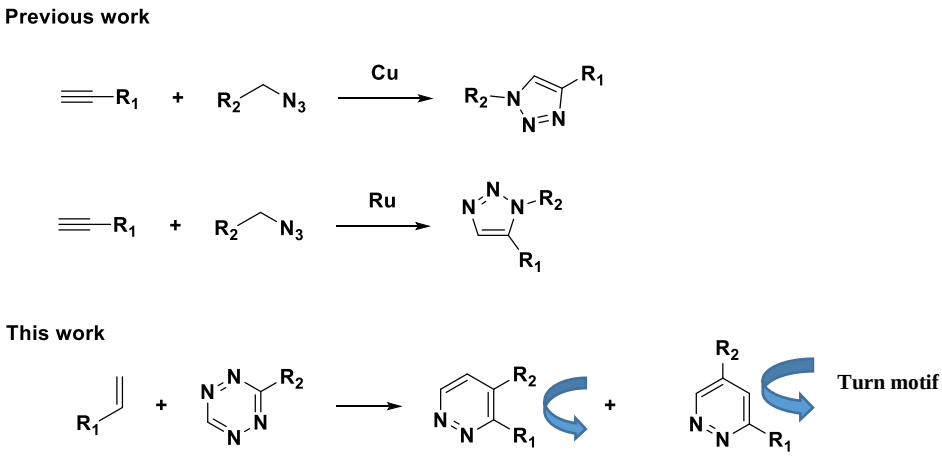


Figure 4-2 *a) CuAAC reaction showing linear triazole product b) iEDDA reaction showing turn like pyridazine product.*

As an alternative approach to mimic a turn structure, the iEDDA reaction between a 1,2,4,5-tetrazine and a chosen dienophile was considered. These reactions often take place at room temperature, they do not require a metal catalyst and a variety of dienophiles have been shown to be successful. Importantly, the resulting pyridazine product gives a turn like structure thought to be an ideal choice as a linker to combine the peptide-small molecule fragments (**Figure 4-2B**).

4.1.3 Inverse electron demand Diels-Alder

4.1.3.1 Mechanism of iEDDA

The mechanism of the iEDDA reaction is a Diels-Alder [4+2] cycloaddition with inverse electron demand (**Figure 4-3**). Differing from the conventional Diels-Alder, where the HOMO serves as the electron rich diene and the LUMO as the electron poor dienophile, the iEDDA is reversed in that the dienophile acts as the HOMO and the diene as the LUMO.

The iEDDA reaction proceeds through the 1,4-addition of the diene system of a tetrazine **4.1** to an alkene, **4.2**, or alkyne, forming a highly strained bicyclic intermediate, **4.3.** This undergoes a further retro-Diels-Alder reaction to give a di-hydropyridazine product, **4.4,** which can be oxidized to give a pyridazine product, **4.5** (**Figure 4-3**).

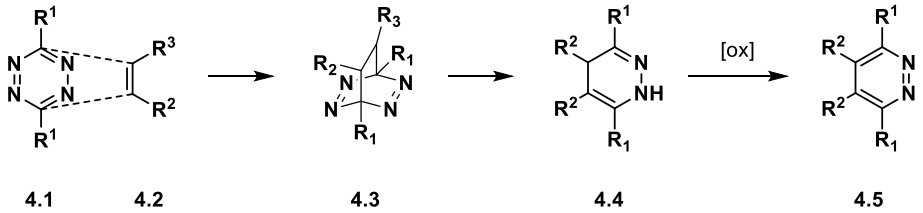


Figure 4-3 *iEDDA reaction involving 1,2,4,5-tetrazine (**4.1**) and an alkene (**4.2**) via a highly strained bicyclic intermediate (**4.3**).*

4.1.3.2 1,2,4,5-tetrazines

Tetrazines consist of a six-membered cyclic ring characterized by the position of the nitrogen atoms to identify them as 1,2,3,4-tetrazines **4.6**, 1,2,3,5-tetrazines **4.7**, and 1,2,4,5-tetrazines **4.8** (**Figure 4-4**).[16]

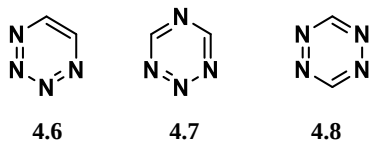


Figure 4-4 *1,2,3,4 tetrazine (**4.6**), 1,2,3,5 tetrazine (**4.7**), 1,2,4,5-tetrazine (**4.8**).*

1,2,4,5-tetrazines contain two sp^2 hybridised carbon atoms and four sp^2 hybridised nitrogen atoms. They can be symmetrically or unsymmetrically (di)-substituted (**Figure 4-5**) with a diverse range of 1,2,4,5-tetrazines with various substituents being reported in literature.[17–20]

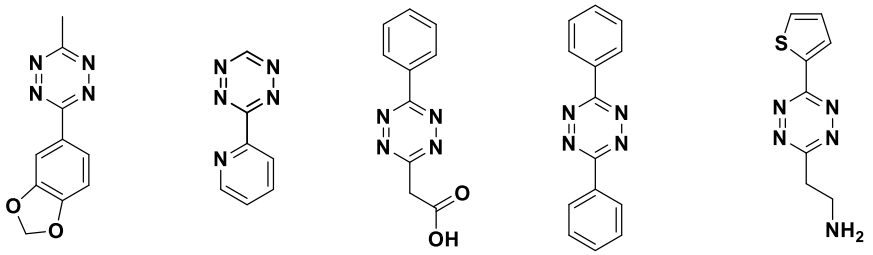


Figure 4-5 *Symmetric and asymmetric (di)-substituted 1,2,4,5-tetrazines.*

The four electronegative nitrogen atoms lead to a low energy π* molecular orbital that is responsible for the characteristic pink and red colours. This is due to a weak n-π* transition in the visible range of the electromagnetic spectrum.[21] Since the first discovery of the 1,2,4,5-tetrazines, their uses have been applied in many areas of research including molecular probing and bioconjugates, explosives, labelling and imaging biomolecules and in nanotechnology.[22–24]

4.1.4 Factors that affect iEDDA reactivity

The iEDDA reaction kinetics are based on the energy gap between the HOMO and LUMO of the reactants. The smaller the energy gap difference between the two energy states, the faster the reaction will take place. Multiple studies have determined different factors to fine tune the iEDDA kinetics into the optimal reaction.[25–27]

4.1.4.1 Electronic Effects

Electron donating groups (EDGs) raise the HOMO and LUMO energy states and electron-withdrawing groups (EWGs) lower the HOMO and LUMO energy levels (**Figure 4-6**). The selection of the substituents for both diene and dienophiles allows the manipulation of the LUMO-HOMO energy gap to enhance reactivity.

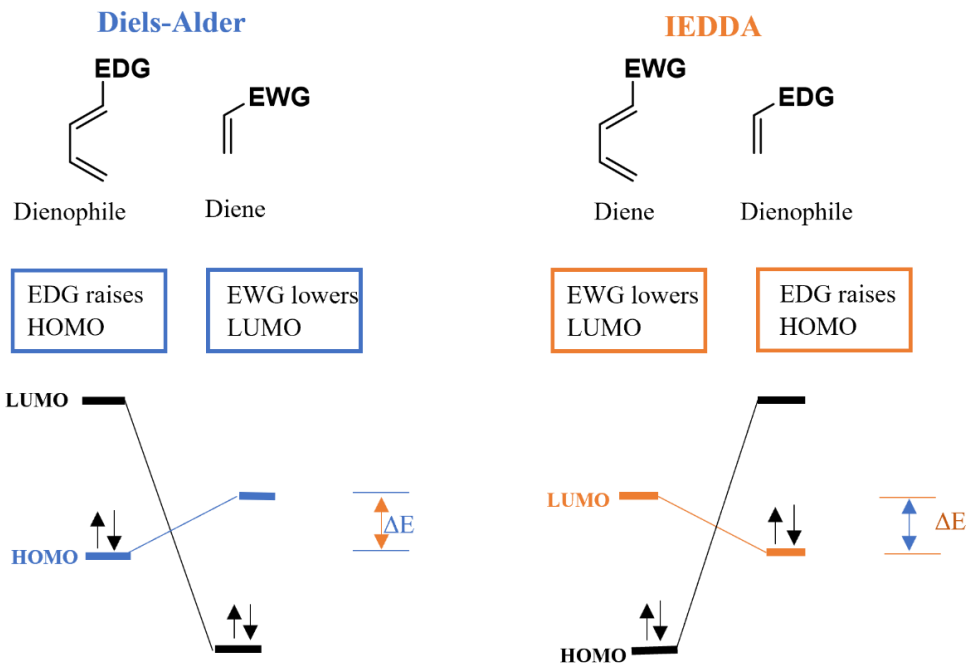


Figure 4-6 *A comparison of the effects of EWG and EDG on both diene and dienophile for the Diels Alder and iEDDA reactions.*

The Boger group compared multiple 1,2,4,5-tetrazine substituents to conclude that electron deficiency lowers the LUMO energy and incorporating an EWG allowed for the acceleration of the iEDDA reactions (**Figure 4-7**).[27] For example, tetrazines with electron withdrawing ester groups, **4.9,** will proceed with faster kinetics than those with a methanethiol, **4.10,** or methoxy group, **4.11**. Another study found that substituting positions C3 and C6 with aromatic rings functionalised by EWGs increased the reaction rate further by decreasing the electron density of the tetrazine.[28,29]

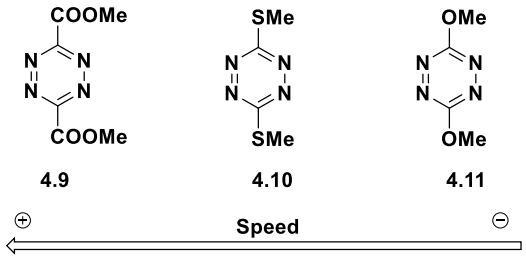


Figure 4-7 *Substituent effects on kinetics of dienes.*

However, the functionality of the dienophile has a bigger impact on the iEDDA kinetics. Electron rich substituents are favoured for achieving fast kinetics.[30] An alkene dienophile will have a faster reaction rate than an alkyne dienophile due to the triple bond being electron withdrawing, therefore lowering the energy of the HOMO.[30,31]

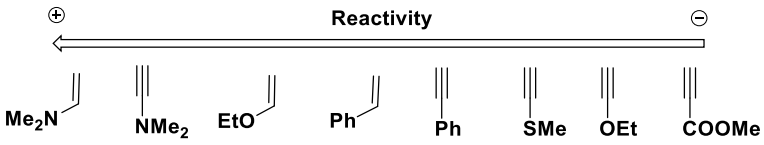


Figure 4-8 *Substituent effects on kinetics of dienophiles.*

When discussing the addition of EDGs, the more electron-rich dienophiles achieve the faster kinetics favouring enamines and ynamines as shown in **Figure 4-8**.[32] Similar patterns between electronics and kinetics are seen if EDGs are introduced to phenylacetylenes and styrenes.[30,31]

4.1.4.2 Strain effect

Ring strain also plays an important role in the iEDDA reaction rate by raising the HOMO of the dienophile.[33] A common dienophile found to be most effective is *trans*-cyclooctene (TCO) **4.12**.[26]



4.12 **4.13**

Figure 4-9 *The conformations of TCO (**4.12**) and cis-cyclo-octene (**4.13**).*

The TCO adopts a 'crown' conformation (**4.12**, **Figure 4-9**) whereas the *cis*-cyclooctene, **4.13,** is found in the 'half chair' conformation. The strained dienophile is more reactive due to the pre-distorted conformation that acts as pre-organisation of the structure for the reaction to proceed. Therefore, less distortion energies are needed for the dienophile to react.[34,35]

For the use as a turn mimic between a peptide and small molecule, TCO would be considered too bulky and potentially could interfere with the turn structure. As such, smaller linear dienophiles were preferential for this study. Linear dienophiles are found to click to 1,2,3,4 tetrazines successfully as noted in **Figure 4-10** where methoxyethyne (**a**), *N*,*N*-diethyl-1-propynylamine (**b**), and methyl prop-2-enoate (**c**) can be seen as examples.[25,27,36] All reactions took place in 1,4 dioxane and took between 0-3 days to react.

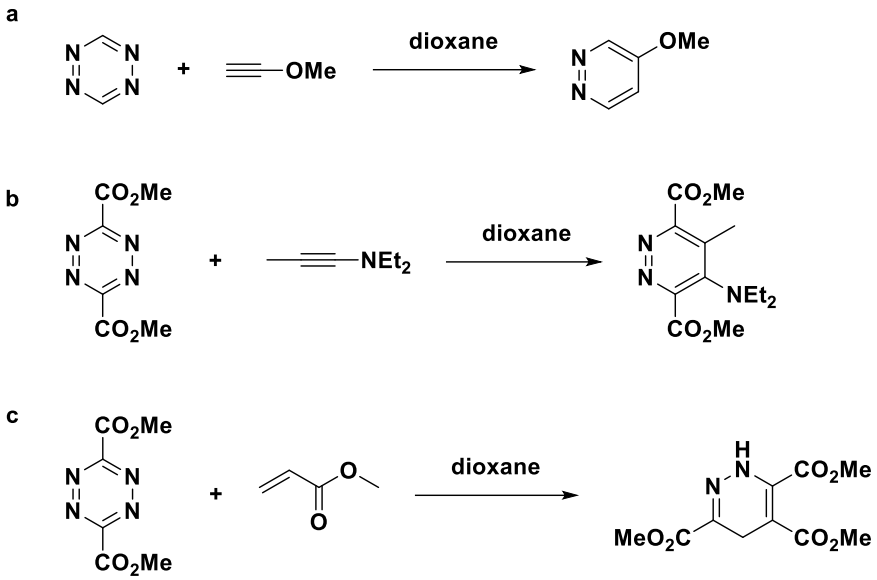


Figure 4-10 *Examples of IEDDA reactions with 1,2,3,4 tetrazines with linear dienophiles methoxyethyne (**a**), N,N-diethyl-1-propynylamine (**b**), methyl prop-2-enoate (**c**) .*

4.1.4.3 Steric effect

The increase of any steric effect on the dienophile will impede its reactivity, as such alkenes and alkynes are more reactive if they are terminal.[37] Furthermore, the steric effect when introducing an EDG must be considered. Despite the high electron deficiency, if the steric effects are also high this will often only lead to a marginal increase in reactivity.[35] Subsequently, mono-substituted tetrazines have faster kinetics than di-substituted tetrazines regardless of strong EWGs substituents.[17,26,38]

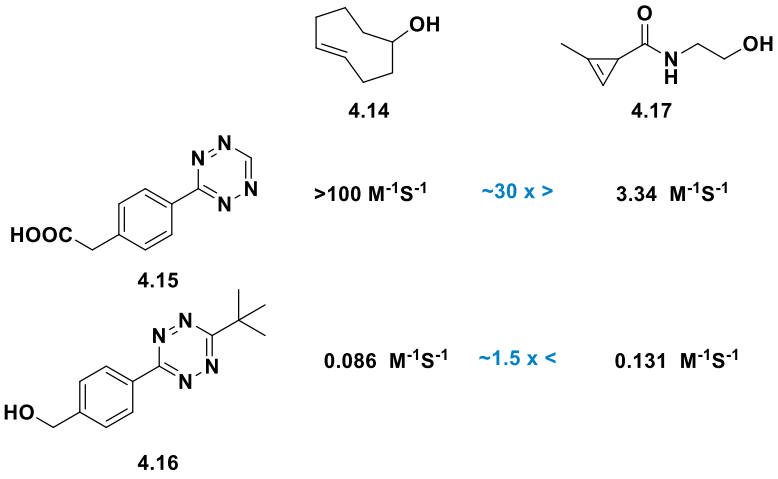


Figure 4-11 *The impact of the steric effect on the iEDDA reaction.*

The discovery of the steric effects has led to the design of iEDDA reactions that balance the dienophile and diene to control the reaction rate. For instance, it was demonstrated that a mono-substituted tetrazine, **4.15**, undergoes iEDDA reaction with

TCO derivative **4.14** 30 times faster than with cyclopropene, **4.17**. However, if that tetrazine is substituted with a bulky group, **4.16**, the unfavourable steric slows the reaction favouring the less bulky cyclopropene (**Figure 4-11**).[32]

4.1.5 iEDDA in peptides

In 2009, a peptide was modified with an iEDDA reaction to enhance the transport of temozolomide (TMZ) to its site of action, mitigating off-target effects. A tetrazine modified TMZ was clicked to a peptide (CRQIKIWFQNRRMKKWKK) acting as a transmembrane shuttle and a nuclear localisation sequence modified with a diene on the C-terminus (KKPKKRKVC).[39] The introduction of dienophiles and dienes to peptides can be achieved through amide couplings. This can be achieved through the backbone of the peptide in solid phase peptide synthesis as seen in **Figure 4-12A** or through post peptide synthesis modification using lysine (**Figure 4-12B**).[40,41] The peptides modified with either a diene or dienophile can proceed with the iEDDA reaction in either solid phase or in solution.[41,42]

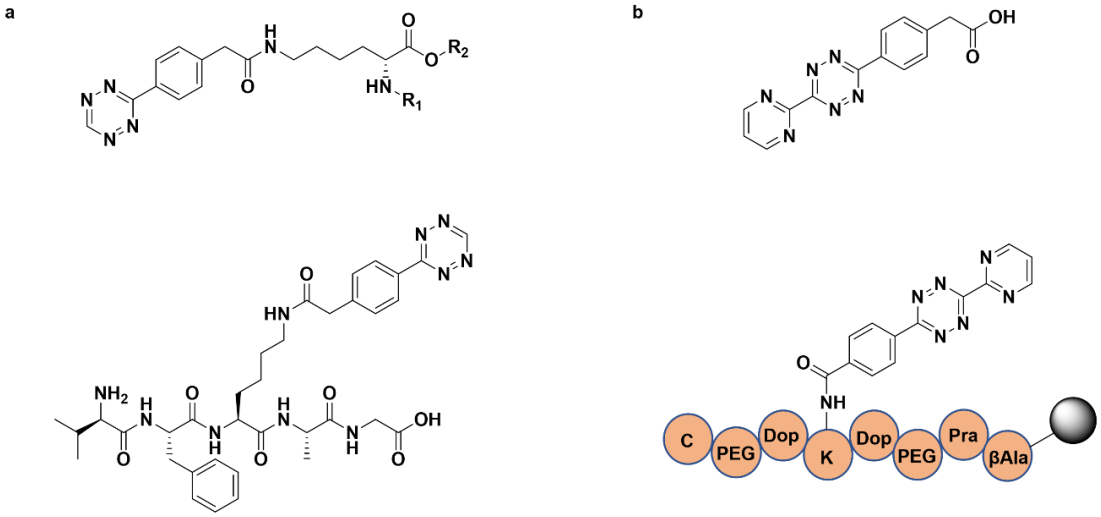


Figure 4-12 *a) A tetrazine modification via the backbone of the peptide showing tetrazine-pentapeptide VF$_T$AG b) Tetrazine modification through the an amide bond using lysine within the sequence of a titanium binding peptide: DOP (dihydroxyphenylalanine), βAla (L-β-alanine) and PEG (polyethylene glycol).*

Notably, tetrazines have been used to modify RGD peptides for cancer targeting, imaging and enhancing cell adhesion to biomaterials. This three amino acid sequence is found in proteins of the extracellular matrix and binds to integrins.[43] The high affinity and selectivity of specific RGD peptides to integrins make them ideal for cancer targeting.[44] Furthermore, the use of this sequence can also increase adhesion of desired cells on biomaterials.[45] A modified c(RGDfK) peptide showed improved cell

adhesion to image and kill cancer cells through the addition of a bicyclic dienophile. Through an iEDDA reaction, the attached dienophile clicked with a tetrazine bearing surface to enhance the adhesive properties of the RGD peptide to cells on silicon and titanium surfaces (**Figure 4-13A**).[41,42,45] Another example used a cyclic RGD peptide modified with a dienophile clicked with a tetrazine that was functionalised with a near-infrared imaging agent to detect human breast carcinoma cells (**Figure 4-13B**).[46] These examples give evidence that iEDDA between tetrazines and alkene/alkynes may be compatible with solid phase and help to make turn mimics for peptide directed binding.

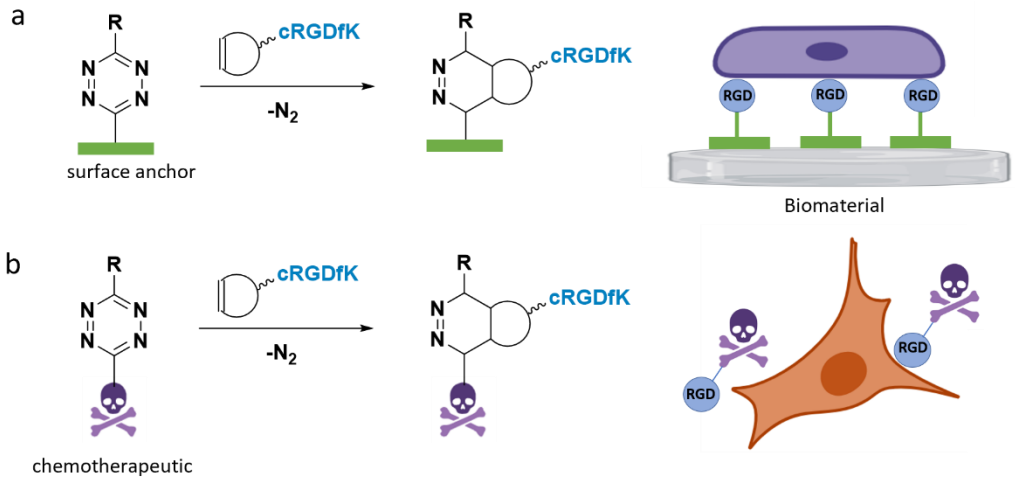


Figure 4-13 *a) Modified RGD peptide with iEDDA reaction to improve cell adhesion for imaging and destroying cancer cells b) Using iEDDA as a ligand between cyclic RGD peptide and a drug (purple) to treat cancer cells (orange).*

4.1.1 Previous syntheses of 1,2,4,5-tetrazines suitable for addition to peptides

The first reported synthesis of the 1,2,4,5-tetrazine was by Pinner in 1893 in a two-step reaction. The first step is the condensation of the nitrile **4.18** with hydrazine to form dihydrotetrazine **4.19,** followed by oxidation to give the di-substituted tetrazine **4.20** (**Figure 4-14**).[47]

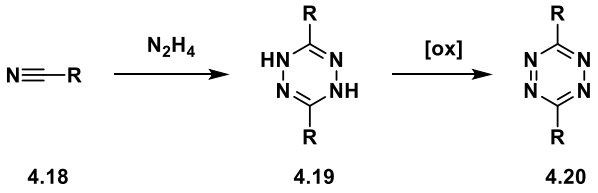


Figure 4-14 *The Pinner synthesis.*

Although successful when synthesising symmetrical tetrazines, the synthesis is limited towards asymmetric tetrazines, with the formation of symmetric tetrazines as a by-product alongside the asymmetric tetrazine.[48] Furthermore, the Pinner synthesis has poor tolerance to alkyl nitriles and is therefore unable to provide tetrazines with alkyl substituents.[49] No mechanism has been confirmed for the Pinner synthesis to date. To activate the alkyl nitriles to promote the addition of hydrazine, metal-catalysed reactions using $Zn(OTf)_2$ and $Ni(OTf)_2$ to act as Lewis acids were developed to improve the Pinner synthesis of alkyl and unsymmetrical di-substituted and mono-substituted tetrazines.[50] Zn and Ni were also used to improve the synthesis of mono-substituted, unsymmetrical tetrazines through the condensation of a formamidine salt and nitrile in which anhydrous hydrazine is used (**Figure 4-15**).[50,51]

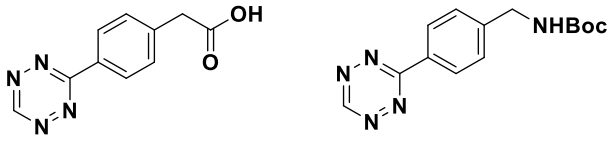
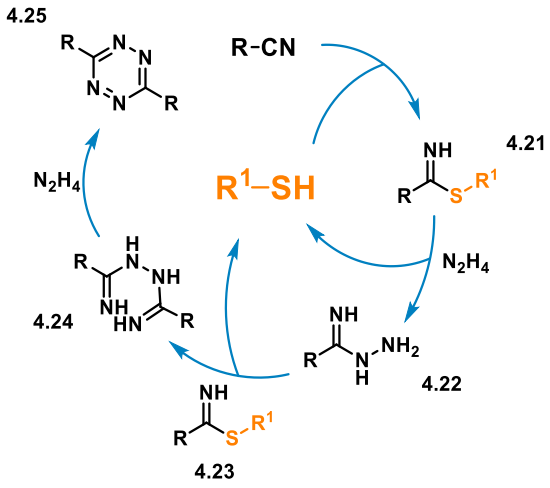


Figure 4-15 *Examples of metal catalysed synthesis of tetrazines products.*

Another approach was reported by the Wu group using an organocatalyst to mitigate the use of the hazardous and reactive anhydrous hydrazine.[20] The Wu group proved that a thiol-containing organocatalyst promotes the reaction between hydrazine hydrate and nitriles with various alkyl- or aryl- functional groups moving.[20] The proposed mechanism shown in **Scheme 4-1** shows the nucleophilic attack on the nitrile by the thiol organocatalyst to form **4.21** that undergoes subsequent nucleophilic substitution by hydrazine to give **4.22** as shown in **Scheme 4-1**. A second nucleophilic substitution by **4.23** leads to **4.24**, which undergoes an intramolecular cyclization and oxidation to give the final product **4.25**.



Scheme 4-1 *Proposed organocatalytic mechanism for 1,2,4,5-tetrazine synthesis.*

This led to the successful synthesis of di-substituted 1,2,4,5-tetrazine derivatives (**Figure 4-16**). Furthermore, the synthesis of a phosphonate 1,2,4,5-tetrazine, **4.26**, was reported that could be used in subsequent Horner-Wadsworth-Emmons (HWE) reactions to form the desired 1,2,4,5-tetrazines. The Wu group used a variety of aldehydes to functionalise 1,2,4,5-tetrazines through an alkene bond as shown in compound **4.27**.[20]

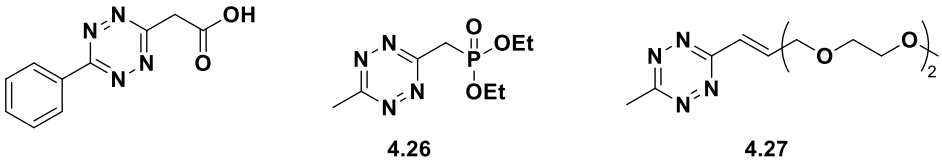


Figure 4-16 *Examples from the Wu group's successful synthesis of 1,2,4,5-tetrazines.*

Transition metal-catalysed coupling reactions have found success in asymmetrical 1,2,4,5-tetrazine synthesis with the metal used to form C-C bonds directly onto the tetrazine.[52] These were found to have modest yields and were dependent on electron donating groups, whereas electron deficient tetrazines tended to decompose. First reported using Sonogashira coupling, other couplings have all reported tetrazines with moderate yields such as Negishi, Suzuki-like and Stille-like couplings.[53,54] In 2020, the Fox group utilized Pd-catalysed cross coupling in a thioether reduction to synthesize mono-substituted 1,2,4,5-tetrazines. In a one pot procedure, carboxylic esters **4.28** and methyl thiocarbohydrazide **4.29** are used to form 3-thiomethyltetrazines **4.30** that can be further reduced to the mono substituted 1,2,4,5-tetrazine **4.31 (Figure 4-17A)**.[55] The carboxylic esters are inexpensive and can be synthesized in a straight forward procedure, providing a different foundation for 3,6

di-substituted tetrazine synthesis and a new synthesis for mono-substituted tetrazines (**Figure 4-17B**).[18]

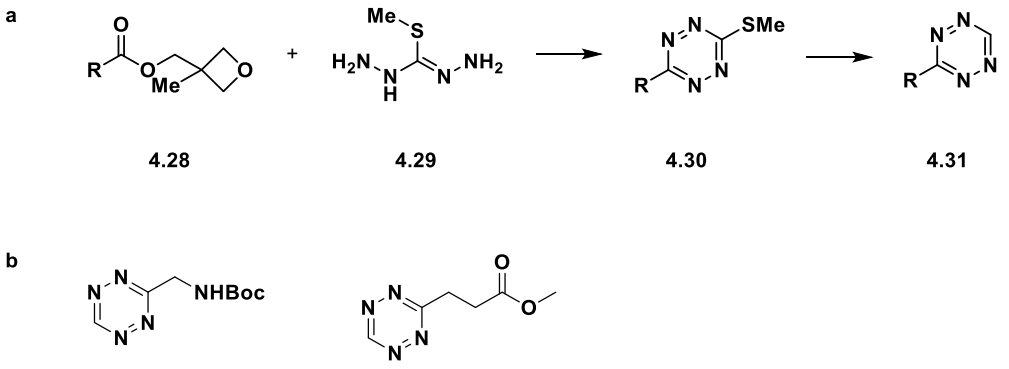


Figure 4-17 *a)1,2,4,5-tetrazine synthesis via carboxylic ester b) Examples of 1,2,4,5-tetrazines synthesised by the Fox group.*

4.2 Chapter Aims

The aim of this chapter was to determine the viable use of click chemistry between a 1,2,4,5-tetrazine derivative and a chosen dienophile to mimic a turn like structure for inhibiting PD-1/PD-L1. The tetrazine would be attached on one of the small molecule fragments or semi-peptides, with the dienophile on the other, and connected using click chemistry to result in a novel small molecule inhibitor. The tetrazine needed to be functionalised with either a carboxylic acid linker or an amine linker to form an amide bond with the terminal ends of a semi-peptide (**Figure 4-18**). Despite tetrazines functionalised with a phenyl group showing excellent reactivity in multiple studies, for this study a smaller tetrazine would be required to prevent interference with the turn structure. Secondly, a reactive dienophile needed to be identified that could be incorporated to the opposing end of the semi-peptide to be readily reacted with the tetrazine. The carboxylic acid derivative was planned for simple coupling onto the free amine following the final Fmoc deprotection of the peptide. The amine tetrazine derivative was proposed for use in conjunction with Dawson's resin to be added to the N-terminus upon cleavage from the resin.

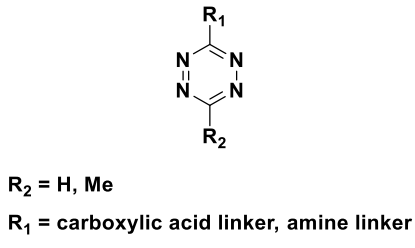
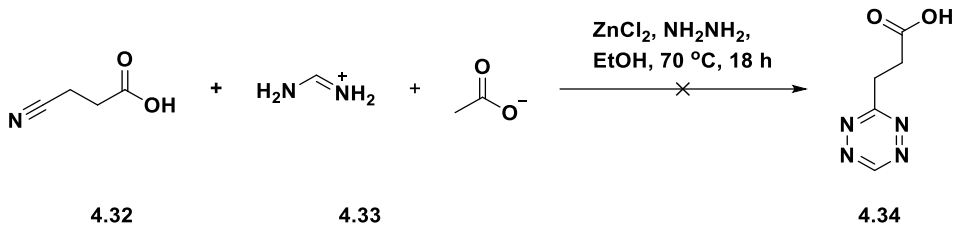


Figure 4-18 *Proposed 1,2,4,5-tetrazine structure for iEDDA to be used in peptide-directed binding.*

4.3 Results and Discussion

4.3.1 Synthesis of 1,2,4,5-tetrazine

The Lewis acid catalysed Pinner synthesis offered the simplest method to the desired mono-substituted tetrazine, **4.34**, and so was attempted first. 3-cyanopropanoic acid, **4.32**, was reacted with formamidine acetate, **4.33**, in the presence of catalytic zinc and anhydrous hydrazine (**Scheme 4-2**).[51] However, even with increased temperature and reaction times this reaction was met with no success, recovering only starting material.



Scheme 4-2 *The Pinner synthesis using Zn as a catalyst with 3-cyanopropanoic acid (**4.32**) and formamidine acetate (**4.33**).*

Moving away from the zinc catalyst and avoiding anhydrous hydrazine, the Wu group reported using an organocatalyst for the synthesis of 1,2,4,5-tetrazines.[20] Initially, the organocatalyst was unsuccessfully attempted with 3-cyanopropanoic acid and acetonitrile replacing the zinc catalyst. However, the reported reaction had one of the reacting nitriles functionalised with a phenyl group, this would become positioned at C3 once the tetrazine was formed (**Figure 4-19**).

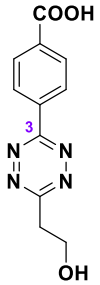
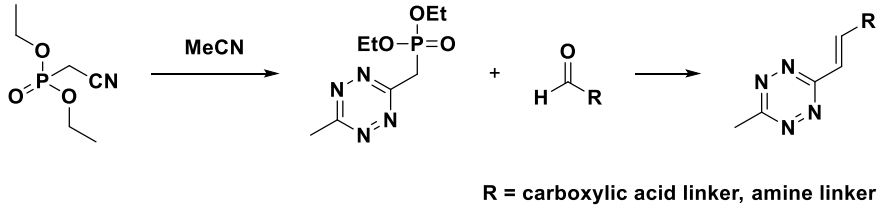


Figure 4-19 *Di-substituted 1,2,4,5-tetrazine showing a phenyl group at C3.*

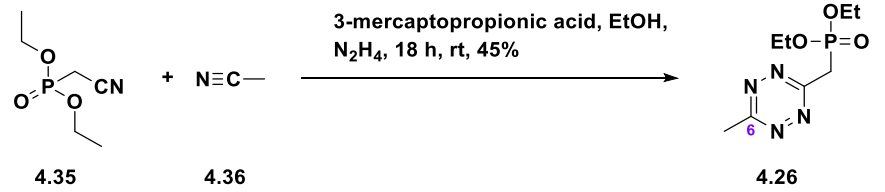
It was concluded that the 3-cyanopropanoic acid lacked the reactivity of the bulky phenyl groups. However, the synthesis of a phosphonate 1,2,4,5-tetrazine was reported that could be used in conjunction in a Horner Wadsworth Emmons (HWE). The examples in the paper showed a variety of aldehydes being used to functionalise 1,2,4,5-tetrazine avoiding the bulky phenyl groups that would be unsuitable for creating that turn like structure to inhibit PD-1/PD-L1.[20] This led to a promising

approach to synthesis a di-substituted 1,2,4,5-tetrazine with a carboxylic acid or amine linker (**Scheme 4-3**).



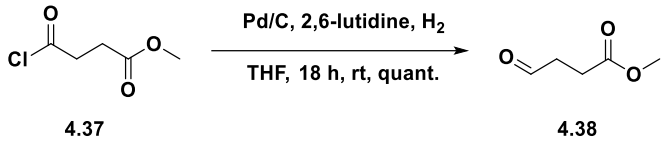
Scheme 4-3 *Proposed pathway to synthesis di-substituted 1,2,4,5-tetrazine with a carboxylic acid or amine linker.*

The synthesis began by making 3-phosphonate-6-methyl-1,2,4,5-tetrazine **4.26**. Diethyl cyanomethyl phosphate **4.35** and acetonitrile **4.36** were activated by 3-mercaptopropionic acid to form the tetrazine ring. After purification *via* flash column chromatography the product **4.26** was obtained as a pink oil in a 45% yield (**Scheme 4-4**). ^{1}H NMR showed confirmation of the tetrazine formation with a singlet at 3.07 ppm integrating to three protons, showing the methyl group at the C6 position. The successful synthesis was further confirmed by obtaining a *m/z* of 269.2, corresponding to the $[M+Na]^{+}$ ion.



Scheme 4-4 *The synthesis of 3-phosphonate-6-methyl-1,2,4,5-tetrazine (**4.26**).*

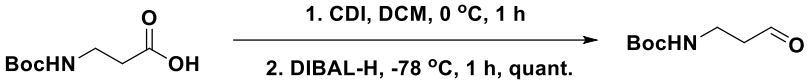
The next step was to synthesise the carboxylic acid and amine functionalised aldehydes, suitable for a HWE coupling. Methyl succinyl chloride **4.37** was reduced using 2,6-lutidine and Pd/C under an atmosphere of H_2 to produce methyl 4-oxobutanoate **4.38** (**Scheme 4-5**).[56] This was produced in a quantitative yield and was used without purification. The catalytic hydrogenation of an acid chloride to form an aldehyde is known as the Rosenmund reaction.[57] The addition of 2,6 lutidine poisons the catalyst preventing overreduction.[57] The crude ^{1}H NMR showed a singlet at 9.69 ppm integrating for one proton confirming the formation of the aldehyde.



4.37 4.38

Scheme 4-5 *The synthesis of methyl 4-oxobutanoate (**4.38**) using a Rosenmund reaction.*

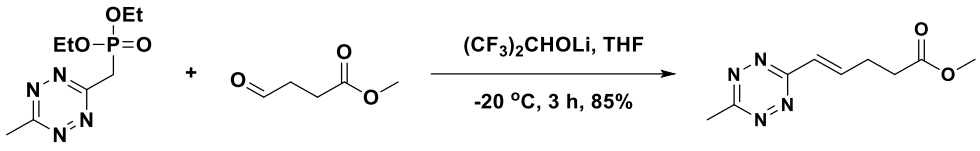
The amine precursor started with Boc-β-alanine, **4.39**, being activated by 1,1'-carbonyldiimidazole (CDI) and reduced by DIBAL-H to give the aldehyde, **4.40**, as a yellow oil that was used crude (**Scheme 4-6**).[58] Again, this was confirmed using the crude ^{1}H NMR showing a singlet that integrated for one proton at 9.75 ppm corresponding to the aldehyde formed.



4.39 4.40

Scheme 4-6 *The reduction of Boc- β -Alanine (**4.38**) using CDI and DIBAL to give the product **4.40**.*

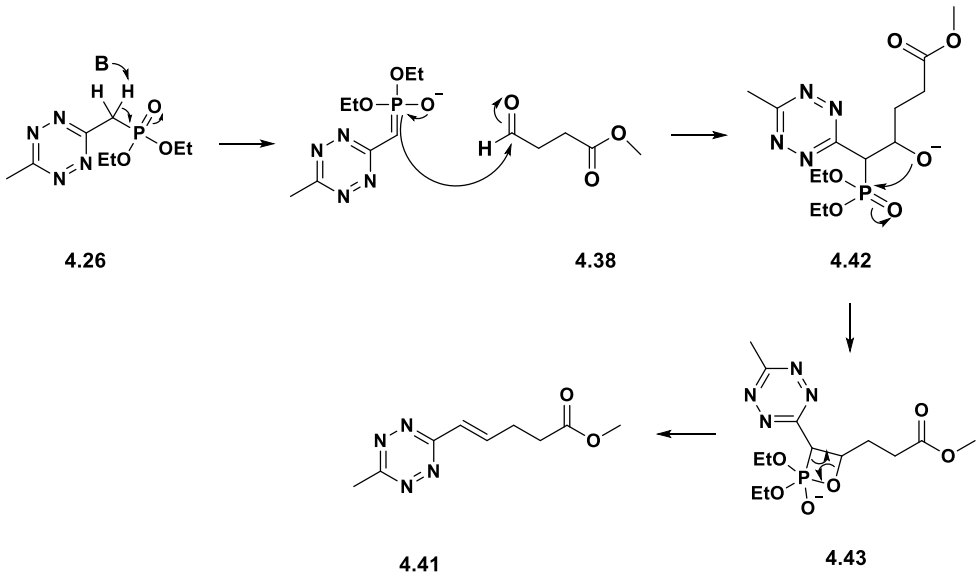
After the successful synthesis of both aldehyde precursors, the next step was to perform the HWE reaction using 3-phosphonate-6-methyl-1,2,4,5-tetrazine, **4.26**. The HWE reacts an aldehyde with a phosphonate to give an alkene, the mechanism for this reaction is similar to the Wittig reaction (**Scheme 4-7**).



4.26 4.38 4.41

Scheme 4-7 *HWE reaction with 3-phosphonate-6-methyl-1,2,4,5-tetrazine (**4.26**) and an ester functionalised aldehyde (**4.38**) to give di-substituted 1,2,4,5-tetrazine (**4.41**).*

Phosphonate esters are typically reacted with strong bases to produce reactive phosphonium anions. The phosphonium anion then undergoes nucleophilic attack towards the aldehyde **4.38** giving the tetrahedral intermediate **4.42**. The final step is the elimination of phosphine oxide, forming an alkene **4.41** (**Scheme 4-8**).

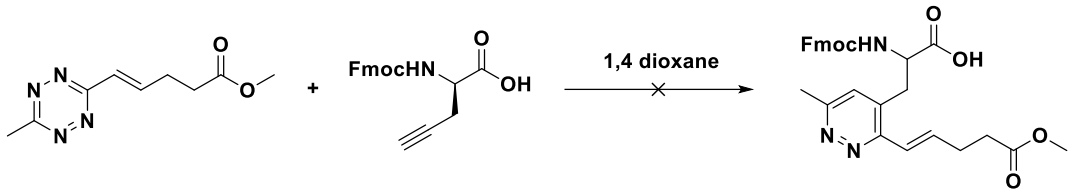


Scheme 4-8 *Horner Wadsworth Emmons reaction mechanism.*

The HWE reaction mechanistically favours the *E* isomer. However, the formation of **4.43** has a reversible nature, therefore the choice of solvent, steric bulk and base was important for *E* isomer selectivity. For this reaction, the based used was lithium hexafluoroisopropoxide ($(CF_3)_2CHOLi$).[59] This weak base was shown to be highly effective with limited epimerization and high *E* selectivity.[59] This was prepared using n-butyllithium added to 1,1,1,3,3,3-hexafluoroisopropanol in dimethoxyethane (DME) to give $(CF_3)_2CHOLi$. Furthermore, the bulky phosphonate group with strong electron withdrawing groups also favours the *E*-alkene. $LiOCH\text{-}(CF_3)_2$ was added to **4.26** and either **4.38** or **4.40** to give the olefin product. For the ester functionalised tetrazine **4.41**, ^{1}H NMR revealed a doublet of triplets at 7.51 ppm and another doublet of triplets at 6.86 ppm integrating to one proton each to confirm the formation of the alkene. The coupling constant (J = 16.3 Hz) and downfield position of the proton peaks confirm the *E* isomer. When forming the di-substituted tetrazine with the amine functional group, the reaction was successful but resulted in two spots on the TLC that were unable to be separated. By using ^{1}H NMR it was determined that with two doublets of triplets observed at 7.45 ppm and 6.87 ppm integrating to one, the product was visible but also an aldehyde peak found at 9.79 ppm corresponding to starting material. As they were unable to be separated, the ester 1,2,4,5-tetrazine was used in iEDDA click attempts.

4.3.2 iEDDA clicks with di-substituted tetrazine

The iEDDA click reactions were attempted using Fmoc-L-propargylglycine and Fmoc-(S)-2-(4-pentyl)Ala-OH as the dienophile. Fmoc protected compounds are suitable to be used in SPPS. As the purpose of the iEDDA reactions is to proceed under mild conditions, initially **4.41** was added in a 1:1 ratio with the Fmoc-L-propargylglycine **4.44** in 1,4-dioxane at room temperature (**Scheme 4-9**).



4.41 **4.44** **4.45**

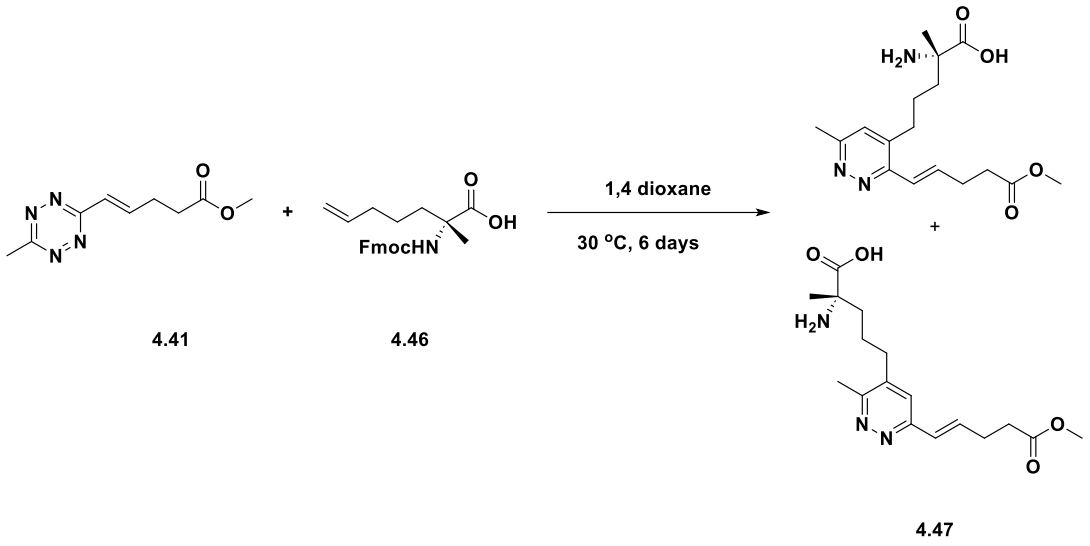
Scheme 4-9 *iEDDA reaction with* ***4.41*** *and Fmoc-L-propargylglycine (****4.44****).*

The reaction was monitored by TLC, showing no change after 7 days. After this time, 90 °C heat was applied for 3 days also noting no change. The Boger group found that tetrazines can be activated for cycloaddition by hydrogen bonding using hexafluoroisopropanol (HFIP).[60] However, when added as the only solvent at 0.1 M solubility was an issue. To combat the insolubility, small amounts of methanol were added but after five days the reaction remained unchanged with starting materials present. It was concluded that for this iEDDA reaction, Fmoc-L-propargylglycine was an unsuitable dienophile.

When using the alkene dienophile, Fmoc-(S)-2-(4-pentyl)Ala-OH **4.46**, for the iEDDA reaction with the di-substituted 1,2,4,5-tetrazine more success was seen. The reaction conditions were repeated, with equimolar reactants in 1,4 dioxane (

Scheme 4-10 *iEDDA reaction with* ***4.41*** *and Fmoc-(S)-2-(4-pentyl)Ala-OH (****4.46****) to give the pyridazine products (****4.47****).*

).



Scheme 4-10 *iEDDA reaction with* ***4.41*** *and Fmoc-(S)-2-(4-pentyl)Ala-OH (****4.46****) to give the pyridazine products (****4.47****).*

The reaction was monitored using TLC. Upon a change in the TLC spot, the mixture was purified using 10% methanol in DCM. When analysed by analytical HPLC to determine the purity, it was clear that the product still contained starting material and required further purification as more than one peak was seen. Preparative RP-HPLC was used for further purification. However, when confirming the purity *via* analytical HPLC it was clear that impurities remained (**Figure 4-20**).

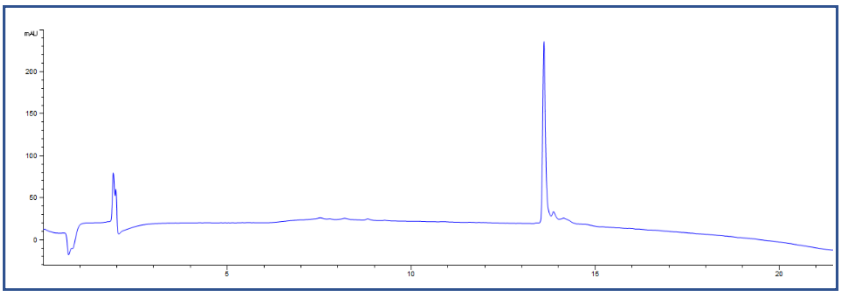


Figure 4-20 *The analytical HPLC traces recorded at 214 nm for* ***4..47*** *after purification via preparative RP-HPLC (Agilent eclipse XDB-C18 column (4.6 x 150 mm, 5 µm) and a flow rate of 1 mL/min. Spectra were run with a solvent gradient of 0-100% B over 20 min. Solvent A: H_2O, 0.05% TFA, solvent B: MeCN, 0.05% TFA).*

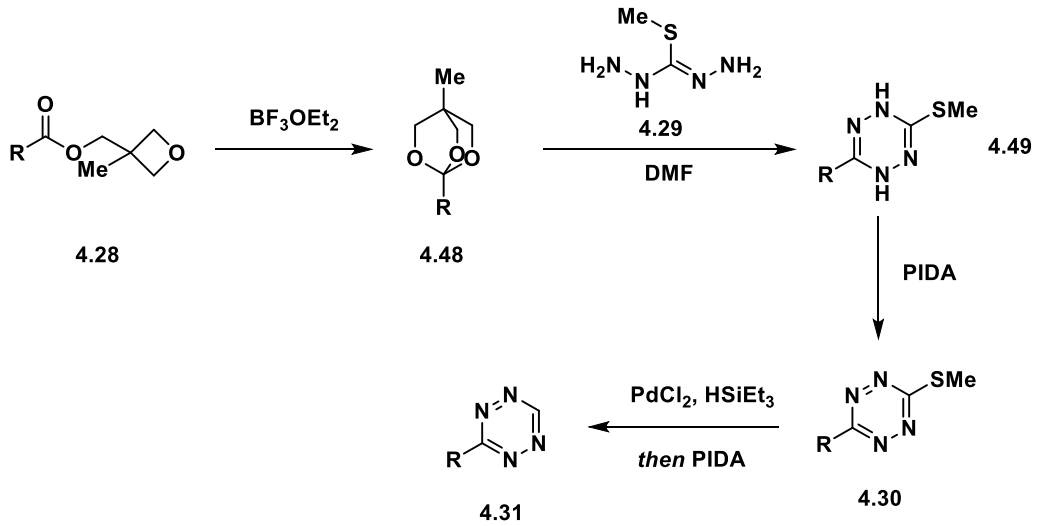
Despite the impurities, there was evidence to suggest the product was there by the mass being seen using high resolution LCMS with the observed *m/z* of 339.2032, matching the expected [M+H]+ of 339.1999. When analysing the mass and the impurities that were seen on TLC, it was determined that the Fmoc-(S)-2-(4-pentyl)Ala-OH was being Fmoc deprotected over the six day reaction due to 1,2,4,5-tetrazines being thought to be weakly basic. The iEDDA addition is not regioselective and produces a mixture of

1,4- and 1,5 isomers.[61,62] After both purifications with further purifications still needed, the remaining yield can be assumed to be less than 20%.

Due to the number of days these reactions were taking to proceed and the low yield, the iEDDA reaction was subjected to microwave heating over a range of temperatures from 50 °C to 80 °C for up to 15 minutes.[37] However, there was either no change in the reaction or degradation was occurring and it was assumed this was unsuitable for these reactions.

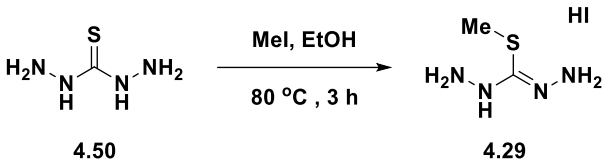
4.3.3 Mono-substituted 1,2,4,5-tetrazine synthesis

Despite the success of the iEDDA reaction with the di-substituted tetrazine, **4.40**, reaction progress was very slow and the yield was too low for use with a library of small molecule fragments. As previously mentioned, mono-substituted tetrazines have faster kinetics than di-substituted tetrazines.[17,26,38] There was some concern that the methyl group was slowing the iEDDA reaction, therefore a different approach was considered to synthesis mono-substituted tetrazines. To synthesis a mono-substituted tetrazine suitable for peptide synthesis, the Fox group's strategy for synthesis was used. In a one pot procedure, carboxylic esters, **4.28**, are used to form 3-thiomethyltetrazines, **4.48**, through the condensation of oxabicyclo[2.2.2]octyl orthoester (OBO), **4.47**, and methyl thiocarbohydrazide, **4.29**, followed by oxidation of **4.49** (**Scheme 4-11**).[18,55]



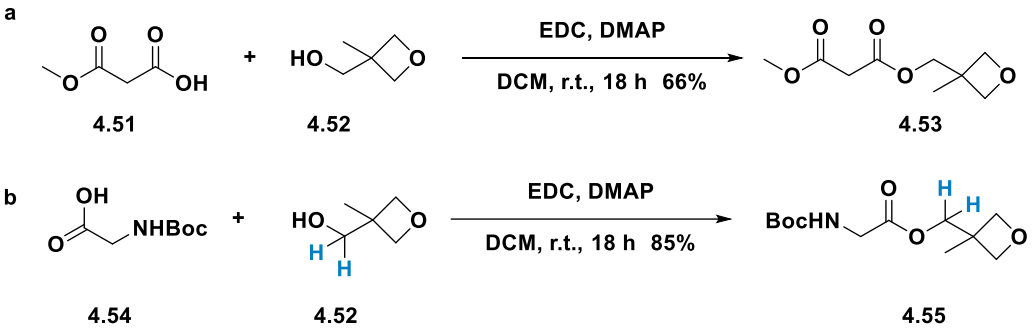
Scheme 4-11 *The overall synthesis using carboxylic acid precursors to form mono-substituted 1,2,4,5-tetrazine (**4.30**).*

The synthesis began with forming methyl thiocarbohydrazide iodide salt **4.29** by refluxing thiocarbohydrazide **4.50** with methyl iodide. This formed a white solid and was used directly without purification (**Scheme 4-12**).[18]



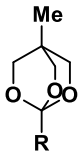
Scheme 4-12 *The methylation of thiocarbohydrazide (**4.50**) to form the product methyl thiocarbohydrazide iodide salt (**4.29**).*

The next step was to synthesise the two oxetane esters, one with an ester functional group **4.53** (**Scheme 4-13A**) and one with a Boc protected amine **4.55** (**Scheme 4-13B**). These were prepared from precursor acids by Steglich esterification using 3-methyl-3-oxetanemethanol **4.52**, EDC and DMAP. ^{1}H NMR showed a downfield shift of the protons that were attached to the alcohol as an ester was formed confirming both products. Further confirmation was provided by LCMS with the observed *m/z* of 203.6 and 260.2, matching the expected [M+H]+ of 203.08 and 260.14 for **4.53** and **4.55** respectively.



Scheme 4-13 *a) Synthesis of ester substituted oxetane ester (**4.53**) b) Synthesis of amine substituted oxetane ester (**4.55**).*

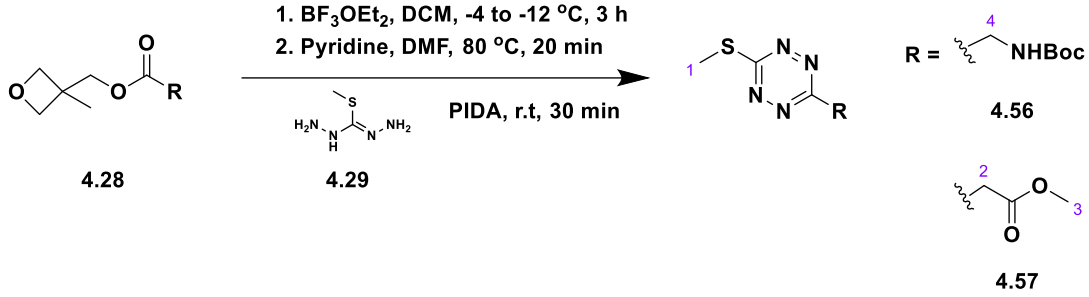
Following this, the one-pot method synthesized 3-thiomethyl-1,2,4,5-tetrazines **4.56** and **4.57** from the prepared esters. The oxetane esters **4.53** and **4.55** were treated with $BF_3.OEt_2$ to form the OBO orthoester (**Figure 4-21**) .[55]



4.47

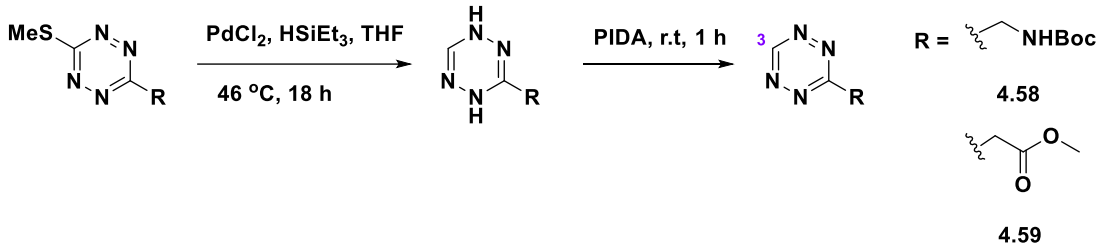
Figure 4-21 *OBO orthoester.*

After 3 hours, pyridine and methyl thiocarbohydrazide iodide salt **4.29** were added. The solvent was also exchanged from DCM to DMF and the mixture was heated at 80 °C for 20 minutes. The dihydrotetrazine solution was cooled to room temperature and treated with phenyliodine(III) diacetate (PIDA) to oxidise to the final 1,2,4,5-tetrazine products. After purification *via* flash column chromatography, the products **4.56** and **4.57** were recovered as a red oil with a 64% yield and a red solid with a 49% yield respectively (**Scheme 4-14**).



Scheme 4-14 *Synthesis of 3-thiomethyl 1,2,3,4 tetrazine with an amine functional group (**4.56**) and an ester functional group (**4.57**).*

Both products were characterized using ^{1}H NMR. The ester showed three singlets, two corresponding to the two methyl groups ($1CH_3$, $3CH_3$, **4.57**) integrating for 3 protons and a singlet ($2CH_2$) integrating for 2 protons (**Scheme 4-14**). The Boc protected amine, **4.56**, showed two singlets, one integrating for 9 protons corresponding to the protecting Boc group and one integrating for 3 protons for the methyl group ($1CH_3$). The ^{1}H NMR also displayed a doublet integrating for 2 protons corresponding to be the CH_2 between the tetrazine ring and the amine ($4CH_2$).

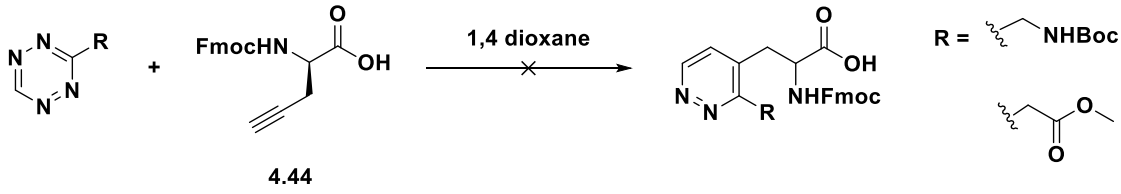


Scheme 4-15 *The reduction of thiomethyl tetrazines to give the mono-substituted amine functionalised tetrazine (**4.58**) and ester functionalised tetrazine (**4.59**).*

The synthesis continued to reduce the thiomethyltetrazines **4.56** and **4.57** using $PdCl_2$ and triethylsilane at 45 °C overnight (**Scheme 4-15**). The mixture was then cooled to room temperature and the oxidising agent PIDA was added for 1 hour to give the mono-substituted tetrazine products **4.58** and **4.59**. The crude products were purified using flash column chromatography with reported yields of 64% for **4.48** and 30% for **4.59** respectively. These products were confirmed using ^{1}H NMR showing a singlet at 10.28 ppm integrating for one proton that corresponds to the proton found at the C3 position (1CH) on the 1,2,4,5-tetrazine (**Scheme 4-15**).

4.3.4 iEDDA clicks with mono-substituted tetrazines

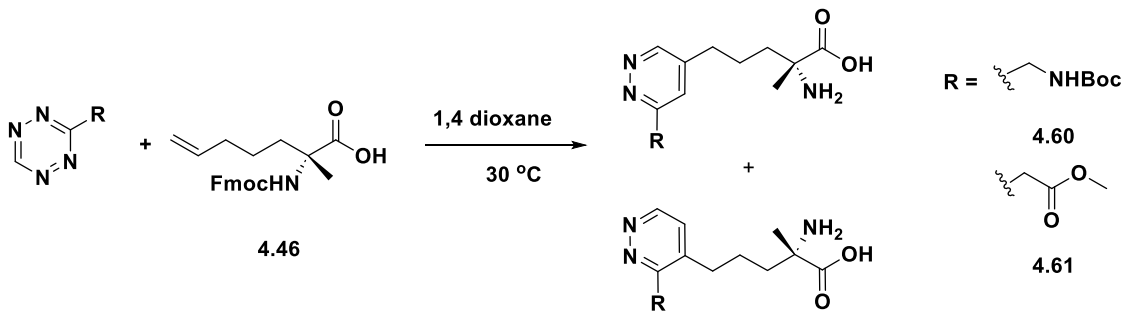
The iEDDA click was attempted first using Fmoc-L-propargylglycine (**4.44**) and the mono-substituted tetrazines **4.58** and **4.59** in hopes that they would be more reactive than the di-substituted tetrazines (**Scheme 4-16**).



Scheme 4-16 *iEDDA click reactions using Fmoc-L-propargylglycine (**4.44**) and mono-substituted tetrazines **4.58** and **4.59**.*

Again, the reactions were monitored by TLC and each showed no change after 10 days. The addition of HFIP and an increase in temperature did not change this result.

When using Fmoc-(S)-2-(4-pentyl)Ala-OH, **4.46**, in the repeated reaction conditions a slight decrease in reaction time was seen from six days to two days for the Boc protected amine, **4.60**, and five days for the ester **4.61** (**Scheme 4-17**).



Scheme 4-17 *iEDDA reactions with Fmoc-(S)-2-(4-pentyl)Ala-OH (**4.46**) and mono-substituted tetrazines **4.60** and **4.61.***

The reactions were monitored with TLC and upon completion there was a distinct colour change from red/pink to colourless. The compounds were analysed using analytical HPLC and the crude traced revealed that were was many peaks corresponding to many side reactions. The compounds were attempted to be purified using preparative RP-HPLC with evidence to suggest the final products **4.60** and **4.61** were present at a retention time of 13.25 and 13.13 min through the observation of an *m/z* of 282.3 and 336.2, corresponding to [M+H]+ of 282.1 and 336.2 respectively. However, when analysing the trace of the analytical HPLC (**Figure 4-22**) after attempted purification minor impurities remained with **4.60** having a low yield of less than 11% and **4.61**, less than 18%. Due to this, the determination of which isomer was present was not concluded due to the practical limitations of the reactions.

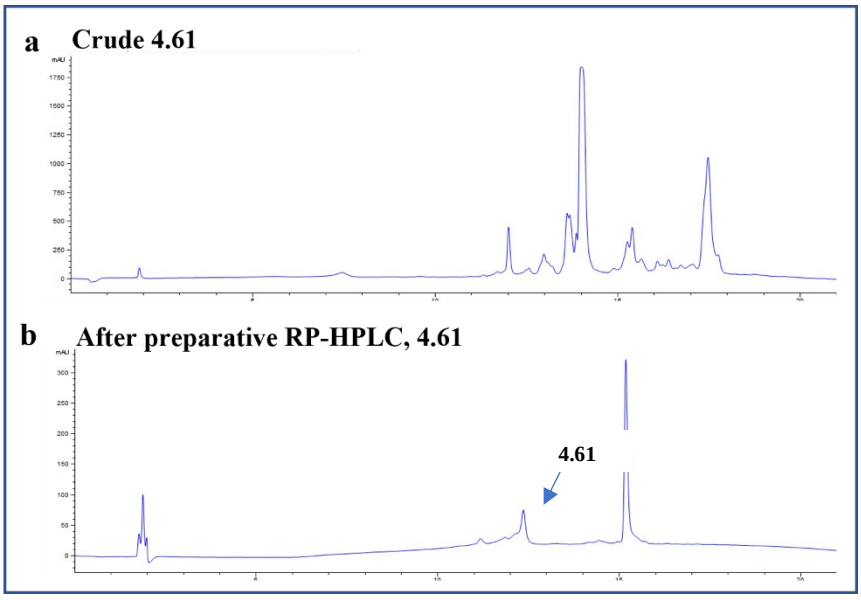
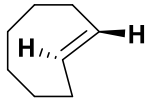


Figure 4-22 *The analytical HPLC traces recorded at 214 nm for **4.61** a) crude b) after purification via preparative RP-HPLC (Agilent eclipse XDB-C18 column (4.6 x 150 mm, 5 µm) and a flow rate of 1 mL/min. Spectra were run with a solvent gradient of 0-100% B over 20 min. Solvent A: H_2O, 0.05% TFA, solvent B: MeCN, 0.05% TFA)*

Again, there was either no change in the reaction or degradation was occurring when the microwave was used. Further, HFIP also did not improve the speed of the reactions nor the yield.

4.3.5 Work towards better dienophiles

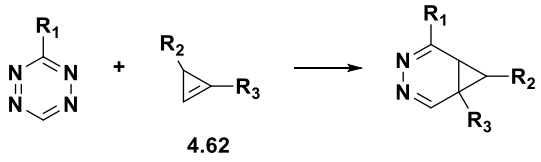
Although the iEDDA reactions showed some success the amount of time the reaction took was not suitable for peptide directed binding. Most studies have found TCO to have the optimal kinetics for an iEDDA reaction, for this project the large structure of TCO would be too bulky (**Figure 4-23**).



4.12

Figure 4-23 *The structure of TCO.*

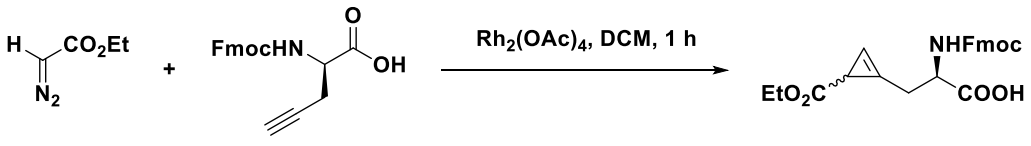
Substituted cyclopropenes, **4.62**, were considered as they are small in size and contain a strained alkene.[63] It was thought that they would be a suitable alternative dienophiles to Fmoc-(S)-2-(4-pentyl)Ala-OH (**4.46**) or Fmoc-L-propargylglycine **4.44** (**Scheme 4-18**).[63]



4.62

Scheme 4-18 *iEDDA reaction between 1,2,4,5-tetrazine and cyclopropene.*

This synthesis of the cyclopropene **4.64** was attempted using the Fmoc-L-propargylglycine, **4.44**, and diazoacetate, **4.63**, in the presence of the catalyst rhodium (II) acetate ($Rh_2(OAc)_4$) (**Scheme 4-19**).[63] By using Fmoc-L-propargylglycine to form the cyclopropene it was hoped it could still be viable for use with SPPS to be inserted into the peptide backbone.



4.63 **4.44** **4.64**

Scheme 4-19 *The synthesis of strained cyclopropene* ***(4.64)*** *using Fmoc-L-propargylglycine* ***(4.44)*** *and diazoacetate* ***(4.63)****.*

Although the reaction was successful in forming the cyclopropene, with two singlets at 6.85 ppm and 6.23 ppm for the two protons found on the alkene observed in the crude ^{1}H NMR, problems arose in the purification. Fmoc deprotection was taking place during the reaction that left a free amine alongside the already unprotected carboxylic acid. During flash column chromatography the product appeared to be too polar to elute from the column. Despite trying to add acid or base to the solvent to protonate or deprotonate the respective acid or amine, the problem was not resolved. If returning to this reaction a different less labile protecting group could be used to protect the amine such as a Boc group. Due to a shortage of time, the click reaction was attempted with the crude product but after 10 days it was concluded that the iEDDA reaction was unsuccessful and purification of the dienophile was necessary.

4.4 Conclusion

When considering peptide-directed binding to create novel small molecule inhibitors for the immune checkpoint pathway PD-1/PD-L1, a turn like structure was beneficial for improving binding affinity to inhibit this interaction. To confirm that the IEDDA reaction could be used as a turn like linker between a peptide and a small molecule, a di-substituted methyl 1,2,4,5 tetrazine with an ester functional group, **4.41**, and two monosubstituted 1,2,4,5 tetrazine, one functionalised with an amine, **4.58**, and the other an ester, **4.59**, were successfully synthesised. Using the dienophiles that could be easily incorporated into a peptide, Fmoc-L-propargylglycine, **4.44**, and Fmoc-(S)-2-(4-pentyl)Ala-OH, **4.46**, the iEDDA reactions were attempted. No reactions were observed with Fmoc-L-propargylglycine for any of the 1,2,4,5 tetrazine derivates. When the IEDDA reactions were repeated with Fmoc-(S)-2-(4-pentyl)Ala-OH, all 1,2,4,5 tetrazine derivates showed successful reactions. However, the reaction times were from 2-6 days and were considered unsuitable for peptide-directed binding. Furthermore, the low yields meant analysis of regioselectivity was inconclusive and would require more investigation. A brief attempt to synthesize a different dienophile that contained a cyclopropene was attempted, but there were problems during purification that could be rectified by using a different protecting group on the amine. Due to the success in other lines of research discussed in chapter 2 and 3, the amount of time spent on this was limited.

In future work, multiple dienophiles with various EWGs could be screened with the 1,2,4,5-tetrazines **4.58** and **4.59** to try optimise the iEDDA reaction, including various ring strained compounds that are less bulky than the commonly used TCO such as the cyclopropene and spirohexene.[64] Solvent can also play an important role in the iEDDA reaction, and future work could include screening multiple solvents to try to determine a reaction with faster kinetics.[37] Further, the addition of HFIP within these various solvents could also be considered.[60] Other potential catalysts could also be considered such as potassium arylethyltrifluoroborate that has been shown to increase reaction time for unstrained dienophiles.[65]

4.5 General procedures

4.5.1 Materials and solvents

All chemicals were purchased from Sigma Aldrich, Fisher Scientific or Fluorochem. Anhydrous solvents were purchased from Sigma Aldrich, used as purchased and assumed to conform to specification.

4.5.2 Instrumental techniques

^{1}H- and ^{13}C- NMR were collected using a Bruker spectrometer operating at 400 MHz (^{1}H) or 101 MHz (^{13}C) using the specified deuterated solvent. The chemical shifts were recorded in ppm and were referenced to the residual solvent peak of DMSO (2.50 ppm) or chloroform (7.26 ppm). Multiplicities in the NMR spectra are described as s = singlet, d = doublet, t = triplet, q = quartet, m = multiplet, and combinations thereof. Coupling constants are reported in Hz. High resolution masses were recorded using Waters Synnapt XS QTOF under electrospray ionisation. Low resolution mass was recorded using an Agilent 1200 Series equipped with a 6460 triple quadrupole.

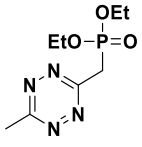
Analytical RP-HPLC was performed using an Agilent 1200 HPLC using an Agilent eclipse XDB-C18 column (4.6 x 150 mm, 5 μm) and a flow rate of 1 mL/min. Spectra were run with a solvent gradient of 0-100% B over 20 min. Solvent A: H_2O, 0.05% TFA, solvent B: MeCN, 0.05% TFA. Detection wavelengths were 214 nm and 254 nm.

Preparative RP-HPLC was performed on an Agilent 1200 HPLC, fitted with an Agilent eclipse XDB-C18 column (21.2 x 150 mm, 5 μM) and a flow rate of 20 mL/min. Purification was run with a solvent gradient of 0-100% B over 15 min. Solvent A: 95%

H2O, 5% MeCN, 0.05% TFA, solvent B: 95% MeCN, 5% H_2O, 0.05% TFA. Detection wavelengths were 214 nm and 254 nm.

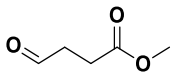
4.5.3 Synthesis 1,2,4,5-tetrazines

4.5.3.1 Di-substituted 1,2,4,5-tetrazine



4.26

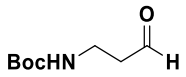
Compound **4.26** was prepared following a published protocol.[20] A solution of diethyl cyanomethyl phosphonate (2.65 g, 2.40 mL, 15.0 mmol), acetonitrile (16 mL, 300 mmol) and 3-mercaptopropionic acid (1.30 mL, 15.0 mmol) in ethanol (5 mL) was cooled to 0 °C and purged with N_2. Hydrazine hydrate (12 mL, 240 mmol) was then added dropwise. The reaction was stirred at room temperature overnight. The reaction was cooled with ice water and an ice water solution of sodium nitrite (15.5 g, 225 mmol) was added dropwise to the reaction. Following this, 1 M HCl was added slowly under intense stirring until gas evolution ceased and pH was 3-4 observed using litmus paper. The reaction colour turned bright pink. The acidic solution was extracted with DCM, washed with brine, dried with Na_2SO_4, filtered and concentrated under vacuum to give a pink oil. Purification was achieved by column chromatography (0.5% acetone in DCM) to afford the tetrazine **4.26** as a pink oil (45%, 1.66 g, 4.33 mmol). Rf 0.28 (0.5% acetone in DCM). The data matched that observed in the literature.[20] (^{1}H NMR (400 MHz, Chloroform-*d*) δ 4.34 – 4.12 (m, 4 H), 3.92 (d, *J* = 22.2 Hz, 2H), 3.07 (s, 3H), 1.33 (t, *J* = 7 Hz, 6H). ^{13}C NMR (101 MHz, $CDCl_3$) δ 167.7 (d, *J* = 3.2 Hz), 164.3 (d, *J* = 9.5 Hz), 63.0, 62.9, 34.4, 33.1, 21.2, 16.4., 16.3. ESI-QQQ $[M+Na]^+$ *m/z* calcd. for $[C_8H_{15}N_4NaO_3P]^+$ 269.09, found 269.2.



4.38

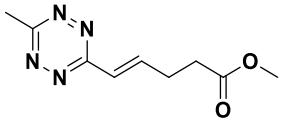
Compound **4.38** was prepared following a published protocol.[56] To a solution of methyl 4-chloro-4-oxobutyrate (0.42 mL, 3.3 mmol) dissolved in THF (8 mL), 2,6-lutidine (0.39 mL, 3.4 mmol) and 10% palladium on carbon (35 mg) was added. The reaction was stirred overnight at room temperature under H_2. The reaction was filtered

through celite and concentrated under vacuum. The product was obtained as a yellow oil (quant.). Continued to next step without purification.



4.40

Compound **4.40** was prepared following a published protocol.[66] Boc-β-Ala-OH (378 mg, 2.00 mmol) was dissolved in anhydrous DCM (10 mL) and cooled to 0 °C. Once cooled, 1,1′-carbonyldiimidazole (357 mg, 2.20 mmol) was added and stirred for 60 mins at 0 °C. The reaction mixture was then cooled to −78 °C and DIBAL-H (3.50 mL, 597 mg, 4.20 mmol) was added dropwise over 20 mins and then stirred for 1 h. The reaction was quenched with ethyl acetate (5 mL) followed by tartaric acid solution (10 mL, 20% in H_2O) with vigorous stirring. The product was extracted using ethyl acetate and washed sequentially with 1 M HCl, $NaHCO_{3(aq)}$ and brine. The combined organic layers were dried with Na_2SO_4, filtered, and concentrated under vacuum to give yellow oil that was used directly without further purification.

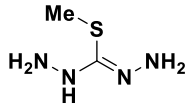


4.41

Compound **4.41** was prepared following a published protocol.[20] LiHFl: 1,1,1,3,3,3-hexafluoroisopropanol (130 µL, 0.21 mmol) in DME (2 mL) was cooled to −14 °C and purged with N_2. Under N_2, n-BuLi in hexanes (396 µL, 2.5 M, 0.198 mmol) was added dropwise. A solution of phosphonate tetrazine derivative (135 mg, 0.549 mmol) and methyl 4-oxobutanoate (58 mg, 0.50 mmol) in anhydrous THF (10 mL) was cooled to −20 °C. To this the LiHFl solution was added dropwise. The reaction was stirred at −20 °C and was monitored using TLC, after 3 hours the reaction was quenched with $NH_4Cl_{(aq)}$. The organic phase was extracted using ethyl acetate, dried with Na_2SO_4, filtered and concentrated under vacuum to give a pink oil. Purification was achieved by column chromatography (15% ethyl acetate in hexane) to yield a pink solid (97 mg, 0.47 mmol, 84%). Rf 0.54 (10% methanol in DCM). ^{1}H NMR (400 MHz, Chloroform-*d*) δ 7.51 (dt, *J* = 16.3, 6.2 Hz, 1H), 6.86 (dt, *J* = 16.3, 1.7 Hz, 1H), 3.71 (s, 3H), 3.02 (s, 3H), 2.78 – 2.71 (m, 2H), 2.61 (td, *J* = 7.3, 1.0 Hz, 2H). ^{13}C NMR (101 MHz, $CDCl_3$) δ 172.9, 166.8, 164.0, 143.3, 124.4, 52.0, 32.7, 28.3, 21.3. IR ν/cm^{-1} 2947,

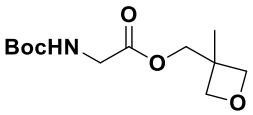
2927, 2862, 1731, 1650, 1405, 1287, 1259, 1193. ESI-QQQ $[M+H]^+$ *m/z* calcd. for $[C_9H_{13}N_4O_2]^+$ 209.2, found 209.1. HRMS (ESI-): $[M+H]^+$ *m/z* calcd. 209.1038, found 209.1039.

4.5.3.2 Mono-substituted 1,2,4,5-tetrazine



4.29

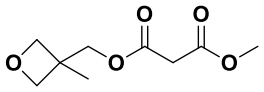
Compound **4.29** was prepared following a published protocol.[18] Thiocarbohydrazide (500 mg, 5 mmol) was suspended in ethanol (15 mL, 0.3 M) and heated under reflux then methyl iodide (323 µL, 735 mg, 5.18 mmol) was added dropwise. The reaction mixture was refluxed for 3 h and then cooled to room temperature. Once cooled, hexane (2 mL) was added and the reaction was left in the freezer overnight. The precipitant formed over night was filtered and washed with hexane: ethanol (1:1) and dried under vacuum to give a white solid (529 mg, 2.13 mmol, 45%) that was used directly without further purification.



4.55

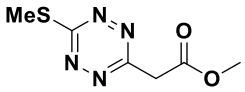
Compound **4.55** was prepared following a published protocol.[18] 3-methyl-3-oxetanemethanol (1.22 mL, 1260 mg, 12.3 mmol), EDC.HCl (2580 mg, 13.5 mmol), and DMAP (137 mg, 1.12 mmol) were dissolved in anhydrous DCM (22 mL) and cooled to 0 °C. Boc-Glycine (350 mg, 2.0 mmol) was added and the reaction was stirred at 0 °C for 15 mins, and then room temperature for 18 h. The reaction completion was determined by TLC (15% ethyl acetate in hexane). The product was diluted with DCM and washed with $Na_2CO_{3(aq)}$, water and brine. The DCM was then dried over Na_2SO_4 and concentrated under vacuum. The crude product was purified using column chromatography (0-15% ethyl acetate in hexane) to give a colourless oil (2470 mg, 9.52 mmol, 85%). Rf 0.15 (15% ethyl acetate in hexane). The data matched that observed in the literature.[18] ^{1}H NMR (400 MHz, Chloroform-*d*) δ 4.48 (d, *J* = 6.0 Hz, 2H), 4.37 (d, *J* = 6.0 Hz, 2H), 4.24 (s, 2H), 3.93 (d, *J* = 5.8 Hz, 2H), 1.43 (s, 9H),

1.32 (s, 3H). ^{13}C NMR (101 MHz, Chloroform-*d*) δ 170.6, 155.8, 80.1, 79.5, 69.5, 42.4, 39.1, 28.3, 21.1. ESI-QQQ $[M+H]^+$ *m/z* calcd. for $[C_{12}H_{22}NO_5]^+$ 260.14, found 260.2.



4.53

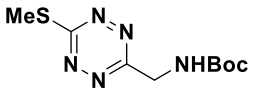
Compound **4.53** was prepared following a published protocol.[18] 3-methyl-3-oxetanemethanol (1960 mg, 11.2 mmol), EDC·HCl (2500 mg, 13 mmol), DMAP (130 g, 13 mmol) were dissolved in anhydrous DCM (22 mL) and cooled to 0 ℃. Once cooled, 3-methoxy-3-oxopropanoic acid (1060 mg, 940 µL, 8.98 mmol) was added dropwise and stirred at 0 ℃ for 15 minutes, then room temperature for 18 h. The reaction completion was determined by TLC (20% ethyl acetate in hexane). The product was diluted with DCM and washed with $Na_2CO_{3(aq)}$, water and brine. The DCM was then dried over Na_2SO_4 and concentrated under vacuum. The oil crude product was purified using a silica plug (0-20% ethyl acetate in hexane) to give a colourless oil (2413 mg, 11.94 mmol, 66%). Rf 0.14 (20% ethyl acetate in hexane). The data matched that observed in the literature.[18] ^{1}H NMR (400 MHz, Chloroform-*d*) δ 4.52 (d, *J* = 6 Hz, 2H), 4.39 (d, *J* = 6.0 Hz, 2H), 4.25 (s, 2H), 3.76 (s, 3H), 3.44 (s, 2H), 1.34 (s, 3H). ^{13}C NMR (101 MHz, $CDCl_3$) δ 166.8, 166.5, 79.4, 69.6, 52.6, 41.2, 39.1, 21.1. ESI-QQQ $[M+H]^+$ *m/z* calcd. for $[C_9H_{15}O_5]^+$ 203.08, found 203.6.



4.57

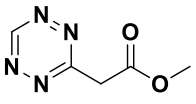
Compound **4.57** was prepared following a published protocol.[18] **4.53** (1300 mg, 6.4 mmol) was dissolved in anhydrous DCM (6 mL) and cooled to −12 ℃. Boron trifluoride etherate (400 µL/460 mg, 3.2 mmol) was added dropwise and stirred for 4 hours. The reaction was monitored by TLC quenching aliquots with triethylamine (20% ethyl acetate in hexane), once the reaction reached completion the reaction was quenched with pyridine. **4.29** (770 mg, 6.4 mmol) and DMF (5 mL) were added and gentle vacuum with vigorous stirring was applied to remove the DCM. The reaction was then heated 80 ℃ and stirred under N_2 for 20 min. After cooling to room temperature, PIDA (3090 mg, 9.60 mmol) was added and stirred for 30 min at room

temperature. The reaction mixture was diluted with DCM and washed three times each with $Na_2CO_{3(aq)}$, water and brine, dried over Na_2SO_4 and concentrated under vacuum. The mixture was purified by column chromatography (20-40% ethyl acetate in hexane) to give a red oil (823 mg, 4.61 mmol, 64%). Rf 0.37 (30% ethyl acetate in hexane). The data matched that observed in the literature.[18] ^{1}H NMR (400 MHz, Chloroform-*d*) δ 4.31 (s, 2H), 3.77 (s, 3H), 2.74 (s, 3H). ^{13}C NMR (101 MHz, $CDCl_3$) δ 176.1, 168.5, 162.3, 52.6, 40.1, 13.3. ESI-QQQ $[M+H]^+$ *m/z* calcd. for $[C_6H_9N_4O_2]^+$ 201.04, found 201.20.



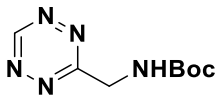
4.56

Compound **4.56** was prepared following a published protocol.[18] **4.55** (1100mg, 4.3 mmol) was dissolved in anhydrous DCM (4.3 mL) and cooled to −12 ℃. Boron trifluoride etherate (264 μL, 304 mg, 2.14 mmol) was added dropwise and stirred for 4 hours. The reaction was monitored by TLC quenching aliquots with triethylamine (15% ethyl acetate in hexane), once the reaction reached completion the reaction was quenched with pyridine. **4.29** (850 mg, 3.4 mmol) and DMF (5 mL) were added and gentle vacuum with vigorous stirring was applied to remove the DCM. The reaction was then heated 80 ℃ and stirred under N_2 for 20 min. After cooling to room temperature, PIDA (1100 mg, 3.4 mmol) was added and stirred for 30 min at room temperature. The reaction mixture was diluted with DCM and washed with $Na_2CO_{3(aq)}$, water and brine, dried over Na_2SO_4 and concentrated under vacuum. The mixture was purified by flash column chromatography (0-15% ethyl acetate in hexane) to give a red solid (539 mg, 2.10 mmol, 49%). Rf 0.35 (15% ethyl acetate in hexane). The data matched that observed in the literature.[18] ^{1}H NMR (400 MHz, Chloroform-*d*) δ 4.89 (d, *J* = 5.8 Hz, 2H), 2.74 (s, 3H), 1.45 (s, 9H). ^{13}C NMR (101 MHz, $CDCl_3$) δ 176.8, 164.5, 80.5, 43.2, 28.4, 13.5. ESI-QQQ $[M+Na]^+$ *m/z* calcd. for $[C_6H_{15}N_5NaO_2S]^+$ 280.08, found 280.20.



4.59

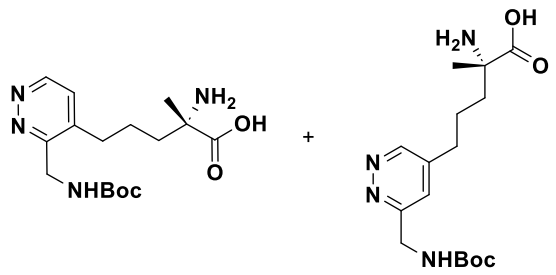
Compound **4.59** was prepared following a published protocol.[18] **4.57** (1000 mg, 6 mmol) and $PdCl_2$ (228 mg, 1.29 mmol) were dissolved in anhydrous THF (40 mL). Triethylsilane (3000 µL, 2260 mg, 19.4 mmol) was added and stirred overnight at 45 °C. Once cooled to room temperature, PIDA (2500 mg, 7.8 mmol) was added and stirred for 1 hour. The reaction mixture was then washed three times each with Na_2CO_3, water and brine then subsequently dried over Na_2SO_4 and concentrated under vacuum to give a red oil. The oil was purified by column chromatography (15% ethyl acetate in hexane) to give a red solid (278 mg, 1.80 mmol, 30%). Rf 0.28 (30% ethyl acetate in hexane). ^{1}H NMR (400 MHz, Chloroform-*d*) δ 10.28 (s, 1H), 4.44 (s, 2H), 3.78 (s, 3H). ^{13}C NMR (101 MHz, $CDCl_3$) δ 168.1, 167.4, 158.2, 52.9, 41.2. ESI-QQQ $[M+Na]^+$ *m/z* calcd. for $[C_6H_6N_4NaO_2]^+$ 177.04, found 177.25.



4.58

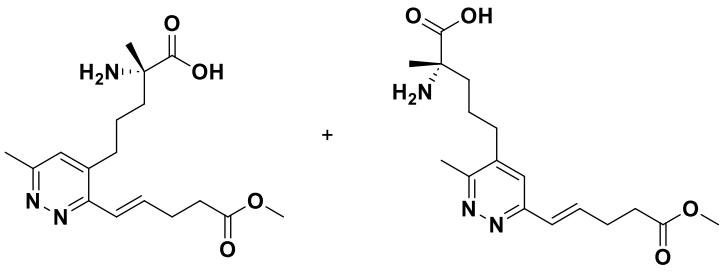
Compound **4.58** was prepared following a published protocol.[18] **4.56** (200 mg, 0.8 mmol) and $PdCl_2$ (14 mg, 0.08 mmol) were dissolved in anhydrous THF (8 mL). Triethylsilane (370 µL, 269 mg, 2.33 mmol) was added and stirred overnight at 45 °C. Once cooled to room temperature, PIDA (300 mg, 0.9 mmol) was added and stirred for 1 hour. The reaction mixture was then washed three times each with $Na_2CO_{3(aq)}$, water and brine then subsequently dried over Na_2SO_4 and concentrated under vacuum to give a red oil. The oil was purified by column chromatography (15% ethyl acetate in hexane) to give a red solid (106 mg, 0.502 mmol, 64%). Rf 0.56 (40% ethyl acetate in hexane). The data matched that observed in the literature.[18] ^{1}H NMR (400 MHz, Chloroform-*d*) δ 10.28 (s, 1H), 5.01 (d, *J* = 6.0 Hz, 2H), 1.46 (s, 9H). ^{13}C NMR (101 MHz, $CDCl_3$) δ 169.6, 158.9, 155.9, 80.7, 43.9, 28.4. ESI-QQQ $[M+H]^+$ *m/z* calcd. for $[C_8H_{13}N_5O_2]^+$ 212.1, found 212.1.

4.5.4 iEDDA click reactions



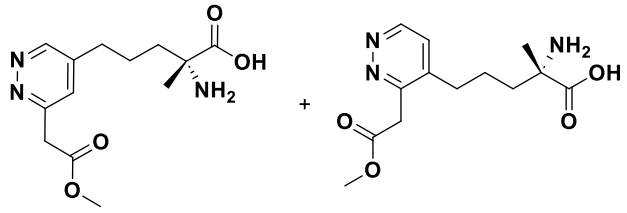
4.60

4.59 (22 mg, 0.1 mmol) and Fmoc-(S)-2-(4-pentyl)alanine (38 mg, 0.1 mmol) were dissolved in 1,4 dioxane (1 mL) and stirred at 30 °C until reaction went to completion as confirmed by TLC, the reaction turned colourless. The crude product was purified by column chromatography (10% methanol in dichloromethane), and further purified with preparative RP-HPLC to give colourless oil. RP-HPLC: t_R = 13.25 min. HRMS (ESI-): $[M+H]^+$ *m/z* calcd. for $[C_{16}H_{27}N_4O_4]^+$ 339.1999, found 339.2032.



4.47

4.41 (10 mg, 0.03 mmol) and Fmoc-(S)-2-(4-pentyl)alanine (10 mg, 0.03 mmol) were dissolved in 1,4 dioxane (1 mL) and stirred at 30 °C until reaction went to completion as confirmed by analytical HPLC, the reaction turned colourless. The crude product was purified with preparative RP-HPLC to give colourless oil. RP-HPLC: t_R = 13.72 min. ESI-QQQ $[M+H]^+$ *m/z* calcd. for $[C_{17}H_{26}N_3O_4]^+$ 336.18, found 336.20.



4.61

4.59 (16 mg, 0.10 mmol) and Fmoc-(S)-2-(4-pentyl)alanine (40 mg, 0.10 mmol) were dissolved in 1,4 dioxane (1 mL) and stirred at 30 °C until reaction went to completion as confirmed by analytical HPLC, the reaction turned colourless. The crude product was purified with preparative RP-HPLC to give colourless oil. RP-HPLC: t_R = 13.13 min. ESI-QQQ $[M+H]^+$ *m/z* calcd. for $[C_{13}H_{20}N_3O_4]^+$ 282.1, found 282.3.

4.6 References

1 A. M. Beekman, M. A. O'Connell and L. A. Howell, *Angew. Chem. Int. Ed.*, 2017, **56**, 10446–10450.
2 H. C. Kolb, M. G. Finn and K. B. Sharpless, *Angew. Chem. Int. Ed.*, 2001, **40**, 2004–2021.
3 V. V. Rostovtsev, L. G. Green, V. V. Fokin and K. B. Sharpless, *Angew. Chem. Int. Ed Engl.*, 2002, **41**, 2596–2599.
4 C. W. Tornøe, C. Christensen and M. Meldal, *J. Org. Chem.*, 2002, **67**, 3057–3064.
5 H. C. Kolb and K. B. Sharpless, *Drug Discov. Today*, 2003, **8**, 1128–1137.
6 J. C. Worch, C. J. Stubbs, M. J. Price and A. P. Dove, *Chem. Rev.*, 2021, **121**, 6744–6776.
7 US. Pat., 0153771 A1, 2003.
8 C. R. Bertozzi, *Acc. Chem. Res.*, 2011, **44**, 651–653.
9 E. Renard, E. Collado Camps, C. Canovas, A. Kip, M. Gotthardt, M. Rijpkema, F. Denat, V. Goncalves and S. A. M. Van Lith, *Cancers*, 2021, **13**, 428.
10 E. Kozma, O. Demeter and P. Kele, *ChemBioChem*, 2017, **18**, 486–501.
11 R. Rossin, R. M. Versteegen, J. Wu, A. Khasanov, H. J. Wessels, E. J. Steenbergen, W. Ten Hoeve, H. M. Janssen, A. H. A. M. Van Onzen, P. J. Hudson and M. S. Robillard, *Nat. Commun.*, 2018, **9**, 1484.
12 J. A. C. M. Goos, A. Cho, L. M. Carter, T. R. Dilling, M. Davydova, K. Mandleywala, S. Puttick, A. Gupta, W. S. Price, J. F. Quinn, M. R. Whittaker, J. S. Lewis and T. P. Davis, *Theranostics*, 2020, **10**, 567–584.
13 W. Jeong, J. Bu, Y. Han, A. J. Drelich, A. Nair, P. Král and S. Hong, *J. Am. Chem. Soc.*, 2020, **142**, 1832–1837.
14 L. Zhang, X. Chen, P. Xue, H. H. Y. Sun, I. D. Williams, K. B. Sharpless, V. V. Fokin and G. Jia, *J. Am. Chem. Soc.*, 2005, **127**, 15998–15999.
15 J. S. Oakdale, V. V. Fokin, S. Umezaki and T. Fukuyama, *Org. Synth.*, 2013, **90**, 96–104.
16 J. Mondal and A. Sivaramakrishna, *Top. Curr. Chem.*, 2022, **380**, 34.
17 M. R. Karver, R. Weissleder and S. A. Hilderbrand, *Bioconjug. Chem.*, 2011, **22**, 2263–2270.
18 Y. Xie, Y. Fang, Z. Huang, A. M. Tallon, C. W. am Ende and J. M. Fox, *Angew. Chem. Int. Ed.*, 2020, **59**, 16967–16973.
19 W. D. Lambert, Y. Fang, S. Mahapatra, Z. Huang, C. W. Am Ende and J. M. Fox, *J. Am. Chem. Soc.*, 2019, **141**, 17068–17074.
20 W. Mao, W. Shi, J. Li, D. Su, X. Wang, L. Zhang, L. Pan, X. Wu and H. Wu, *Angew. Chem. Int. Ed.*, 2019, **58**, 1106–1109.
21 Y.-H. Gong, F. Miomandre, R. Méallet-Renault, S. Badra, L. Galmiche, J. Tang, P. Audebert and G. Clavier, *Eur. J. Org. Chem.*, 2009, **2009**, 6121–6128.

22 Y. B. Rus, M. Bosmi, S. Maisonneuve, V. Guérineau, V. Noël, A. Courty and F. Miomandre, *RSC Adv.*, 2021, **11**, 7043–7050.
23 X. Jiang, M. Li, Y. Wang, C. Wang, Y. Wang, T. Shen, L. Shen, X. Liu, Y. Wang and X. Li, *Nat. Commun.*, 2023, **14**, 1401.
24 L. L. Fershtat, *FirePhysChem*, 2023, **3**, 78–87.
25 J. Sauer, D. K. Heldmann, J. Hetzenegger, J. Krauthan, H. Sichert and J. Schuster, *Eur. J. Org. Chem.*, 1998, **1998**, 2885–2896.
26 F. Thalhammer, U. Wallfahrer and J. Sauer, *Tetrahedron Lett.*, 1990, **31**, 6851–6854.
27 D. L. Boger, R. P. Schaum and R. M. Garbaccio, *J. Org. Chem.*, 1998, **63**, 6329–6337.
28 D. Wang, W. Chen, Y. Zheng, C. Dai, K. Wang, B. Ke and B. Wang, *Org. Biomol. Chem.*, 2014, **12**, 3950.
29 C. Li, H. Ge, B. Yin, M. She, P. Liu, X. Li and J. Li, *RSC Adv.*, 2015, **5**, 12277–12286.
30 J. Sauer and D. Lang, *Angew. Chem.*, 1964, **76**, 603–603.
31 D. R. Soenen, J. M. Zimpleman and D. L. Boger, *J. Org. Chem.*, 2003, **68**, 3593–3598.
32 B. L. Oliveira, Z. Guo and G. J. L. Bernardes, *Chem. Soc. Rev.*, 2017, **46**, 4895–4950.
33 J. Sauer and R. Sustmann, *Angew. Chem. Int. Ed. Engl.*, 1980, **19**, 779–807.
34 F. Liu, R. S. Paton, S. Kim, Y. Liang and K. N. Houk, *J. Am. Chem. Soc.*, 2013, **135**, 15642–15649.
35 F. Liu, Y. Liang and K. N. Houk, *J. Am. Chem. Soc.*, 2014, **136**, 11483–11493.
36 J. Sauer, A. Mielert, D. Lang and D. Peter, *Chem. Ber.*, 1965, **98**, 1435–1445.
37 A.-C. Knall and C. Slugovc, *Chem. Soc. Rev.*, 2013, **42**, 5131.
38 G. Cserép, O. Demeter, E. Bätzner, M. Kállay, H.-A. Wagenknecht and P. Kele, *Synthesis*, 2015, **47**, 2738–2744.
39 K. Braun, M. Wiessler, V. Ehemann, R. Pipkorn, H. Spring, J. Debus, B, Didinger, M. Koch, G. Muller and W. Waldeck, *Drug Des. Devel. Ther.*, 2009, **2**, 289-301.
40 B. M. Zeglis, F. Emmetiere, N. Pillarsetty, R. Weissleder, J. S. Lewis and T. Reiner, *ChemistryOpen*, 2014, **3**, 48–53.
41 M. Pagel, R. Meier, K. Braun, M. Wiessler and A. G. Beck-Sickinger, *Org. Biomol. Chem.*, 2016, **14**, 4809–4816.
42 R. Hassert, M. Pagel, Z. Ming, T. Häupl, B. Abel, K. Braun, M. Wiessler and A. G. Beck-Sickinger, *Bioconjug. Chem.*, 2012, **23**, 2129–2137.
43 S. L. Bellis, *Biomaterials*, 2011, **32**, 4205–4210.
44 C. Mas-Moruno, F. Rechenmacher and H. Kessler, *Anticancer Agents Med. Chem.*, 2010, **10**, 753–768.
45 M. Pagel and A. G. Beck-Sickinger, *Biol. Chem.*, 2017, **398**, 3–22.
46 M. Wiessler, U. Hennrich, R. Pipkorn, W. Waldeck, L. Cao, J. Peter, V. Ehemann, W. Semmler, T. Lammers and K. Braun, *Theranostics*, 2011, **1**, 381–394.
47 In *Comprehensive Organic Name Reactions and Reagents*, John Wiley & Sons, Inc., Hoboken, NJ, USA, 2010, p. conrr504.
48 A. Pinner, *Justus Liebigs Ann. Chem.*, 1897, **297**, 221–271.
49 C. Larsen, E. Binderup and J. Moller, *Acta Chem. Scand.*, 1967, **21**, 2855–2858.
50 J. Yang, M. R. Karver, W. Li, S. Sahu and N. K. Devaraj, *Angew. Chem. Int. Ed.*, 2012, **51**, 5222–5225.

51 US. Pat., 065860 Al, 2014.
52 E. Ros, A. Prades, D. Forson, J. Smyth, X. Verdaguer, L. R. de Pouplana and A. Riera, *Chem. Commun.*, 2020, **56**, 11086–11089.
53 A. M. Bender, T. C. Chopko, T. M. Bridges and C. W. Lindsley, *Org. Lett.*, 2017, **19**, 5693–5696.
54 Z. Novák and A. Kotschy, *Org. Lett.*, 2003, **5**, 3495–3497.
55 E. J. Corey and N. Raju, *Tetrahedron Lett.*, 1983, **24**, 5571–5574.
56 T. Zhao, K. Kurpiewska, J. Kalinowska-Tłuścik, E. Herdtweck and A. Dömling, *Chem. Eur. J.*, 2016, **22**, 3009–3018.
57 A. W. Burgstahler, L. O. Weigel and C. G. Shaefer, *Synthesis*, 1976, **1976**, 767–768.
58 J. Ivkovic, C. Lembacher-Fadum and R. Breinbauer, *Org. Biomol. Chem.*, 2015, **13**, 10456–10460.
59 L. K. Blasdel and A. G. Myers, *Org. Lett.*, 2005, **7**, 4281–4283.
60 Z. Zhu, C. M. Glinkerman and D. L. Boger, *J. Am. Chem. Soc.*, 2020, **142**, 20778–20787.
61 K. Lang, L. Davis, J. Torres-Kolbus, C. Chou, A. Deiters and J. W. Chin, *Nat. Chem.*, 2012, **4**, 298–304.
62 N. K. Devaraj, R. Weissleder and S. A. Hilderbrand, *Bioconjug. Chem.*, 2008, **19**, 2297–2299.
63 P. Kumar, W. Huang, D. Shukhman, F. M. Camarda and S. T. Laughlin, *Tetrahedron Lett.*, 2019, **60**, 1476–1480.
64 C. P. Ramil, M. Dong, P. An, T. M. Lewandowski, Z. Yu, L. J. Miller and Q. Lin, *J. Am. Chem. Soc.*, 2017, **139**, 13376–13386.
65 Z. Zawada, Z. Guo, B. L. Oliveira, C. D. Navo, H. Li, P. M. S. D. Cal, F. Corzana, G. Jiménez-Osés and G. J. L. Bernardes, *Bioconjug. Chem.*, 2021, **32**, 1812–1822.
66 Y. Zhang, P. Ji, Y. Dong, Y. Wei and W. Wang, *ACS Catal.*, 2020, **10**, 2226–2230.

Chapter 5

Cyclic Peptides to Inhibit PD-1/PD-L1

5.1 Introduction

Due to the negative drawbacks of monoclonal antibodies that are currently used to inhibit PD-1/PD-L1 there is a high demand to find an alternative inhibitor. Research into small molecule inhibitors has been challenging with only one small molecule presently in clinical trials.[1] Cyclic peptides overcome many of the limitations of their linear counterparts owing to their constrained conformation that offers pre-arrangement and a turn structure for increased binding affinity.[2] As discussed in chapter 3, peptide-directed binding is the method of using peptides to identify the key characteristics required for inhibiting a PPI and applying those to the development a novel small molecule. Due to the benefits of the cyclic peptide turn structure, they are an ideal candidate to apply to peptide-directed binding for the development of a novel small molecule due to their preferential traits for binding to PD-1/PD-L1.

5.1.1 Cyclic peptides

Cyclic peptides have found an important role in the pharmaceutical industry. Of the >60 approved peptide drugs, two-thirds are cyclic.[3,4] Their functions include protein-protein interaction (PPI) inhibition, enzyme inhibition and antimicrobial agents.[5] When targeting PPIs, peptides offer several advantages over small molecules such as having a larger more diverse structure to interact with the large surface area of the PPIs. They are capable of forming more interactions due to this diverse structure and have the ability to be engineered for specificity. Furthermore, cyclisation of linear peptides has the potential to improve structural and pharmacokinetic properties over their linear counterparts.[6] The fixed cyclic structure also produces fewer alternate conformations, reducing non-specific binding and ultimately improving targeting.[7] The conformational rigidity reduces the ability of the cyclic peptide to fit into the catalytic site of proteases and this, alongside the lack of carboxyl and amino ends, improves proteolytic resistance.[8] Cyclic peptides have a larger contact area with PPIs due to their looped structure allowing them to form more interactions than their linear counterparts.[9] The structural advantages of cyclic peptides improve absorption and membrane permeability.[10] The constrained cyclic nature lowers the energy barrier for adapting to the membrane environment and binding to transport proteins. This can increase both passive and active transport allowing the cyclic peptide to reach challenging targets.[11] As discussed in chapter one, cyclic and turn structured peptides

have become a starting point in the discovery of novel small molecules to target PPIs due to their structural advantages that lead to enhanced binding.

5.1.2 Cyclic peptides that target PD-1 or PD-L1

The PD-1/PD-L1 pathway is a prominent immune checkpoint that has been targeted to create a more effective cancer treatment within immunotherapy. The interface between these interacting proteins is governed by β-sheets and β-strands.[12] It has been found that peptides that contain a turn like structure are effective inhibitors of β-sheet protein surfaces possessing the potential to have increased binding.[13] Cyclic peptides can mimic this turn due to their rigid cyclic structure offering pre-organization and fixed conformation.[3] As discussed in chapter 1, PD-1/PD-L1 is currently inhibited using monoclonal antibodies that face the drawbacks of no oral bioavailability, immune related adverse reactions, and high cost.[14]As an alternative inhibitor for PD-1/PD-L1 to antibodies, cyclic peptides are a viable option. Gao *et al.* developed a novel cyclic peptide that binds to PD-1 by using phage display technology. They used microscale thermophoresis (MST) to determine the K_D values revealing the structure **5.1** (**C8**) to have the highest affinity for PD-1 (K_D = 0.64 μM). **5.1** can effectively block the binding of PD-1 to PD-L1 and can activate T-cells comparably to a PD-1 antibody. *In vivo* studies revealed C8 killed tumours by activating only $CD8^+$ T-cells and were found only in draining lymph nodes.[15]

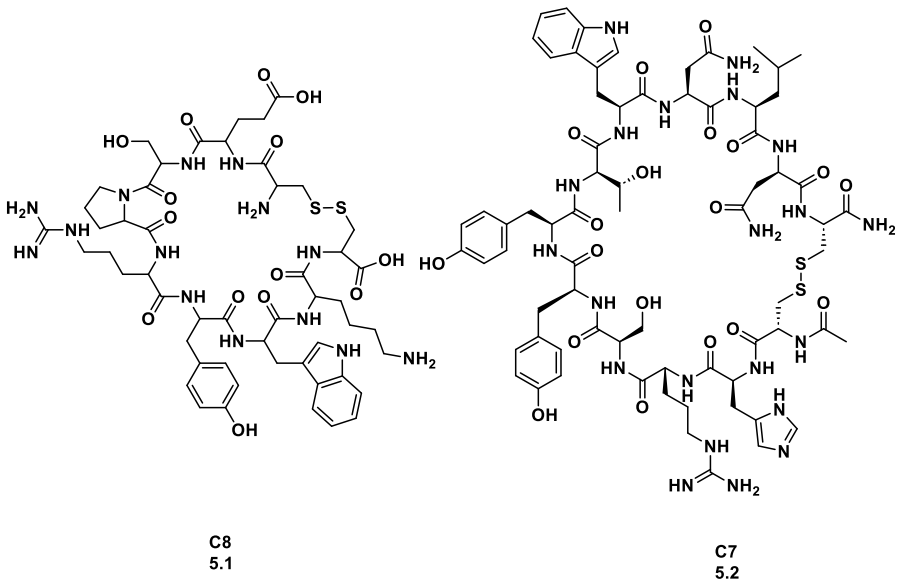


Figure 5-1 *Structures of C8 (**5.1**) and C7 (**5.2**), both cyclic peptide inhibitors of PD-1/PD-L1.*

Other work has focused on taking linear peptides and cyclising them to improve binding affinity and stability to degradation. A linear peptide discovered using phage display was screened with side chain macrocyclisation using cysteine.[16,17] This was followed by disulfide bond formation between two cysteine residues resulting in the cyclic peptide C7 (**5.2**). Analysed using surface resonance plasmon (SPR), **5.2** showed binding to PD-L1 with an IC_{50} value of 119 nM, and a 1.7 fold increase in blocking efficiency over its linear counterpart, highlighting the power of cyclisation.[17]

5.1.1 Previous *N*-methylated peptide syntheses

The coupling of *N*-methylated amino acids can be challenging due to the presence of the methyl group on the nitrogen causing steric hindrance. Furthermore, this addition reduces the nucleophilicity of the amino group, hindering the nitrogen's nucleophilic attack on the carbonyl to form an amide bond. Both solution phase and solid phase synthesis can be used to couple *N*-methylated amino acids. However, solution phase is associated with low yields and risk of racemization. Solid phase synthesis of peptides containing *N*-methylated amino acids was aided by the development of 1-hydroxy-7-azabenzotriazole (HOAt) (**Figure 5-2**). Carpino *et al.* demonstrated the superiority of HATU-HOAt over HBTU-HOBt synthesising MeLeu-MeLeu-MeVal showing a purity of 85% v 8% of the final product.[18] Since this discovery, these coupling agents have seen success in multiple studies synthesising *N*-methylated peptides.[19–21] Other methods were also developed to enhance the coupling of *N*-methylated amino acids such as the development of 4-nitro-9-(trifluoromethyl)benzotriazole-1-yloxy]tris (pyrrolidino) phophonium hexafluorophosphate (CF_3-NO_2-PyBOP) by modifying the structure of 1-hydrobenzotriazole (HOBt) to become very effect in performing hindered coupling (**Figure 5-2**).[22] The acid chloride method also found success in enhancing coupling but was limited due to Fmoc amino acid chlorides containing acid-labile protecting groups on their side chains. In an attempt to overcome this problem, triphosgene was used to generate Fmoc-amino acid chloride in situ but this requires extreme anhydrous conditions or the peptide sequence becomes cleaved from the resin.[23–25] Ethyl 2-cyano-2-(hydroxyamino)actate (oxyma) was the next development in coupling agents that could outperform HOBt, used alongside *N,N*'-diisopropylcarbodiimide (DIC) for successful synthesis of *N*-methylated amino acid containing cyclic peptides (**Figure**

5-2).[26,27] The effect of microwave coupling also resulted in superior coupling, reducing the reaction time from 1 or 2 h to 20 mins and with higher yields.[28]

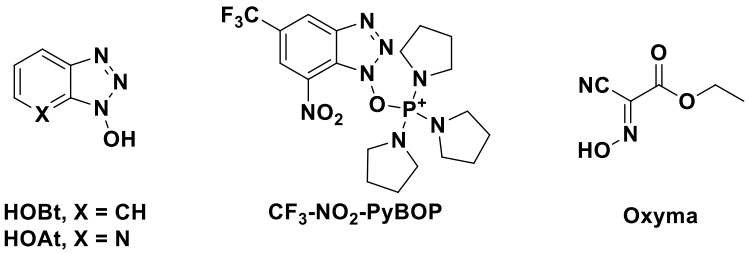


Figure 5-2 *Structures of HOBt, HOAt, Oxyma, CF_3NO_2PyBOP.*

5.1.2 Bristol Myers Squibb Peptides

Bristol Myer Squibb (BMS) has released multiple patents reporting cyclic peptides that inhibit PD-1/PD-L1 determined through a homologous time resolved fluorescence (HTRF) assay and cell-based experiments.[29–31] The reported macrocycles enhance T-cell response and therefore "switch on" the immune system. The general structure disclosed in **Figure 5-3** shows multiple *N*-methylated amino acids and in all cases a thioether bond.[29,30]

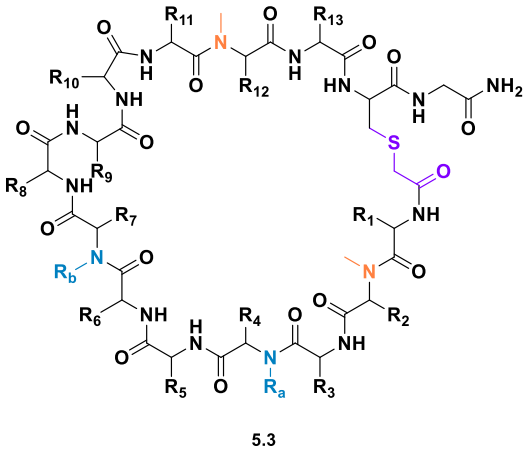


Figure 5-3 *General structure published in BMS patent: thioether bond (purple), N-methylated amino acids (orange), modified N groups (blue)[29,30].*

5.1.2.1 Unnatural amino acids

Cyclic peptides can be further improved by introducing non-canonical amino acids. Inspired by natural products, the addition allows for the fine-tuning of solubility, metabolic stability, and oral bioavailability.[32] Non-canonical amino acids are amino acids outside of the 20 canonical amino acids, often also called unnatural amino acids, nonstandard amino acids and non-natural amino acids.[33] They are often precursors,

analogues, or metabolic intermediates of the 20 amino acids.[32] These modifications can include unnatural L-amino acids (**Figure 5-4, 5.4**), D-amino acids (**Figure 5-4, 5.5**), *N*-methylated (**Figure 5-4, 5.6**), α-substituted (**Figure 5-4, 5.7**), and β-substituted (**Figure 5-4, 5.8**) amino acids.[32]

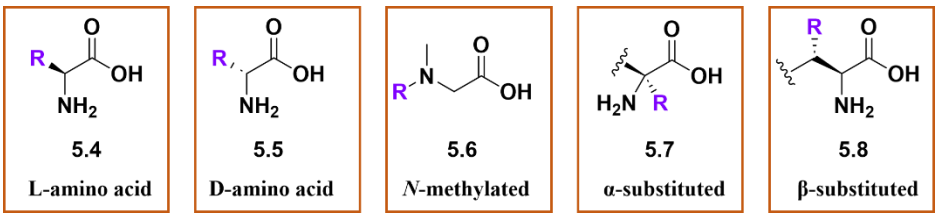


Figure 5-4 *Unnatural amino acid examples including L-amino acid (**5.4**), D-amino acid (**5.5**), N-methylated (**5.6**), α-substituted (**5.7**), β-substituted (**5.8**).*

These modifications of amino acids often enhance peptidase resistance.[34] Further, *N*-methylation modulates the conformation of cyclic peptides as this depends on the steric interactions between the *N*-methyl group and the carbonyl oxygen and/or the substituent of the α carbon of the next amino acid, not by the side chain functionality.[35] Evidence has been found to support that this conformational rigidity introduced by the *N*-methylated amino acid can function to induce a turn, similar to that of a proline.[36] Other modifications to form unnatural amino acids found in BMS macrocyclic peptides that inhibit PD-1/PD-L1 include, but are not limited to, halogenation (**Figure 5-5**, **5.9**), introduction of ring strain through cyclopropane (**Figure 5-5, 5.10**), and the introduction of functional groups such as a methyl or ether groups (**Figure 5-5, 5.11** and **5.12**).[29–31] The inclusion of halogen atoms can modulate the binding to PD-L1 through steric effects while enhancing hydrogen bond formation.[37,38] Further structural control can be implemented through the introduction of the sterically restrained cyclopropane. It is known to cause changes in conformation such as β-turns, and this can increase binding affinity and stability.[39] The methylation of lysine has the ability to form a salt bridge with negatively charged amino acids and has been linked to enhanced binding affinity through enhanced cation-π interactions.[40] Furthermore, the methyl groups enhance the overall size and hydrophobicity of the peptide.[40] Other modifications such as the addition of an ether group can improve solubility and are considered when enhancing bioavailability.[41]

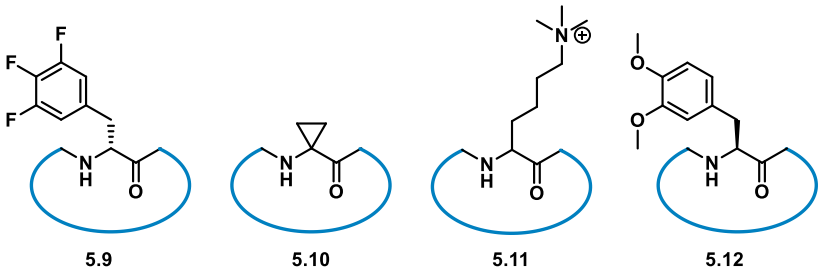


Figure 5-5 *Examples of unnatural amino acids found in BMS patent including halogenation (**5.9**), introduction of ring strain (**5.10**) and introduction of a functional group via a methyl (**5.11**) or ether (**5.12**) group.* [29–31]

5.1.3 BMS peptide-57, peptide-71 and peptide-101

Holak *et al.* analysed three of the BMS macrocyclic peptides shown in **Figure 5-6**, peptide-57 (p57) **5.14**, peptide-71 (p71) **5.13** and peptide-101 (p101) **5.15**. P57 and p71 contain unnatural amino acids while p101 is built of only canonical amino acids. Activity levels of each peptide within cells were measured and compared to FDA approved antibodies that target PD-1/PD-L1. Although not as potent as the antibodies, all three peptides dose dependently restored the activity of the T-cell receptor-responsive promoter.[42,43]

X-ray crystallography was used to obtain structural data about the binding properties for each peptide with PD-L1. The three peptides bind at the interface where PD-1 binds to PD-L1. Despite being found in the same binding site on PD-L1, no single residue of one peptide mimics the binding of any residue on another.

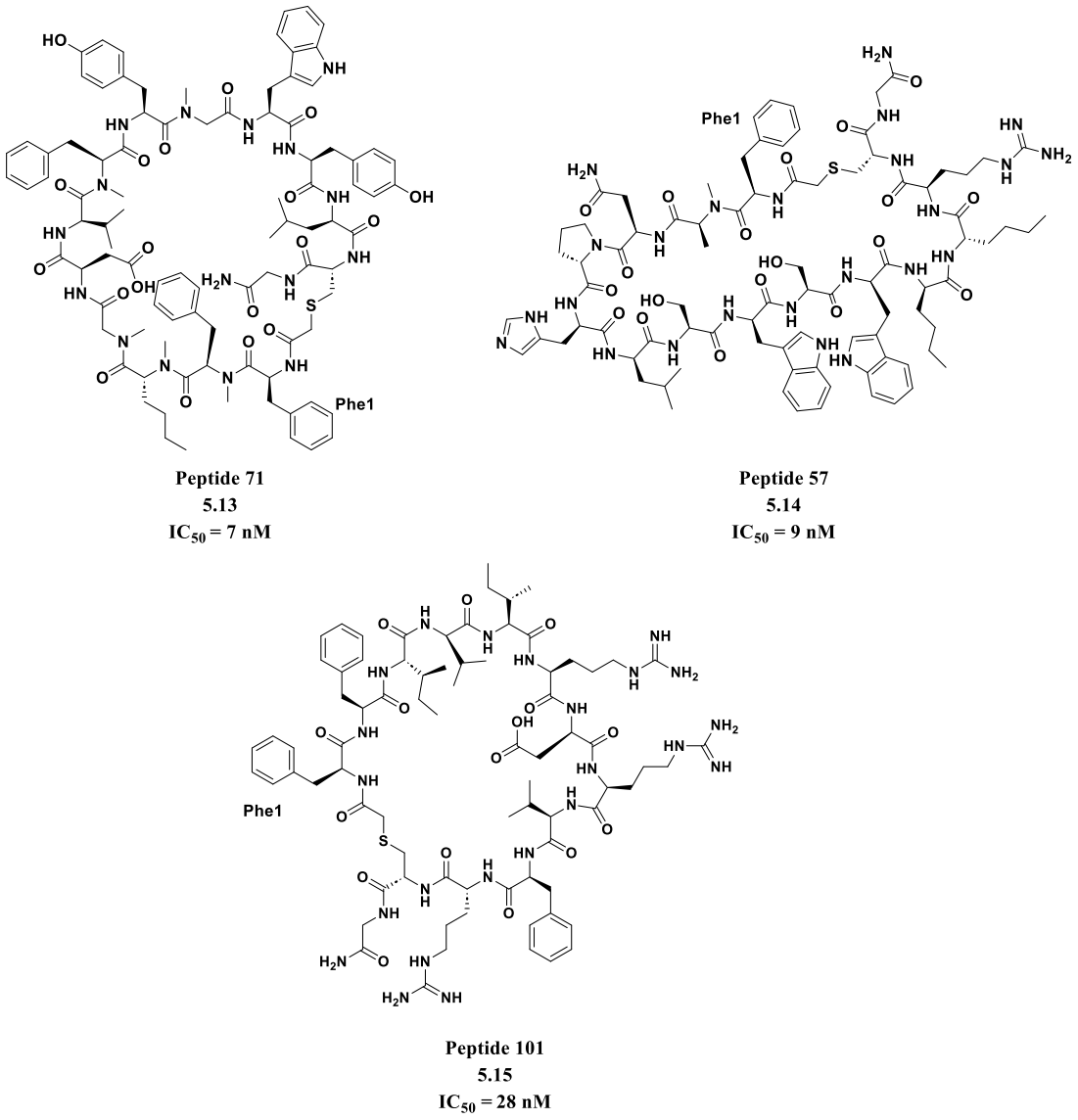


Figure 5-6 *BMS cyclic peptide p71 (**5.9**), p57 (**5.10**) and p101 (**5.11**) including the reported IC_{50} values for the inhibition of PD-1/PD-L1.*

5.1.3.1 Structural data for p57/PD-L1

The structure of p57 is stabilized by intermolecular hydrogen bonding that forms multiple turns through residues Phe1-Arg13, and Phe1-Asn3. The residues of the peptide are positioned so that all polar groups are above the ring plane and the hydrophobic residues are below the ring plane. The hydrophobic residues of Phe1, Trp8, Trp10, NMeNle11 and NMeNle12 dominate the interactions (**Figure 5-7A**, yellow). The indole moieties of Trp8 and Trp10 fill two pockets on PD-L1, one of those pockets overlaps the binding area of PD-1. Here, Trp10 interacts with $_{PD\text{-}L1}$Tyr56 and $_{PD\text{-}L1}$Tyr123 accommodating the pocket that is surrounded by Arg113 and Glu58.[42] Tyr123 has been highlighted previously as an important binding residue for targeting

PD-L1.[12] Overall, the interaction of p57 and PD-L1 is guided by π- π interactions of the Trp8 and Trp10 found in two pockets. These interactions are supplemented by weak hydrophobic effects from side chains surrounding the indole sidechains.

5.2 Structural data for p71/PD-L1

P71 binds in a relatively hydrophobic area of PD-L1. Like p57, the ring plane is decorated with hydrophobic residues that drives the interaction with PD-L1. The three aromatic residues Phe1, NMePhe7, and Trp10 dominate these interactions and are supplemented with NMeNle3 and Val6. These interactions form two hotspots, one of which directly overlaps with the binding site of PD-1 with NMePhe7 interacting with $_{PD\text{-}L1}$Met115 and Trp10 being stabilized with $_{PD\text{-}L1}$Tyr123 (**Figure 5-7B**, pink).[42] Notably, this is not the same pocket on PD-L1 that p57 overlaps with. Further, like Tyr123, Met115 has also been highlight as being an important residue when targeting PD-L1.[12] The second binding pocket is formed by Phe1, completed by intermolecular interactions with NMeNle3 and NMePhe7. Overall, the interaction area between PD-L1 and p71 is relatively shallow and is governed by many low energy interactions rather than one defining pocket.[42]

5.2.1.1 Structural data for p101/PD-L1

P101 binds at the same interface as PD-1, with a higher affinity than PD-1. Upon binding to PD-L1, p101 forms a β-hairpin turn, comparable to the β-strands of PD-1.[12] Phe10 is found in one of the shallow pockets on PD-L1 interacting with Tyr123 and Tyr56. Arg6 also shows interaction with Tyr123.[43] P101 also has interesting, bifurcated binding as shown in **Figure 5-7C**. This means that the peptide binds in more than one interaction site. The two alternative conformations have their own distinct interaction sites on PD-L1, although they mostly overlap. Through NMR spectra it seems that neither one of the binding conformations is preferred or there is a fast exchange between the two conformations.[43]

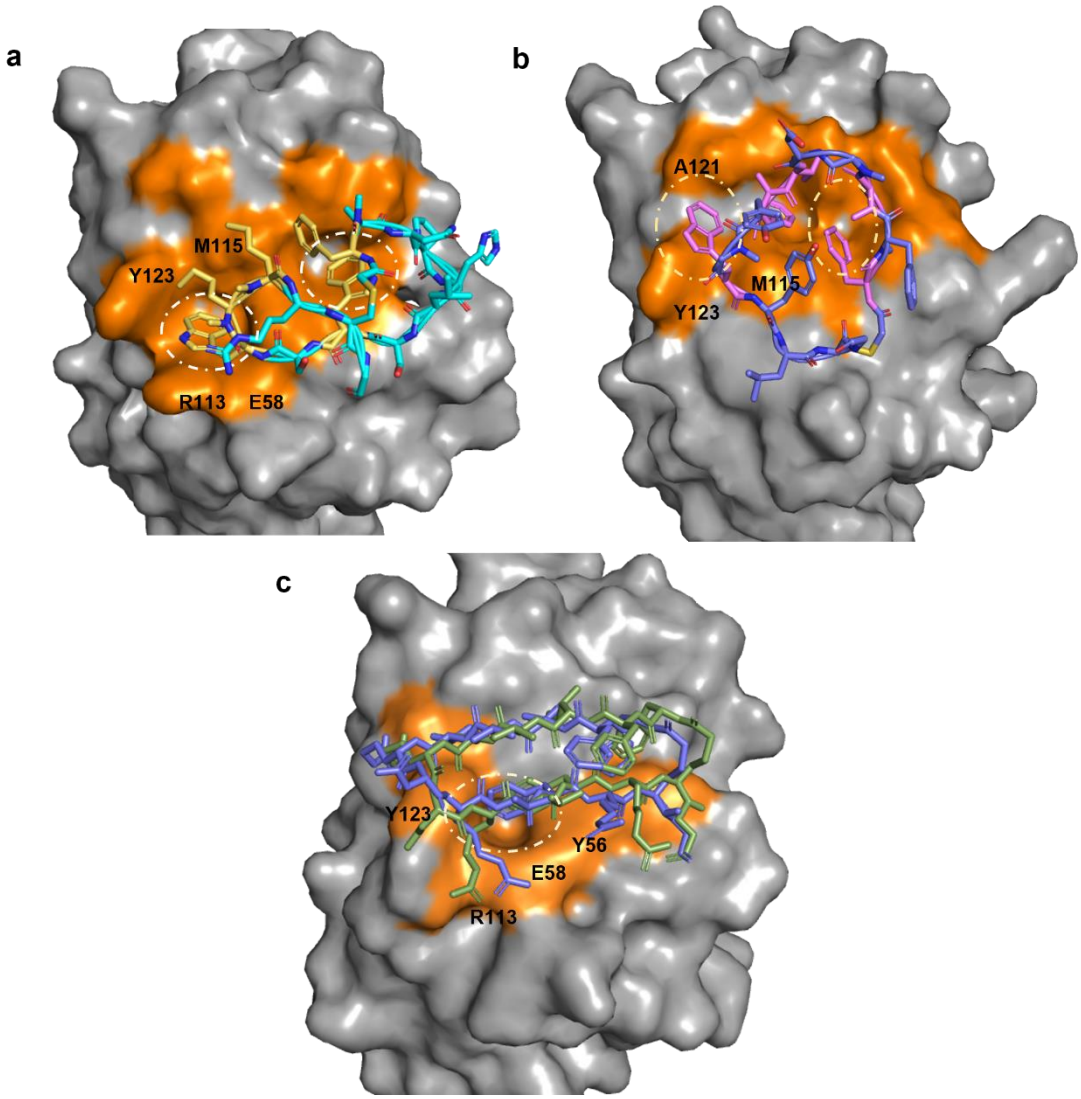


Figure 5-7 *a) Crystal structure of PD-L1 and p57 (cyan) showing the residues of p57 (yellow) that interact with two binding pockets (circled) on PD-L1 (orange) (PDB ID 5O4Y) b) Crystal structure of PD-L1 and p71(purple) showing the residues of p71 (pink) that interact with two binding pockets (circled) on PD-L1 (orange) (PDB ID 5O45) c) Bifurcated binding shown with the alternative conformations of p101 (purple and green) showing one binding pocket (circled) on PD-L1 (orange) (PDB ID 6YCR).*

While the crystal structure of the peptide/protein complex provides a detailed description of the interactions that take place, an alanine scan can provide further insight into the structure-function relationship of the peptide.[44] Through using an alanine scan, the amino acids that are essential for the peptide's biological activity can be highlighted, validating the crystal structure. The knowledge of these important interactions can then be applied as a starting point when developing novel small molecule inhibitors.

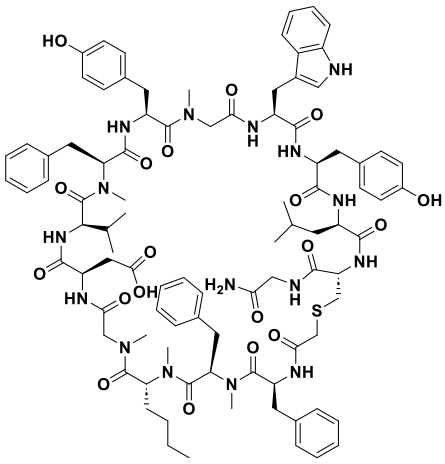
5.3 Chapter Aims

The potency of these peptides to inhibit PD-1/PD-L1 and the detailed description of their binding interactions with PD-L1 highlights these peptides to be advantageous to be used in peptide directed binding, discussed in chapter 3. Furthermore, peptide directed binding has not yet been proven on cyclic peptides offering a further, novel application of the technique. In this chapter, the applicability of p57, p71 and p101 for peptide directed binding will be investigated. The aim of synthesising these peptides was to determine which amino acids were essential for binding to PD-L1 through an alanine scan. This information will establish whether these residues are dispersed around the ring in a way that was possible to split the peptide in half and therefore if the peptides are applicable for peptide directed binding.

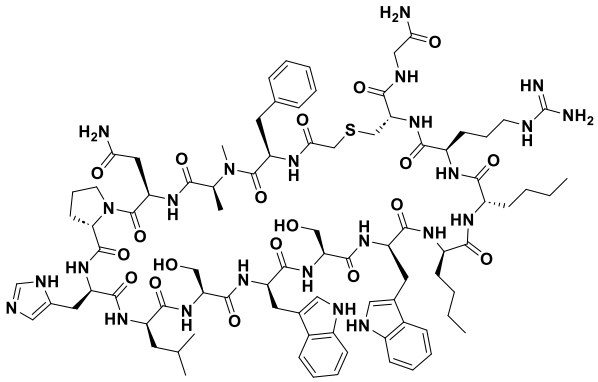
5.4 Results and Discussion

5.4.1 P71 and p57 synthesis

Magiera-Mularz *et al*. reported using the coupling agents DIC and oxyma when synthesising p71 and p57 (**Figure 5-8**) that both include *N*-methylated amino acids. The couplings for the *N*-methylated amino acids were performed in the microwave at 75 °C for 15 minutes twice, with a further 6 hours at room temperature before continuing with the remainder of the sequence. Further, the amino acid that follows the *N*-methylated amino acids were also coupled twice at 75 °C for 15 minutes to ensure successful coupling.[42] Due to their success, this published method was attempted.



Peptide 71
5.13
IC_{50} = 7 nM



Peptide 57
5.14
IC_{50} = 9 nM

Figure 5-8 *The structures of p71 (**5.13**) and p57 (**5.14**) including the reported IC_{50} values for the inhibition of PD-1/PD-L1.*

In their report they described that the linear peptide was synthesised, capped with chloroacetic acid, and cleaved from the resin. The cyclisation of the peptide happened under basic conditions *via* the formation of a thioether bond (**Figure 5-9**).

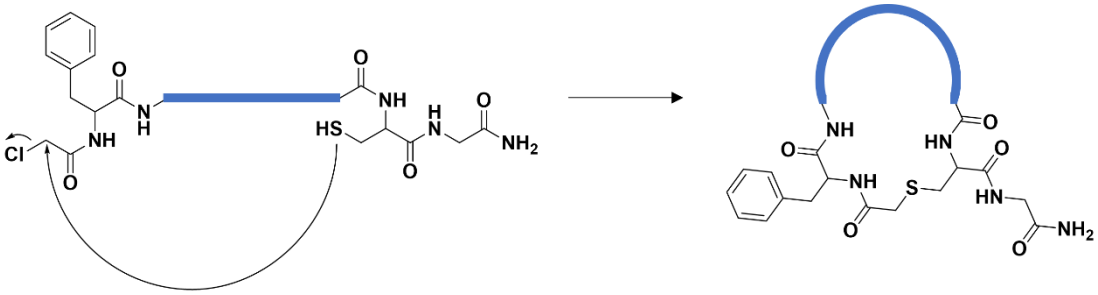
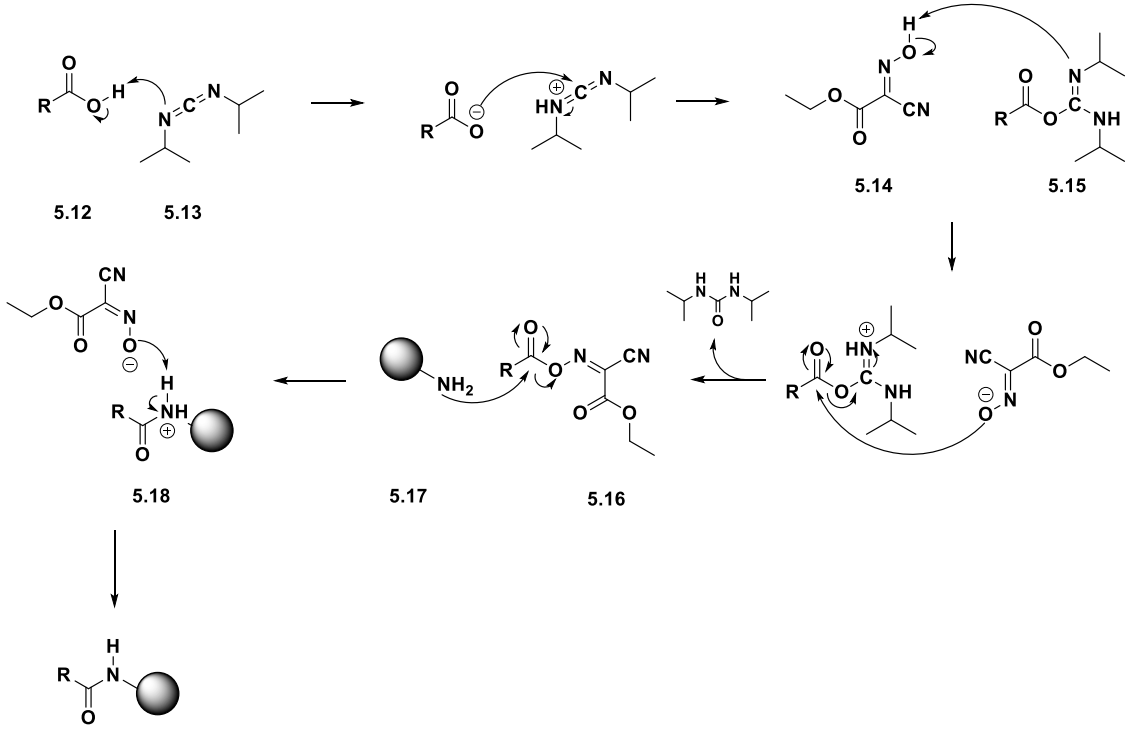


Figure 5-9 *The formation of a thioether bond to form a cyclic peptide.*

As such, the synthesis began by swelling the resin for 20 minutes in DMF before being Fmoc deprotected with 20% piperidine for 10 minutes, twice. Five equivalents of the next Fmoc-protected amino acid were added to the resin with five equivalents of DIC and ten equivalents of oxyma in DMF. The coupling agents DIC and oxyma were chosen due to these peptides containing multiple *N*-methylated amino acids that are known to be more difficult to synthesize.[26] Oxyma has shown to produce peptides with an increased yield compared to the alternative peptide coupling additive HOBt, while avoiding side reactions associated with high levels of base.[26] This improved efficiency is thought to be attributed to oxyma remaining in solution where HOBt has the potential to precipitate out. It also is more stable, allowing for extending coupling reactions and harsher conditions.[26]

Mechanistically, oxyma follows the same route as HOBt. The carbodiimide (**5.13**) and the acid (**5.12**) form an O-acylurea (**5.15**), as shown in **Scheme 5-1.** The O-acylurea deprotonates the oxime hydrogen of oxyma (**5.14**) leaving a nucleophile that can attack the carbonyl of the O-acylurea, eliminating diisoproplyurea. The activated acid (**5.16**) can undergo a nucleophilic attacked by the amine on resin (**5.17**) to form an amide bond (**5.18**) that eliminates deprotonated oxyma.

Each coupling took place at 75 °C for 15 minutes except histidine and cysteine that were coupled once for 15 mins at 50 °C as both are susceptible to racemization at higher temperatures.[45] *N*-methylated amino acids and the amino acids that followed them in the sequence were double coupled to ensure successful coupling as often they can be difficult to incorporate. Arginine was also double coupled as it is susceptible to γ-lactam formation that reduces coupling efficiency.[46]



Scheme 5-1 *Oxyma and DIC coupling mechanism for SPPS.*

Rink Amide MBHA resin (**Figure 5-10**, **5.19**) was used initially. This resin has an acid labile linker and after cleavage provides an amide on the C-terminal. This provides a non-reactive terminal to the synthesized peptides. Despite following the reported procedure for optimal synthesis, finding a defining mass using MALDI was inconclusive for both p57 and p71. To improve the synthesis, various coupling

conditions were trialled, including double coupling every amino acid twice for 15 mins at 75 °C except arginine, histidine, and cysteine that remained at their specific coupling procedures. By double coupling each amino acid it was thought to increase the success of the coupling but there was no change with the mass of the peptide still being unconfirmed. Holak *et al.* reported after the doubling coupling at 75 °C a further 6-hour coupling continued at room temperature for *N*-methylated amino acids, but this did not improve the synthesis in this study.

In another effort to overcome this challenging synthesis, three other resins were considered with different functionalities that provide a variety of advantages during SPPS. Rink amide AM (**Figure 5-10**, **5.20**) is a polystyrene-based resin similar to Rink amide MBHA, differing only in the bond between the linker and the resin bead.

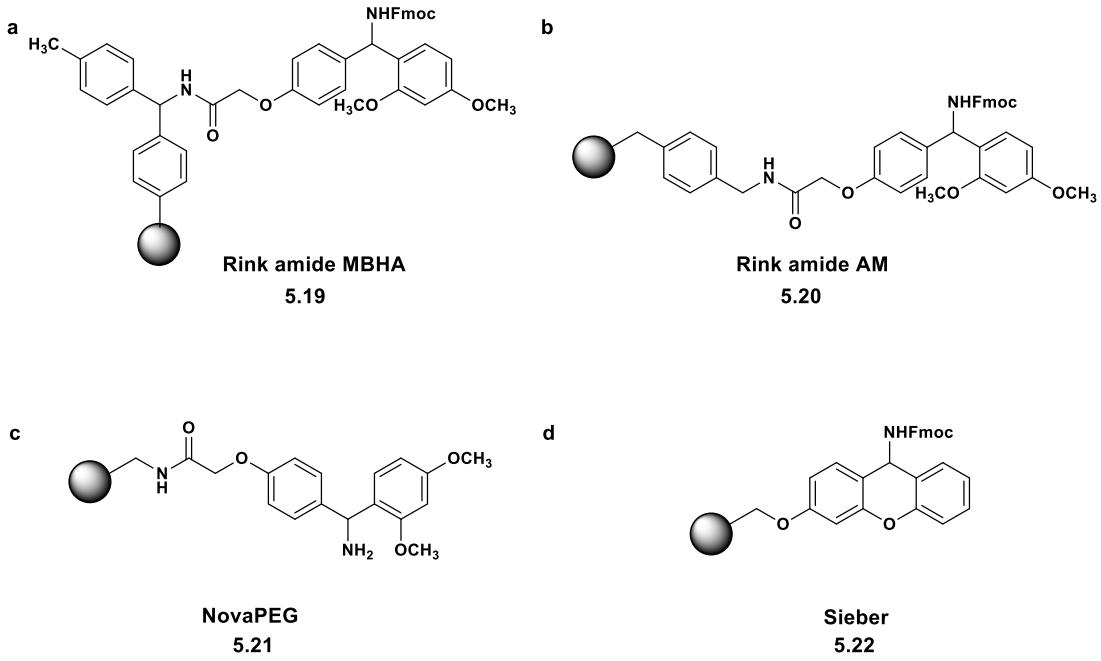


Figure 5-10 a) *Rink amide MBHA (**5.19**) b) Rink amide AM (**5.20**) c) NovaPEG (**5.21**) d) Sieber (**5.22**) resins.*

NovaPEG (**Figure 5-10, 5.21**) is a type of polyethylene glycol (PEG)-based resin that has a unique porous structure that allows for rapid diffusion of reagents leading to an optimised peptide synthesis strategy. Further, it has a high loading capacity and a low level of non-specific binding that can reduce aggregation. Despite these benefits reported for both resins, neither p57 nor p71 were confirmed by MALDI mass spectrometry using these resins (**Figure 5-11B/C**).

Also a polystyrene-base resin, the Sieber resin (**Figure 5-10**, **5.22**) is capable of a high degree of swelling leading to efficient coupling of difficult amino acids. It also has the

benefit of the ability to be cleaved in very mild acidic conditions. [47] The benefits of the Sieber were thought advantageous when trying to synthesize the more difficult *N*-methylated amino acids. The analytical HLPC for the crude linear peptide of p57 using the Sieber resin showed aggregation as seen in **Figure 5-11A** but also confirmed *m/z* at 1799.2 which matched the expected molecular weight of 1799.9. However, p71 was still unconfirmed.

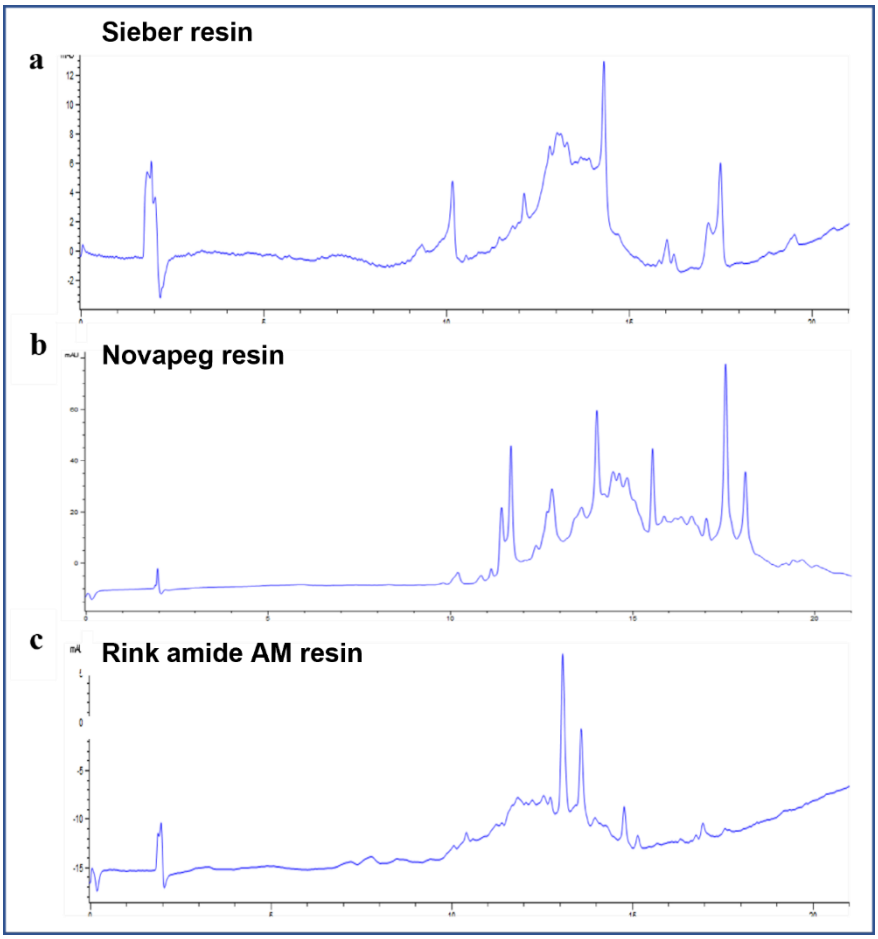


Figure 5-11 *The analytical HPLC trace recorded at 214 nm of crude linear peptide 57 a) Sieber resin b) Novapeg resin c) Rink amide Am resin (Agilent eclipse XDB-C18 column (4.6 x 150 mm, 5 µm) and a flow rate of 1 mL/min. Spectra were run with a solvent gradient of 0-100% B over 20 min. Solvent A: H_2O, 0.05% TFA, solvent B: MeCN, 0.05% TFA).*

When analysing the MALDI results and considering the aggregation present in the analytical HPLC trace, a recurring problem appeared that the first amino acid, glycine, was not coupling to the resin. To rectify this, glycine was doubled coupled and the resin was acetylated with acetic anhydride (4 eq) and DIPEA (4 eq) for 45 minutes before the peptide synthesis continued. With this additional coupling and acetylation, the mass was confirmed for the linear peptide of p57 on the Sieber resin (**Figure 5-12A**).

There was some concern that perhaps the degradation was occurring during the cleavage of the peptide. Four cleavage conditions were trialled, including varying the time spent cleaving and percent of TFA. The Sieber resin has been demonstrated to show successful cleaving time of as short as 1.5 hours and could be cleaved in low percentages of TFA.

In hopes to reduce degradation the shorter cleaving time was tried. However, this showed no improvement analysed through the analytical HPLC traces (**Figure 5-12D**) and showed a severe drop in yield. This was also emulated when the percent of TFA was decreased (**Figure 5-12C**). The cleavage condition that contained TFA:TIPS:DODT:H_2O with the ratios of 92.5:2.5:2.5:2.5 (**Figure 5-12B**) in comparison showed a cleaner trace with limited degradation. However, the cleavage conditions of TFA:TIPS:DODT:H_2O and 94:1:2.5:2.5 (**Figure 5-12A**) over 3 hours was significantly superior, showing a cleaner analytical HPLC trace and a large product peak.

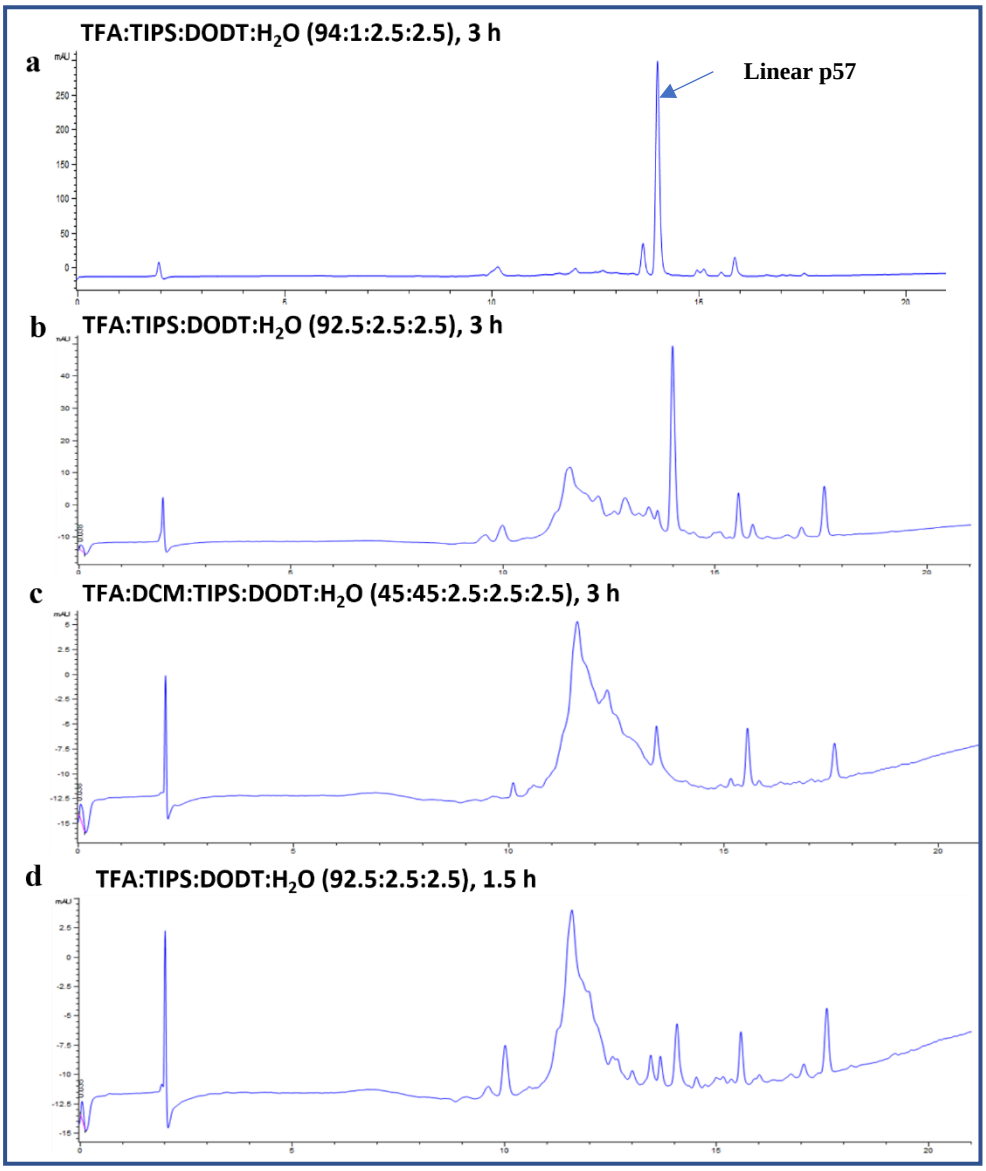


Figure 5-12 *The analytical HPLC traces recorded at 214 nm for p57 with a) TFA:TIPS:DODT:H₂O (94:1:2.5:2.5) for 3 h b) TFA:TIPS:DODT:H₂O (92.5:2.5:2.5:2.5) for 3 h c) TFA:DCM:H₂O:TIPS:DODT (45:45:2.5:2.5:2.5) for 3 h d) TFA:TIPS:DODT:H₂O (95:2.5:2.5:2.5) for 1.5 h (Agilent eclipse XDB-C18 column (4.6 x 150 mm, 5 µm) and a flow rate of 1 mL/min. Spectra were run with a solvent gradient of 0-100% B over 20 min. Solvent A: H₂O, 0.05% TFA, solvent B: MeCN, 0.05% TFA).*

5.4.2 Capping the peptide with a chloroacetyl group

With the synthesis and cleavage optimised to be able to produce the linear peptide of p57, the next step was to add the chloroacetyl cap for the cyclisation. It had been reported that the chloroacetyl cap was incorporated through an amide bond with chloroacetic acid on the N-terminal of the peptide, coupling with chloroacetic acid for 15 min at 75 °C.[42] However, despite confirming a mass for the cleaved linear peptide before the chloroacetic acid coupling, after the acid coupling there was no mass

evidence supporting the linear peptide with the chloroacetyl cap was present. The analytical HPLC also showed degradation (**Figure 5-13B**).

It was attempted to replace the chloroacetic acid with chloroacetyl chloride and DIPEA at 75 °C for 15 mins, but the results also showed degradation as seen in **Figure 5-13C**. Further, no mass was confirmed for the linear peptide of p57 nor the linear peptide containing the chloroacetyl cap.

To make the conditions milder to preventing degradation, the chloroacetyl cap was coupled at room temperature overnight using chloroacetic acid (25 eq) and DIC (0.02 eq) in DMF. Although the mass of p57 with the chloroacetic cap was confirmed the analytical HPLC showed degradation making purification difficult (**Figure 5-13D**). The Sieber resin is hyper acid labile indicating that its possible during the capping step degradation of the resin was occurring. Furthermore, chloroacetyl groups can undergo side reactions with side chains of the amino acids causing fragmentation also leading to degradation.

Considering the overarching aim was the alanine scan of these cyclic peptides to determine which residues were key to PD-L1 binding, a further fifteen peptides were needed to be prepared. Due to this degradation, and the practically of repeating this procedure a further fifteen times, it was decided to progress forward without using p57 or p71.

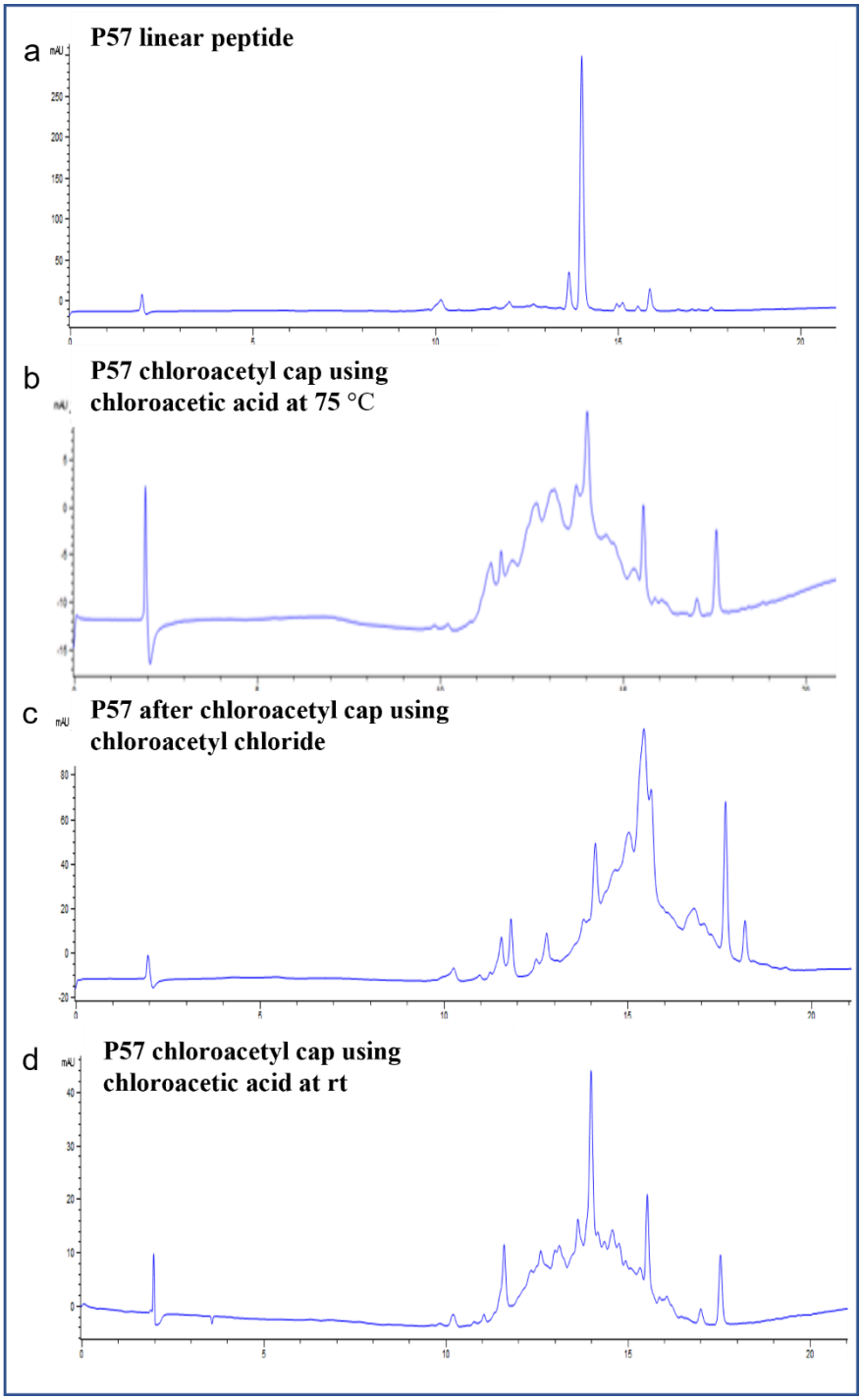
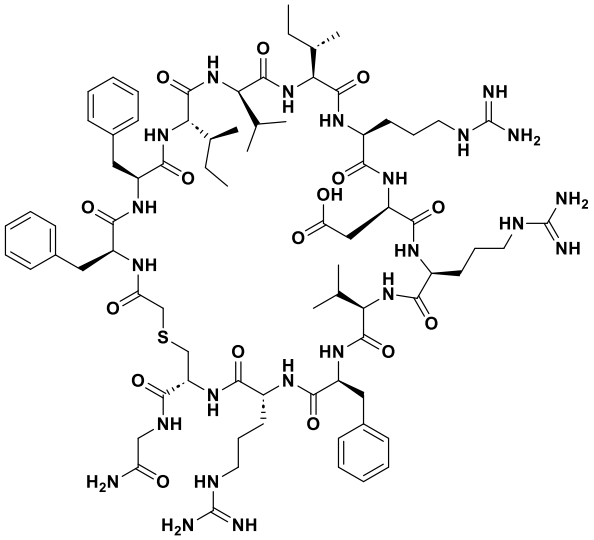


Figure 5-13 *The analytical HPLC traces recorded at 214 nm for p57 a) linear b) after chloroacetic cap using DIC/Oxyma with chloroacetic acid for 15 mins at 75 °C c) after chloroacetyl chloride and DIPEA for 15 mins at 75 °C d) after chloroacetic cap using chloroacetic acid and DIC overnight at room temperature (Agilent eclipse XDB-C18 column (4.6 x 150 mm, 5 µm) and a flow rate of 1 mL/min. Spectra were run with a solvent gradient of 0-100% B over 20 min. Solvent A: H_2O, 0.05% TFA, solvent B: MeCN, 0.05% TFA).*

5.4.3 P101 synthesis

As p101 is made up of canonical amino acids it was expected that the synthesis would be simpler. P101 (**Figure 5-14**, **5.11**) was synthesised as described in chapter 2, using Fmoc SPPS initially using the NovaPEG resin with the coupling agents HOBt, HBTU and DIPEA. The couplings were performed twice at room temperature for 45 minutes. Once the linear peptide was synthesised, it was washed and cleaved using the cleavage cocktail of TFA/TIPS/H_2O/DODT (94:1:2.5:2.5) over 3 hours.



Peptide 101
5.11
IC_{50} = 28 nM

Figure 5-14 *The structure of peptide 101 (**5.11**).*

The linear peptide of p101 was confirmed by the observation of *m/z* 1702.79 matching the expected molecular weight $[M+H]^+$ 1702.86. However, the analytical HPLC showed multiple peaks suggesting side reactions were taking place (**Figure 5-15**).

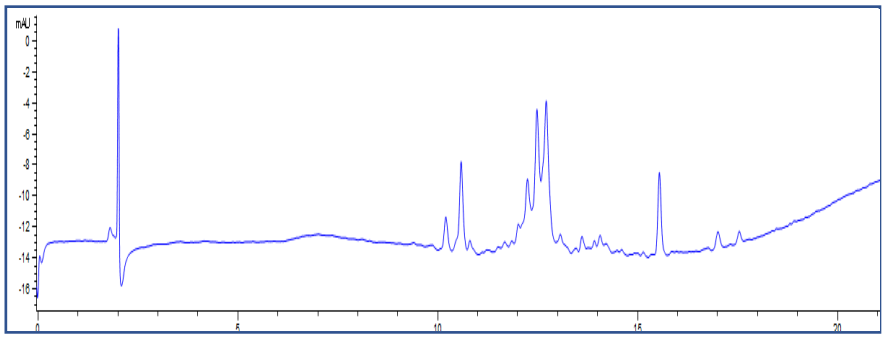
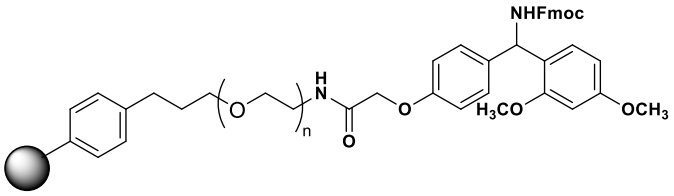


Figure 5-15 *The analytical HPLC trace recorded at 214 nm showing crude linear p101 on NovaPEG resin using HBTU/HOBt at RT (Agilent eclipse XDB-C18 column (4.6 x 150 mm, 5 µm) and a flow rate of 1 mL/min. Spectra were run with a solvent gradient of 0-100% B over 20 min. Solvent A: H_2O, 0.05% TFA, solvent B: MeCN, 0.05% TFA).*

To try and produce a cleaner analytical trace to make purification easier, microwave SPPS was used as discussed for the synthesis of p71 and p57. Furthermore, the TentaGel S RAM resin (**Figure 5-16**, **5.20**) was used citing the benefits of being a high-capacity PEG-based resin with a large surface area and low levels of non-specific binding, both suggested to reduce aggregation and aid the synthesis.[48]



TentaGel S RAM resin

5.20

Figure 5-16 *The structure of TentaGel S RAM resin (**5.20**).*

By heating the couplings and using the different coupling agents of DIC and oxyma there was a positive difference as the crude analytical HPLC was much cleaner showing one major peak (**Figure 5-17A**). The linear peptide was confirmed through the observation of *m/z* 1702.6 matching the expected molecular weight $[M+H]^+$ 1702.9.

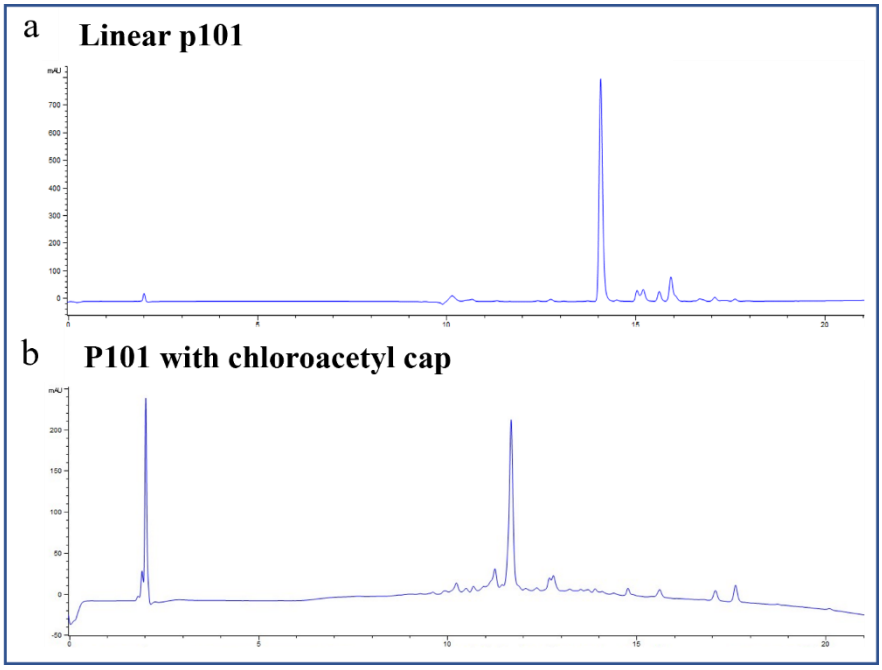


Figure 5-17 *a) The analytical HPLC trace recorded at 214 nm of crude p101 using Tentagel S RAM resin and the coupling DIC/Oxyma at 75 °C b) the analytical HPLC trace recording 214 nm of crude linear p101 with chloroacetyl cap (Agilent eclipse XDB-C18 column (4.6 x 150 mm, 5 µm) and a flow rate of 1 mL/min. Spectra were run with a solvent gradient of 0-100% B over 20 min. Solvent A: H_2O, 0.05% TFA, solvent B: MeCN, 0.05% TFA).*

Once the linear peptide was confirmed, the chloroacetyl cap needed to be added to the N-terminus. From the findings after attempting to synthesize p57 and p71, the milder chloroacetic acid capping method at room temperature with DIC was tried, providing a successful result with a slight shift in the analytical HPLC from a retention time of 14.1 mins to 11.6 mins (**Figure 5-17B**). This was confirmed with an *m/z* of 1702.52 corresponding to the $[M+H]^+$.

5.4.3.1 Cyclisation of p101

Once the chloroacetyl group was confirmed for p101, the cyclisation was attempted with 0.1 M ammonium carbonate buffer (pH 8.5) and acetonitrile (1:2 v/v) at a concentration of 1 mg/mL. This was stirred overnight at room temperature. The thioether macrocyclization occurs spontaneously under basic conditions. The crude analytical HPLC showed multiple peaks very close together with no defining peak to say which peak was definitively the cyclised p101 (**Figure 5-18A**). This hinted to degradation or many side reactions taking place, making the purification challenging.

Due to how close the peaks were on the analytical HPLC, semi-preparative HPLC was used to purify and try isolate which peak was cyclic p101. The analytical HPLC after purification (**Figure 5-18B**) shows the cyclised p101 at 11.6 min. However, it is found alongside some impurities and a peak corresponding to the ammonium carbonate buffer that is used in the cyclisation step of the peptide at 2.1 min shown in **Figure 5-18C.** The cyclic p101 showed an *m/z* of 833.8 corresponding to $[M+2H]^{2+}$, matching the peak found on the analytical HPLC *via* UV-Vis. Despite being able to isolate the cyclised p101, the many peaks seen in the crude analytical HPLC inferring degradation and side reactions taking place means the practicality of repeating this procedure to complete an alanine scan impractical. Furthermore, with no majority peak and accounting for the other impurities being seen it can be assumed that the yield would be poor. These reasons, alongside the success seen in other chapters of this thesis, led to the discontinuation of the synthesis of the alanine scan of p101.

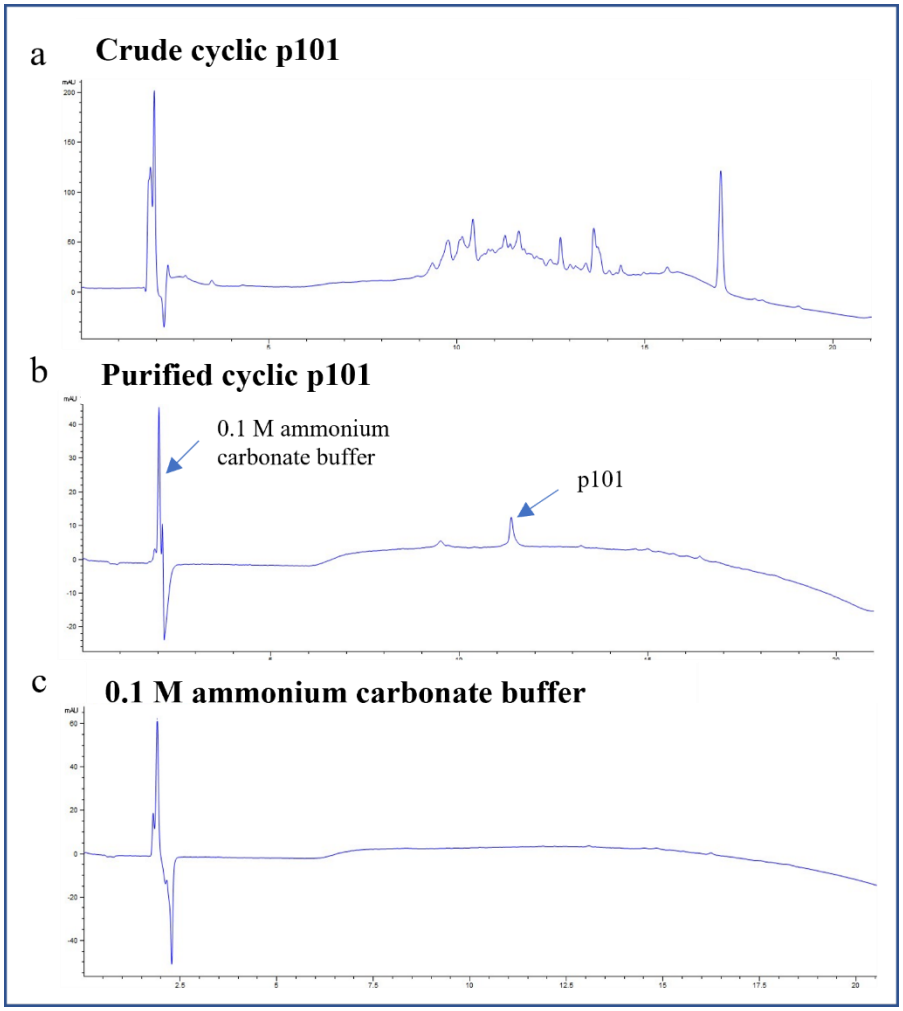


Figure 5-18 *a) The analytical HPLC trace recording of 214 nm of the crude cyclised p101 b) The analytical HPLC trace recording of 214 nm of the crude cyclised p101 c) The analytical HPLC trace recording of 214 nm of ammonium carbonate buffer (Agilent eclipse XDB-C18 column (4.6 x 150 mm, 5 µm) and a flow rate of 1 mL/min. Spectra were run with a solvent gradient of 0-100% B over 20 min. Solvent A: H_2O, 0.05% TFA, solvent B: MeCN, 0.05% TFA).*

5.5 Conclusion

Cyclic peptides have proven their importance within the pharmaceutical industry in targeting PPIs. Their rigid conformation restricts alternative conformations, improving off-targeting binding, while reducing the likelihood of proteolytic degradation.[8] The loop structure adopted by the cyclisation also allows for a larger contact area with PPIs than their linear counterparts, allowing them to form more interactions resulting in enhancing binding affinity.[9] Furthermore, it has been suggested that cyclic or turn structured peptides have the potential to be effective inhibitors of β-sheet protein surfaces. As the PD-1/PD-L1 proteins are formed of β-sheets and β-strands cyclic peptides make the ideal choice to pursue.[12] BMS has released multiple patents containing cyclic peptide inhibitors for PD-1/PD-L1.[29,30,49] Three peptides were

extracted from one of the patents and crystallised with PD-L1 to highlight key interactions (**Figure 5-7**).[42,43] P57, **5.9,** and p71, **5.10**, contained multiple *N*-methylated amino acids, while p101, **5.11**, contained only proteinogenic amino acids. The synthesis of p57 and p71 was challenging due to *N*-methylated amino acids. Through the screening of four resins, it was found that the Sieber resin was the most promising in the synthesis of the linear peptide of p57. The synthesis of the linear peptide of p71 was not successful after trying multiple conditions. It was found that the first amino acid of p57 (glycine) was not completing a full coupling, the coupling was doubled and the resin was acetylated before continuing with the peptide synthesis. Following the complete synthesis, the chloroacetyl cap needed to be added. However, despite altering the conditions and trying different reagents, p57 faced degradation during this step. Due to the degradation occurring during synthesis, proceeded by the practically of repeating this procedure for the remainder of the alanine scanned peptides, it was decided to progress forward without p57 or p71. The synthesis of p101 was found most successful using the TentaGel S Ram resin and capping the peptide with chloroacetic acid at room temperature with DIC. However, during the cyclisation step analysis hinted towards degradation or many side reactions taking place, making purification challenging. Due to these drawbacks and the success found in other chapters within this thesis, it was decided to continue without the use of p101.

To combat the difficulties faced in the synthesis of p71, smaller parts of the peptides could have been synthesised and then combined in solution phase. The future work surrounding p101 could have included screening different cyclisation strategies. The thioether bond forms under basic conditions, both DMSO and triethylamine have been used to lower the pH for cyclisation and could be effective.[50,51] Further, a different method to chloroacetylate p57 could be utilized. Chloroacetyl *N*-hydroxysuccinimide ester chloromethylcarbonyloxysuccinimide in NMP has been effective and could be tried to improve degradation.[51]

5.6 Experimental

5.6.1 Materials and solvents

All chemicals were purchased from Sigma Aldrich, Fisher Scientific or Fluorochem unless otherwise specified. Fmoc-amino acids and coupling agents were purchased from Novabiochem, Fluorochem or AGTC Bioproducts.

5.6.2 Instrumental techniques

Analytical RP-HPLC was performed using an Agilent 1200 HPLC, fitted with an Agilent eclipse XDB-C18 column (4.6 x 150 mm, 5 μm) and a flow rate of 1 mL/min. Spectra were run with a solvent gradient of 0-100% B over 20 min. Solvent A: H_2O, 0.05% TFA, solvent B: MeCN, 0.05% TFA. Detection wavelengths were 214 nm and 254 nm. Semi-preparative RP-HPLC was performed using an Agilent 1200 HPLC, fitted with an Agilent eclipse XDB-C18 column (9.4 x 250 mm, 5 μm) and a flow rate of 3 mL/min. Spectra were run with a solvent gradient of 1-100% B over 20 min. Solvents: A = H_2O, 0.05% TFA, B: MeCN, 0.05% TFA. Detection wavelengths were 214 nm and 254 nm. Preparative RP-HPLC was performed using an Agilent 1200 HPLC, fitted with an Agilent eclipse XDB-C18 column (21.2 x 150 mm, 5 μM) and a flow rate 20 mL/min. Spectra were run with a solvent gradient of 0-100% B over 15 min. Solvent A: 95% H_2O, 5% MeCN, 0.05% TFA, solvent B: 95% MeCN, 5% H_2O, 0.05% TFA. Detection wavelengths were 214 nm and 254 nm.

MALDI was performed on a Kratos Analytical Axima-CFR MALDI-ToF, using sinapinic acid as the matrix.

Low resolution mass was recorded using an Agilent 1200 Series equipped with a 6460 triple quadrupole.

Automated peptide synthesis was performed using a CEM Liberty Lite.

5.6.3 Solid phase peptide synthesis

All peptides synthesised in this chapter were synthesised via Fmoc-solid phase peptide synthesis. Sieber or TentaGel S RAM resin was swelled for 30 minutes in DMF.
For automated peptide synthesis the resin was deprotected with 20% piperidine in DMF for 20 minutes twice, followed by washing the resin three times with DMF. The coupling of Fmoc-protected amino acids (4 eq) was completed with DIC (5 eq) and

oxyma (10 eq) and bubbled with N_2 for 15 mins at 75 ℃. Except for when coupling histidine and cysteine which were reacted for 15 mins at 50 ℃. Each peptide coupling was followed by the resin being washed three times with DMF and deprotection of the peptide chain with piperidine.

Cleavage of the peptide from the resin was completed in 94:1:2.5:2.5 TFA:TIPS:H_2O:DODT with shaking for three hours. The resulting solution was evaporated to dryness and washed with cold ether. Peptides were purified by preparative HPLC and their purity confirmed using analytical HPLC.

5.6.4 Synthesis of linear p57 (5.10)

5.10 was synthesised following the general procedure described in section 5.4.3 using the Sieber resin with the following modification. The first amino acid, Fmoc-glycine, was doubled coupled and acetylated with acetic anhydride (4 eq) and DIPEA (4 eq) for 45 minutes. The resin was washed with DMF (x 3), and the peptide synthesis continued as described. P57 was purified by preparative HPLC to collect a white solid, its purity was confirmed using analytical HPLC. RP-HPLC: t_R = 14.1 min. MALDI-ToF $[M+H]^+$ *m/z* calcd. for $[C_{87}H_{123}N_{24}O_{19}S]^+$ 1799.0; found 1799.2.

5.6.5 Synthesis of p101 (5.11)

5.11 was synthesised following the general procedure described in section 5.4.3 using the TentaGel S RAM resin. Once peptide synthesis was completed, chloroacetic acid (25 eq), DIC (0.02 eq) in DMF was added to the resin and shaken overnight at room temperature. The resin was then washed three times with DMF, dichloromethane and methanol. Once cleaved from the resin the peptide was cyclised. For the cyclisation, the precipitated peptide was dissolved in 0.1 M ammonium carbonate buffer pH 8.5:acetonitrile (1:2 v/v) at 1 mg/mL and stirred overnight at room temperature. The solution was concentrated under vacuum and purification was performed using semi-preparative HPLC. RP-HPLC: t_R = 11.7 min. ESI-QQQ $[M+3H]^{3+}$ *m/z* calcd. for $[C_{78}H_{122}N_{23}O_{16}S]^{3+}$ 833.9, found 833.8.

5.7 References

1 B. Musielak, J. Kocik, L. Skalniak, K. Magiera-Mularz, D. Sala, M. Czub, M. Stec, M. Siedlar, T. A. Holak and J. Plewka, *Molecules*, 2019, **24**, 2804.

2 L. K. Buckton, M. N. Rahimi and S. R. McAlpine, *Chem. Eur. J.*, 2021, **27**, 1487–1513.

3 A. Zorzi, K. Deyle and C. Heinis, *Curr. Opin. Chem. Biol.*, 2017, **38**, 24–29.
4 THPdb: Database of FDA-approved peptide and protein therapeutics - PubMed, https://pubmed.ncbi.nlm.nih.gov/28759605/, (accessed 20 May 2023).
5 J.-S. Choi and S. H. Joo, *Biomol. Ther.*, 2020, **28**, 18–24.
6 D. A. Horton, G. T. Bourne and M. L. Smythe, *Chem. Rev.* 2003, **103**, 893-930.
7 C. Sohrabi, A. Foster and A. Tavassoli, *Nat. Rev. Chem.*, 2020, **4**, 90–101.
8 D. J. Craik, *Science*, 2006, **311**, 1563–1564.
9 A. Angelini, L. Cendron, S. Chen, J. Touati, G. Winter, G. Zanotti and C. Heinis, *ACS Chem. Biol.*, 2012, **7**, 817–821.
10 Y. Li, W. Li and Z. Xu, *Marine Drugs*, 2021, **19**, 311.
11 M. Dathe, H. Nikolenko, J. Klose and M. Bienert, *Biochemistry*, 2004, **43**, 9140–9150.
12 K. M. Zak, R. Kitel, S. Przetocka, P. Golik, K. Guzik, B. Musielak, A. Dömling, G. Dubin and T. A. Holak, *Structure*, 2015, **23**, 2341–2348.
13 K. Wang, Y. Song, Y. Su, Y. Liang and L. Wang, *Biochem. Biophys. Res. Commun.*, 2020, **527**, 453–457.
14 R. C. Acúrcio, S. Pozzi, B. Carreira, M. Pojo, N. Gómez-Cebrián, S. Casimiro, A. Fernandes, A. Barateiro, V. Farricha, J. Brito, A. P. Leandro, J. A. R. Salvador, L. Graça, L. Puchades-Carrasco, L. Costa, R. Satchi-Fainaro, R. C. Guedes and H. F. Florindo, *J. Immunother. Cancer*, 2022, **10**, e004695.
15 W. Zhai, X. Zhou, M. Zhai, W. Li, Y. Ran, Y. Sun, J. Du, W. Zhao, L. Xing, Y. Qi and Y. Gao, *Sci. China Life Sci.*, 2021, **64**, 548–562.
16 H. Liu, Z. Zhao, L. Zhang, Y. Li, A. Jain, A. Barve, W. Jin, Y. Liu, J. Fetse and K. Cheng, *J. Immunother. Cancer*, 2019, **7**, 270.
17 J. Fetse, Z. Zhao, H. Liu, U.-F. Mamani, B. Mustafa, P. Adhikary, M. Ibrahim, Y. Liu, P. Patel, M. Nakhjiri, M. Alahmari, G. Li and K. Cheng, *J. Med. Chem.*, 2022, **65**, 12002–12013.
18 L. A. Carpino, A. El-Faham, C. A. Minor and F. Albericio, *J. Chem. Soc., Chem. Commun.*, 1994, 201.
19 Y. M. Angell, C. García-Echeverría and D. H. Rich, *Tetrahedron Lett.*, 1994, **35**, 5981–5984.
20 C. U. Hjørringgaard, J. M. Pedersen, T. Vosegaard, N. Chr. Nielsen and T. Skrydstrup, *J. Org. Chem.*, 2009, **74**, 1329–1332.
21 A. C. Sapia, U. Slomczynska and G. R. Marshall, *Lett. Pept. Sci.*, 1995, **1**, 283–290.
22 J. C. H. M. Wijkmans, F. A. A. Blok, G. A. Van Der Marel, J. H. Van Boom and W. Bloemhoff, *Tetrahedron Lett.*, 1995, **36**, 4643–4646.
23 S. Fuse, Y. Mifune and T. Takahashi, *Angew. Chem. Int. Ed.*, 2014, **53**, 851–855.
24 B. Thern, J. Rudolph and G. Jung, *Tetrahedron Lett.*, 2002, **43**, 5013–5016.
25 A. R. Katritzky, E. Todadze, P. Angrish and B. Draghici, *J. Org. Chem.*, 2007, **72**, 5794–5801.
26 R. SubirÃ^{3}s-Funosas, R. Prohens, R. Barbas, A. El-Faham and F. Albericio, *Chem. Eur. J.*, 2009, **15**, 9394–9403.
27 R. Subirós-Funosas, A. El-Faham and F. Albericio, *Organic Syntheses*, eds. A. S. Kende and J. P. Freeman, Wiley, 1st edn., 2014, pp. 306–315.
28 A. Adamska-Bartłomiejczyk, A. Janecka, M. R. Szabó, M. C. Cerlesi, G. Calo, A. Kluczyk, C. Tömböly and A. Borics, *Bio. Med. Chem. Lett.*, 2017, **27**, 1644–1648.
29 US. Pat., 0294898 A1, 2014.
30 US. Pat., 0340391 A1, 2016.

31 US. Pat., 102507A1, 2023.
32 A. A. Vinogradov, Y. Yin and H. Suga, *J. Am. Chem. Soc.*, 2019, **141**, 4167–4181.
33 A. Rezhdo, M. Islam, M. Huang and J. A. Van Deventer, *Curr. Opin. Biotechnol.*, 2019, **60**, 168–178.
34 D. Meister, S. M. Taimoory and J. F. Trant, *Pept. Sci.*, 2019, **111**, e24058.
35 J. Chatterjee, B. Laufer and H. Kessler, *Nat. Protoc.*, 2012, **7**, 432–444.
36 B. Laufer, J. Chatterjee, A. O. Frank and H. Kessler, *J. Pept. Sci.*, 2009, **15**, 141–146.
37 Y. Lu, Y. Wang, Z. Xu, X. Yan, X. Luo, H. Jiang and W. Zhu, *J. Phys. Chem. B*, 2009, **113**, 12615–12621.
38 S. Z. Borozan and S. Đ. Stojanović, *Comput. Biol. Chem.*, 2013, **47**, 231–239.
39 B. Moreau and A. B. Charette, *J. Am. Chem. Soc.*, 2005, **127**, 18014–18015.
40 M. Luo, *Chem. Rev.*, 2018, **118**, 6656–6705.
41 L. W. Peterson and C. E. McKenna, *Expert Opin. Drug Deliv.*, 2009, **6**, 405–420.
42 K. Magiera-Mularz, L. Skalniak, K. M. Zak, B. Musielak, E. Rudzinska-Szostak, Ł. Berlicki, J. Kocik, P. Grudnik, D. Sala, T. Zarganes-Tzitzikas, S. Shaabani, A. Dömling, G. Dubin and T. A. Holak, *Angew. Chem. Int. Ed.*, 2017, **56**, 13732–13735.
43 K. Magiera-Mularz, K. Kuska, L. Skalniak, P. Grudnik, B. Musielak, J. Plewka, J. Kocik, M. Stec, K. Weglarczyk, D. Sala, B. Wladyka, M. Siedlar, T. A. Holak and G. Dubin, *Adv. Therap.*, 2021, **4**, 2000195.
44 F. Lefevre, *Nucleic Acids Research*, 1997, **25**, 447–448.
45 S. A. Palasek, Z. J. Cox and J. M. Collins, *J. Pept. Sci.*, 2007, **13**, 143–148.
46 M. Alhassan, A. Kumar, J. Lopez, F. Albericio and B. G. de la Torre, *Int. J. Mol. Sci.*, 2020, **21**, 4464.
47 P. Sieber, *Tetrahedron Lett.*, 1987, **28**, 2107–2110.
48 A. Lone, A. Arnous, P. R. Hansen, B. Mojsoska and H. Jenssen, *Front. Chem.*, 2020, **8**, 370.
49 US. Pat., 194307-A1, 2018.
50 T. Miura, T. R. Malla, C. D. Owen, A. Tumber, L. Brewitz, M. A. McDonough, E. Salah, N. Terasaka, T. Katoh, P. Lukacik, C. Strain-Damerell, H. Mikolajek, M. A. Walsh, A. Kawamura, C. J. Schofield and H. Suga, *Nat. Chem.*, 2023, **15**, 998–1005.
51 A. Kawamura, M. Münzel, T. Kojima, C. Yapp, B. Bhushan, Y. Goto, A. Tumber, T. Katoh, O. N. F. King, T. Passioura, L. J. Walport, S. B. Hatch, S. Madden, S. Müller, P. E. Brennan, R. Chowdhury, R. J. Hopkinson, H. Suga and C. J. Schofield, *Nat. Commun.*, 2017, **8**, 14773.

Chapter 6

Conclusion

6.1 Summary

Within this thesis there was a strong focus on finding alternative turn mimics to design peptide and small molecule inhibitors for PD-1/PD-L1. In chapter 2, an azobenzene was inserted into the backbone of a known peptide inhibitor of PD-1/PD-L1. The different isomeric states allowed for photo-controllable inhibition of this interaction, where the *cis* isomer acted as the turn mimic. Within chapter 3, a small molecule inserted into the peptide backbone was demonstrated to be an effective turn mimic in developing peptide-small molecule hybrids. Finally, in chapter 4 by using the inverse electron demand Diels-Alder reaction with a tetrazine and alkyne or alkene, it was hoped that would have provided a further example of a turn mimic.

WHFSYNWRWLPP
(6.1)
WHFSYNARWLPP
(6.2)
WHFSANWRWLPP
(6.3)
WHFSYN-AMPP-RWLPP
(6.4)

Figure 6-1 *The peptide sequences of CLP003 (**6.1**) and the three peptides designed within this thesis, **6.2**, **6.3**, **6.4**. Alanine substitutes are in blue, [3-(3-Aminomethyl)phenylazo]phenylacetic acid (AMPP) in orange.*

Excitingly in chapter 2, the development of a photo-controlled inhibitor was designed using **6.1** (IC_{50} of 0.8 µM [0.72,0.11]) as the foundation, demonstrating the ability to inhibit PD-1/PD-L1 in the *cis* isomer *via* peptide **6.4** (**Figure 6-1**).[1] The *cis* isomer of [3-(3-Aminomethyl)phenylazo]phenylacetic acid (AMPP) acts as a turn like structure within **6.4** demonstrating an IC_{50} value of 0.3 µM [0.15,0.56] while showing limited inhibition in the more linear *trans* isomer.[2] Further analysis using surface plasmon resonance (SPR) or a T-cell based assay would reinforce the success of **6.4**. Within this chapter when analysing **6.1** with an alanine scan, two modified peptides, **6.2** and **6.3**, were discovered to show a superior inhibition of PD-1/PD-L1 with IC_{50} values of 0.052 µM [0.028, 0.10] and 0.025 µM [0.013, 0.052] respectively (**Figure 6-2**). These modified peptides suggest that the flexibility of the alanine could have the potential to improve binding, through X-ray crystallography it would be interesting to see how the removal of these structurally robust and polar amino acids, tryptophan, and tyrosine, would change the interaction with PD-L1. Furthermore, after considering the discoveries within chapter 3 where the semi-peptide WHFSYN was shown to have superior inhibition of PD-1/PD-L1 in comparison to **6.4**, it would be interesting to re-

evaluate the design of the azobenzene peptides to within this shorter sequence as **6.4** was the only peptide of six that showed inhibition ability and was also the only peptide to involve that sequence.

Further developments to discover an alternative inhibitor for PD-1/PD-L1 are found in chapter 3 *via* the design of peptide-small molecule hybrids. The known peptide inhibitor, CLP003, **6.1**, was split into two peptides with the alternative sides being replaced with a small molecule fragment in a screening process.[1] To implement the turn structure and to act as a linker between the peptide and the small molecule, *cis*-2-aminocyclohexanecarboxylic acid was used (**Figure 6-2**, purple). When utilising semi-peptide 1 (-NWRWLPP), ten out of the twenty peptide-small molecule hybrids showed inhibition of PD-1/PD-L1 with two compounds, **6.5** and **6.6**, showing an IC_{50} value in the nanomolar range. For semi-peptide 2 (WHFSYNP-) an alternative approach was used replacing *cis*-2-aminocyclohexanecarboxylic acid with a proline pre-loaded resin. This commercially available resin evaded the need for coupling the first residue onto a chlorotrityl resin while still offering a turn inducing moiety.

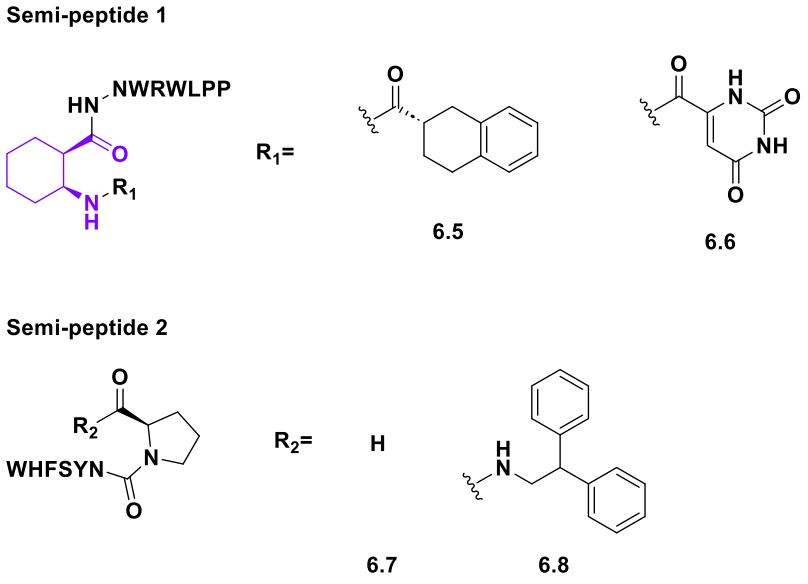


Figure 6-2 *The structures of peptide-small molecule hybrids designed and synthesised in chapter 2,* ***6.5****,* ***6.6****,* ***6.8****, (cis-2-aminocyclohexanecarboxylic acid in purple) and the peptide WHFYSNP that showed superior inhibition of PD-1/PD-L1,* ***6.7****.*

As mentioned, the semi peptide WHFSYNP, **6.7**, demonstrated superior inhibition of PD-1/PD-L1 in comparison to **6.1** demonstrating an IC_{50} value of 2.3 nM [1.1, 5.0]. It would be valuable to perform a second alanine scan on this truncated peptide to determine which amino acids were now considered essential for inhibition of PD-1/PD-L1. Further, a crystal structure of both **6.1** and **6.7** would determine if the binding

sites on PD-L1 remained the same or differ. Also, further biological testing would determine if this enhanced inhibition translated to a cell-based assay or SPR.

In continuation with peptide-directed binding, one peptide-small molecule fragment, **6.8**, retained the ability to inhibit PD-1/PD-L1. To create a novel small molecule inhibitor, these fragments could be combined to create a library of small molecules connected with turn structure to be screened for inhibition of PD-1/PD-L1 with examples shown in **Figure 6-3**.

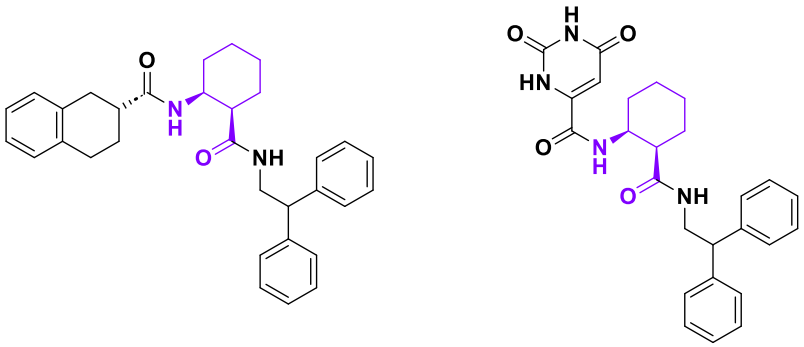


Figure 6-3 *Two structural examples of combining the small molecules highlighted in the peptide-small molecule hybrids screening using cis-2-aminocyclohexanecarboxylic acid to create small molecule mimics of CLP003,* ***6.1****.*

Another approach towards the completion of peptide-directed binding, would be using semi-peptide 2 without the proline and incorporating *cis*-2-Fmoc-aminocyclohexanecarboxylic acid using the reaction involving isobutyl chloroformate (**Figure 6-4**). This reaction originally was not attempted due to time constraints and the chlorotrityl resin being challenging to load. This would account for any difference in the structure that proline causes allowing for equal evaluation of both sides of the peptide. Also, retesting these peptides following acetylation would also be interesting to determine if there is any difference as acetylation is known to improve stability of peptides making them more resistant to degradation.

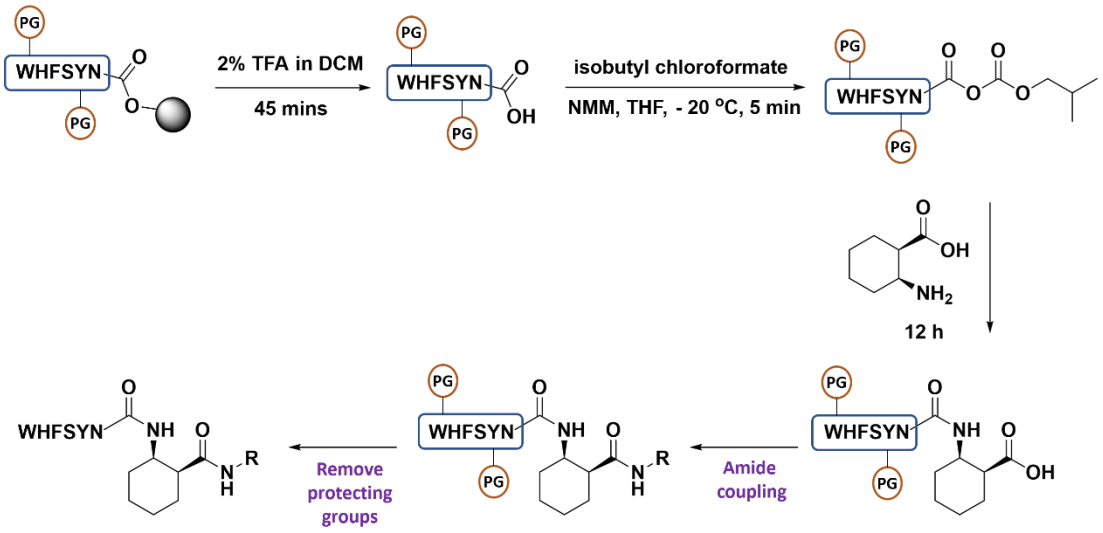


Figure 6-4 *Schematic illustration of cleaving the peptide WHFSYN from 2-chlorotrityl resin, amide coupling with cis-2-aminocyclohexanecarboxylic acid followed by another coupling with an amine small molecule, followed by deprotection for the final product, peptide-small molecule hybrid.*

In chapter four the investigation on whether IEDDA reaction between a tetrazine and a linear alkyne or alkene could be used in replacement of *cis*-2-Fmoc-aminocyclohexanecarboxylic acid as the turn mimic was carried out. The results of this reaction varied with the mono-substituted 1,2,4,5-tetrazines and Fmoc-(S)-2-(4-pentyl)Ala-OH showing the most promising outcome. However, poor yields and elongated reaction times limited this reaction from being used. Reports of IEDDA with tetrazines in the literature use a bulky, sterically hindered dienophile for this reaction but for use in peptide-directed binding as a turn mimic a smaller, more linear structure was advantageous.[3,4] Investigations into more reactive dienophiles could continue by looking into cyclopentene structures and trialling various solvents and temperatures to optimise the conditions.

Chapter five describes work towards synthesising cyclic peptides known to inhibit PD-1/PD-L1 and establishing a binding pharmacophore with an alanine scan. Through the modifications of a published procedure, the linear peptide of p57 and p101 were successfully synthesised.[5,6] For p57, the resin was change from rink amide AM to the sieber resin and was followed by double coupling the first amino acid (glycine). The couplings time and temperature for the remaining amino acids remained the same, removing the added six hour coupling at room temperature for N-methylated amino acids as this was not shown to improve coupling efficiency. When cleaving the peptide, the cleavage conditions were changed to use TFA:TIPS:DODT:H_2O

(94:1:2.5:2.5) instead of TFA/tioanisole/EDT/anisole (90:5:3:2), giving a cleaner analytical HPLC trace. However, despite attempting multiple conditions to add the chloroacetyl cap p57 showed degradation. P101 was synthesised using the TentaGel S Ram resin and was originally reported to use microwave coupling but room temperature coupling showed less aggregation. Despite the chloroacetyl cap being successfully added, when attempting the cyclisation to form the thioether bond the analysis suggested degradation and side reactions were taking place. To combat these challenges, the N-methylated containing peptides, p57 and p71, could potentially be synthesized in smaller sections and combined in solution phase. P101 would benefit from cyclisation optimisation through various cyclisation strategies. This could include using DMSO or triethylamine to lower the pH for cyclisation.

6.2 Conclusion

Throughout this thesis the theme of investigating turn mimic structures within novel inhibitors for PD-1/PD-L1 is prevalent. The design of a photo-switchable inhibitor in chapter 2 and the peptide-small molecule hybrid compounds found in chapter 3 demonstrate the value of a turn mimic when inhibiting PD-1/PD-L1. In particular, compounds **6.5** and **6.6** that showed IC_{50} values of 123 nM and 0.368 nM respectively. These compounds show comparable IC_{50} values to INCB086550 that is currently in clinical trials and of the antibody inhibitor, pembrolizumab.[7,8] These compounds stand to be the foundation of a lead compound that could be further modified and improved. Furthermore, the findings of the modified alanine scanned peptides and the shortened truncated peptides that showed superior inhibition of PD-1/PD-L1 in comparison to CLP003 also open an avenue of investigation to be continued.

6.3 References

1 H. Liu, Z. Zhao, L. Zhang, Y. Li, A. Jain, A. Barve, W. Jin, Y. Liu, J. Fetse and K. Cheng, *J. Immunother. Cancer*, 2019, **7**, 270.
2 A. Aemissegger and D. Hilvert, *Nat. Proto.c*, 2007, **2**, 161–167.
3 F. Liu, R. S. Paton, S. Kim, Y. Liang and K. N. Houk, *J. Am. Chem. Soc.*, 2013, **135**, 15642–15649.
4 F. Liu, Y. Liang and K. N. Houk, *J. Am. Chem. Soc.*, 2014, **136**, 11483–11493.
5 K. Magiera-Mularz, L. Skalniak, K. M. Zak, B. Musielak, E. Rudzinska-Szostak, Ł. Berlicki, J. Kocik, P. Grudnik, D. Sala, T. Zarganes-Tzitzikas, S. Shaabani, A. Dömling, G. Dubin and T. A. Holak, *Angew. Chem. Int. Ed.*, 2017, **56**, 13732–13735.

6 K. Magiera-Mularz, K. Kuska, L. Skalniak, P. Grudnik, B. Musielak, J. Plewka, J. Kocik, M. Stec, K. Weglarczyk, D. Sala, B. Wladyka, M. Siedlar, T. A. Holak and G. Dubin, *Adv. Therap.*, 2021, **4**, 2000195.
7 M. Chatterjee, D. C. Turner, E. Felip, H. Lena, F. Cappuzzo, L. Horn, E. B. Garon, R. Hui, H.-T. Arkenau, M. A. Gubens, M. D. Hellmann, D. Dong, C. Li, K. Mayawala, T. Freshwater, M. Ahamadi, J. Stone, G. M. Lubiniecki, J. Zhang, E. Im, D. P. De Alwis, A. G. Kondic and Ø. Fløtten, *Annals of Oncol.*, 2016, **27**, 1291–1298.
8 H. K. Koblish, L. Wu, L.-C. S. Wang, P. C. C. Liu, R. Wynn, J. Rios-Doria, S. Spitz, H. Liu, A. Volgina, N. Zolotarjova, K. Kapilashrami, E. Behshad, M. Covington, Y. Yang, J. Li, S. Diamond, M. Soloviev, K. O'Hayer, S. Rubin, C. Kanellopoulou, G. Yang, M. Rupar, D. DiMatteo, L. Lin, C. Stevens, Y. Zhang, P. Thekkat, R. Geschwindt, C. Marando, S. Yeleswaram, J. Jackson, P. Scherle, R. Huber, W. Yao and G. Hollis, *Cancer Discov.*, 2022, **12**, 1482–1499.